SOLID-PHASE SYNTHESIS OF RECYCLABLE PHOSPHORUS DONOR LIGANDS FOR THE DEVELOPMENT OF IMMOBILIZED TRANSITION-METAL CATALYST LIBRARIES

Robert Konrath

A Thesis Submitted for the Degree of PhD
at the
University of St Andrews

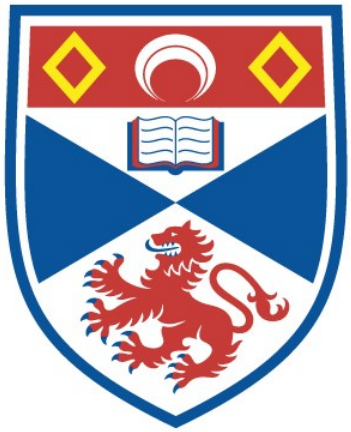

2019

Solid-Phase Synthesis of Recyclable Phosphorus Donor Ligands for the Development of Immobilized Transition-Metal Catalyst Libraries

Robert Konrath

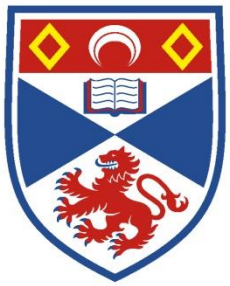

University of
St Andrews

This thesis is submitted in partial fulfilment for the degree of

Doctor of Philosophy (PhD)

at the University of St Andrews

April 2019

Declarations

Candidate's declarations:

I, Robert Konrath, do hereby certify that this thesis, submitted for the degree of PhD, which is approximately 63,000 words in length, has been written by me, and that it is the record of work carried out by me, or principally by myself in collaboration with others as acknowledged, and that it has not been submitted in any previous application for any degree.
I was admitted as a research student at the University of St Andrews in October 2015.
I received funding from an organisation or institution and have acknowledged the funder(s) in the full text of my thesis.

Date: 10.06.2019 Signature of candidate:

(Robert Konrath)

Funding

This work was supported by the Engineering and Physical Sciences Research Council Studentship Block Grant (Award Reference 1658187); and the University of St Andrews (School of Chemistry).

Date: 10.06.2019 Signature of candidate:

(Robert Konrath)

Research Data/Digital Outputs access statement

Research data underpinning this thesis are available at https://doi.org/10.17630/ea8ec4c1-1c2a-4bd7-8718-5e2d2009c667.

Date: 10.06.2019 Signature of candidate:

(Robert Konrath)

Supervisor's declaration:

I, Paul C. J. Kamer, hereby certify that the candidate has fulfilled the conditions of the Resolutions and Regulations appropriate for the degree of PhD in the University of St Andrews and that the candidate is qualified to submit this thesis in application for that degree.

Date: 10.06.2019 Signature of supervisor

(Prof. Paul C. J. Kamer)

I, Andrew Smith, hereby certify that the candidate has fulfilled the conditions of the Resolutions and Regulations appropriate for the degree of PhD in the University of St Andrews and that the candidate is qualified to submit this thesis in application for that degree.

Date: 10.06.2019 Signature of supervisor:

(Prof. Andrew Smith)

Permission for publication:

In submitting this thesis to the University of St Andrews we understand that we are giving permission for it to be made available for use in accordance with the regulations of the University Library for the time being in force, subject to any copyright vested in the work not being affected thereby. We also understand, unless exempt by an award of an embargo as requested below, that the title and the abstract will be published, and that a copy of the work may be made and supplied to any bona fide library or research worker, that this thesis will be electronically accessible for personal or research use and that the library has the right to migrate this thesis into new electronic forms as required to ensure continued access to the thesis.

I, Robert Konrath, confirm that my thesis does not contain any third-party material that requires copyright clearance.

The following is an agreed request by candidate and supervisor regarding the publication of this thesis:

Printed copy

Embargo on all of print copy for a period of 2 years on the following ground(s):

- Publication would preclude future publication

Supporting statement for printed embargo request

I have publications pending

Electronic copy

Embargo on all of electronic copy for a period of 2 years on the following ground(s):

- Publication would preclude future publication

Supporting statement for electronic embargo request

I have publications pending

Title and Abstract

- I agree to the title and abstract being published.

Date: 10.06.2019 Signature of candidate:

(Robert Konrath)

Date: 10.06.2019 Signature of supervisor:

(Prof. Paul C. J. Kamer)

Date: 10.06.2019 Signature of supervisor:

(Prof. Andrew Smith)

Underpinning research data or digital outputs

Candidate's declaration:

I, Robert Konrath, understand that by declaring that I have original research data or digital outputs, I should make every effort in meeting the University's and research funders' requirements on the deposit and sharing of research data or research digital outputs.

Date: 10.06.2019 Signature of candidate:

(Robert Konrath)

Permission for publication of underpinning research data or digital outputs

We understand that for any original research data or digital outputs which are deposited, we are giving permission for them to be made available for use in accordance with the requirements of the University and research funders, for the time being in force.

We also understand that the title and the description will be published, and that the underpinning research data or digital outputs will be electronically accessible for use in accordance with the license specified at the point of deposit, unless exempt by award of an embargo as requested below.

The following is an agreed request by candidate and supervisor regarding the publication of underpinning research data or digital outputs:

Embargo on all of electronic files for a period of 2 years on the following ground(s):

- Publication would preclude future publication

Supporting statement for embargo request

I have publications pending

Date: 10.06.2019 Signature of candidate:

(Robert Konrath)

Date: 10.06.2019 Signature of supervisor:

(Prof. Paul C. J. Kamer)

Date: 10.06.2019 Signature of supervisor:

(Prof. Andrew Smith)

Of all human activities, writing is the one for which it is easiest to find excuses not to begin – the desk's too big, the desk's too small, there's too much noise, there's too much quiet, it's too hot, too cold, too early, too late.

Robert HarriS

Acknowledgements

Looking back on the past 3.5 years, it has been a rewarding but also a rocky road, which ultimately culminated in this PhD thesis. On that way, many institutions and collaborators as well as colleagues, friends and family have a great share in the successful completion of this work. Hence, I would like to express my gratitude in the following lines.

First I would like to thank my supervisor, Professor Paul Kamer, for the opportunity to do a PhD in his group and all the fruitful discussions about the project but also about political developments in the European Union, which happened to affect us directly. Speaking about Brexit, I deeply appreciate his efforts to enable me finishing my research studies in his current institution, the Leibniz Institut für Katalyse in Rostock, Germany. This turned out to be a win-win collaboration, which made significant contributions to this thesis. Moreover, I would like to thank Paul for giving me the freedom to follow my own ideas in the development of new projects. This is something truly unique these days that, in my opinion, tremendously helps to become an independent researcher.

Many thanks to my formal supervisor, Prof. Andrew Smith, who made sure that, despite the relocation circumstances, everything proceeded smoothly and that the work in St Andrews as well as in Rostock remained unaffected.

I would also like to thank various other people in St Andrews who contributed to the realization of this thesis. First of all, cheers to my predecessor, Frank Heutz, who enabled me a flying start into this PhD. He not only introduced me into the world of resin chemistry but also supported me with constructive discussions long after he left St Andrews. I hope I could satisfy the expectations of the resinator community (#solidphasechemistry). During my time in St Andrews, I was given the opportunity to guide several project students who made valuable contributions to this work. In particular I would like to point out the CRITICAT CDT students Connor and Sophie, who, I am confident, are doing their own successful PhD at the moment after they had to experience the ups and downs in solid-phase synthesis during their first training year. Best of luck to Sven Wendholt, who visited as an Erasmus student and who mastered the frustration of resin-clogged needles with dignity. Without technical support, this thesis would contain only a fraction of content. Thanks to Melanja, Thomas and Daniel for providing outstanding NMR support. Many thanks to Brian and Bobby, who helped to fix any technical issues.

Inside and outside the lab, I met a lot of people of which many have turned into good friends and I am still in contact with despite the distances these days. Cheers to all the members of the PCJK group during my time in St Andrews. Especially Lorenzo, Ciaran and Rebecca for unforgettable fun times in the lab. Sherry for cooking incredibly tasty dumplings for us on a lonely New Year's Eve in St Andrews as well as for cat-sitting on many occasions. Luke, despite his awful taste in music in the lab, for all the help during moving. And of course to Amanda and all the other members of the group for help and advice.

I am glad that I could join the Monday Badminton sessions to escape the lab for exciting rallies and matches. In St Andrews, I discovered the world of whisky and many other enjoyable beverages at several memorable tastings. I need to highlight the splendid whisky trip to Islay. 3.5 days, 8 distilleries, delicious whisky, beautiful landscape and the best company from Frank, Rik and Stefan. Thanks to the Whey Pat young team, in particular Joe, Ciaran, Andrew, Reuben and Sam, for very special Darts & Dominos nights at the pub (DAAAAARTS!). I should not forget to mention fantastic Beer & Burger nights and extremely dramatic games of Resistance. Cheers to Sam, one of the best friends and origami artists I have met in St Andrews. Thanks for hanging out so many times and all the best for your future and I truly hope we keep in contact.

Concerning my stay in Germany, I would like to thank the Leibniz Institut für Katalyse for hosting me as a gust researcher. It was tough to say good bye to people in St Andrews but I was warmly welcomed in Likat. Especially by the new research group in Rostock but also by several colleagues who have a big share on the successful completion of this thesis. Thanks to Nils for Raman measurements, to Marcel for supplying the phospholane and to Jacob and Jens for great discussions. And of course to Bernhard, Pim, Brian, Christoph and Tommy who helped out in the lab on several occasions and who were good company outside Likat.

Finally, I would like to express my gratitude to both my family and friends, who supported me during this time. All the joyful visits in our little St Andrian house made the whole experience even better.

The last lines are reserved for the certainly most important person, my fiancé Franziska, who did not only share this adventure with me but also helped me to forget about all the PhD troubles when necessary. I cannot appreciate enough that you decided to join me in St Andrews and in Rostock, especially since it was always a challenging task to find your own way whenever we changed location. Vielen Dank.

Abstract

Phosphorus-based ligands play a key role in a plethora of transition-metal catalyzed transformations. To date, only a few privileged ligand motifs have been developed for high performance application in a wide range of reactions. Despite the advances in rational design of highly selective phosphorus-based ligands in (asymmetric) homogeneous catalysis, synthetic approaches through trial-and-error remain the most common methodologies for the discovery of new powerful catalysts. High throughput experimentation has been embraced by both academia and industry to accelerate catalyst optimization requiring accesses to large and diverse ligand libraries. There is, however, still a lack of efficient combinatorial techniques enabling the synthesis and screening of vast phosphorus-based ligand libraries.

Solid-phase synthesis (SPS) offers an useful tool towards the parallel synthesis of large multidentate ligand libraries. While being covalently bound to an insoluble polymeric support, a stepwise preparation of modular ligands can be realized via systematic variation of various building blocks. Moreover, purification procedures can be greatly simplified when employing this SPS approach, often requiring only easy filtration steps. Another advantage offered by immobilization of homogeneous catalysts on insoluble supports is the facilitated catalyst recovery and recycling as catalyst separation remains one of the major problems in applied homogenous catalysis. Consequently, resin-bound catalysts represent promising candidates for application in continuously operated processes.

This thesis presents the efficient preparation of multidentate phosphorus ligand libraries using as solid-phase synthesis approach. Chapter 2 describes the modular access to a large and highly diverse supported phosphine-phosphite ligand library for application in asymmetric hydrogenation of enamides. The synthesis of a supported PNP pincer ligand library for application in ester reduction underlines the versatility of this SPS approach (chapter 3). Furthermore, the combinatorial ligand synthesis on a solid support has been successfully transferred to chiral PNP-type ligands (chapter 4). In chapter 5, a series of supported tripodal phosphorus ligand-based ruthenium complexes has been employed in nitrile hydrogenation providing tunable product selectivity by a simple change in the catalyst structure. Ultimately, the recovery and reusability of these heterogenized homogeneous catalysts has been investigated under batch and continuous flow conditions.

Table of Contents

Declarations iii

Acknowledgements xi

Abstract xiii

Table of Contents xv

List of Abbreviations xix

Chapter 1 1

1.1 Introduction 2

1.2 Heterogenization of Homogeneous Catalysts 6

1.2.1 Organic Supports 10

1.2.2 Inorganic Supports 14

1.2.4 Continuously Operated Processes 15

1.3 Solid-Phase Synthesis 18

1.3.1 Supported Multidentate Phosphorus Ligands 18

1.4 Project Aim 25

1.5 References 27

Chapter 2 33

2.1 Introduction 34

2.2 Solid-Phase Synthesis of a Supported Phosphine-Phosphite Ligands 38

2.2.1 Synthesis of Resin-Bound β-Hydoxyalkyl Phosphines 39

2.2.2 *O*-Phosphorylation of Resin-Bound Phosphino Alcohols 44

2.3 Rhodium-Catalyzed Asymmetric Hydrogenation 49

2.3.1 Synthesis of Supported Rhodium-P-OP Complexes 49

2.3.2 Catalytic Screening 50

2.4 Catalytic Recycling 58

2.4.1 Batch Recycling 58

2.4.2 Continuous Flow Hydrogenation 60
2.5 Conclusion and Outlook 63
2.6 Experimental 65
2.7 References 78
Chapter 3 81
3.1 Introduction 82
3.2 Solid-Phase Synthesis of PNP Ligand Library 87
3.3 Synthesis of Supported Ruthenium-PNP Complexes 94
3.3.1 Gel-phase ^{31}P NMR 95
3.3.2 Solid-State NMR 96
3.4 Synthesis of unsymmetrical homogeneous Ru-PNP complex 8 98
3.5 Application in Ester Hydrogenation 100
3.5.1 Catalytic Screening 100
3.5.2 Substrate Scope 103
3.5.3 Reaction Profile 104
3.6 Catalytic Recycling 105
3.7 Conclusion and Outlook 107
3.8 Experimental 109
3.9 References 129
Chapter 4 133
4.1 Introduction 134
4.2 Solid-Phase Synthesis 138
4.2.1 Synthesis of Cyclic Sulfamidates 138
4.2.2 Synthesis of Supported PN Ligands 139
4.2.3 Synthesis of Supported (a)chrial PNP Ligands 145
4.2.4 Synthesis of Supported Chiral Pyridine-based PNP Ligand L_{13} 150
4.3 Application in Asymmetric Ketone Hydrogenation 152
4.3.1 Synthesis of Supported Ru-PNP Complexes 152

4.3.2 Catalytic Screening 155
4.4 Conclusion and Outlook 161
4.5 Experimental 163
4.6 References 178
Chapter 5 181
5.1 Introduction 182
5.2. Solid-Phase Synthesis of Supported Triphos Derivatives 187
5.3. Solid-Phase Synthesis of Supported Ruthenium-Triphos Complexes 189
5.3.1 Gel-phase ^{31}P NMR 190
5.3.2 Solid-State NMR 192
5.3.3 ATR-FTIR Spectroscopy 193
5.3.4 Raman Spectroscopy 195
5.4 Application of Supported Ru-Triphos Complexes in Catalysis 197
5.4.1 Deaminative Hydrogenation of Nitriles to Primary Alcohols 197
5.4.2 Hydrogenation of Nitriles to Primary Amines 199
5.5 Catalytic Recycling 204
5.5.1 Batch Recycling 204
5.5.2 Continuous Flow Hydrogenation 205
5.6 Conclusion and Outlook 211
5.7 Experimental 213
5.8 References 219
List of Publications 222

List of Abbreviations

δ	chemical shift
Δ	difference operator
ν	wavenumber
Å	Ångström
ac	acetyl
acac	acetylacetonate
Ad	adamantyl
AIBN	azobisisobutyronitrile
Ar	aromatic
ATR	attenuated total reflectance
BINAL-H	binaphthol-modified lithium aluminum hydride
BINAP	bis(diphenylphosphino)-1,1′-binaphthalene
BINOL	1,1'-bi-2-naphthol
Boc	*tert*-butoxycarbonyl
br	broad
BSA	*O*,*N*-bis(trimehtylsilyl)acetamide
Bu	butyl
BuLi	butyllithium
Bz	benzyl
°C	degrees Celsius
cat.	catalyst
CBS	Corey-Bakshi-Shibata catalyst
cod	cyclooctadiene
CP	cross-polarization
Cy	cyclohexyl
d	doublet
DABCO	1,4-diazabicyclo[2.2.2]octane
DCM	dichloromethane
DIBAL-H	diisobutylaluminium hydride
DIOP	2,3-*o*-isopropylidene-2,3-dihydroxy-1,4-bis(diphenylphosphino)butane
DIPAMP	1,2-bis[(2-methoxyphenyl)(phenylphosphino)]ethane
DIP-Cl™	chlorodiisopinocampheylborane

DMC	dimethyl carbonate
DMSO	dimethyl sulfoxide
DPEN	1,2-diphenyl-1,2-diaminoethane
DVB	divinylbenzene
EMR	enzyme-membrane reactor
equiv.	equivalent
Et	ethyl
FID	flame ionization detector
FT	Fourier transformation
g	grams
GC	gas chromatography
h	hours
HPA	heteropolyacid
HPLC	high performance liquid chromatography
Hz	Hertz
i	*iso*
ICP-OES	inductively coupled plasma optical emission spectrometry
i.e.	id est
IR	infrared spectroscopy
J	coupling constant (Hz)
JJ	JandaJel™ resin
KHMDS	potassium bis(trimethylsilyl)amide
LDA	lithium diisopropylamide
m	multiplet (NMR), medium (IR)
M	moles per liter
MAS	magic angle spin
Me	methyl
MF	Merrifield resin
min	minutes
MOF	metal organic framework
mol	moles
Ms	mesyl
n	linear
nbd	norbornadiene
NMR	nuclear magnetic resonance

O	*ortho*
OTs	tosylate
P	pressure
PEG	polyethylene glycol
Ph	phenyl
P-OP	phosphine-phosphite
ppm	parts per million
Pr	propyl
PS	polystyrene resin
PTA	phosphotungstic acid
PTSA	*p*- toluenesulfonic acid
rt	room temperature
s	singlet (NMR), strong (IR)
$scCO_2$	supercritical carbon dioxide
SHOP	Shell higher olefin process
SILP	supported ionic liquid phase
SPS	solid phase synthesis
t	*tert*
T	temperature
TADDOL	$\alpha,\alpha,\alpha,\alpha$-tetraaryl-1,3-dioxolane-4,5-dimethanol
TBAF	tetra-n-butylammonium fluoride
TBS	*tert*-butyldimethylsilyl
TFA	trifluoroacetic acid
THF	tetrahydrofuran
TMOF	trimethyl orthoformate
TOF	turnover frequency
Tol	tolyl
TON	turnover number
TOS	time-on-stream
TPPTS	3,3′,3″-phosphanetriyltris(benzenesulfonic acid) trisodium salt
Triphos	1,1,1-tris(diphenylphosphinomethyl)ethane
w	weak

Chapter 1

Heterogenization of Homogeneous Catalysts and Solid-Phase Synthesis of Phosphorus-based Ligands

Abstract: *Despite the advances in rational design of highly selective phosphorus-based ligands in (asymmetric) homogeneous catalysis, synthetic approaches through trial-and-error remain the most common methodologies for catalyst optimization. There is, however, still a lack of efficient combinatorial methods enabling the synthesis and screening of chiral phosphorus ligand libraries. Solid-phase synthesis (SPS) offers a facile tool for a stepwise ligand production by employing insoluble organic supports enabling simplified purification procedures. Systematic variation of building blocks can lead to a rapid access towards large and diverse supported multidentate phosphorus ligand libraries. When employed in a catalytic reaction, this approach can facilitate the recovery of heterogenized catalysts and potentially even enable their reusability. This can be of great importance due to the inherent separation issue associated with applied homogeneous catalysis. Ample catalyst immobilization approaches have been studied involving the use of solid and soluble supports as well as multiphasic and multidisciplinary techniques. As the topics of this thesis involve the solid-phase synthesis of multidentate phosphorus ligands and the recovery of immobilized catalysts, an overview is presented in this introductory chapter.*

1.1 Introduction

Crude oil, still representing the most important raw material followed by coal, natural gas and renewable feedstocks, is processed daily on a multiton scale for the production of platform chemicals.[1] These bulk chemicals serve as raw materials for the manufacture of increasingly desired fine chemicals, agrochemicals and pharmaceuticals. The rising demand for reduced waste production and energy consumption has led to widespread application of atom-economical and environmentally more benign catalytic processes.[2]

To date, heterogeneous catalysts play a predominant role in industrial production of liquid fuels and bulk chemicals owing to their high stability and robustness under harsh reaction conditions as well as their applicability in continuous processes. Since the discovery of the so-called *oxo synthesis* by Otto Roelen in 1938,[3] the field of homogeneous catalysis has gained significant importance for both academia and industry.[4] While a growing but still limited number of homogenously catalyzed processes has been implemented in the petrochemical industries, homogeneous catalysis provides an essential tool to fine chemical and pharmaceutical synthesis especially in the production of optically pure compounds. Ultimately, the tremendous achievements in the field of asymmetric catalysis were rewarded with the Nobel Prize in chemistry for W. S. Knowles,[5] R. Noyori[6] and K. B. Sharpless.[7]

In comparison to heterogeneous catalysts, the use of homogeneously catalyzed processes remains heavily underrepresented. Milestones in large scale productions employing homogeneous transition-metal catalysts are the hydroformylation of propene to *n*-butanal (Ruhrchemie/Rhône-Poulenc process),[8] the production of linear α-olefins (SHOP process)[9] as well as the carbonylation of methanol (Monsanto and CATIVA process).[10] Moreover, industrial processes reliant on asymmetric transformations have successfully applied homogeneous catalysts featuring enantioselective bidentate phosphorus ligands. The Antiparkinson's disease drug L-DOPA (L-3,4-dihydroxyphenylalanine) is produced in the Monsanto amino acid process with 94% *ee* using a Rh-DIPAMP catalyst (Figure 1).[11] An Ir catalyst based on a chiral diphosphine ligand was used by Ciba-Geigy to manufacture the herbicide (*S*)-Metolachlor on an annual >10000 ton scale.[12] Another landmark example was introduced by Takasago Perfumery Co. Ltd. for the stereoselective Rh-catalyzed isomerization of a key intermediate in the L-menthol production employing Noyori's BINAP ligand (see Figure 1).[13]

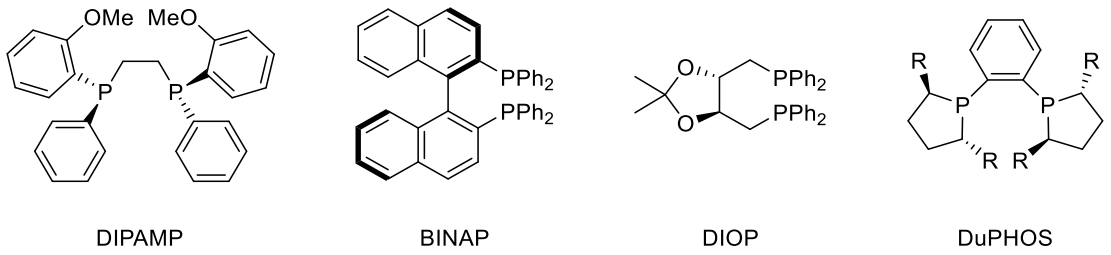

Figure 1 Selected examples of privileged bidentate phosphorus ligands in asymmetric catalysis.

Despite the few successful industrial applications and the undeniable potential of homogeneous asymmetric catalysis, the discovery of highly selective catalysts remains challenging. In fact, only a small number of so-called privileged ligands, such as the chiral diphosphines DIPAMP and BINAP, displays high activity, selectivity and longevity in a broad range of transformations (see Figure 1 for selected examples).[14] Huge advances in the field of asymmetric transition-metal catalysis have been made in recent years, especially due to the benefits of modern computational techniques. However, the discovery of high performance catalysts still relies mainly on empirical trial-and-error methodologies.[15]

Initially used as an indispensable tool in biotechnology, automated high-throughput experimentation has found widespread application in both academia and industry for the discovery of new efficient catalysts.[16] The advantage of *in situ* generated homogeneous catalysts by mixing metal precursor with commercially available ligands offers a myriad of combinations requiring efficient analysis strategies such as iterative or deconvolution approaches. However, often fine-tuning of ligand properties becomes necessary in order to achieve excellent catalytic performances for specific substrates. Since subtle changes in ligand structure can have a profound impact on activity and selectivity, the application of modular (chiral) ligand libraries in high-throughput screenings has proven to be highly beneficial.[16-17] In a seminal report from 1996 by Burgess and co-workers, a series of 13 different phosphine oxazolines was prepared starting from a common synthon and subsequently screened in Pd-catalyzed allylic alkylation of *rac*-1,3-diphenyl-2-propenyl acetate with dimethyl malonate in a 34-well microtiter plate (Scheme 1).[18]

In essence, the success of this screening approach relies on efficient protocols in order to access large and highly diverse ligand libraries. However, combinatorial synthetic methodologies towards chiral phosphorus containing multidentate ligands, which are of significant importance in asymmetric transition-metal catalyzed reactions, remain scarce.[15]

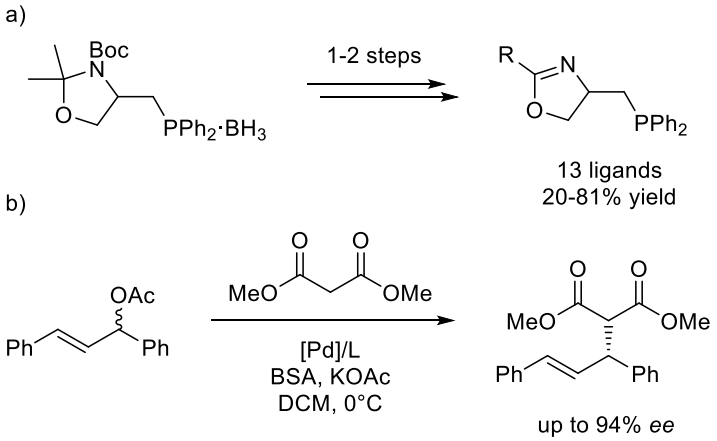

Scheme 1 a) Modular approach towards phosphine oxazoline ligands and b) application in Pd-catalyzed asymmetric allylic alkylation (BSA = *O*,*N*-bis(trimehtylsilyl)acetamide).[18]

This can be attributed to the intrinsically more complicated synthesis of these compounds often containing highly air and moisture sensitive phosphine and phosphite moieties.[19]

Combinatorial approaches for the solution phase synthesis of ligand libraries have mainly focused on monodentate phosphorus containing ligands.[20] The extension of this methodology to bidentate or even terdentate phosphorus ligand libraries turned out to be much more complicated in terms of time-consuming and often low-yielding purification steps.[16] The utilization of solid-phase synthesis strategies provides an alternative approach towards the access of highly diverse multidentate ligand libraries, which can be generated by a modular step-by-step ligand synthesis while being bound to a resin bead throughout the procedure. In contrast to conventional synthetic techniques, solid-phase synthesis (SPS) offers the advantage of simple purification steps by employing easy filtrations and decantations which consequently allows the use of excess reagents to achieve quantitative yields.[19b] Using such a divergent SPS approach significantly accelerates the preparation of new ligands for utilization in subsequent screenings in various catalytic transformations.

The fact that only a few catalytic processes employing homogeneous catalysts have been commercialized is associated with the intrinsic difficulties in product separation of these often toxic and expensive ligands and transition-metals.[21] Catalyst immobilization via SPS offers the advantage of facile recovery and reusability as the catalyst remains covalently bound to the insoluble support. Moreover, resin-bound catalysts make promising candidates for application in continuous flow processing avoiding the change in conditions during the product separation step.[22] However, problems involving catalysts deactivation resulting in metal and ligand leaching into the

product phase have hampered commercialization on large scale so far apart from niche applications in pharmaceutical industry.[23]

Since the ideal catalyst would combine the best of both worlds, i.e. high activity, selectivity and tunability of homogeneous catalysis and the ease of separation and recycling of heterogeneous catalysts, a tremendous research effort has been devoted to the development of heterogenized homogeneous catalysts in the past decades.[21b,24] A plethora of immobilization strategies has emerged over the years including multiphasic catalysis,[25] immobilization on (in)organic supports,[26] physical entrapment methodologies[24c,27] as well as multidisciplinary techniques such as separation by size-exclusion using membrane reactors.[28] Nevertheless, in many cases, the heterogenization of homogeneous catalysts is associated with reduced activity and (enantio)selectivity compared to their solution-phase analogues. Especially from the field of applied homogeneous catalysis, reduced performances combined with the prevailing issue of metal leaching have raised concerns about the suitability of these hybrid-type catalysts for industrial applications.[29]

In fact, significant progress has been made in the field of catalyst immobilization in particular when aiming for solutions to overcome the above mentioned limitations.[30] However, research combining the advantages of both the combinatorial synthesis of multidentate ligand libraries as well as the preparation of reusable immobilized catalysts is still restricted to a few literature reports.[31] The research presented in this work aims to connect the benefits of the solid-phase synthesis of supported multidentate phosphorus ligand libraries with efficient catalyst screening in catalytic reactions. In particular, the recovery and recyclability of the resin-bound catalysts will be investigated under batch and continuous flow conditions.

In the first section of this chapter, strategies towards catalyst immobilization and their applications are discussed (section 1.2). Section 1.3 outlines the benefits of a solid-phase synthetic approach towards the generation of multidentate phosphorus ligand libraries on solid supports. In the final section, the specific aims of this research are presented (section 1.4).

1.2 Heterogenization of Homogeneous Catalysts

In spite of the huge advantages offered by homogeneous catalysis compared to heterogeneous catalysis (see Table 1), such as high activity, selectivity and catalyst tunability, commercialization remains limited as a consequence of one major drawback. Unlike heterogeneous catalysis, all involved compounds in homogeneous catalysis are situated in a monophasic system which significantly complicates the recovery of these often costly and toxic transition-metal complexes.

Table 1 Homogeneous versus heterogeneous catalysis.

	Homogeneous Catalysis	**Heterogeneous Catalysis**
Activity (relative to metal content)	High	Low/moderate
Selectivity	High	Low/moderate
Reaction conditions	Mild	Harsh
Thermal stability	Low/moderate	High
Longevity	Low/moderate	Long
Sensitivity towards catalyst poisons	Low	High
Mass and heat transfer limitations	None	Possible
Mechanistic understanding	Reasonably well understood	Less Well Understood
Tunability	Facile	Complicated
Catalyst Recovery and Recycling	Challenging/expensive	Facile

For example, tailored chiral diphosphine ligands for applications in asymmetric reactions are generally prepared in multistep procedures leading to an overall cost between 5,000 and 20,000 €/kg, which rationalizes the desire for ligand recovery.[29] However, separation and purification procedures, often involving fractional distillations, can be expensive, energy intensive and troublesome also due to the limited thermal stability of homogeneous catalysts. This in turn explains the preference for heterogeneously operated processes in industrial settings.

The hydroformylation of propene or higher olefins for the production of linear aldehydes represents one of the few successful examples of industrially applied homogeneous catalysis.[32] The pioneering high-pressure hydroformylation processes, dating back to the early 1950s, were based on cobalt catalysts such as $HCo(CO)_4$.[33] Initially, catalyst separation was accomplished by disintegration of the homogeneous complex by changing the oxidation state via hydrothermal treatment (older Ruhrchemie process) or by oxygen treatment under acidic conditions (BASF process) followed by catalyst regeneration. The Kuhlmann/Exxon process enabled the preservation of the catalyst oxidation state involving aqueous basic extraction and conversion of the sodium cobalt salt into the active cobalt hydride catalyst. A significantly improved approach for the production of *n*-butanal employed a water-soluble rhodium catalyst based on a *meta*-sulfonated triphenylphosphine ligand (TPPTS, Ruhrchemie/Rhône-Poulenc process, Scheme 2).[8,34] The insolubility of the Rh-catalyst in the product phase facilitates the aqueous biphasic separation of the product and catalyst-containing layer in a decanter unit. Subsequently, the catalyst is returned to the reactor for the next reaction cycle.

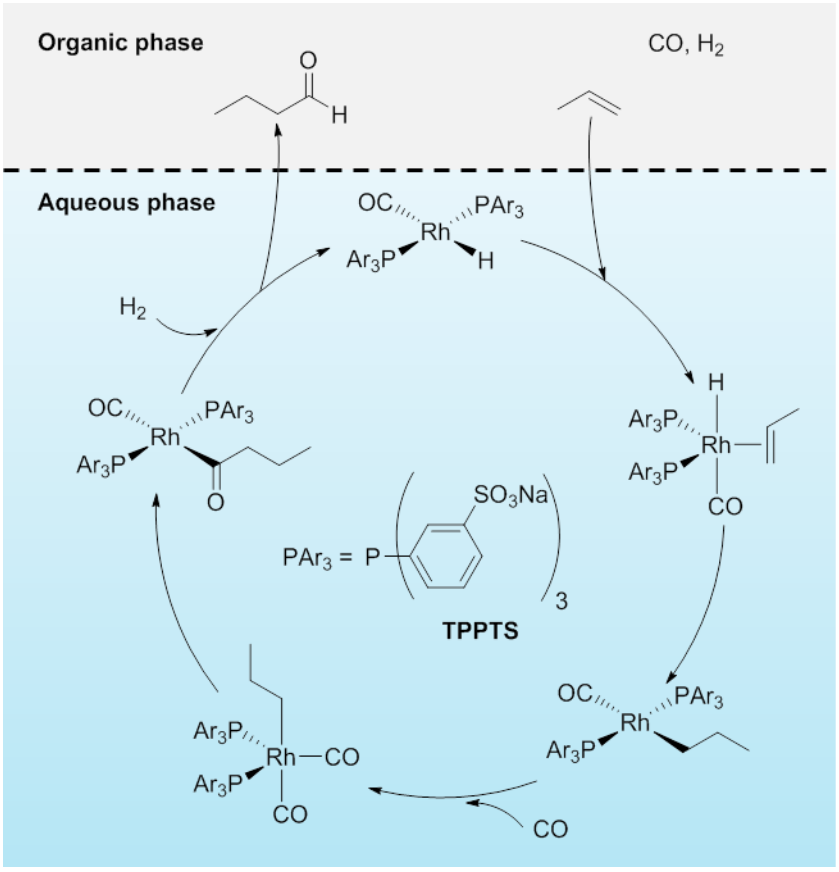

Scheme 2 Ruhrchemie/Rhône-Poulenc process for aqueous biphasic Rh-catalyzed hydroformylation.

Further important processes employing liquid-liquid partitioning for homogeneous catalyst separation are Kuraray's hydrodimerization of butadiene,[35] the Shell higher olefin process (SHOP)[9] for the production of linear α-olefins as well as the adiponitrile synthesis via hydrocyanation of butadiene (DuPont).[36]

Limited applicability to a wider range of processes and thus the necessity for the development of tailor-made separation methods in all cases has triggered the desire in both academia and industry to explore alternative recovery strategies. In order to develop an ideal heterogenized homogeneous catalyst, which combines the best of both disciplines (see Table 1), a tremendous research effort has been devoted to immobilization strategies beyond classical biphasic systems (Figure 2).

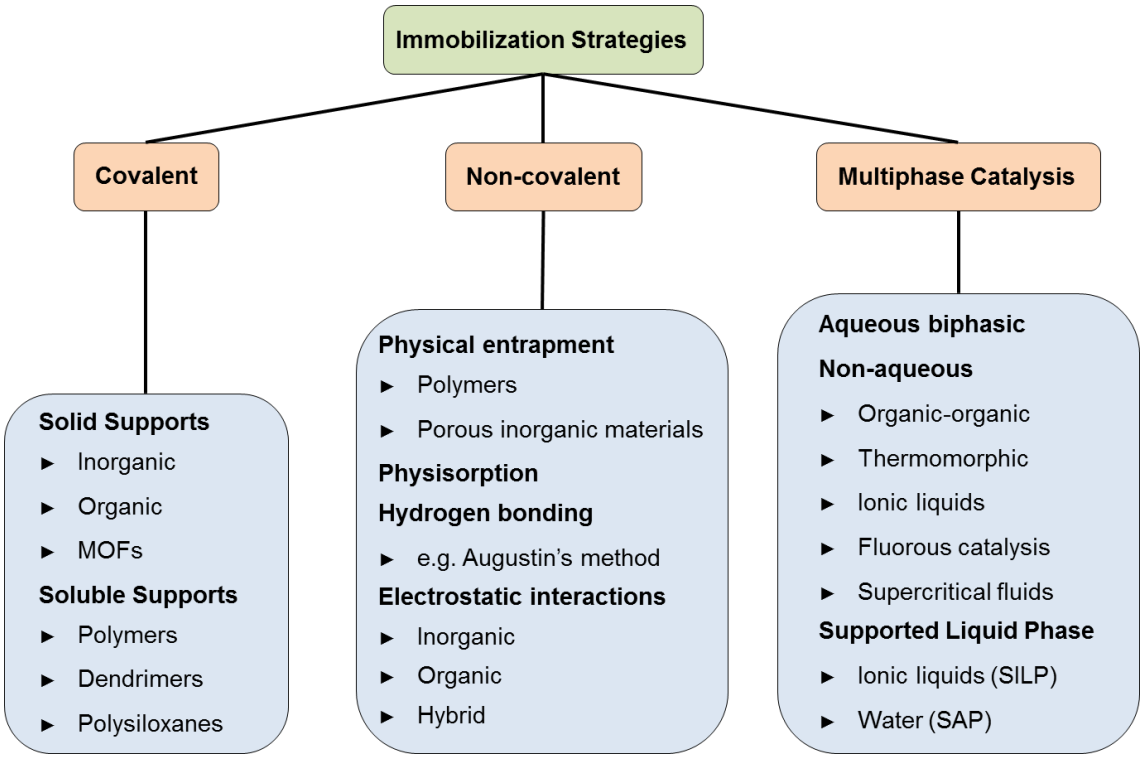

Figure 2 Selected strategies towards the immobilization of homogeneous catalysts.

Among the field of multiphase catalysis, alternative reaction media, such as ionic liquids, fluorous and supercritical fluids have been applied, which all require a tailor-made catalyst to provide selective solubility under separation conditions.[25] On the other hand, thermomorphic catalysts can be separated from the product by phase separation induced upon change of temperature.[37] Supported liquid phase catalysis represents a more advanced hybrid approach, which involves immobilization of a homogeneous catalyst within a thin film of a particular medium distributed over the

surface area of an insoluble support.[38] Another non-covalent strategy uses physical entrapment of a homogeneous catalyst inside the porous structure of an inorganic support, such as the 'ship-in-a-bottle' methodology, or by entanglement into a polymer.[27] A broad research area has focused on tethering homogeneous catalysts onto organic, inorganic supports[26] as well as on metal organic frameworks (MOF)[39] via covalent, electrostatic or other non-covalent interactions. While solid support materials remain insoluble in the reaction medium often leading to reduced catalyst performance due to mass-transfer limitations, also soluble polymeric supports have been introduced commonly employing polyethylene glycols (PEG).[40] This gives the opportunity to apply the supported catalyst in a monophasic system and subsequent separation is facilitated by precipitation and filtration techniques. Alternative approaches follow a molecular weight enlargement strategy by anchoring the catalyst onto dendrimers or polysilsesquioxanes (POSS) which in turn makes them suitable candidates for application in multidisciplinary ultra- and nanofiltration processes.[28]

Many of the above mentioned immobilization methodologies suffer from severe catalyst leaching due to insufficient precipitation in case of soluble supports or limited retention in the catalyst phase regarding biphasic approaches. Hence, the concept of anchoring a homogenous catalyst onto a solid support provides a more promising approach towards efficient catalyst recovery and recycling. Commercialized examples of immobilized catalysts remain limited to the Acetica process developed by Chiyoda and UOP for the production of acetic acid via carbonylation of methanol.[41] In this case the anionic rhodium complex $[RhI_2(CO)_2]^-$ is immobilized on a thermally robust polyvinyl pyridine resin by strong ionic interactions. At process temperatures between 160-200 °C and pressures of up to 60 bar, the catalyst remained active for >7000 hours when used in a continuous bubble reactor. Despite the obvious advantages and the tremendous research effort over the last 40 years, no chiral supported catalyst has been implemented into an industrial process. So far, the separation and recycling benefits associated with immobilized catalysts have failed to outbalance the downsides such as reduced catalytic performances due to mass-transfer limitations, additional preparative costs for ligand tailoring and catalysts leaching.[29,42] To overcome these issues, the development of widely applicable single-site heterogeneous catalysts, exhibiting improved performances as well as enhanced support and catalyst stability, remains of high interest to many research groups. Since insoluble supports play a predominant role, the following sections will focus on examples of catalyst immobilized on organic (1.2.1) and inorganic supports (1.2.2).

1.2.1 Organic Supports

Since the seminal work of Merrifield in the 1960s, polymeric supports have been frequently investigated as materials for the heterogenization of homogeneous catalyst.[43] Among the different types of polymers that have emerged over the last decades, a general differentiation can be made between soluble polymers and insoluble resins. Opposed to their insoluble cross-linked counterparts, soluble supports can offer reduced mass-transfer limitations. However, efficient recovery and recycling remain challenging for soluble polymeric supports whereas heterogeneous polymers can greatly facilitate the separation from the liquid phase. In some cases, immobilization on these insoluble types of supports can exert a beneficial effect on the catalyst stability, for example by catalyst site isolation preventing decomposition pathways such as dimerization of transition-metal complexes.[19a] Moreover, some resin examples can even provide an environment similar to those of homogeneous systems. Since the support plays a non-innocent role, detrimental impacts on supported catalyst activity and enantioselectivity are often reported.[29] On the other hand, many studies could demonstrate a beneficial effect on the catalyst performance when compared to their homogeneous analogues.[30]

The most common insoluble polymeric support materials are usually based on functionalized polystyrene and styrene/divinylbenzene (PS-DVB) co-polymers varying in the percentage of divinylbenzene (DVB) crosslinking.[44] An additional differentiation can be made into highly crosslinked macroporous resins (>5% DVB, up to 25% DVB) and weakly crosslinked microporous polymers (1-2% DVB). Macroporous resins typically possess a permanent pore structure and hence show solvent independent properties, which often lead to reduced catalyst activities.[45] In the case of microporous, also called gel-type resins, the DVB-crosslinked polystyrenes, such as the well-known Merrifield resin (Figure 3, left) and 4-bromopolystyrene (Figure 3, middle), represent examples of frequently employed insoluble supports. Low cost and commercial availability of these resins combined with their advantages for recycling of expensive catalysts has led to an indispensable tool in combinatorial chemistry and catalyst immobilization techniques.[19b,46]

One of the main drawbacks of microporous resins is their lower mechanical and thermal strength compared to higher crosslinked materials. Sufficient swelling properties of these resins are generally obtained in solvents such as THF, 1,4-dioxane, dichloromethane (DCM) and toluene, which in turn enables catalytic reactions to take place under solution-like conditions.

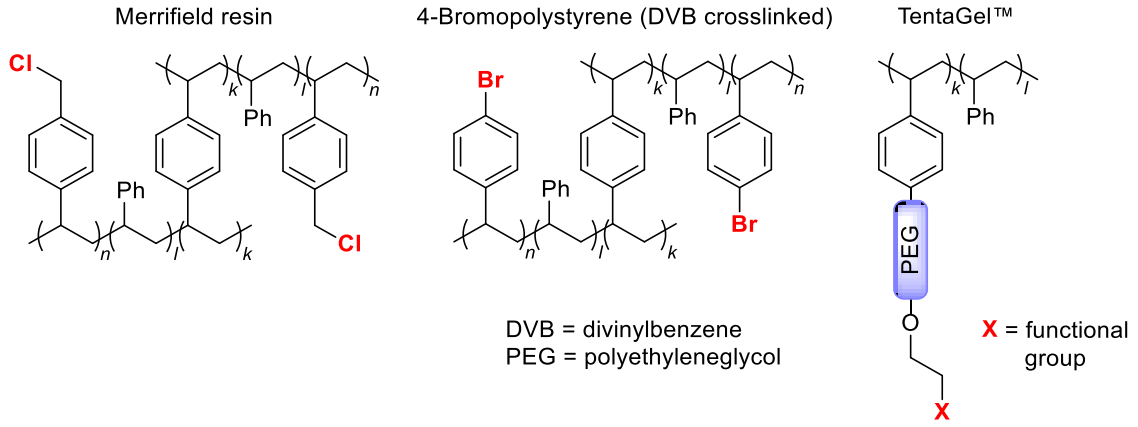

Figure 3 Merrifield resin (left), DVB crosslinked 4-bromopolystyrene (middle) and TentaGel™(right).

However, in protic media, such as alcohols, swelling properties can be severely reduced.[19b] In order to circumvent solvent dependency, amphiphilic hybrid PS-resins, like TentaGel™ (Figure 3, right), incorporating polyethyleneglycol (PEG) linkers have been introduced.[47] In addition to classical PS-DVB co-polymers, a range of other polymeric supports has been studied for catalyst immobilization purposes such as polyacrylates, polyvinyls or cellulose.[30]

Anchoring of the ligand to the polymeric support can be accomplished via covalent and non-covalent bonding.[26d,40b] The advantage of covalently-bound catalysts is the significantly reduced risk of metal or ligand leaching. Two synthetic strategies have been developed, which differ in the sequence in which the catalyst is incorporated into the polymeric structure. The bottom-up approach relies on the co-polymerization of functional monomers with a specifically modified ligand or complex, which leads to homogeneously distributed functionalities among the main chain of the polymer (Figure 4, left). An alternative approach is based on the post-modification strategy, which involves tethering of a ligand or the active catalyst onto the side-chains of a preformed, functionalized polymer (Figure 4, right).[48]

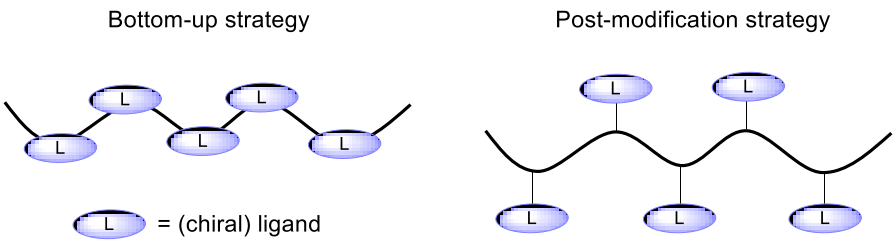

Figure 4 Bottom-up and post-modification strategies in the synthesis of polymer-supported catalysts.

In a recent example, the bottom-up approach was applied to the preparation of a chiral BINAP-based porous organic polymer via radical-induced polymerization of vinyl-functionalized (*S*)-BINAP with DVB (Scheme 3).[49] The corresponding supported ruthenium-diphosphine complexes were employed in the Ru-catalyzed asymmetric hydrogenation of β-keto esters giving enantioselectivities of up to 94%. Subsequent recycling experiments were performed at full substrate conversion, which hampers the monitoring of actual catalyst deactivation. However, the product selectivity remained fairly stable over six consecutive runs and Ru metal leaching was found to be less than 0.06 ppm per run.

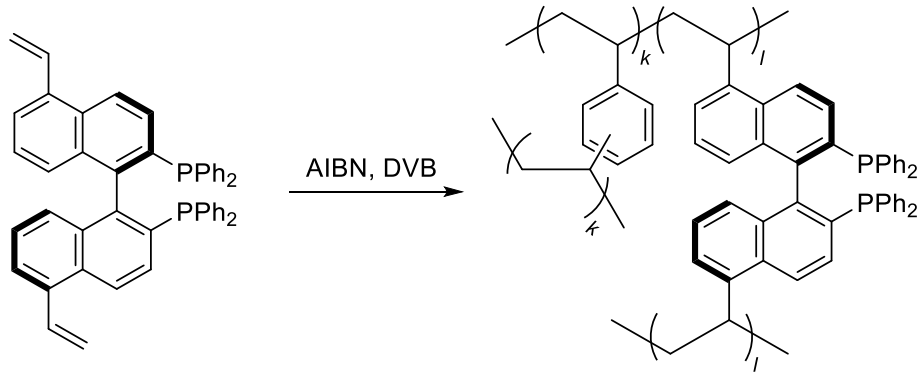

Scheme 3 Synthesis of chiral BINAP-based porous organic polymer by using a bottom-up approach.[49]

More recently, a knitting strategy developed by Tan and co-workers has attracted attention for the synthesis of porous organic polymer supported catalysts as a radical-free alternative to the more common co-polymerization approaches described above.[50] The preparation is based on $FeCl_3$ catalyzed Friedel-Crafts alkylation involving the crosslinking of simple aromatic building blocks, such as benzene, with aryl groups present in the ligand structure via rigid methylene bridges. This knitting strategy was applied by Wang *et al.* in 2016 for the preparation of (*S*)-BINAP immobilized in a hypercrosslinked polymeric aromatic network (Scheme 4).[51] Conveniently, ligand pre-modification with groups required for co-polymerization, such as vinyl moieties, could be avoided in this case. High activities at a catalysts loading of about 0.02 mol% and enantioselectivities of up to 98% were obtained in the Ru-catalyzed asymmetric hydrogenation of methyl acetoacetate. Preliminary recycling experiments performed at full substrate conversion revealed a slight drop in selectivity of about 1% over four consecutive runs. Potential leaching of the catalyst into the product phase was not investigated.

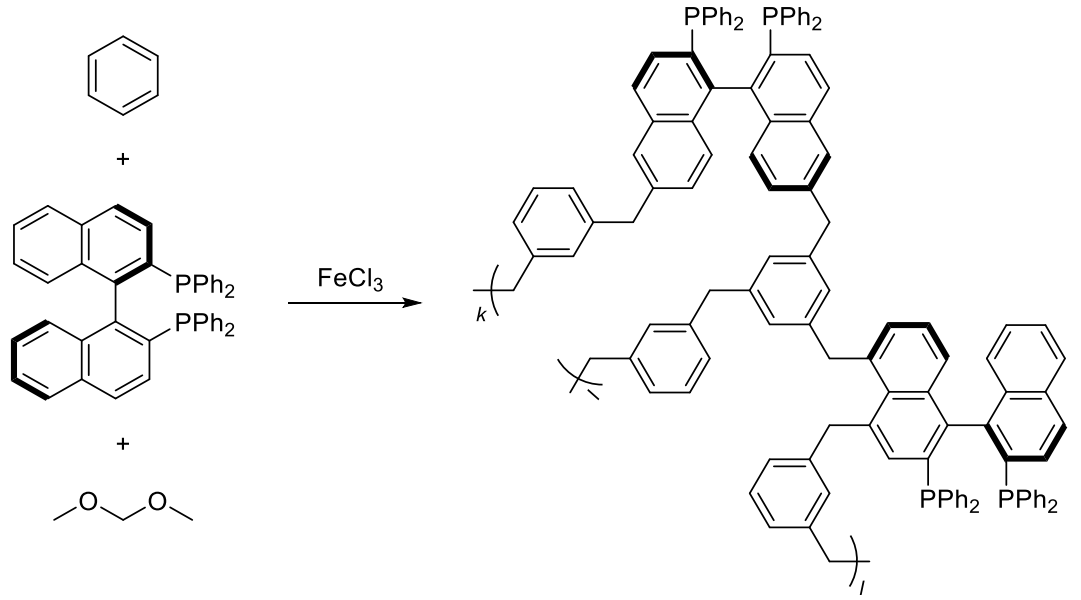

Scheme 4 Knitting strategy for the preparation of porous polymer supported BINAP ligand.[51]

The chiral salen-manganese complex, known as the Jacobsen's catalyst, was grafted onto pre-made polymeric supports, such as crosslinked acetoxy-functionalized polystyrene and methacrylate-based resins, by using a post-modification approach (Figure 5).[52] Application of the supported Jacobsen's catalysts in the asymmetric epoxidation of 1-phenylcyclohex-1-ene gave similar enantioselectivities for the methacrylate-supported Mn-catalyst compared to those obtained for homogeneous analogues. However, the catalyst recovery and reusability was not explored.

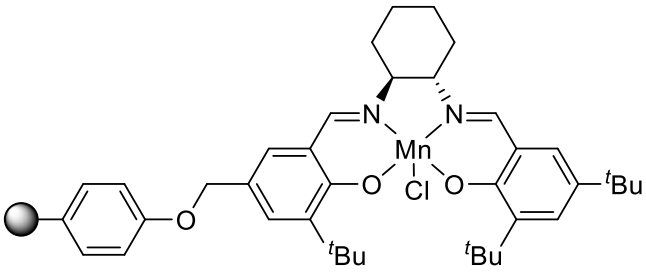

Figure 5 Immobilized Jacobsen's catalyst prepared via post-modification.[52]

Linear polystyrene as well as PEG-based polymers, such as MeO–PEG_{5000}–OH, have been widely studied for supported solution-phase catalysts. The potential for catalyst recovery relies on the solubility in solvents like water, toluene and chlorinated solvents whereas polymer precipitation is obtained in hexanes and diethyl ether. This facilitates catalyst recovery by simple filtration steps but quantitative recovery remains

challenging. Common issues are associated with polymer leaching often requiring large amounts of solvent for efficient catalyst recovery as well as co-precipitation of reaction products and by-products, which can lead to catalyst contaminations.[53]

1.2.2 Inorganic Supports

Opposed to organic polymeric supports, inorganic supports can offer a highly defined morphology together with a large surface area, which are important criteria for isolated single-site heterogeneous catalysts. Moreover, high thermal and mechanical stability as well as the lack of solvent dependent properties has led to the utilization of many well-established inorganic materials for catalyst immobilization.[54] In terms of costs and the high control over properties during synthesis, reported research mainly focuses on widely applied mesoporous silica-based materials, but also alumina, other single and mixed oxides, clays and zeolites are commonly applied. More recently, carbon-based materials, such as graphite and nanotubes, have attracted attention.[55]

Catalyst immobilization on silica-based supports can be achieved via covalent as well as non-covalent interactions with surface silanol groups. Anchoring of the homogeneous catalyst involving non-covalent interactions, such as hydrogen bonding, van der Waals or electrostatic interactions, often leads to weakly bound catalysts. Especially if purification procedures require the use of protic, polar solvents, catalyst leaching from the surface of the support can be significant.

The Augustine's strategy employs anionic heteropolyacids (HPA) functioning as anchoring agents, which are fixated on supports like alumina via weak hydrogen bond interactions (Figure 6, left). Electrostatic interactions between HPA and a cationic metal complex, such as $[(DIPAMP)Rh(cod)]^+$ (cod = cyclooctadiene), enable immobilization of a homogeneous catalyst onto the inorganic material. In the pioneering work of Augustine *et al.*, various alumina/PTA supported (PTA = phosphotungstic acid) rhodium catalysts based on chiral diphosphines were applied in the asymmetric hydrogenation of methyl 2-acetamidoacrylate showing at least equal and in some cases even superior activities and enantioselectivities when compared to their solution-phase analogues.[56] Leaching of Rh from the support was found to be below 1 ppm.

Covalent anchoring of homogeneous catalysts onto the surface of inorganic supports, such as silica, can be accomplished by a post-synthetic grafting strategy. This approach requires a pre-made ligand modified with an alkoxysilane linker, which can undergo a condensation with the surface silanol groups of the support.

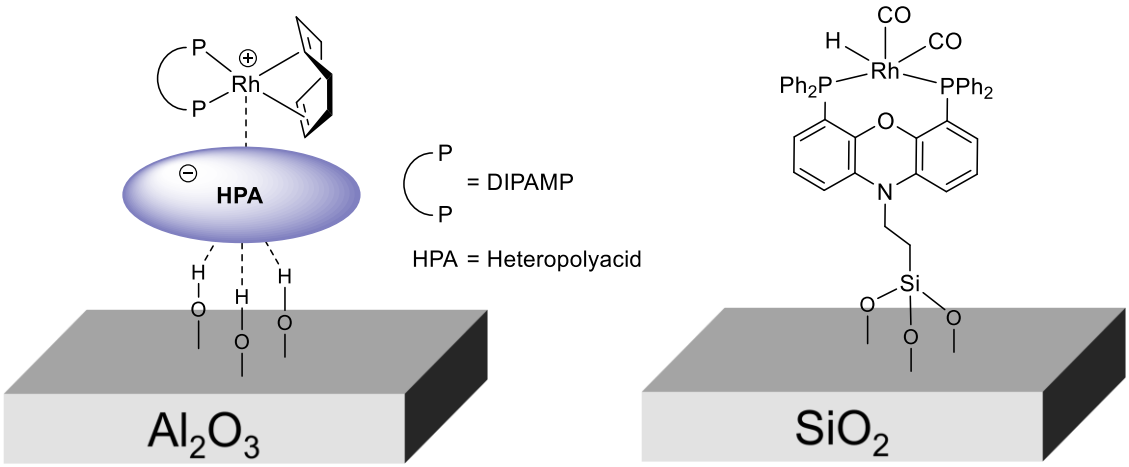

Figure 6 Alumina-supported Rh-diphosphines via Augustine's strategy[56] (left) and silica-bound Rh-siloxantphos synthesized by sol-gel process (right).[57]

However, both an inhomogeneous distribution of catalytic sites on the surface as well as limited mass transport inside the pores are downsides often associated with this post-synthetic strategy.[58]

An alternative approach in order to obtain a more homogeneous surface distribution of the catalyst is via a sol-gel process by performing a polycondensation of tetra-alkoxysilanes and functionalized tri-alkoxysilanes under mild synthetic conditions.[59] Following this approach, van Leeuwen and co-workers immobilized a rhodium siloxantphos catalyst, which was successfully applied and recycled in the Rh-catalyzed hydroformylation of 1-octene (Figure 6, right).[57] The desired linear aldehyde was obtained in 95% purity over eight consecutive cycles together with a total Rh leaching of <1%.

More recently, various advanced inorganic materials with advantageous properties, such as controllable morphology and large surface area, have been employed in this field. Supports, like MCM-type mesoporous silicas or mesoporous mixed metal oxides, are widely studied for the synthesis of supported catalysts.[54] In this work, however, the research will focus on insoluble polymeric supports for the preparation of multidentate ligands using a solid-phase synthetic approach.

1.2.4 Continuously Operated Processes

The benefits of large scale continuous processing have long been recognized by the oil and petrochemical industries. More recently, though, vast progress in the development of microreactor and flow chemistry technology has triggered increased attention to both

synthetic as well as process chemists in the fine chemical industries.[23b,60] Especially the continuous production of active pharmaceutical ingredients (APIs) has found widespread application but also the preparation of agrochemicals, polymers, nanomaterials and other platform chemicals.[23a,61] Continuous flow processing offers several advantages over batch processes such as improved control over heat and mass-transfer, which in turn facilitates reaction scale-up.[62] Usually harsher conditions can be applied compared to reactions in a batch reactor. The use of smaller reactor dimensions combined with high catalyst to substrate ratios leads to significantly reduced residence times in flow. Consequently, substrates and products are only exposed to these conditions for a short period minimizing the potential for side-product formation as well as providing a safer alternative for exothermic reactions.[63] The main advantage of continuous flow technology, however, is the high process efficiency having a significantly reduced impact on the environment due minimized production of waste.[60a,64] Continuous formation of product combined with simultaneous separation of the catalyst results in an intensified process avoiding the often laborious and energy demanding recovery of the typically very expensive and toxic homogeneous catalyst.

Heterogenized homogeneous catalysts can be readily integrated into a packed-bed reactor setup remaining located at a specific part of the reactor while the reaction mixture flows through. Since mechanical deterioration of the supporting material can be largely prevented compared to stirred batch processing and catalyst recycling is greatly simplified, numerous literature examples of immobilized catalysts used in continuous flow processes have appeared over the last two decades.[22,65]

One selected example reported by Meehan *et al.* employs a previously mentioned silica-bound siloxantphos ligand in the Rh-catalyzed continuous hydroformylation of 1-octene in supercritical carbon dioxide ($scCO_2$, Scheme 5).[66]

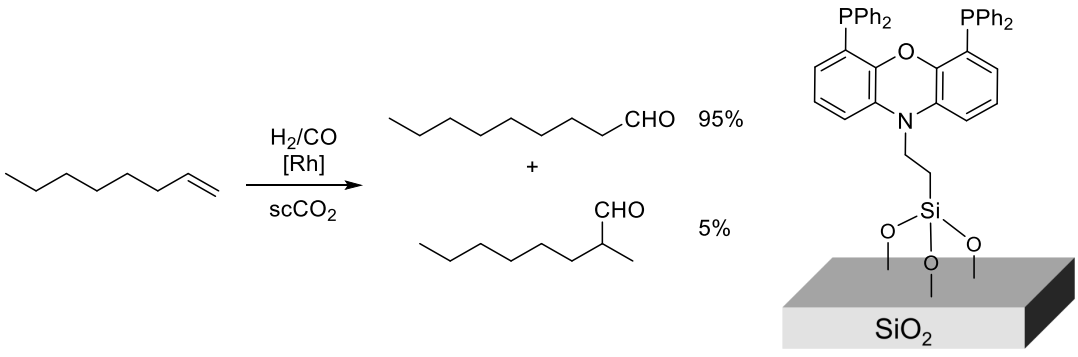

Scheme 5 Continuous hydroformylation of 1-octene using a SiO_2-grafted siloxantphos ligand.[66]

In this process, the catalyst proved to be very robust showing no significant activity and selectivity drop over six non-consecutive days together with only 0.2% of Rh metal leached into the product phase. Moreover, the organic phase could be easily separated from $scCO_2$ by depressurization.

A continuous hydrogenation process by Cole-Hamilton and co-workers employed a Rh-MeDuPHOS catalyst immobilized on alumina/PTA using the Augustine's method (Scheme 6).[67] For 23 hours on stream, the heterogenized catalysts converted >99% of dibutyl itaconate to the corresponding (*S*)-configured product with 98% *ee* under solvent-free conditions resulting in a total TON of 2638. The rhodium leaching during this period was found to be less than <50 ppb. After 23 hours on stream, the enantioselectivity decreased steadily to 65% over the next 50 hours along with a drop in activity to 68%.

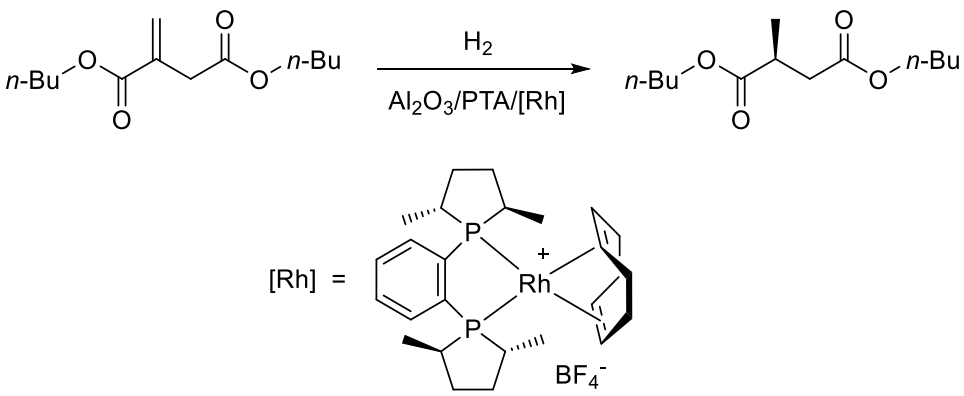

Scheme 6 Continuous hydrogenation of dibutyl itaconate using Rh-MeDuPhos immobilized on Al_2O_3/PTA.[67]

Another multidisciplinary alternative to classical flow reactor set-ups are membrane reactors coupling homogeneous catalysis with ultra- and nanofiltration techniques.[24e,28b] Since the development of the continuously operated enzyme-membrane reactors (EMR) used for the manufacture of amino acids at Degussa[68], the field of organic solvent nanofiltrations has rapidly expanded.[65] In many cases, weight enlarged homogeneous catalysts based on dendrimers or soluble polymers are employed but also non-modified catalysts have found application. As the catalyst remains in a homogeneous system, the obvious advantage of this technology is the high activity and selectivity provided by homogeneous catalysis. Limitations of this technique are often associated with membrane fouling and decomposition due to precipitation of compounds during the process.

Finally, facile optimization of processes parameters, such as temperature, pressure and reaction time, has led to a significant contribution of fully automated continuous flow processes to high-throughput experimentation.[16,69]

1.3 Solid-Phase Synthesis

Solid-phase synthesis (SPS) was initially developed for the preparation of polypeptides pioneered by Merrifield in 1963.[43] Since then, the methodology has found widespread application in the linear supported synthesis of oligonucleotides and oligosaccharides. Moreover, the immobilization of acceptor molecules and even the stabilization of explosive compounds could be accomplished when using SPS.[70] The main advantage of SPS is the utilization of functionalized insoluble polymers, which serve as a common synthon for a step-by-step synthesis of the desired compound while being covalently bound to a resin bead throughout the whole sequence. Excess reagents and side-products present in the supernatant solution can be easily removed by simple purification steps such as decantation or filtration. Hence, SPS has proven to be highly beneficial for the rapid combinatorial synthesis of compound libraries and has thus been used extensively in automated synthesis and high-throughput screening techniques, particularly in the pharmaceutical industry.[16] Taking the previously mentioned difficulties in the discovery of new high performance catalysts into account (see chapter 1.1), it is only a logical consequence that the SPS methodology was expanded towards the combinatorial synthesis of supported ligand and catalyst libraries and their subsequent screening in catalytic transformations.[46] In particular the generation of large and diverse multidentate phosphorus ligand libraries can tremendously benefit from a solid-phase synthetic approach applied in a combinatorial fashion since efficient solution-phase protocols still remain scarce.[15,19b,31b-d,71] The following section highlights the early and most recent achievements in the efficient SPS synthesis of resin-bound multidentate (chiral) phosphorus ligands and the advantages in terms of screening and recycling in catalysis.

1.3.1 Supported Multidentate Phosphorus Ligands

As mentioned previously, the number of privileged ligands applicable in a wide range of catalytic transformations can be pinned down to only a handful of examples.[14a] Techniques used to predict activities and selectivities of potential ligands are often still

lacking the required accuracy. That is why trial-and-error methodologies still remain the most common approaches for the discovery of high performance catalysts. Since this is generally realized in high-throughput experimentation settings, the rapid access to large and diverse ligand libraries is essential.[16] Especially in the case of phosphorus-containing ligands, which are of significant importance in (asymmetric) catalysis, solution-phase methodologies aiming for ligand optimization commonly involve troublesome and laborious protocols. The inherently more challenging synthesis of these multidentate phosphorus ligands has led to only a small number of homogeneous and more recent supramolecular approaches to libraries of ligands.[14b,15,72]

SPS offers a practical tool for a stepwise ligand build-up while remaining covalently bound to an insoluble polymer throughout the sequence. The treatment of a commercially available functionalized resin, such as Merrifield, with suitable phosphorus reagents leads to resin-bound phosphines ($\mathbf{P^{a\text{-}c}}$) serving as universal library synthons (Scheme 7). Employing a systematic variation of multiple building blocks, such as chiral backbones or amine bridges ($\mathbf{B^{1\text{-}2}}$) and additional phosphorus moieties ($\mathbf{P^{d\text{-}f}}$), enables the rapid access to large and structurally diverse supported multidentate ligand libraries. The benefit of this approach over conventional approaches is the ease of purification. The synthesis of typically air and moisture sensitive homogeneous phosphorus ligands often requires tedious purification steps, such as column chromatography under inert atmosphere.

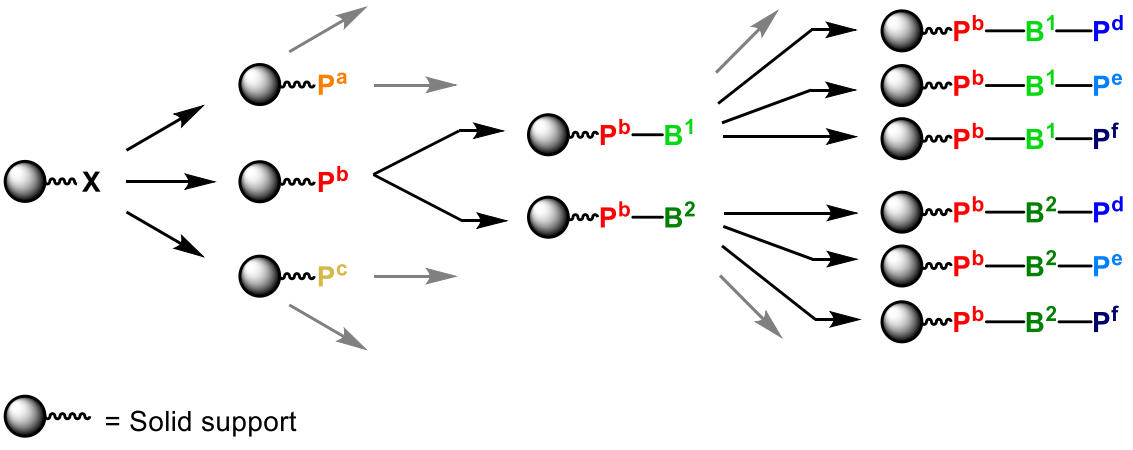

Scheme 7 Schematic representation of a modular solid-phase synthetic approach towards supported multidentate phosphorus ligands.

In contrast, only simple filtration or decantation steps to separate the support from the reaction mixture are required when using SPS. Consequently, this allows for the use of reagents in large excess to ensure full conversion for each reaction step, which is essential since supported by-products remain covalently bound to the support and cannot be removed. Another advantage offered by SPS is the possibility for facilitated catalyst recovery and recycling in catalytic transformations.

Over the last two decades, ample examples of monodentate phosphorus containing ligands synthesized by using an SPS approach and their application in (asymmetric) catalysis have appeared in literature.[15,73] However, reports on supported multidentate phosphorus ligand libraries remain relatively scarce.

Gilbertson and co-workers were the first to employ combinatorial methodologies in the development of supported bidentate phosphorus ligand libraries.[74] By using solid-phase peptide synthesis, a library of 63 undecapeptides was prepared, which include two different phosphinoserine amino acids in the peptide sequence (Figure 7). The peptide chain was designed in such a way that the resulting helical structure enabled chelating coordination of the phosphines to a rhodium centre.

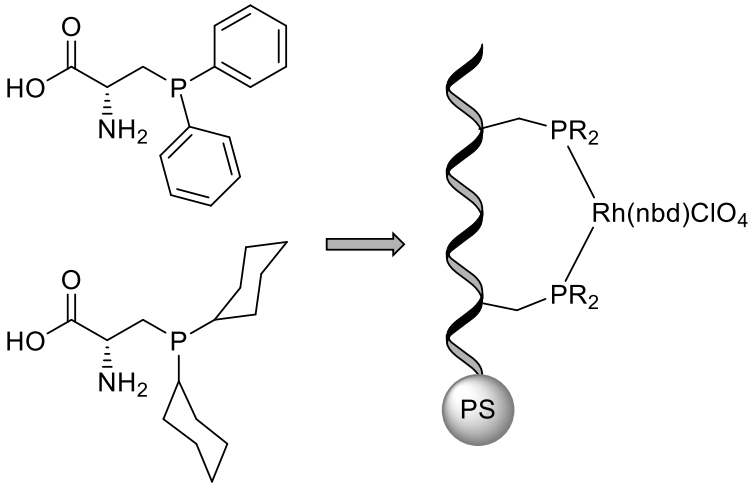

Figure 7 Amino acid-derived phosphines (left) and Rh-catalyst bound to peptide supported phosphinoserine amino acids (right).[74]

Subsequent screening of the supported ligand library in the Rh-catalyzed asymmetric hydrogenation of methyl 2-acetamidoacrylate resulted in low enantioselectivities but demonstrated the potential of screening phosphorus ligands libraries. In the following reports by the same group, the enantioselectivity was improved by second-generation peptide supported diphosphines.[75] A year later, the methodology could be extended to a library of 96 peptides based on a β-turn motive.

These were composed of nine amino acids, of which three positions were altered and two positions were kept constant for the metal binding phosphinoserine amino acids. When applied in the Pd-catalyzed asymmetric allylic alkylation of cyclopentenyl and cyclohexenyl acetate with dimethyl malonate, up to 80% *ee* were achieved.[76]

In 2001, Li and co-workers showcased the versatility of the SPS methodology by generating a library of 15 different bidentate phosphorus ligands. Starting from a *tert*-butylamine functionalized Merrifield resin, the chlorinated aminophosphine-phosphine synthon could be accessed by treatment with an excess of 1,2-bis(dichlorophosphanyl)ethane (Scheme 8, middle). Further modifications using a series of nucleophiles, such as organolithium reagents or alcoholates, led to a diverse library of bidentate ligands, which could be cleaved from the support via treatment with PCl_3.[77]

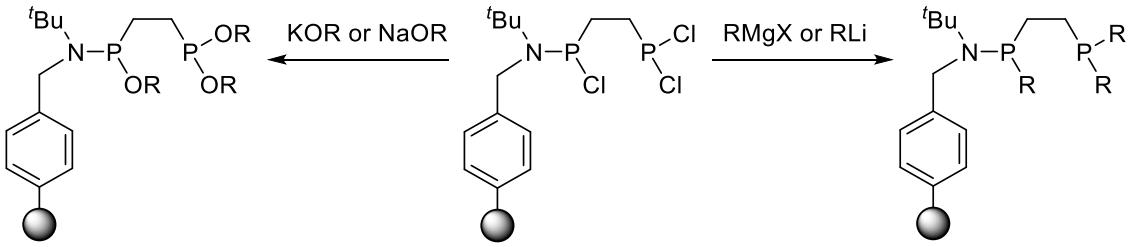

Scheme 8 SPS approach towards resin-bound bidentate phosphorus ligands by Li *et al*.[77]

Following a similar approach, Mansour and Portnoy developed a modular SPS protocol for the synthesis of 10 different supported bidentate aminophosphines-phosphine and phosphinite ligands starting from various resin-bound amino alcohols.[78] Subsequent ligand screening in the Pd-catalyzed Heck reaction of bromobenzene and methyl acrylate gave only low to moderate activities.

The parallel synthesis of a supported bidentate phosphorus ligand library featuring a *P*-stereogenic resin-bound phosphorus atom was demonstrated by the Kamer group in 2008.[31a] The resin-bound *P*-stereogenic aminophosphine moiety was introduced into the solid-phase synthesis by using a general synthetic route developed by Jugé *et al*. for solution-phase analogues (Scheme 9).[79] A series of oxazaphospholidine borane building blocks carrying various R^1 substituents were prepared by following synthetic routes described by Jugé *et al*.[80] (Route A) or by Xiao *et al*. (Route B).[81] Subsequent stereoselective ring-opening by reacting the heterocycles with lithiated 4-bromopolystyrene led to the formation of supported *P*-chiral hydroxyalkyl aminophosphine boranes.

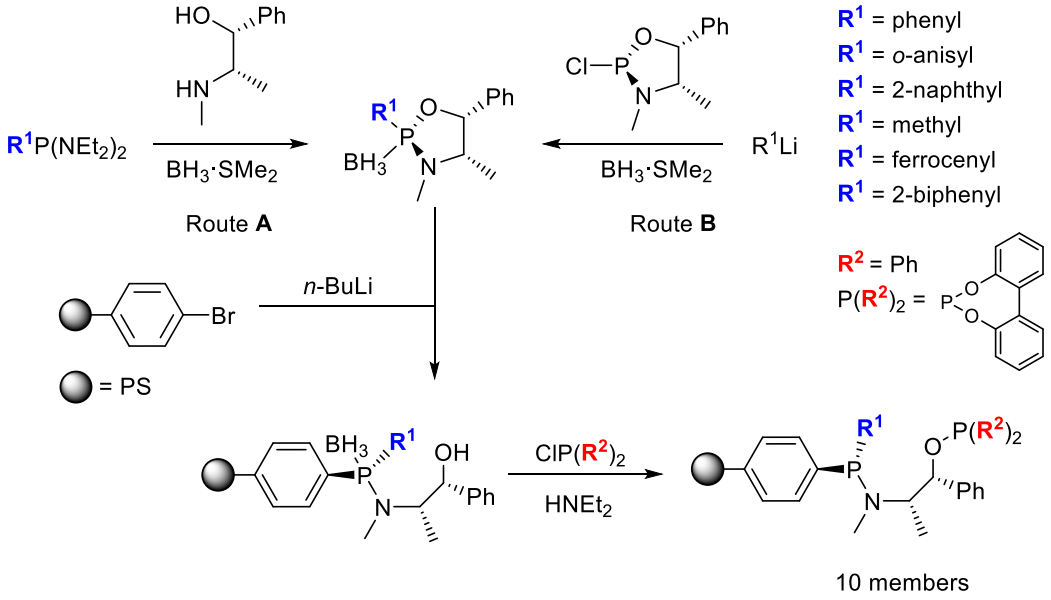

Scheme 9 SPS of supported aminophosphine-phosphite and -phosphinite ligand library.[31a]

Treatment with chlorophosphorus reagents followed by borane removal yielded six different supported chiral aminophosphine-phosphite and four aminophosphine-phosphinite ligands in high purity. Subsequent screening in Rh-catalyzed asymmetric hydrogenation of two benchmark enamides and dimethyl itaconate gave moderate to good *ee* of up to 89% in case of methyl α-acetamidoacrylate. A selected member of the supported library was compared to its homogeneous analogue showing 20% lower enantioselectivity (59% versus 79% *ee*). The general potential for catalyst recovery and recyclability of one of the aminophosphine-phosphite ligands was demonstrated in the asymmetric hydrogenation of methyl α-acetamidoacrylate. Over three consecutive reaction cycles, an activity loss of 13% together with an 8% drop in *ee* was observed. Nevertheless, these results clearly highlight the capability of a solid-phase synthetic methodology to create a diverse and reusable multidentate phosphorus ligand library for application in asymmetric catalysis.

More recently, the Kamer group reported on a facile SPS approach towards highly modular supported diphosphine ligands.[31b,31d] Starting from commercially available 4-bromopolystyrene crosslinked with DVB (PS), Merrifield (MF) and JandaJel™ (JJ) resins, a large and diverse resin-bound ligand library of 18 members was prepared in high purity and in quantitative yields (Scheme 10, Route A). Structural ligand diversity was readily introduced via systematic variation of three main building blocks as well as the nature of the polymeric support. Phosphine-bound substituents R^1 and R^3 could be varied by choosing a suitable primary and secondary lithium

phosphide. The chain length (l) of the chiral backbone and R^2 were altered via ring-opening of several cyclic sulfates. The supported library was screened in Rh-catalyzed asymmetric hydrogenation of three prochiral enamides showing high activities and enantioselectivities between 2% and 83%. In subsequent recycling experiments, a selected MF-bound diphosphine achieved constant conversion over six consecutive runs while a stable *ee* was obtained over eleven cycles. Moreover, the authors could demonstrate the applicability of these resin-bound diphosphines combined with several diamines in Ru-catalyzed ester hydrogenation under mild conditions.[82]

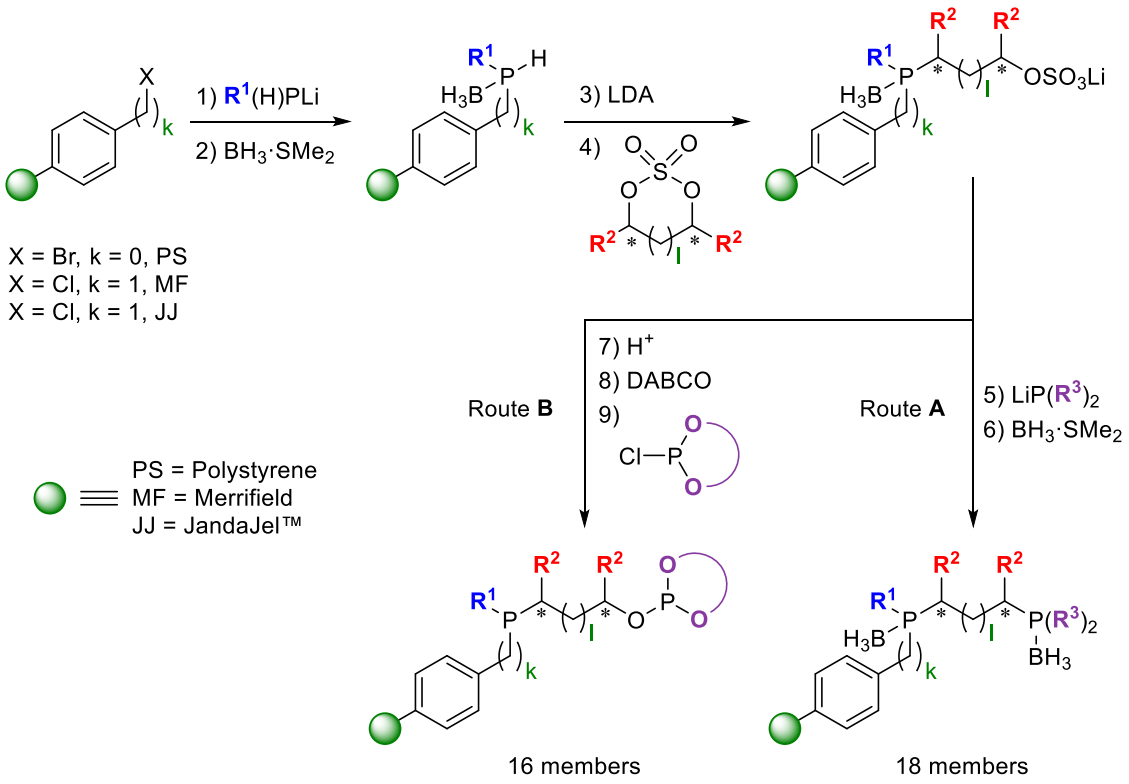

Scheme 10 Modular SPS of resin-bound diphosphine and phosphine-phosphite ligand libraries.

This versatility of the this SPS approach for immobilized bidentate phosphorus ligands was nicely shown by the Kamer group when the same sequence was adapted for the synthesis of resin-bound phosphine-phosphite (P-OP) ligands.[31c] Instead of treating the supported phosphine-borane sulfates with lithium phosphide reagents, as used in Route **A**, a hydrolysis step followed by reaction with a range of chlorophosphites led to a resin-bound P-OP ligand library of 16 members in high yield and purity (Scheme 10, Route **B**). The library was applied in Rh-catalyzed asymmetric hydrogenation of enamide benchmark substrates. With high activities and enantioselectivities of up to 98% *ee*, the supported P-OP ligands were able to compete

and in some cases even outperform their homogeneous analogues. This indicates that catalyst immobilization did not have a detrimental effect on the performance as observed for many heterogenized systems. Studies towards the recoverability reusability showed only a minor drop of activity (3%) over eleven consecutive runs together with no loss in enantioselectivity. About 1.3 ppm of leached Rh metal per run was detected by ICP-OES analysis of the liquid phases. These results underline the remarkable stability of these inherently sensitive types of ligands and their application in continuous flow processes would thus be the next logical step.

1.4 Project Aim

Encouraged by the recent progress in the field of catalyst immobilization addressing the inherent separation issue of homogeneous catalysts, the overall aim of this project is to find an efficient access to immobilized catalysts based on multidentate phosphorus ligands. Building on the success of a highly versatile solid-phase synthesis approach developed within the Kamer group, the focus of this project will be on both the diversification and extension of heterobidentate ligand libraries and the efficient access to novel (hetero)tridentate phosphorus ligands bound to a polymeric support.

Starting from one common synthon, namely a resin-bound secondary phosphine, it is possible to create a large supported phosphine-phosphite ligand library as described in chapter 2 (Scheme 11).

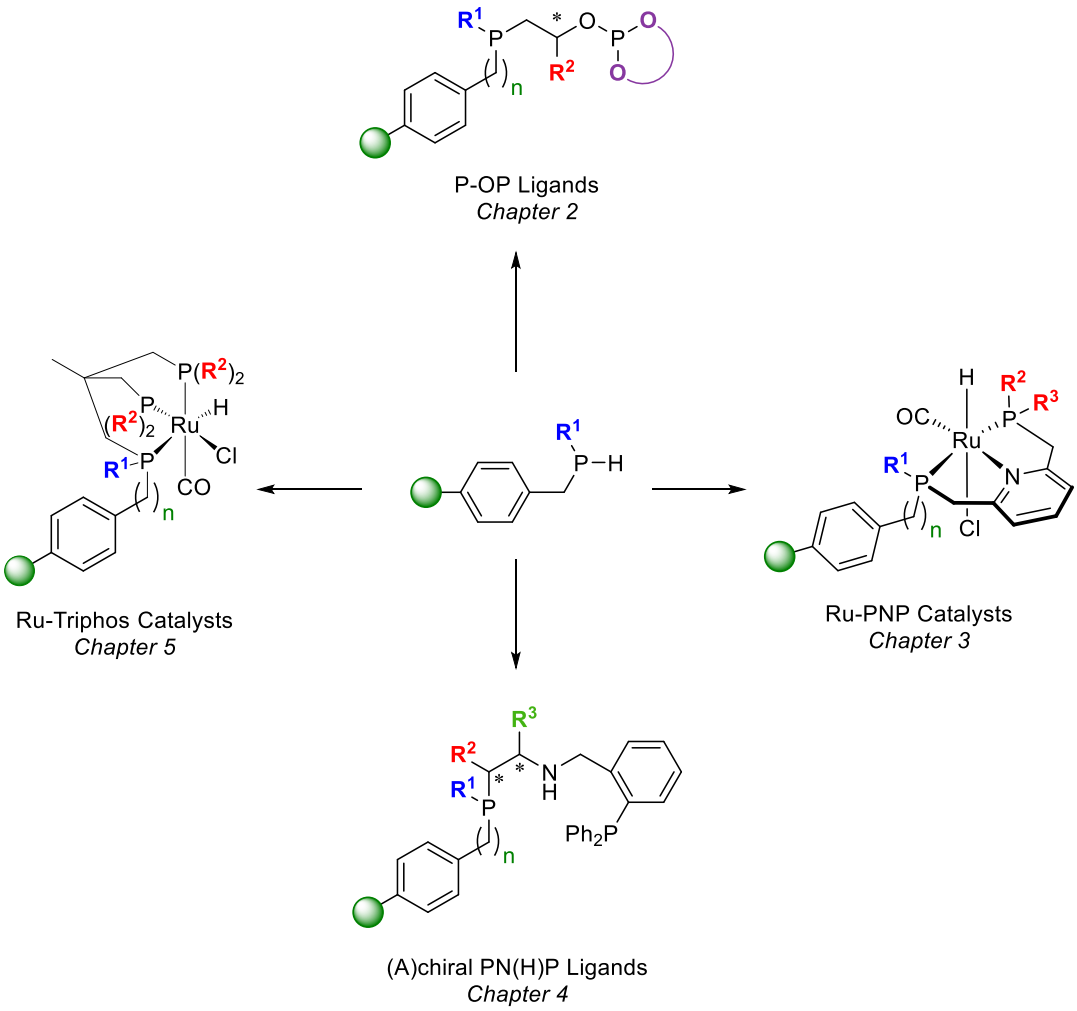

Scheme 11 Versatile SPS approach towards diverse multidentate phosphorus ligand and Ru-catalyst libraries.

The synthetic sequence encompasses a step-by-step ligand build-up on the support by using three main building blocks in a combinatorial manner. This in turn allows for subtle changes in ligand properties facilitating the fine-tuning of the corresponding catalysts for rapid screening in asymmetric catalysis.

The ligand class of PNP-pincer ligands has found widespread application in the field of homogeneous catalysis for a myriad of transformations. Although ample ligand motifs have been reported, synthetic protocols to efficiently tune the properties of both achiral and chiral PNP ligands remain elusive. In chapter 3, the solid-phase synthesis approach is extended towards a series of resin-bound pyridine-based PNP pincer ligands and their corresponding ruthenium complexes. Since this methodology offers a convenient route to introduce two phosphine moieties differing in the groups **R**^{1}, **R**^{2} and **R**^{3}, the effect of unsymmetrical substitution is examined in the catalytic hydrogenation of carboxylic esters. By using the advantages of the SPS tool to install ligand chirality, a novel modular route towards supported chiral PN(H)P ligands is investigated in chapter 4.

In both previous studies as well as in this work (chapter 2, 3 and 5), the benefits of having a ligand covalently anchored to a support have been demonstrated in terms of catalyst separation and recycling. Inevitably, the application in a continuously operated process represents the next logical step. Chapter 5 investigates the catalyst stability of a heterogeneous equivalent to the well-known tripodal Triphos ligand in the selective reduction of nitriles compounds under continuous flow conditions.

Eventually, the research presented in this thesis will contribute to the increasing need of large and diverse multidentate phosphorus ligand libraries for high-throughput experimentation. Moreover, it will showcase the suitability of resin-bound catalysts for efficient recycling in batch and continuously operated processes.

1.5 References

[1] P. C. J. Kamer, D. Vogt, J. W. Thybaut, *Contemporary Catalysis: Science, Technology, and Applications*, The Royal Society of Chemistry, **2017**.

[2] a) B. E. Leach, *Applied Industrial Catalysis*, Academic Press, **1983**; b) J. Hagen, *Industrial Catalysis: A Practical Approach*, Wiley-VCH Verlag GmbH & Co. KGaA, **2015**.

[3] O. Roelen, Chemische Verwertungsgesellschaft Oberhausen m.b.H, *DE 849.548*, **1938/1952**.

[4] a) P. W. N. M. van Leeuwen, *Homogeneous Catalysis: Understanding the Art*, Kluwer Academic Publishers, Dordrecht, The Netherlands, **2004**; b) B. Cornils, W. A. Herrmann, M. Beller, R. Paciallo, *Applied Homogeneous Catalysis with Organometallic Compounds*, 3 ed., Wiley-VCH, **2018**.

[5] W. S. Knowles, *Angew. Chem. Int. Ed.* **2002**, *41*, 1998-2007.

[6] R. Noyori, *Angew. Chem. Int. Ed.* **2002**, *41*, 2008-2022.

[7] K. B. Sharpless, *Angew. Chem. Int. Ed.* **2002**, *41*, 2024-2032.

[8] S. Bhaduri, D. Mukesh, *Hydroformylation*, in *Homogeneous Catalysis*, John Wiley & Sons, Inc., **2002**, pp. 85-103.

[9] S. Bhaduri, D. Mukesh, *Other Alkene-based Homogeneous Catalytic Reactions*, in *Homogeneous Catalysis*, John Wiley & Sons, Inc., **2002**, pp. 133-170.

[10] P. W. N. M. van Leeuwen, J. C. Chadwick, *Carbonylation Reactions*, in *Homogeneous Catalysts*, Wiley-VCH Verlag GmbH & Co. KGaA, **2011**, pp. 213-278.

[11] W. S. Knowles, *Asymmetric Hydrogenations – The Monsanto L-Dopa Process*, in *Asymmetric Catalysis on Industrial Scale* (Eds.: H.-U. Blaser, E. Schmidt), Wiley-VCH Verlag GmbH & Co. KGaA, Weinheim, **2004**, pp. 21-38.

[12] H.-U. Blaser, R. Hanreich, H.-D. Schneider, F. Spindler, B. Steinacher, *The Chiral Switch of Metolachlor: The Development of a Large-Scale Enantioselective Catalytic Process*, in *Asymmetric Catalysis on Industrial Scale* (Eds.: H.-U. Blaser, E. Schmidt), Wiley-VCH Verlag GmbH & Co. KGaA, Weinheim, **2004**, pp. 55-70.

[13] a) R. Noyori, *Science* **1990**, *248*, 1194-1199; b) R. Noyori, H. Takaya, *Acc. Chem. Res.* **1990**, *23*, 345-350.

[14] a) T. P. Yoon, E. N. Jacobsen, *Science* **2003**, *299*, 1691-1693; b) J. Wassenaar, J. N. H. Reek, *Org. Biomol. Chem.* **2011**, *9*, 1704-1713.

[15] P. E. Goudriaan, P. W. N. M. van Leeuwen, M. N. Birkholz, J. N. H. Reek, *Eur. J. Inorg. Chem.* **2008**, *2008*, 2939-2958.

[16] M. Renom-Carrasco, L. Lefort, *Chem. Soc. Rev.* **2018**, *47*, 5038-5060.

[17] a) C. Gennari, U. Piarulli, *Chem. Rev.* **2003**, *103*, 3071-3100; b) C. Jakel, R. Paciello, *Chem. Rev.* **2006**, *106*, 2912-2942.

[18] A. M. Porte, J. Reibenspies, K. Burgess, *J. Am. Chem. Soc.* **1998**, *120*, 9180-9187.

[19] a) P. W. N. M. van Leeuwen, J. C. Chadwick, *Homogeneous Catalysts*, Wiley-VCH Verlag GmbH & Co. KGaA, **2011**; b) M. C. Samuels, B. H. G. Swennenhuis, P. C. J. Kamer, *Solid-phase Synthesis of Ligands*, in *Phosphorus(III) Ligands in Homogeneous Catalysis: Design and Synthesis* (Eds.: P. C. J. Kamer, P. W. N. M. v. Leeuwen), John Wiley & Sons, Ltd, Chichester, **2012**, pp. 463-479; c) B. Zhang, H. Jiao, D. Michalik, S. Kloß, L. M. Deter, D. Selent, A. Spannenberg, R. Franke, A. Börner, *ACS Catal.* **2016**, *6*, 7554-7565.

[20] M. J. Johansson, S. Berglund, Y. Hu, K. H. O. Andersson, N. Kann, *ACS Combi. Sci.* **2012**, *14*, 304-308.

[21] a) D. J. Cole-Hamilton, *Science* **2003**, *299*, 1702-1706; b) D. J. Cole-Hamilton, R. P. Tooze, *Homogeneous Catalysis - Advantages and Problems*, in *Catalyst Separation, Recovery and Recycling: Chemistry and Process Design* (Eds.: D. J. Cole-Hamilton, R. P. Tooze), Springer Netherlands, Dordrecht, **2006**, pp. 1-8.

[22] a) A. Kirschning, G. Jas, *Top. Curr. Chem.* **2004**, *242*, 209-239; b) A. Kirschning, W. Solodenko, K. Mennecke, *Chem. Eur. J.* **2006**, *12*, 5972-5990; c) D. Cantillo, C. O. Kappe, *ChemCatChem* **2014**, *6*, 3286-3305.

[23] a) C. C. Russell, J. R. Baker, P. J. Cossar, A. McCluskey, *Recent Developments in the Use of Flow Hydrogenation in the Field of Medicinal Chemistry*, IntechOpen, **2017**, pp. 269-288; b) D. L. Hughes, *Org. Process Res. Dev.* **2018**, *22*, 13-20.

[24] a) M. Benaglia, *Recoverable and Recyclable Catalysts* John Wiley & Sons, Ltd, **2009**; b) P. Barbaro, F. Liguori, *Heterogenized Homogeneous Catalysts for Fine Chemicals Production, Vol. 33*, Springer, Dordrecht, **2010**; c) Q.-H. Fan, K. Ding, *Top. Organomet. Chem.* **2011**, *36*, 207-245; d) R. Šebesta, *Enantioselective Homogeneous Supported Catalysis*, The Royal Society of Chemistry, **2012**; e) R. Konrath, F. J. L. Heutz, P. C. J. Kamer, D. Vogt, *Catalyst Separation*, in *Contemporary Catalysis* (Eds.: P. C. J. Kamer, D. Vogt, J. W. Thybaut), The Royal Society of Chemistry, **2017**, pp. 711-747.

[25] a) B. Cornils, W. A. Herrmann, I. T. Horváth, W. Leitner, S. Mecking, H. Oliver-Bourbigou, D. Vogt, *Multiphase Homogeneous Catalysis, Vol. 1*, Wiley-VCH Verlag GmbH & Co. KGaA, Weinheim, **2005**; b) L. Xu, J. Xiao, *Asymmetric Catalysis in Ionic Liquids*, in *Recoverable and Recyclable Catalysts* (Ed.: M. Benaglia), John Wiley & Sons, Ltd, **2009**, pp. 259-300; c) S. L. Desset, D. J. Cole-Hamilton, *Biphasic Catalysis: Catalysis in Supercrtical CO_2 and in Water*, in *Recoverable and Recyclable Catalysts* (Ed.: M. Benaglia), John Wiley & Sons, Ltd, **2009**, pp. 199-258.

[26] a) N. E. Leadbeater, M. Marco, *Chem. Rev.* **2002**, *102*, 3217-3274; b) C. A. McNamara, M. J. Dixon, M. Bradley, *Chem. Rev.* **2002**, *102*, 3275-3300; c) C. E. Song, S.-g. Lee, *Chem. Rev.* **2002**, *102*, 3495-3524; d) J. N. H. Reek, P. W. N. M. van Leeuwen, A. G. J. van der Ham, A. B. de Haan, *Supported Catalysts*, in *Catalyst Separation, Recovery and Recycling: Chemistry and Process Design* (Eds.: D. J. Cole-Hamilton, R. P. Tooze), Springer Netherlands, Dordrecht, **2006**, pp. 39-69.

[27] J. M. Fraile, J. I. Garcia, C. I. Herrerias, J. A. Mayoral, E. Pires, *Non-covalent Immobilization*, in *Enantioselective Homogeneous Supported Catalysis* (Ed.: R. Šebesta), The Royal Society of Chemistry, **2012**, pp. 237-274.

[28] a) C. Müller, M. G. Nijkamp, D. Vogt, *Eur. J. Inorg. Chem.* **2005**, *2005*, 4011-4021; b) N. J. Ronde, D. Vogt, *Separation by Size-Exclusion Filtration*, in *Catalyst Separation, Recovery and Recycling: Chemistry and Process Design* (Eds.: D. J. Cole-Hamilton, R. P. Tooze), Springer Netherlands, Dordrecht, **2006**, pp. 73-102; c) M. Janssen, J. Wilting, C. Muller, D. Vogt, *Angew. Chem. Int. Ed.* **2010**, *49*, 7738-7741.

[29] S. Hübner, J. G. d. Vries, V. Farina, *Adv. Synth. Catal.* **2016**, *358*, 3-25.

[30] B. Altava, M. I. Burguete, E. Garcia-Verdugo, S. V. Luis, *Chem. Soc. Rev.* **2018**, *47*, 2722-2771.

[31] a) R. den Heeten, B. H. G. Swennenhuis, P. W. N. M. van Leeuwen, J. G. de Vries, P. C. J. Kamer, *Angew. Chem.* **2008**, *120*, 6704-6707; b) F. J. L. Heutz, M. C. Samuels, P. C. J. Kamer, *Catal. Sci. Technol.* **2015**, *5*, 3296-3301; c) F. J. Heutz, P. C. Kamer, *Dalton Trans.* **2016**, *45*, 2116-2123; d) M. C. Samuels, F. J. L. Heutz, A. Grabulosa, P. C. J. Kamer, *Top. Catal.* **2016**, *59*, 1793-1799.

[32] C. W. Kohlpaintner, *Hydroformylation - Industrial*, in *Encyclopedia of Catalysis*, John Wiley & Sons, Inc., **2002**.

[33] C. D. Frohning, C. W. Kohlpaintner, H.-W. Bohnen, *Hydroformylation (Oxo Synthesis, Roelen Reaction)*, in *Applied Homogeneous Catalysis with Organometallic Compounds, Vol. 1*, 2nd ed. (Eds.: B. Cornils, W. A. Herrmann), Wiley-VCH Verlag GmbH, Weinheim, **2002**, pp. 31-103.

[34] C. W. Kohlpaintner, R. W. Fischer, B. Cornils, *Appl. Catal. A* **2001**, *221*, 219-225.

[35] N. Yoshimura, *Telomerization (Hydrodimerization) of Olefines*, in *Applied Homogeneous Catalysis with Organometallic Compounds, Vol. 1*, 2nd ed. (Eds.: B. Cornils, W. A. Herrmann), Wiley-VCH Verlag GmbH, Weinheim, **2002**, pp. 361-367.

[36] K. Huthmacher, S. Krill, *Reactions with Hydrogen Cyanide (Hydrocyanation)*, in *Applied Homogeneous Catalysis with Organometallic Compounds* (Eds.: B. Cornils, W. A. Herrmann), Wiley-VCH Verlag GmbH, Weinheim, **2008**, pp. 468-490.

[37] D. E. Bergbreiter, *Thermomorphic Catalysts*, in *Recoverable and Recyclable Catalysts* (Ed.: M. Benaglia), John Wiley & Sons, Ltd, **2009**, pp. 117-154.

[38] a) P. Wasserscheid, M. Haumann, *Catalyst Recycling using Ionic Liquids*, in *Catalyst Separation, Recovery and Recycling: Chemistry and Process Design* (Eds.: D. J. Cole-Hamilton, R. P. Tooze), Springer Netherlands, Dordrecht, **2006**, pp. 183-214; b) C. M. Gordon, W. Leitner, *Supercritical Fluids*, in *Catalyst Separation, Recovery and Recycling: Chemistry and Process Design* (Eds.: D. J. Cole-Hamilton, R. P. Tooze), Springer Netherlands, Dordrecht, **2006**, pp. 215-236.

[39] M. Rimoldi, A. Nakamura, N. A. Vermeulen, J. J. Henkelis, A. K. Blackburn, J. T. Hupp, J. F. Stoddart, O. K. Farha, *Chem. Sci.* **2016**, *7*, 4980-4984.

[40] a) T. Chinnusamy, P. Hilgers, O. Reiser, *Catalysts Bound to Soluble Polymers*, in *Recoverable and Recyclable Catalysts* (Ed.: M. Benaglia), John Wiley & Sons, Ltd, **2009**, pp. 77-100; b) C. Jimeno, S. Sayalero, M. A. Pericàs, *Covalent Heterogenization of Asymmetric Catalysts on Polymers and Nanoparticles*, in *Heterogenized Homogeneous Catalysts for Fine Chemicals Production, Vol. 33* (Eds.: P. Barbaro, F. Liguori), Springer, Dordrecht, **2010**, pp. 123-170.

[41] N. Yoneda, S. Kusano, M. Yasui, P. Pujado, S. Wilcher, *Appl. Catal. A* **2001**, *221*, 253-265.

[42] B. Pugin, H.-U. Blaser, *Top. Catal.* **2010**, *53*, 953-962.

[43] R. B. Merrifield, *J. Am. Chem. Soc.* **1963**, *85*, 2149-2154.

[44] a) A. Akelah, D. C. Sherrington, *Chem. Rev.* **1981**, *81*, 557-587; b) J. Lu, P. H. Toy, *Chem. Rev.* **2009**, *109*, 815-838.

[45] G. Zhao, Z. Chai, *Insoluble Resin-supported Catalysts*, in *Recoverable and Recyclable Catalysts* (Ed.: M. Benaglia), John Wiley & Sons, Ltd, **2009**, pp. 49-76.

[46] S. E. Booth, C. M. Dreef-Tromp, P. H. H. Hermkens, J. A. P. A. de Man, H. C. J. Ottenheijm, *Survey of Solid-Phase Organic Reactions*, in *Combinatorial Chemistry* (Ed.: G. Jung), Wiley-VCH Verlag GmbH, Weinheim, **1999**, pp. 35-76.

[47] R. Quarrell, T. D. W. Claridge, G. W. Weaver, G. Lowe, *Mol. Divers.* **1996**, *1*, 223-232.

[48] T. E. Kristensen, T. Hansen, *Synthesis of Chiral Catalysts Supported on Organic Polymers*, in *Catalytic Methods in Asymmetric Synthesis* (Eds.: M. Gruttadauria, F. Giacalone), John Wiley & Sons, Inc., Hoboken, New Jersey, **2011**, pp. 209-256.

[49] T. Wang, Y. Lyu, K. Xiong, W. Wang, H. Zhang, Z. Zhan, Z. Jiang, Y. Ding, *Chin. J. Catal.* **2017**, *38*, 890-897.

[50] a) B. Li, R. Gong, W. Wang, X. Huang, W. Zhang, H. Li, C. Hu, B. Tan, *Macromolecules* **2011**, *44*, 2410-2414; b) B. Li, Z. Guan, W. Wang, X. Yang, J. Hu, B. Tan, T. Li, *Adv. Mater.* **2012**, *24*, 3390-3395; c) X. Wang, E. A. P. Ling, C. Guan, Q. Zhang, W. Wu, P. Liu, N. Zheng, D. Zhang, S. Lopatin, Z. Lai, K. W. Huang, *ChemSusChem* **2018**, *11*, 3591-3598.
[51] T. Wang, Y. Lyu, X. Chen, C. Li, M. Jiang, X. Song, Y. Ding, *RSC Adv.* **2016**, *6*, 28447-28450.
[52] L. Canali, E. Cowan, C. L. Gibson, D. C. Sherrington, H. Deleuze, *Chem. Commun.* **1998**, 2561-2562.
[53] D. E. Bergbreiter, S. D. Sung, *Adv. Synth. Catal.* **2006**, *348*, 1352-1366.
[54] B. G. Trewyn, H.-T. Chen, V. S. Y. Lin, *Surface-Functionalized Nanoporous Catalysts for Renewable Chemistry*, in *Recoverable and Recyclable Catalysts* (Ed.: M. Benaglia), John Wiley & Sons, Ltd, **2009**, pp. 15-47.
[55] L. M. Esteves, H. A. Oliveira, F. B. Passos, *J. Ind. Eng. Chem.* **2018**, *65*, 1-12.
[56] R. Augustine, S. Tanielyan, S. Anderson, H. Yang, *Chem. Commun.* **1999**, 1257-1258.
[57] A. J. Sandee, L. A. van der Veen, J. N. H. Reek, P. C. J. Kamer, M. Lutz, A. L. Spek, P. W. N. M. van Leeuwen, *Angew. Chem. Int. Ed.* **1999**, *38*, 3231-3235.
[58] a) C. Lesaint, B. Lebeau, C. Marichal, J. Patarin, *Microporous Mesoporous Mater.* **2005**, *83*, 76-84; b) M. Matheron, A. Bourgeois, T. Gacoin, A. Brunet-Bruneau, P. A. Albouy, J. P. Boilot, J. Biteau, P. Lacan, *Thin Solid Films* **2006**, *495*, 175-179.
[59] A. Stein, B. J. Melde, R. C. Schroden, *Adv. Mater.* **2000**, *12*, 1403-1419.
[60] a) F. M. Akwi, P. Watts, *Chem. Commun.* **2018**, *54*, 13894-13928; b) C. Wiles, P. Watts, *Eur. J. Org. Chem.* **2008**, *2008*, 1655-1671; c) S. V. Luis, E. Garcia-Verdugo, *Chemical Reactions and Processes under Flow Conditions*, RSC Green Chemistry, **2010**; d) J. Hartwig, J. B. Metternich, N. Nikbin, A. Kirschning, S. V. Ley, *Org. Biomol. Chem.* **2014**, *12*, 3611-3615; e) C. Wiles, P. Watts, *Green Chem.* **2014**, *16*, 55-62.
[61] a) P. Poechlauer, J. Colberg, E. Fisher, M. Jansen, M. D. Johnson, S. G. Koenig, M. Lawler, T. Laporte, J. Manley, B. Martin, A. O'Kearney-McMullan, *Org. Process Res. Dev.* **2013**, *17*, 1472-1478; b) B. Gutmann, D. Cantillo, C. O. Kappe, *Angew. Chem. Int. Ed.* **2015**, *54*, 6688-6728; c) S. K. Teoh, C. Rathi, P. Sharratt, *Org. Process Res. Dev.* **2016**, *20*, 414-431.
[62] Z. Amara, M. Poliakoff, R. Duque, D. Geier, G. Franciò, C. M. Gordon, R. E. Meadows, R. Woodward, W. Leitner, *Org. Process Res. Dev.* **2016**, *20*, 1321-1327.
[63] D. Macquarrie, *Fine Chemical Synthesis Through Heterogenized Catalysts: Scope, Challenges and Needs*, in *Heterogenized Homogeneous Catalysts for Fine Chemicals Production, Vol. 33* (Eds.: P. Barbaro, F. Liguori), Springer, Dordrecht, **2010**, pp. 1-36.
[64] a) C. G. Frost, L. Mutton, *Green Chem.* **2010**, *12*, 1687-1703; b) S. G. Newman, K. F. Jensen, *Green Chem.* **2013**, *15*, 1456-1472.
[65] I. Vural Gürsel, T. Noël, Q. Wang, V. Hessel, *Green Chem.* **2015**, *17*, 2012-2026.
[66] N. J. Meehan, A. J. Sandee, J. N. H. Reek, P. C. J. Kamer, P. W. N. M. van Leeuwen, M. Poliakoff, *Chem. Commun.* **2000**, 1497-1498.
[67] R. Duque, P. J. Pogorzelec, D. J. Cole-Hamilton, *Angew. Chem. Int. Ed.* **2013**, *52*, 9805-9807.
[68] a) C. Wandrey, E. Flaschel, K. Schügerl, *Chem. Ing. Tech.* **1977**, *49*, 257; b) U. Kragl, D. Gygax, O. Ghisalba, C. Wandrey, *Angew. Chem. Int. Ed.* **1991**, *30*, 827-828.
[69] D. K. B. Mohamed, X. Yu, J. Li, J. Wu, *Tetrahedron Lett.* **2016**, *57*, 3965-3977.

[70] D. Obrecht, J. M. Villalgordo, *Introduction, Basic Concepts and Strategies*, in *Solid-Supported Combinatorial and Parallel Synthesis of Small-Molecular-Weight Compound Libraries*, Elsevier Science ltd., Oxford, **1998**, pp. 1-184.
[71] F. J. L. Heutz, P. C. J. Kamer, *PhD Thesis* **2016**.
[72] N. Llorente, H. Fernández-Pérez, L. Núñez-Rico José, L. Carreras, A. Martínez-Carrión, E. Iniesta, A. Romero-Navarro, A. Martínez-Bascuñana, A. Vidal-Ferran, in *Pure Appl. Chem., Vol. 91*, **2019**, pp. 3-15.
[73] a) O. Huttenloch, E. Laxman, H. Waldmann, *Chem. Eur. J.* **2002**, *8*, 4767-4780; b) S. Doherty, E. G. Robins, I. Pál, C. R. Newman, C. Hardacre, D. Rooney, D. A. Mooney, *Tetrahedron: Asymmetry* **2003**, *14*, 1517-1527; c) A. Mandoli, M. Calamante, B. L. Feringa, P. Salvadori, *Tetrahedron: Asymmetry* **2003**, *14*, 3647-3650; d) W. Chen, S. M. Roberts, J. Whittall, *Tetrahedron Lett.* **2006**, *47*, 4263-4266; e) Z.-D. Jiang, Z.-H. Meng, *Chin. J. Chem.* **2007**, *25*, 542-545; f) B. H. Swennenhuis, R. Chen, P. W. van Leeuwen, J. G. de Vries, P. C. Kamer, *Org. Lett.* **2008**, *10*, 989-992; g) B. H. G. Swennenhuis, R. Chen, P. W. N. M. van Leeuwen, J. G. de Vries, P. C. J. Kamer, *Eur. J. Org. Chem.* **2009**, *2009*, 5796-5803.
[74] S. R. Gilbertson, X. Wang, *Tetrahedron Lett.* **1996**, *37*, 6475-6478.
[75] S. R. Gilbertson, X. Wang, *Tetrahedron* **1999**, *55*, 11609-11618.
[76] S. R. Gilbertson, S. E. Collibee, A. Agarkov, *J. Am. Chem. Soc.* **2000**, *122*, 6522-6523.
[77] G. Y. Li, P. J. Fagan, P. L. Watson, *Angew. Chem. Int. Ed.* **2001**, *40*, 1106-1109.
[78] A. Mansour, M. Portnoy, *Tetrahedron Lett.* **2003**, *44*, 2195-2198.
[79] a) D. Moulin, C. Darcel, S. Jugé, *Tetrahedron: Asymmetry* **1999**, *10*, 4729-4743; b) C. Darcel, D. Moulin, J.-C. Henry, M. Lagrelette, P. Richard, P. D. Harvey, S. Jugé, *Eur. J. Org. Chem.* **2007**, *2007*, 2078-2090.
[80] S. Juge, M. Stephan, J. A. Laffitte, J. P. Genet, *Tetrahedron Lett.* **1990**, *31*, 6357-6360.
[81] D. Vinci, N. Mateus, X. Wu, F. Hancock, A. Steiner, J. Xiao, *Org. Lett.* **2006**, *8*, 215-218.
[82] F. J. L. Heutz, C. Erken, M. J. B. Aguila, L. Lefort, P. C. J. Kamer, *ChemCatChem* **2016**, *8*, 1896-1900.

Chapter 2

Solid-Phase Synthesis of a Reusable Phosphine-Phosphite Ligand Library

Abstract: *Although homogeneous asymmetric catalysis offers a powerful key to access enantiomerically pure compounds, the development of highly selective catalysts remains challenging. Despite all advances, catalyst discovery still relies heavily on trial-and-error methodologies, which in turn calls for more efficient combinatorial protocols for ligand and catalyst library preparation. This chapter presents the facile access to highly modular hybrid phosphine-phosphite ligands in high purity by using a solid-phase synthetic approach requiring only minimal purification efforts. The large and diverse ligand library, containing 37 members immobilized on insoluble polymeric supports, provided excellent enantioselectivities of up to 99% in Rh-catalyzed hydrogenation of prochiral enamides. Moreover, preliminary data concerning the recoverability and recyclability of immobilized phosphine-phosphites under batch and continuous flow conditions showed high TONs and good stability.*

2.1 Introduction

Over the past decades, the increasing demand for enantiopure chemicals, such as flavors, fragrances, pharmaceuticals and agrochemicals, has led to the emergence of homogeneous asymmetric transition metal catalysis as an essential tool to fine chemical manufacturing (see chapter 1.1).[1] However, the discovery of highly active and selective catalysts remains a challenging task. In fact, only a small number of so-called privileged ligands (e.g. DIOP, BINAP and DUPHOS) based on chelating phosphorus-containing ligand scaffolds were found to be applicable in a wide range of relevant transformations.[2]

The C_2-symmetric ligand scaffold was associated with the beneficial restriction of the potential number of competing diastereomeric transition states in chiral transformations. However, the subsequent development of ligand structures occupying C_1-symmetry disproved the inherent superiority in enantioselectivity of C_2-symmetric ligands.[3] In fact, hybrid ligands bearing two donor moieties differing in electronic properties have demonstrated enhanced enantiocontrol opposed to C_2-symmetric ligands due to electronic effects such as the *trans* influence limiting potential competing reaction pathways.[4] Consequently, this has led to the development of a myriad of bidentate mixed-donor ligands either involving a second heteroatom (e.g. PN, PS and PO ligands) or two inequivalent phosphorus donor groups as in phosphine-phosphoramidites or phosphine-phosph(in)ites.[5] In particular phosphine-phosphites (P-OP), carrying an electron donating phosphine unit combined with a strong phosphite π-acceptor, have attracted tremendous attention in recent years. Since the pioneering works of Takaya and Nozaki introducing the BINAPHOS ligand (**I**)[6] as well as Pringle's P-OP ligand **II**[7] for application in asymmetric catalysis (Figure 1), a plethora of phosphine-phosphite ligand motifs has showcased high performances in various asymmetric transformations.[8] Widespread applicability was demonstrated in asymmetric hydrogenation reactions of functionalized alkenes and imines but also in hydroformylation, allylic alkylation, hydroboration and hydrophosphorylation.

The emergence of a vast number of P-OP-type ligands can be attributed to the intrinsic modular ligand nature. Ample diversification strategies targeting the (a)chiral phosphine unit as well as the more flexible phosphite group often based on axial chiral biaryl or *C*-chiral TADDOL derived backbones have been established.[8-9] Additional stereogenic centers could be introduced via the linker between phosphine and phosphite using sources from the chiral pool such as carbohydrates[10] but also via ring-opening of chiral oxiranes and cyclic sulfates.[11]

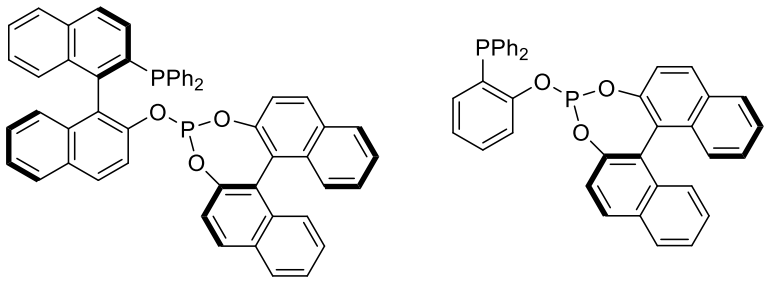

(*R*,*S*)-BINAPHOS (**I**) **II**

Figure 1 (*R*,*S*)-BINAPHOS by Takaya and Nozaki[6] and P-OP ligand **II** by Pringle.[7]

In terms of ligand discovery the modular scaffold of P-OP-type ligands makes them promising candidates for the combinatorial synthesis and high-throughput automated screening of ligand libraries.[4c,12] This in turn allows for efficient fine-tuning of ligand properties as subtle changes in ligand structure can have a profound impact on the enantioselectivity.[13] In order to access broad P-OP ligand libraries for combinatorial processes, the development of efficient modular synthetic approaches is required. The groups of Pizzano[12a,14] and Schmalz[13] reported on a modular ligand design based on the structural motif **III**, which provides an (un)functionalized aryl or an ethane C_2-carbon bridge in addition to various phosphine and phosphite building blocks (Figure 2). When van Leeuwen and co-workers employed chiral epoxides, up to three stereogenic centers could be systematically installed in the ligand structure **IV**, which are localized at the *P*-stereogenic phosphine, the C_2-C_3 carbon linker and in the phosphite moiety.[11a-c] Similar to that, the group of Vidal-Ferran utilized Sharpless epoxy ethers to create a small ligand library of **V**.[11d,15] However, implementation in combinatorial processes is hampered by the intrinsically more complicated synthesis of these highly air and moisture sensitive types of ligands often requiring arduous and low yielding purification procedures.

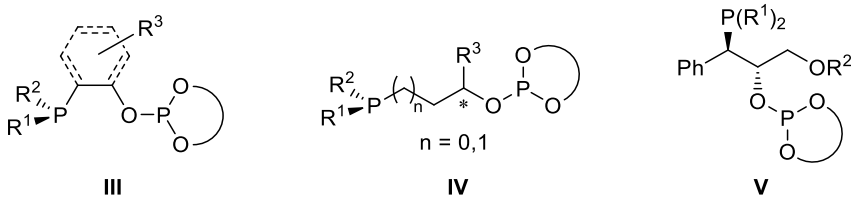

Figure 2 Representative ligand motifs for modular approaches towards P-OP ligand libraries.

Solid-phase synthesis (SPS) can provide an alternative approach towards the parallel synthesis of hybrid phosphine-phosphite ligand libraries, as outlined in chapter

1.3. This enables the access towards highly diverse ligand libraries by preparing ligand structures in a combinatorial fashion while being bound to a resin bead throughout the synthesis. In contrast to conventional solution-phase synthesis, SPS offers the advantage of simplified workup procedures by employing easy filtration or decantation steps which in turn allows the use of excess reagents to achieve quantitative conversions.[16] Consequently, this methodology can be a suitable approach for automated ligand synthesis and subsequent high-throughput screening in various catalytic transformations. Despite the advantages of solid-phase synthetic strategies towards the synthesis of hybrid ligand libraries, examples remain limited to aminophosphines-phosphite and -phosphinite as well as phosphine-phosphite ligand libraries reported by the Kamer group.[17] In the latter case, a supported P-OP ligand library of 16 members was efficiently prepared using a modular SPS approach. Various chiral cyclic sulfates providing two *C*-stereogenic centers in the C3 or C4 carbon linkers were employed in addition to axial chiral biaryl moieties in the phosphite backbones (**VI**, Figure 3) Moreover, the successful application of the supported library in Rh-catalyzed hydrogenation of enamides was demonstrated achieving up to 98% *ee*.

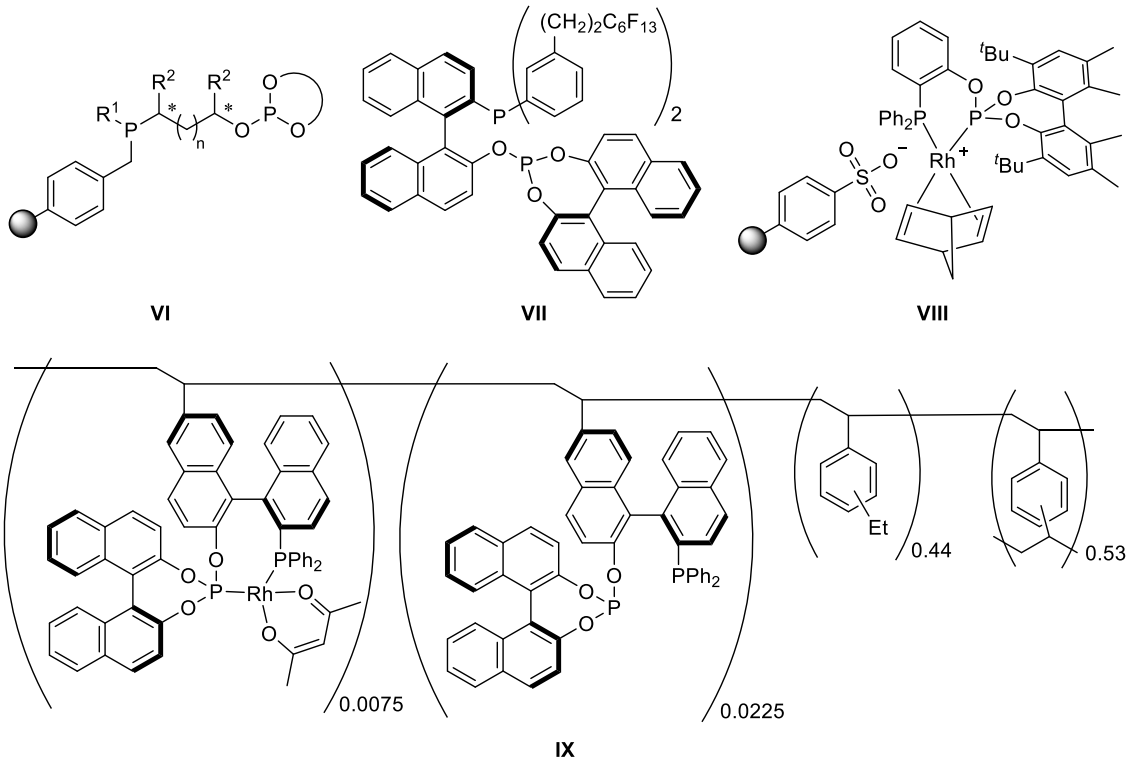

Figure 3 Representative examples of heterogenized P-OP ligands.

Having the homogeneous catalyst covalently bound to a solid support can be highly beneficial in terms of catalyst recovery and reusability as catalyst separation remains one of the major problems in applied homogenous catalysis.[18] In case of polymer-bound P-OP ligands **VI** facile catalyst separation from the product phase as well as recycling of up to 8 times with only a minor drop in activity was demonstrated.[17b] However, most attempts towards immobilization of P-OP-type ligands rely on inefficient post-modification strategies. This often requires cumbersome and non-modular syntheses of ligands modified with specific groups for subsequent immobilization in a multiphasic system or anchoring to an insoluble support. The group of Leitner, for example, designed a perfluoroalkylated BINAPHOS derivative (**VII**, Figure 3) enabling sufficient solubility of the corresponding Rh-complex in supercritical CO_2 for application in biphasic asymmetric hydrogenation.[19] In 2015, Kleman *et al.* reported on Rh-phosphine-phosphite catalyst **VIII** bound to a sulfonated polystyrene through ionic interactions, which was applied in the asymmetric hydrogenation of alkenes in aqueous medium.[20] Despite achieving high enantioselectivities severe loss in activity was encountered when employed in recycling experiments. Finally, BINAPHOS was immobilized on polystyrene by Nozaki *et al.* following a bottom-up approach.[21] This involved the ligand being modified with vinyl groups and subsequently incorporated via co-polymerization with ethylstyrene and divinylbenzene followed by complexation with $Rh(acac)(CO)_2$ (**IX**, Figure 3).

The potential for application under continuous flow conditions represents another advantage of a heterogenized homogeneous catalyst. Although continuously operated processes offer a more economical and less dangerous alternative for multiphasic hydrogenation reactions as opposed to batch processes,[22] reports on phosphine-phosphite ligands employed in flow remain scarce.[23]

This chapter presents a highly efficient solid-phase synthetic protocol providing access to a large and diverse heterobidentate ligand library of supported phosphine-phosphites. This combinatorial synthetic approach via regioselective ring-opening of chiral epoxides provides fast access to a large library of P-OP ligands bearing a chiral C2 backbone. The great potential of such a large and recyclable ligand library for screening in Rh-catalyzed asymmetric hydrogenation of alkenes as well as the applicability under continuous flow conditions is demonstrated.

2.2 Solid-Phase Synthesis of a Supported Phosphine-Phosphite Ligands

In the last two decades, various vicinal phosphine-phosphite (P-OP) ligands have been synthesized in solution-phase employing regioselective ring-opening of chiral epoxide building blocks (see Figure 4 for representative examples **X-XIII**).[11b,11d-f] However, despite the modular nature of hybrid P-OP ligands, efficient modular protocols remain scarce (see chapter 2.1). In this work, the rapid and highly modular synthesis of a large P-OP ligand library of 37 members via a solid-phase synthetic methodology is shown. The library was obtained via systematic variation of four different building blocks throughout the combinatorial synthesis allowing for efficient fine-tuning of ligand properties. The general ligand structure bound to the support is depicted in Figure 4 (**L_1-L_{37}**). While the resin-bound phosphine moiety could be readily altered by employing different **R^1** substituents, chiral **R^2** groups were introduced into the C2 ligand backbone structure by choosing a suitable chiral epoxide. Moreover, enhanced diversity could be created by employing a series of phosphites (**–OP**) as well as by changing the type of polymeric support from Merrifield (**MF**) crosslinked with 1% divinylbenzene to polystyrene (**PS**).

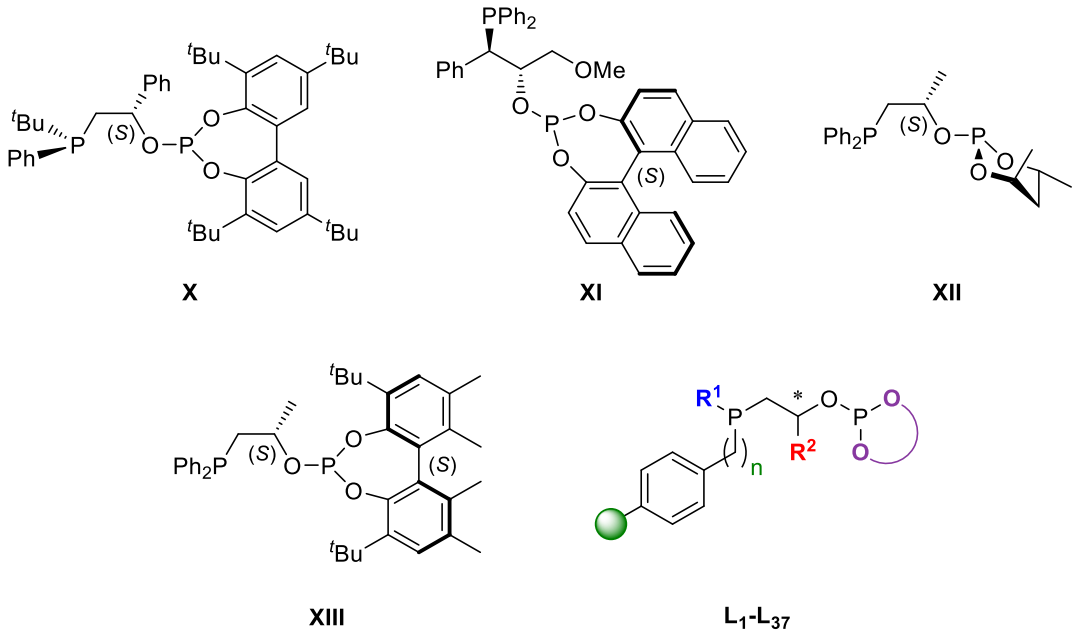

Figure 4 Representative examples of vicinal P-OP ligands reported by the groups of van Leeuwen (**X**),[11b] Vidal-Ferran (**XI**),[11d] Bakos (**XII**)[11f] and Pizzano (**XIII**)[11e] and the general structure of supported P-OP ligands **L_1-L_{37}**.

2.2.1 Synthesis of Resin-Bound β-Hydoxyalkyl Phosphines

In analogy to the reported solid-phase synthesis of phosphine-phosphite ligands bearing C3 and C4 ligand backbones,[17b] the modular sequence for vicinal P-OP ligands starts with resin-bound secondary phosphines **1a-d**, which were prepared according to literature procedures.[24] Diversity was readily introduced using a phenyl or a cyclohexyl substituent attached to the phosphorus atom, which is immobilized on Merrifield support crosslinked with either 1% (**1a** and **1c**) or 4% divinylbenzene (**1b**). In addition, a more bulky *tert*-butyl phosphine bound to polystyrene support (**1d**) was used as a synthon. Next, the resin-bound phosphines **1a-d** were deprotonated using an excess (10 equiv.) of lithium diisopropylamide (LDA) at room temperature, which resulted in dark orange colored resins (Scheme 1, step 1).

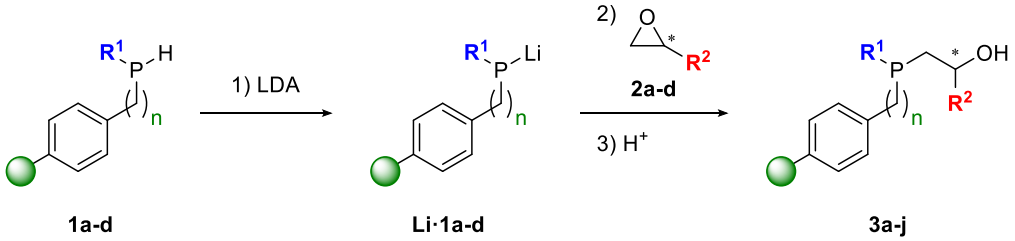

1a-d **Li·1a-d** **3a-j**

1a: MF, n = 1, R^1 = Ph
1b: MF 4%, n = 1, R^1 = Ph
1c: MF, n = 1, R^1 = Cy
1d: PS, n = 0, R^1 = ^{t}Bu

2a: R^2 = Me (S_C)
2b: R^2 = Me (R_C)
2c: R^2 = Et (S_C)
2d: R^2 = Et (R_C)

3a: MF, R^1 = Ph, R^2 = Me (S_C)
3b: MF 4%, R^1 = Ph, R^2 = Me (S_C)
3c: MF, R^1 = Ph, R^2 = Me (R_C)
3d: MF, R^1 = Ph, R^2 = Et (S_C)
3e: MF, R^1 = Ph, R^2 = Et (R_C)
3f: MF, R^1 = Cy, R^2 = Me (S_C)
3g: MF, R^1 = Cy, R^2 = Me (R_C)
3h: MF, R^1 = Cy, R^2 = Et (S_C)
3i: MF, R^1 = Cy, R^2 = Et (R_C)
3j: PS, R^1 = ^{t}Bu, R^2 = Me (S_C)

Scheme 1 Solid-phase synthetic approach towards supported chiral phosphino alcohols **3a-j**.

LDA was preferred over *n*-BuLi as lithiation agent due to competing deprotonation of the benzylic position observed for *n*-BuLi causing the formation of by-products in subsequent treatment with electrophiles. The reaction progress was conveniently monitored by gel-phase ^{31}P NMR revealing quantitative phosphine lithiation after two hours. For **Li·1a** and **Li·1b** very broad signals at δ = -39.5 ppm were detected whereas significant peak shifts for **Li·1c** (δ = -21.2 ppm) and **Li·1d** (δ = 4.3 ppm) were observed.

In the following reaction step, a series of β-phosphino alcohols **3a-j** bearing a single *C*-chiral center was accessed via ring-opening of chiral epoxides **2a-d** followed by hydrolysis of the corresponding lithium alkoxides (Scheme 1, steps 2 and 3). The S_N2 reaction proceeds by a nucleophilic attack of the resin-bound lithium phosphides **Li·1a-d** at the less sterically hindered carbon atom of the respective propylene or butylene oxide. Upon epoxide addition at room temperature a color change of the resin from dark orange to light orange was observed. Unfortunately, following the reaction by ^{31}P and ^{7}Li-NMR proved to be impossible due to significant peak broadening of the respective resin-bound lithium alkoxides. After the subsequent hydrolysis step using a 1:1 mixture of THF:H_2O, quantitative conversion towards the desired β-phosphino alcohols **3a-j** was confirmed by ^{31}P NMR. In the corresponding spectra, the light yellow resins **3a-e** exhibit broad resonances in the range from δ = -18.4 to -26.0 ppm appearing as two narrow peaks in a 1:1 ratio, which can be attributed to the presence of the two resin-bound phosphine epimers (see Figure 5 for spectrum of **3d**).[17b] The chemical shifts are in agreement with solution-phase analogues reported by the Pizzano and co-workers.[11e]

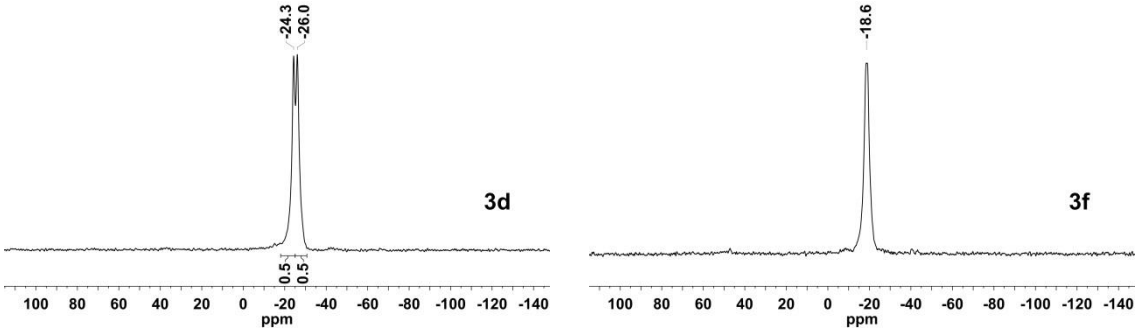

Figure 5 Gel-phase ^{31}P NMR spectra of supported phosphino alcohols **3d** (left) and **3f** (right).

In case of cyclohexyl substituted phosphino alcohols **3f-l** a significant downfield shift of $\Delta\delta$ = 22 ppm compared to the supported secondary phosphine **1c** was observed showing signals at δ = -17.4 to -19.7 ppm (see Figure 5 for spectrum of **3f**). Opposed to the phenyl substituted analogues, only **3h** showed two peaks associated with different stereoisomers whereas **3f-g** and **3i** revealed a single broad resonance, probably due to overlap of the epimer signals. Similar to that, a single peak at δ = -5.6 ppm was observed for the ^{t}Bu substituted derivative **3j**.

In order to confirm the regioselective ring-opening of propylene and butylene oxide and hence the unambiguous installation of the *C*-chiral center in the β-position to

the phosphorus atom, the corresponding supported phosphino alcohol **5** was prepared carrying an (*S*)-methyl group in α-position. After deprotonation of secondary phosphine **1a** using an excess of LDA as described previously, the lithiated species was treated with (*R*)-1-((*tert*-butyldimethylsilyl)oxy)propan-2-yl methanesulfonate (1.5 equiv.) resulting in the quantitative formation of the silyl ether protected phosphine **4** with full inversion of the stereo center (Scheme 2, steps 1 and 2).

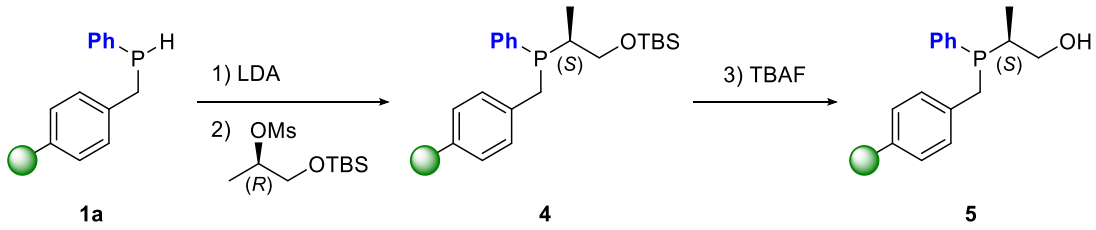

Scheme 2 Solid-phase synthesis of chiral phosphino alcohol **5**.

In the corresponding ^{31}P NMR spectrum, a single broad peak at δ = -10.2 ppm was observed for **4** accompanied by a minor signal of a species at δ = -24.4 ppm, which could be assigned to the β-substituted regioisomers **3a** or **3c** due to potential loss of the *tert*-butyldimethylsilyl (TBS) group. Subsequently, the TBS group was removed by using an excess of TBAF leading to the desired α-methylated resin-bound phosphino alcohol **5** (Scheme 2, step 3). Upon deprotection, again a splitting of the corresponding ^{31}P NMR peak at δ = -5.6 and -8.2 ppm occurred caused by the presence of a 1:1 mixture of epimers at the phosphine group while the resonance of the impurity remained unchanged. However, the chemical shift of the α-substituted phosphino alcohol **5** on support is in agreement with those observed for homogeneous counterparts, which in turn indicates full regioselectivity in the ring-opening of alkyl-substituted epoxides.[11e]

Building on the successful incorporation of chiral methyl and ethyl substituents in β-position of the ligand backbone, it was intended to apply this strategy to aromatic substituents by using styrene oxide. In previous attempts within the Kamer group, (*S*)-styrene oxide was employed in the solid-phase synthesis of *P*-chiral phosphine phosphinites on polystyrene support (Scheme 3).[25] However, lithiation of the resin-bound borane protected phosphine followed by epoxide ring-opening and subsequent *O*-phosphorylation with chlorodiphenylphosphine led to a mixture of α- and β-substituted regioisomers due to unselective S_N2 attack.

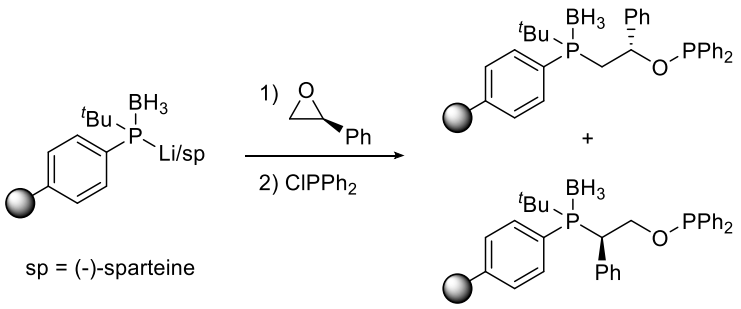

Scheme 3 Attempted synthesis of chiral PS-supported phosphine-phosphites by M. Samuels.[25]

It was decided to investigate the regioselectivity of the styrene oxide ring-opening reaction in Merrifield-based systems. Therefore, MF-resin-bound borane-protected secondary phosphine **1a·BH$_3$** bearing a phenyl substituent was lithiated with LDA to form **Li·1a·BH$_3$** analogous to the procedure described for **Li·1a** (Scheme 4, step 1). Subsequently, the lithiated phosphine was treated with a slight excess of (*S*)-styrene oxide at room temperature leading to an instant resin color change from dark orange to light yellow. Upon hydrolysis a single resonance emerged at δ = 15.6 ppm belonging to the desired β-substituted resin-bound phosphino alcohol **3k** accompanied by a minor set of two signals in a 1:1 ratio at δ = 23.2 and 20.6 ppm (Figure 6, left spectrum). The latter species can be attributed to a mixture of epimers of the α-substituted regioisomer **3l**, which is present in a ratio of 1:3 with respect to **3k**.

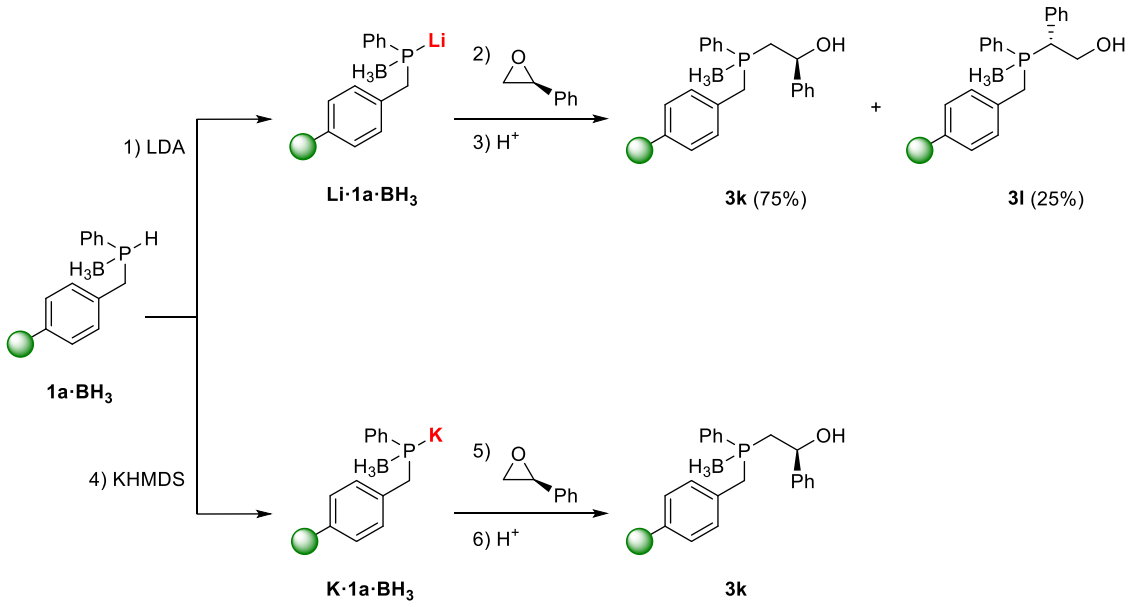

Scheme 4 Synthetic attempts towards regioselective ring-opening of (*S*)-styrene oxide.

This outcome is in line with the unselective ring-opening of styrene oxide observed for PS-supported systems. Similar regioselectivity issues were encountered in solution-phase systems. In the reaction of lithium diphenylphosphide with styrene oxide a regioisomeric mixture comprising α:β substitution in a 3:7 ratio was obtained.[26] Early studies on the impact of basicity in ring-opening of epoxides indicated that an increase in basicity results in decreasing attack of the secondary carbon center of styrene oxide.[27]

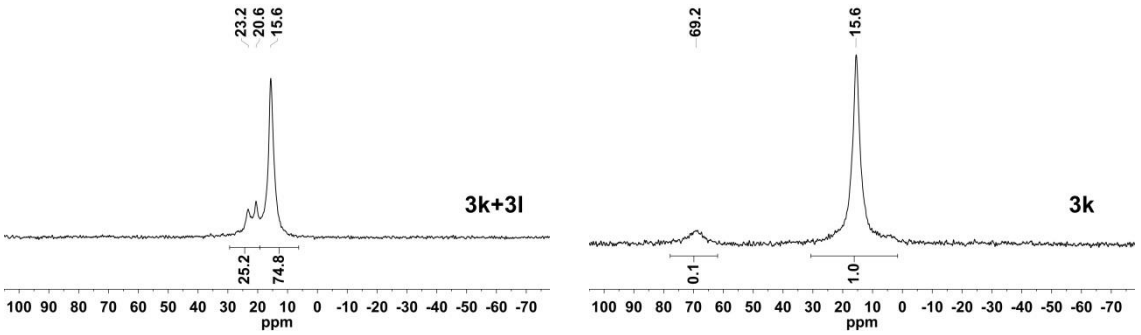

Figure 6 Gel-phase ^{31}P NMR spectra of a regioisomeric mixture of **3k** and **3l** (left) and selective formation of **3k** (right).

Consequently, LDA was exchanged for potassium bis(trimethylsilyl)amide (KHMDS) for the deprotonation of **1a·BH$_3$** to obtain the corresponding BH_3-protected potassium phosphide **K·1a·BH$_3$** as a bright orange resin (Scheme 4, step 4). Subsequent addition of (*S*)-styrene oxide followed by hydrolysis led to the regioselective formation of the supported β-substituted phosphino alcohol **3k** confirmed by a single resonance at δ = 15.6 ppm in the ^{31}P NMR spectrum (Figure 6, right spectrum). A similar improvement in the regioselectivity when changing from lithium to potassium phosphides has been reported by Vidal-Ferran and co-workers.[28] Despite the achievement of full selectivity when using a supported potassium phosphide, the appearance of a minor resin-bound impurity exhibiting a chemical shift of δ = 69.2 ppm was detected. This phosphorus species was exclusively observed when reacting phenyl- and cyclohexyl-substituted resin-bound potassium phosphides with styrene oxide whereas no by-product formation occurred in case of propylene oxide. Upon borane removal via treatment with 1,4-diazabicyclo[2.2.2]octane (DABCO) at 50 °C no change in chemical shift was observed for the by-product. Since further reaction optimization is required to avoid the by-product formation, **3k** was not used in the following reactions.

2.2.2 *O*-Phosphorylation of Resin-Bound Phosphino Alcohols

Prior to the synthesis of the target resin-bound phosphine-phosphite ligands via *O*-phosphorylation of the chiral phosphino alcohol intermediates, the preparation of a corresponding phosphine-phosphinite was attempted to evaluate the suitability of this reaction step. Hence, supported P–OH **3c** was treated with a slight excess of chlorodiphenylphosphine under basic conditions affording the desired resin-bound phosphine-phosphinite **6** as a pale yellow resin (Scheme 5).

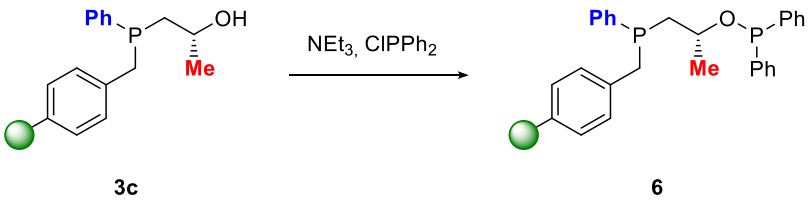

Scheme 5 Solid-phase synthesis of resin-bound phosphine-phosphinite **6**.

Quantitative incorporation of the remote phosphorus moiety could be confirmed by ^{31}P NMR showing the appearance of a second signal in the phosphinite region at δ = 105.4 ppm in a 1:1 ratio with the peak corresponding to the resin-bound phosphine moiety (Figure 7). Upon separation of the resin from the supernatant solution by filtration, several washing cycles with DCM facilitated the removal of extensive amounts of ammonium salts formed during the reaction followed by washing with THF and diethyl ether.

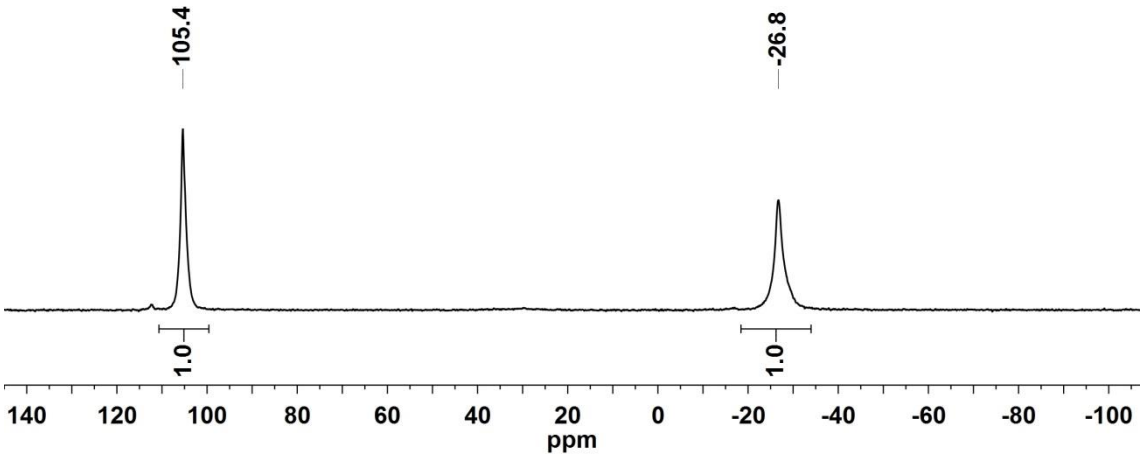

Figure 7 Gel-phase ^{31}P NMR spectrum of supported phosphine-phosphinite **6**.

On the basis of the successful *O*-phosphorylation reaction to access phosphine-phosphinites on a polymeric support, an analogous procedure was employed to

synthesize a resin-bound library of phosphine-phosphite ligands (P-OP). Accordingly, the series of supported phosphino alcohols **3a-j** was treated with 2-3 equivalents of a respective chlorophosphite **7a-f** at 0 °C in THF and in the presence of triethylamine (Scheme 6).

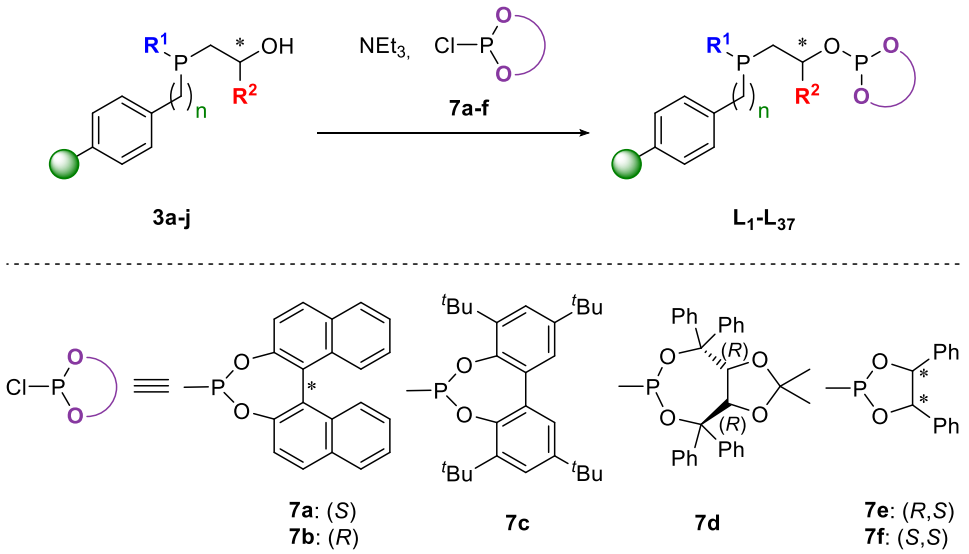

Scheme 6 Solid-phase synthesis of resin-bound phosphine-phosphite ligands $\mathbf{L_1}$-$\mathbf{L_{37}}$.

A variety of different -OP moieties was introduced ranging from (*R*)- and (*S*)-BINOL-derived chlorophosphites (**7a** and **7b**), which provide additional axial chirality to the overall ligand structure, to an achiral but sterically more demanding *tert*-butyl-functionalized bisphenol group (**7c**). Furthermore, two additional chiral chlorophosphites were employed, namely a (*R*,*R*)-TADDOL-derived moiety (**7d**) as well as simplified hydrobenzoin-based groups with both (*R*,*S*)- and (*S*,*S*)-configuration at the five-membered ring (**7e** and **7f**). Systematic variation of supported P–OH and -OP building blocks enabled rapid access to a large library of 37 different P-OP ligands bound to two types of polymeric supports, which underlines the power of solid-phase synthesis as a valuable synthetic tool for combinatorial ligand preparation. In case of **3b** supported on MF crosslinked with 4% DVB, substantial side-product formation occurred, which could be attributed to the reaction of the chlorophosphite with free OH groups present on the support. For the majority of the library members, high yields and purity were confirmed by ^{31}P NMR and FT-IR spectroscopy and the actual phosphorus loading for representative ligands $\mathbf{L_{13}}$ and $\mathbf{L_{20}}$ was determined by elemental analysis. The entire modular library of supported P-OP ligands is depicted in Figure 8.

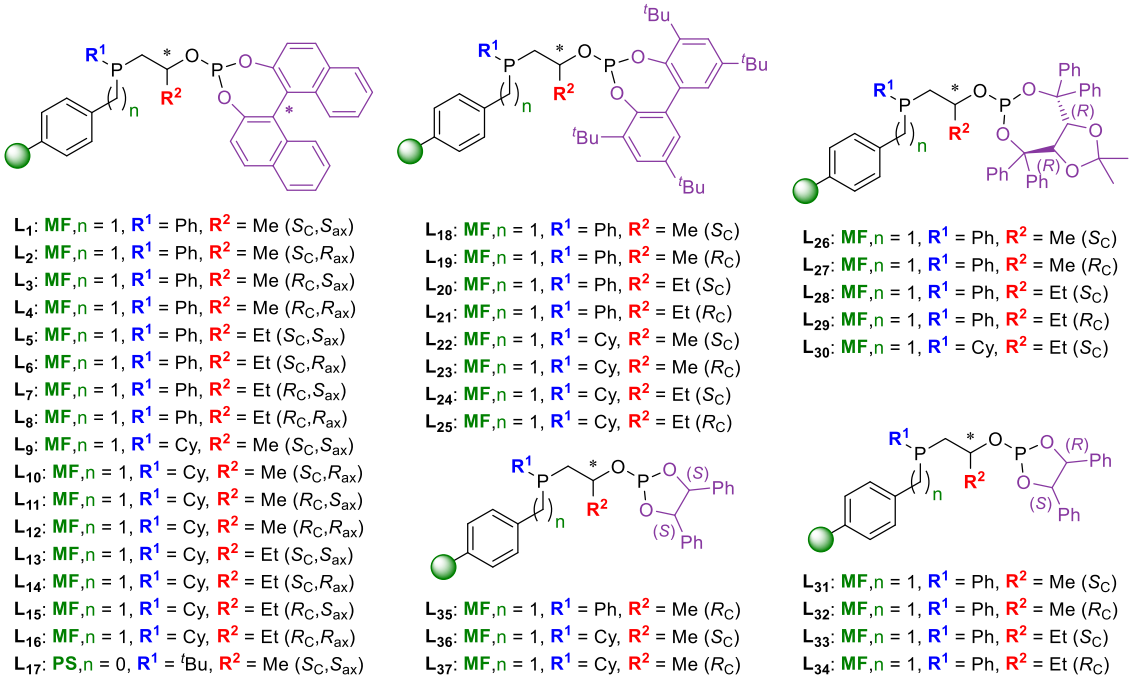

L_1: MF,n = 1, R^1 = Ph, R^2 = Me (S_C,S_{ax})
L_2: MF,n = 1, R^1 = Ph, R^2 = Me (S_C,R_{ax})
L_3: MF,n = 1, R^1 = Ph, R^2 = Me (R_C,S_{ax})
L_4: MF,n = 1, R^1 = Ph, R^2 = Me (R_C,R_{ax})
L_5: MF,n = 1, R^1 = Ph, R^2 = Et (S_C,S_{ax})
L_6: MF,n = 1, R^1 = Ph, R^2 = Et (S_C,R_{ax})
L_7: MF,n = 1, R^1 = Ph, R^2 = Et (R_C,S_{ax})
L_8: MF,n = 1, R^1 = Ph, R^2 = Et (R_C,R_{ax})
L_9: MF,n = 1, R^1 = Cy, R^2 = Me (S_C,S_{ax})
L_{10}: MF,n = 1, R^1 = Cy, R^2 = Me (S_C,R_{ax})
L_{11}: MF,n = 1, R^1 = Cy, R^2 = Me (R_C,S_{ax})
L_{12}: MF,n = 1, R^1 = Cy, R^2 = Me (R_C,R_{ax})
L_{13}: MF,n = 1, R^1 = Cy, R^2 = Et (S_C,S_{ax})
L_{14}: MF,n = 1, R^1 = Cy, R^2 = Et (S_C,R_{ax})
L_{15}: MF,n = 1, R^1 = Cy, R^2 = Et (R_C,S_{ax})
L_{16}: MF,n = 1, R^1 = Cy, R^2 = Et (R_C,R_{ax})
L_{17}: PS,n = 0, R^1 = ^{t}Bu, R^2 = Me (S_C,S_{ax})

L_{18}: MF,n = 1, R^1 = Ph, R^2 = Me (S_C)
L_{19}: MF,n = 1, R^1 = Ph, R^2 = Me (R_C)
L_{20}: MF,n = 1, R^1 = Ph, R^2 = Et (S_C)
L_{21}: MF,n = 1, R^1 = Ph, R^2 = Et (R_C)
L_{22}: MF,n = 1, R^1 = Cy, R^2 = Me (S_C)
L_{23}: MF,n = 1, R^1 = Cy, R^2 = Me (R_C)
L_{24}: MF,n = 1, R^1 = Cy, R^2 = Et (S_C)
L_{25}: MF,n = 1, R^1 = Cy, R^2 = Et (R_C)

L_{35}: MF,n = 1, R^1 = Ph, R^2 = Me (R_C)
L_{36}: MF,n = 1, R^1 = Cy, R^2 = Me (S_C)
L_{37}: MF,n = 1, R^1 = Cy, R^2 = Me (R_C)

L_{26}: MF,n = 1, R^1 = Ph, R^2 = Me (S_C)
L_{27}: MF,n = 1, R^1 = Ph, R^2 = Me (R_C)
L_{28}: MF,n = 1, R^1 = Ph, R^2 = Et (S_C)
L_{29}: MF,n = 1, R^1 = Ph, R^2 = Et (R_C)
L_{30}: MF,n = 1, R^1 = Cy, R^2 = Et (S_C)

L_{31}: MF,n = 1, R^1 = Ph, R^2 = Me (S_C)
L_{32}: MF,n = 1, R^1 = Ph, R^2 = Me (R_C)
L_{33}: MF,n = 1, R^1 = Ph, R^2 = Et (S_C)
L_{34}: MF,n = 1, R^1 = Ph, R^2 = Et (R_C)

Figure 8 Complete immobilized P-OP ligand library.

The progress of the *O*-phosphorylation reaction was monitored by gel-phase ^{31}P NMR showing the appearance of a second characteristic phosphite signal in the range of about $\delta = 150$ to 134 ppm depending on the nature of the -OP moiety. A representative synthesis of resin-bound P-OP ligand **L_{12}** followed by ^{31}P NMR is depicted in Figure 9. For BINOL and hydrobenzoin-based ligands **L_1**-**L_{17}** and **L_{31}**-**L_{37}**, a 1:1 ratio of both signals was typically achieved within 6-16 hours after warming the reaction mixture to room temperature. In case of sterically more demanding *tert*-butyl-functionalized bisphenol and TADDOL-derivatives **L_{18}**-**L_{30}**, prolonged reaction times of up to 10 days were required. Moreover, it was found that elevated reaction temperatures up to 40 °C were necessary combined with frequent addition of fresh equivalents (up to 8 equiv.) of chlorophosphites to drive the reaction to full conversion. However, these conditions possibly led to the formation of small amounts of resin-bound phosphine oxides for some examples. Upon completion, the resin was washed with DCM multiple times to ensure full removal of excess reagents and ammonium salts followed by washing steps with THF and Et_2O. Figure 10 shows representative ^{31}P NMR spectra of selected resin-bound phosphine-phosphite ligands and their characteristic chemical shifts, which are in agreement with those for similar immobilized phosphine-phosphites previously reported by the Kamer group.[17b]

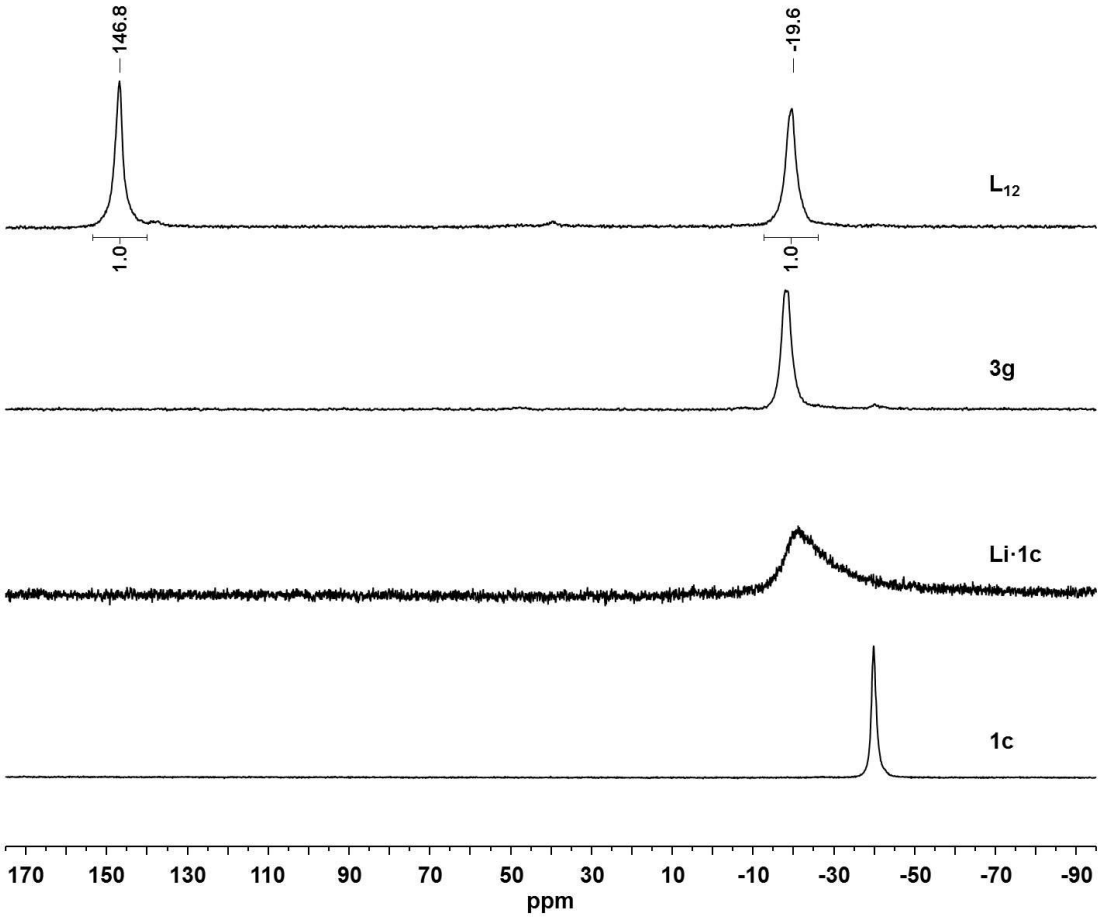

Figure 9 Solid-phase synthesis of supported P-OP ligand **L_{12}** monitored by ^{31}P NMR.

For some ligand library members a splitting of the phosphite resonance was observed (Figure 10, top left). Again, their appearance in a 1:1 ratio can be attributed to a mixture of two phosphine epimers present in each ligand as observed previously (see Figure 5, left). Peak splitting occurred for all BINOL-derived P-OP ligands possessing a R_C,S_{ax} or S_C,R_{ax} stereochemistry in the ligand backbone but also in a few cases involving TADDOL and hydrobenzoin functionalities. For most immobilized ligands, however, single phosphite peaks are visible most likely due to overlapping of the two epimer signals. Studies by Deerenberg *et al.* for similar homogeneous P-OP ligand systems, such as ligand **X** (see Figure 4), have pointed out that the combination of the configuration of carbon backbone and phosphite mainly determine the chiral induction in asymmetric transformations rather than the influence of the *P*-configuration of phosphine part.[11c] Consequently it was anticipated that the epimeric mixtures present in each supported ligand could achieve high enantioselectivities in asymmetric catalysis.

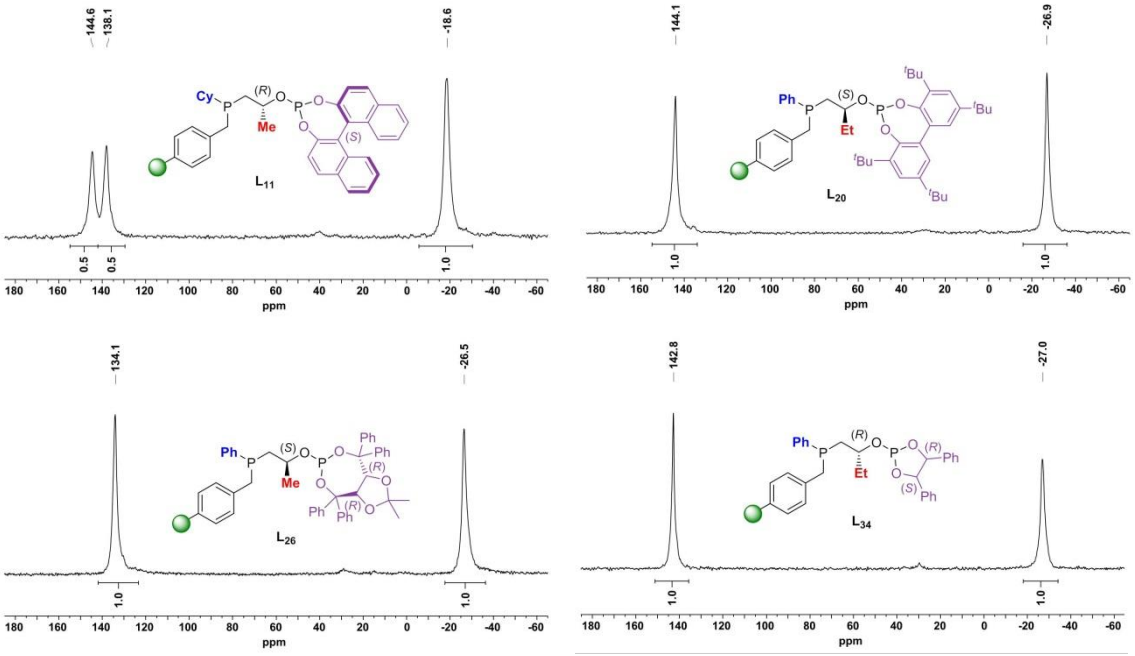

Figure 10 Representative ^{31}P NMR spectra of supported P-OP ligands **L_{11}** (top left), **L_{20}** (top right), **L_{26}** (bottom left) and **L_{34}** (bottom right).

The installation of a variety of different **R^1** and **R^2** substituents combined with the diversity introduced by the **–OP** groups allows for a comprehensive library screening in asymmetric catalysis. Influences of the matched/mismatched effect in case of (*R*)- and (*S*)-BINOL moieties as well as the impact of bulky phosphites on the catalytic performances was investigated as shown in the following chapter.

2.3 Rhodium-Catalyzed Asymmetric Hydrogenation

Since hybrid-type phosphine-phosphite ligands have proven their versatile applicability in a broad range of catalytic enantioselective reactions (see chapter 2.1),[8-9] it was decided to investigate the performance of the highly diverse supported P-OP ligand library in asymmetric catalysis. Therefore, all 37 members were screened in the stereoselective hydrogenation of three prochiral enamide benchmark substrates, namely methyl α-acetamidoacrylate (**S$_1$**), methyl (*Z*)-α-acetamidocinnamate (**S$_2$**) and α-acetamidocinnamic acid (**S$_3$**), employing the corresponding P-OP-based rhodium complexes.

2.3.1 Synthesis of Supported Rhodium-P-OP Complexes

Prior to catalytic screening, catalyst preformation was accomplished following a procedure reported for similar resin-bound diphosphine and phosphine-phosphite systems.[17b,24a] Hence, a previously prepared supported P-OP ligand was suspended in a solution of the metal precursor [Rh(cod)$_2$]X (cod = cyclooctadiene, X = BF_4, SbF_6, 0.9 equiv.) dissolved in DCM (see Scheme 7 for representative example).

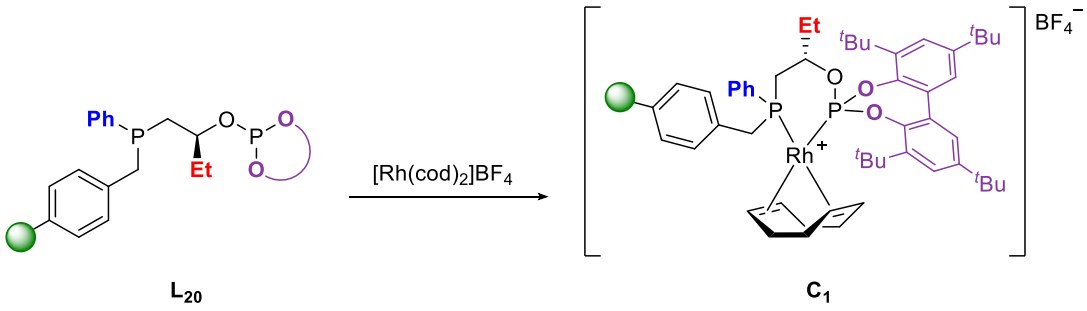

L$_{20}$ **C$_1$**

Scheme 7 Solid-phase synthetic approach towards supported Rh-complex **C$_1$**.

Full complexation was typically reached within 1-2 hours indicated by a resin color change from pale yellow to bright orange while the previously orange supernatant solution decolorized entirely. Subsequent washing steps using DCM, THF and diethyl ether ensured full removal of remaining rhodium metal. The progress of the complexation was monitored by gel-phase ^{31}P NMR which indicates a chelating coordination geometry of the ligand to the Rh-center due to a gradual decline of the ligand signals in a 1:1 ratio. For most library members however, significant peak broadening of the new supported transition-metal complex limited further spectroscopic characterization as observed for similar resin-bound systems.[17b] In case of the

rhodium-P-OP complex **C_1** featuring a bulky and hence less flexible *tert*-butyl-functionalized bisphenol group, two new broad signals are visible at δ = 129.0 ppm and δ = 3.3 ppm belonging to the –OP and the resin-bound phosphine moiety, respectively (Figure 11). Unfortunately, coupling constants could not be determined due to severe peak broadening. Despite full consumption of ligand **L_{20}**, only a phosphite to phosphine peak ratio of 0.8:1 was observed. This may be attributed to partial disappearance of the –OP signal in the baseline. However, the chemical shifts are in the expected range of similar solution-phase Rh/P-OP analogues reported by Pizzano and co-workers.[11e,29]

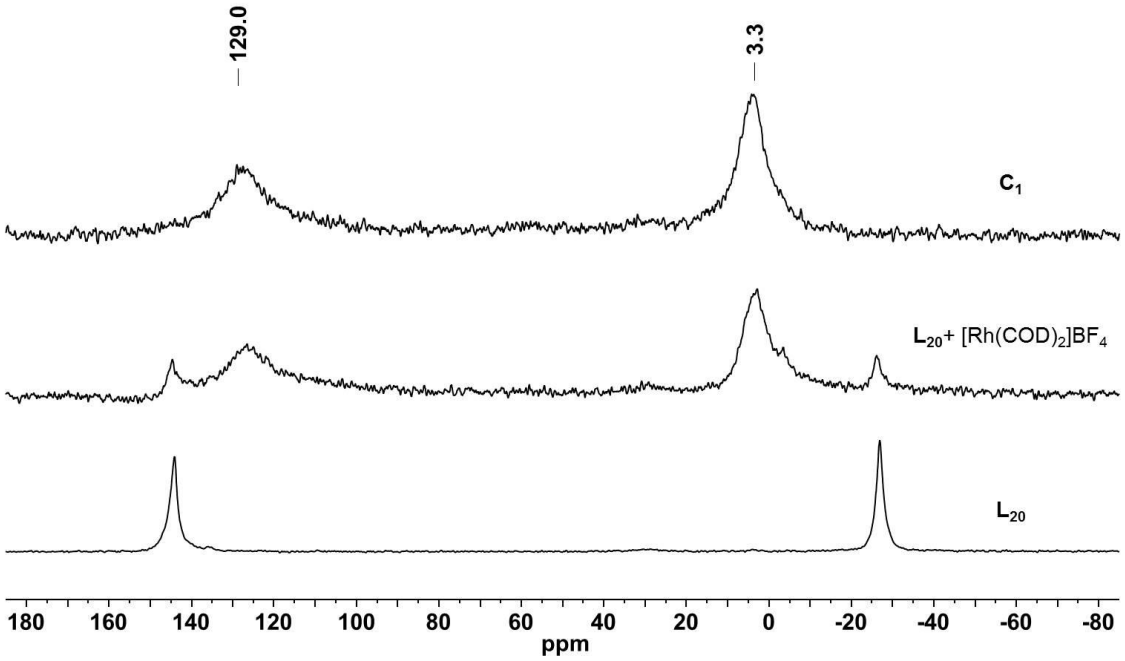

Figure 11 Solid-phase synthesis of resin-bound rhodium phosphine-phosphite complex **C_1** monitored by ^{31}P NMR.

2.3.2 Catalytic Screening

Having preformed the whole set of supported Rh/P-OP complexes, all library members were subsequently screened in the Rh-catalyzed asymmetric hydrogenation of the prochiral enamides **S_1-S_3**. Selected results are depicted in the following Tables 1-3.

Initially, the catalytic performances of Merrifield supported ligands **L_1-L_{16}** as well as polystyrene-bound **L_{17}** were examined (Table 1). All of these ligands have an axially chiral BINOL-derived phosphite moiety in common but differ in the phosphine substituent **R^1** (Ph or Cy) and the **R^2** group (Me or Et) located in the *C*-chiral backbone.

Table 1 Results of Rh-catalyzed asymmetric hydrogenation using **L_1-L_{17}**.[a]

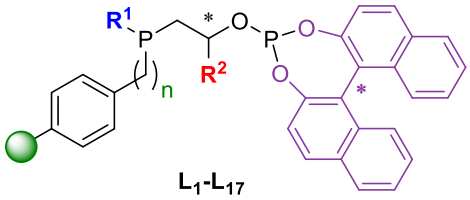

L_1-L_{17}

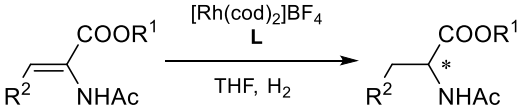

S_1: R^1 = Me, R^2 = H
S_2: R^1 = Me, R^2 = Ph
S_3: R^1 = H, R^2 = Ph

Entry	Ligand	R^1	R^2	Configuration	**S_1** ee [%][b]	**S_2** ee [%][b]	**S_3** ee [%][b]
1	**L_1**	Ph	Me	(S_C,S_{ax})	89 (*R*)	85 (*R*)	87 (*R*)
2	**L_2**	Ph	Me	(S_C,R_{ax})	57 (*S*)	70 (*S*)	68 (*S*)
3	**L_3**	Ph	Me	(R_C,S_{ax})	57 (*R*)	70 (*R*)	62 (*R*)
4	**L_4**	Ph	Me	(R_C,R_{ax})	90 (*S*)	84 (*S*)	86 (*S*)
5	**L_5**	Ph	Et	(S_C,S_{ax})	93 (*R*)	87 (*R*)	90 (*R*)
6	**L_6**	Ph	Et	(S_C,R_{ax})	68 (*S*)	80 (*S*)	76 (*S*)
7	**L_7**	Ph	Et	(R_C,S_{ax})	69 (*R*)	80 (*R*)	77 (*R*)
8	**L_8**	Ph	Et	(R_C,R_{ax})	91 (*S*)	86 (*S*)	89 (*S*)
9	**L_9**	Cy	Me	(S_C,S_{ax})	97 (*R*)	93 (*R*)	96 (*R*)
10	**L_{10}**	Cy	Me	(S_C,R_{ax})	62 (*S*)	33 (*S*)	23 (*S*)
11	**L_{11}**	Cy	Me	(R_C,S_{ax})	64 (*R*)	29 (*R*)	20 (*R*)
12	**L_{12}**	Cy	Me	(R_C,R_{ax})	97 (*S*)	91 (*S*)	96 (*S*)
13	**L_{13}**	Cy	Et	(S_C,S_{ax})	98 (*R*)	93 (*R*)	96 (*R*)
14	**L_{14}**	Cy	Et	(S_C,R_{ax})	67 (*S*)	41 (*S*)	37 (*S*)
15	**L_{15}**	Cy	Et	(R_C,S_{ax})	67 (*R*)	40 (*R*)	36 (*R*)
16	**L_{16}**	Cy	Et	(R_C,R_{ax})	97 (*S*)	92 (*S*)	97 (*S*)
17	**L_{17}**	^{t}Bu	Me	(S_C,S_{ax})	87 (*R*)	88 (*R*)	83 (*R*)
18[c]	**L_5**	Ph	Et	(S_C,S_{ax})	95 (*R*)	90 (*R*)	93 (*R*)
19[c]	**L_{13}**	Cy	Et	(S_C,S_{ax})	**99 (*R*)**	**95 (*R*)**	**97 (*R*)**

[a] Reaction conditions: Rh/substrate = 1:30, H_2 = 1.2 bar, *T* = 25 °C, *t* = 16 h, 0.5 mL of THF, quantitative conversion in all cases, conversion was determined by GC. [b] Enantiomeric excess of product determined by chiral GC (absolute configuration drawn in parenthesis). [c] Using $[Rh(cod)_2]SbF_6$ as metal precursor.

In all cases, full conversions towards the desired amides were obtained along with up to 98% *ee* for substrate **S_1** when employing ligand **L_{13}** and $[Rh(cod)_2]BF_4$ as metal precursor (Table 1, entry 13). Exchanging the BF_4^- counter-ion for SbF_6^- appears

to have a beneficial impact on the stereoselectivity giving up to 3% higher *ee* for **L_5** and **L_{13}** reaching a maximum *ee* of 99% (see entries 5 and 13 versus 18 and 19). This counter-ion effect has been observed before for similar immobilized and solution-phase phosphite-type ligands.[17b,30]

Moreover, a distinct matched/mismatched effect is evident for the supported diastereomeric catalysts.[31] In case of ligands occupying a matched pair configuration of (S_C,S_{ax}) or (R_C,R_{ax}), high enantioselectivities for all substrates were obtained whereas mismatched configurations (S_C,R_{ax}) and (R_C,S_{ax}) led to significantly reduced *ee*. The stereogenic axis of the BINOL moiety governs the stereochemical outcome in the asymmetric hydrogenation of **S_1**-**S_3**, which is in agreement with literature-known heterogeneous and homogeneous systems.[17b,32] While the (*S*)-BINOL group consistently yields the (*R*) hydrogenation product, (*S*)-selectivity is produced by the (*R*)-BINOL regardless of the configuration of the *C*-chiral ligand backbone. However, high enantioselectivities depend on the cooperativity of both stereocenters, more precisely on the pre-orientation of the BINOL moiety by the *C*-chiral substituent. Ligand **L_5**, for instance, possessing (S_C,S_{ax}) configuration achieved up to 24% higher selectivity for **S_1** compared to its diastereomeric analogues **L_6** and **L_7** occupying (S_C,R_{ax}) and (R_C,S_{ax}) combinations of stereogenic elements, respectively (see entry 5 versus 6 and 7). For ligands bearing a cyclohexyl group attached to the phosphine moiety instead of a phenyl group, the cooperative effect between the two chiral groups is more pronounced for substrates **S_2** and **S_3**. In case of matched pair ligand **L_9** and mismatched analogue **L_{11}** a difference in *ee* of up to 76% was observed for **S_3** (see entries 9 and 11).

For ligands occupying a matched configuration, only a single phosphite peak is observed in the corresponding ^{31}P NMR spectrum, whereas their mismatched counterparts exhibit a peak splitting attributable to the different epimers. Notably, mismatched ligands **L_{10}** and **L_{11}** showed the largest splitting of over $\Delta\delta$ = 6 ppm combined with the lowest *ee* in asymmetric hydrogenation of **S_2** and **S_3** (entries 10 and 11, see Figure 10 for ^{31}P NMR of **L_{11}**, top left spectrum).

Regarding the impact of the **R^1** group, cyclohexyl-substituted matched pair ligands showed higher enantioselectivity opposed to phenyl-based analogues (for example entry 1 versus 9) while the reversed effect is observed for mismatched configurations (for example entry 6 versus 14). Polystyrene-bound **L_{17}** featuring a ^{t}Bu-substituted phosphine moiety resulted in similar selectivity compared to the phenyl-substituted counterpart **L_1** (entry 1 versus 17). Moreover, the slightly more bulky ethyl substituent (**R^2**) seemed to have a small but beneficial effect on the enantioselectivity

compared to a methyl group. When comparing **L_1** with **L_5** (entries 1 and 5) it can be seen that the latter example bearing an ethyl group reaches up to 4% higher *ee*.

In fact, very high enantioselectivities were obtained throughout the catalytic screening of most ligands despite the phosphorus of the phosphine part being present as a 1:1 mixture of epimers. This seems to be in line with findings by Deerenberg *et al.* reporting on the minor influence of the *P*-chiral center on the enantioselective induction in homogeneous systems.[11c]

Fine-tuning the properties of the phosphite moiety in heterobidentate phosphorus ligands can have a profound impact on the corresponding performance in catalysis. Hence, the influence of different phosphite moieties was studied in the asymmetric hydrogenation of **S_1-S_3**. The results for ligands **L_{18}-L_{25}**, which bear a more bulky *tert*-butyl-functionalized bisphenol group lacking a stereogenic center, are depicted in Table 2.

Table 2 Results of Rh-catalyzed asymmetric hydrogenation using **L_{18}-L_{25}**.[a]

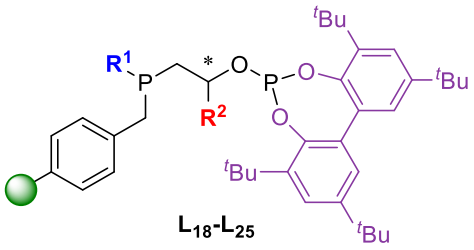

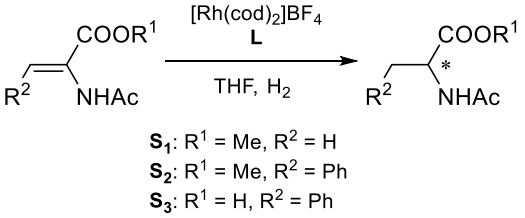

Entry	Ligand	R^1	R^2	S_1	S_2	S_3
				ee [%][b]	ee [%][b]	ee [%][b]
1	L_{18}	Ph	Me (*S*)	74 (*S*)	6 (*R*)	34[c] (*R*)
2	L_{19}	Ph	Me (*R*)	72 (*R*)	6 (*S*)	40 (*S*)
3	L_{20}	Ph	Et (*S*)	91 (*S*)	43 (*S*)	1[c] (*R*)
4	L_{21}	Ph	Et (*R*)	90 (*R*)	44 (*R*)	3[c] (*S*)
5	L_{22}	Cy	Me (*S*)	95 (*S*)	89 (*S*)	75 (*S*)
6	L_{23}	Cy	Me (*R*)	95 (*R*)	91 (*R*)	75 (*R*)
7	L_{24}	Cy	Et (*S*)	94 (*S*)	83 (*S*)	82 (*S*)
8	L_{25}	Cy	Et (*R*)	94 (*R*)	84 (*R*)	85 (*R*)
9[d]	L_{24}	Cy	Et (*S*)	96 (*S*)	87 (*S*)	88 (*S*)

[a] Reaction conditions: Rh/substrate = 1:30, H_2 = 1.2 bar, *T* = 25 °C, *t* = 16 h, 0.5 mL of THF, quantitative conversion in all cases unless stated otherwise, conversion was determined by GC. [b] Enantiomeric excess of product determined by chiral GC (absolute configuration drawn in parenthesis). [c] Conversion: 70-85%. [d] Using $[Rh(cod)_2]SbF_6$ as metal precursor.

When employing phenyl-substituted ligands **L_{18}** and **L_{19}** in the hydrogenation of **S_1**, up to 18% lower *ee*s were observed as opposed to their above mentioned BINOL-derived analogues **L_1** and **L_4** (Table 2, entries 1 and 2 versus Table 1, entries 1 and 4). However, changing to an ethyl group in the chiral carbon backbone resulted in similar selectivities of 90-91% *ee* for **L_{20}** and **L_{21}** when compared to BINOL-ligands **L_5** and **L_8** (Table 2, entries 3 and 4 versus Table 1, entries 5 and 8). These results may seem surprising as the product configuration is mainly determined by the stereocenter located in the phosphite backbone. In fact, for the *tert*-butyl-functionalized bisphenol group a fast interconversion of the potential atropisomers around the biaryl linkage due to a low energy barrier can lead to the presence of the two diastereoisomers **C_{1A}** and **C_{1B}** (Scheme 8).[33]

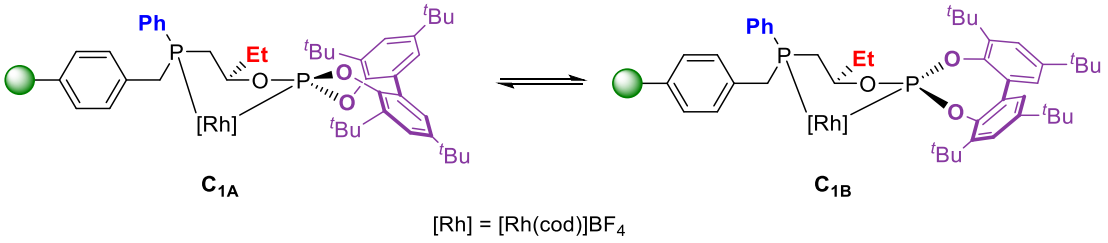

Scheme 8 Interconversion of atropisomers **C_{1A}** and **C_{1B}**.

Consequently, a significantly decreased enantioselectivity would be expected supported by observations made for homogeneous phosphine-phosphite and diphosphite systems.[12a,34] Yet, high stereoselectivities obtained for some supported P-OP ligands carrying an achiral bisphenol-based phosphite moiety can be attributed to a preformed ligand configuration enforced by the *C*-stereogenic center. This in turn leads to an *in-situ* selection of one of the catalyst diastereoisomers **C_{1A}** and **C_{1B}** as reported for chiral diphosphite ligands by Buisman *et al*.[35]

In analogy to their BINOL derivatives, slightly increased enantioselectivities of up to 95% for **S_1** were obtained when changing from a phenyl to a cyclohexyl substituent (Table 2, entries 5 and 6). High to moderate *ee*s ranging from 91-75% in case of substrates **S_2** and **S_3** were reached when using ligands **L_{22}-L_{25}** (Table 2, entries 5-8). Employing Ph-substituted ligands **L_{18}-L_{21}** in the hydrogenation of phenyl-containing enamides **S_2** and **S_3** gave only low selectivities and in some cases even a complete loss in *ee* was found. While Me-substituted ligands **L_{18}** and **L_{19}** gave no selectivity for substrate **S_2** and low selectivities for **S_3** (34-40% *ee*, Table 2, entries 1 and 2), the reverse outcome occurred for Et-substituted ligands **L_{20}** and **L_{21}** (Table 2, entries 3 and

4). Moreover, full conversion was not reached when employing **L_{18}**, **L_{20}** and **L_{21}** in the hydrogenation of **S_3**. By employing $[Rh(cod)_2]SbF_6$ as the metal precursor, again a positive counter-ion effect resulted in up to 6% higher *ee* (Table 2, entry 7 versus 9).

Reports on homogeneous TADDOL-derived P-OP ligands employed in catalytic asymmetric hydrogenation reactions remain scarce. A modular library reported by Robert *et al.* for application in asymmetric hydroformylation of styrene enabled product selectivities of up to 85% *ee*.[13] Moreover, (*S*,*S*)-TADDOL-based ligands provided the best chemo-, diastereo- and enantioselectivity among a range of different P-OP ligands in the hydrogenative desymmetrization of 1,4-dienes.[36] When supported (*R*,*R*)-TADDOL-derived P-OP ligands **L_{26}-L_{30}** were employed in the Rh-catalyzed asymmetric hydrogenation of **S_1-S_3**, significantly lower selectivities were obtained compared to most BINOL- and bulky biaryl-derived P-OP analogues (see Table 5, section 2.6). **L_{27}** possessing a matched (*R*,*R*,*R*) configuration gave the highest *ee* of 63% for the (*S*)-product of **S_1**. Since substituents R^1 and R^2 were found to have a minor impact on the chiral induction, the drop in enantioselectivity may be associated with the reduced phosphite rigidity as opposed to the biaryl counterparts. Similar performances were observed for even more simplified and less bulky hydrobenzoin-derived ligands **L_{31}-L_{37}** achieving up to 65% *ee* for **S_1** when applying cyclohexyl-substituted ligand **L_{37}** providing a cooperative (*R*,*S*,*S*)-combination of stereogenic centers (see Table 6, section 2.6).

In Table 3 the supported C2-bridged ligand **L_{13}** showing the best catalyst performance in the asymmetric hydrogenation of all three substrates **S_1-S_3** is compared to the resin-bound phosphine-phosphite ligand **VI** as well as to similar solution-phase analogues **X**, **XI** and **XIII** having the same chelate ring-size (Figure 12).[11c,11e,15,17b] Excellent and competitive selectivities were obtained for **L_{13}** which, in some cases, even outperformed its heterogeneous and homogeneous counterparts. Furthermore, **L_{13}** was tested in the hydrogenation of dimethyl itaconate (**S_4**) yielding the corresponding (*R*)-product in 95% *ee* slightly exceeding the performance of the structurally similar ligand **XIII** by about 2% (Table 3, entries 1 and 5). Finally, the tetralone-derived α-enamide **S_5** was employed in Rh-catalyzed hydrogenation using **L_{13}**. This cyclic *E*-configured substrate has proven to be significantly more challenging to hydrogenate selectively compared to substrates equipped with an adjacent electron-withdrawing group.[37] A moderate *ee* of 59% towards the (*R*)-amide was obtained still outperforming the homogeneous ligand **XI** reported by Vidal-Ferran and co-workers (Table 3, entries 1 and 4).[15]

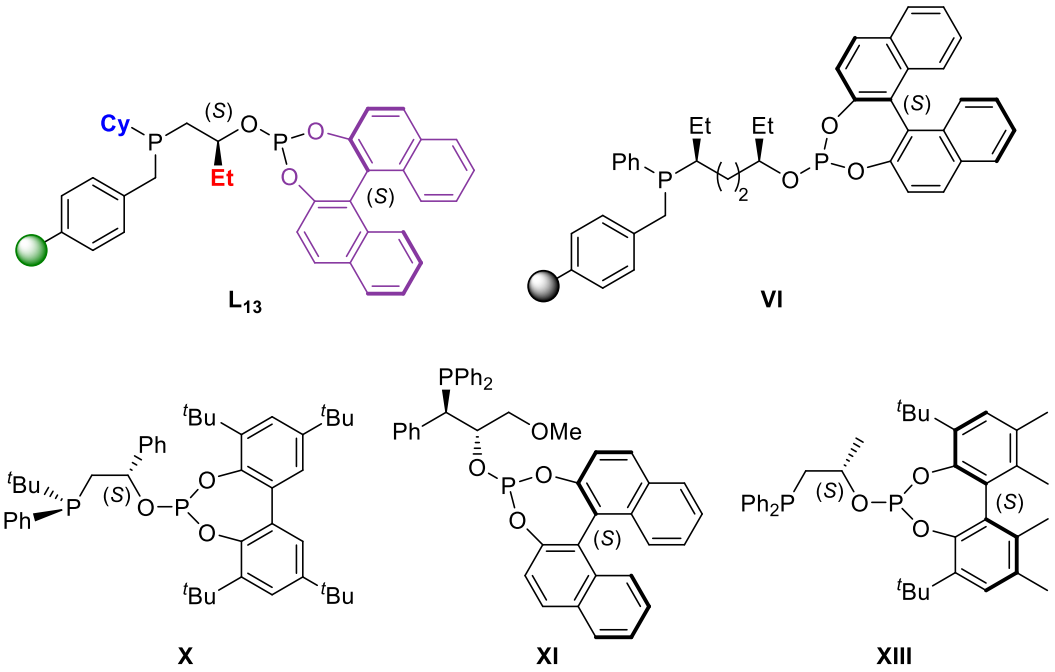

Figure 12 Best performing supported P-OP ligand $\mathbf{L_{13}}$ and similar heterogeneous and homogeneous ligands for comparison of performances (see Table 3).

Table 3 $\mathbf{L_{13}}$ in Rh-catalyzed asymmetric hydrogenation of $\mathbf{S_1}$-$\mathbf{S_5}$ compared to literature examples.

Entry	Ligand	$\mathbf{S_1}$	$\mathbf{S_2}$	$\mathbf{S_3}$	$\mathbf{S_4}$	$\mathbf{S_5}$
		ee [%]	ee [%]	ee [%]	ee [%]	ee [%]
1[a]	$\mathbf{L_{13}}$	99 (*R*)	95 (*R*)	97 (*R*)	95 (*R*)[b]	59 (*R*)[b]
2[c]	**VI**	96 (*R*)	98 (*R*)	91 (*R*)	-	-
3[d]	**X**	99 (*R*)	97 (*R*)	-	-	-
4[e]	**XI**	99 (*R*)	99 (*R*)	-	99 (*R*)	57 (*R*)
5[f]	**XIII**	-	99 (*R*)	-	93 (*S*)	-

[a] Reaction conditions: $[Rh(cod)_2]SbF_6$ as metal precursor, Rh/substrate = 1:30, H_2 = 1.2 bar, *T* = 25 °C, *t* = 16 h, 0.5 mL of THF, full conversion in all cases, conversion was determined by GC. Enantiomeric excess of product determined by chiral GC (absolute configuration drawn in parenthesis). All reaction were performed in duplo. [b] $[Rh(cod)_2]BF_4$ as metal precursor; H_2 = 10 bar. [c] Data taken from reference [17b]. [d] Data taken from reference [11c]. [e] Data taken from reference [15]. [f] Data taken from reference [11e].

Overall, the screening results presented above clearly showcase the dependency on trial-and-error methodologies for catalyst discovery as the majority of the employed P-OP ligands delivered inconsistent performances in the asymmetric hydrogenation of alkenes. Discovering universal chiral ligands remains challenging and often requires tailoring of ligand properties for each substrate as subtle changes in structure can have a profound impact on the selectivity. Modular solid-phase synthesis provides an invaluable tool for automated parallel ligand synthesis in order to efficiently access large and diverse P-OP ligand libraries for subsequent high-throughput screening.[12b] As demonstrated, this approach can lead to highly selective and hence competitive supported catalysts in which the support does not seem to exert a detrimental effect on the enantioselectivity as opposed to many known immobilized examples.

2.4 Catalytic Recycling

2.4.1 Batch Recycling

Subsequently, the recovery and recycling capabilities of the immobilized P-OP ligands were investigated. Therefore, BINOL-derived (S_C,S_{ax})-ligand **L_1** was employed in the asymmetric hydrogenation of **S_2** adapting a procedure reported for similar supported diphosphines and phosphine-phosphites.[17b,24a] For practical reasons the batch reaction cycles were performed in a Schlenk tube under a gentle flow of hydrogen gas instead of an autoclave. It was decided to reduce the reaction time from 16 hours to 27.5 minutes to enable monitoring of the effects on the catalyst stability at lower conversions. After each run, the supernatant solution was removed followed by a washing step while maintaining a H_2 atmosphere before a fresh portion of substrate was added to start the next cycle. The batch recycling results for ligand **L_1** in the asymmetric hydrogenation of **S_2** are summarized in Table 4.

Within the first three runs a constant increase in activity from 46% to 71% indicated a slow formation of the catalytically active species (Table 4, entries 1-3). This may be attributed to incomplete hydrogenation of cyclooctadiene bound to the rhodium/P-OP precursor resulting in delayed accessibility of all active sites. No significant drop in activity was observed in the following five reaction cycles while retaining a constant enantioselectivity of 86% (Table 4, entries 4-8). A maximum turnover frequency (TOF) of 52.5 h^{-1} was achieved in run 7 (Table 4, entry 7). After run 8, a slight activity loss was observed with a total drop of Δ8% in the subsequent three cycles. One explanation could be catalyst degradation caused by mechanical abrasion through magnetic stirring and hence the production of finely ground particles present in the supernatant solution. The introduction of small quantities of air and moisture as well as an inconsistent H_2 atmosphere during the recycling experiment may represent further reasons for catalyst deactivation. Phosphine-phosphite ligands are intrinsically sensitive to air and moisture since phosphines are typically prone to oxidation whereas P–O bonds in phosphites are easily solvolyzed by water.[38] Accordingly the supported P-OP ligand **L_1** exhibits a remarkable recyclability showing no significant loss in activity over 8 cycles accompanied by a steady enantioselectivity throughout the full extent of the recycling experiments. Resin-bound P-OP ligands with increased chelate ring-sizes, such as **VI** (see Figure 12), showed similar robustness over eleven cycles in the hydrogenation of **S_2** with only a minimal drop in activity of Δ3% after the seventh run.[17b] In contrast to that, Rh/P-OP catalyst **VIII** anchored via ionic interactions (see

Figure 3) showed a rapid decline in activity after the fourth reaction cycle under aqueous conditions.[20]

Table 4 Catalyst recycling experiments using $\mathbf{L_1}$ in asymmetric hydrogenation of $\mathbf{S_2}$.

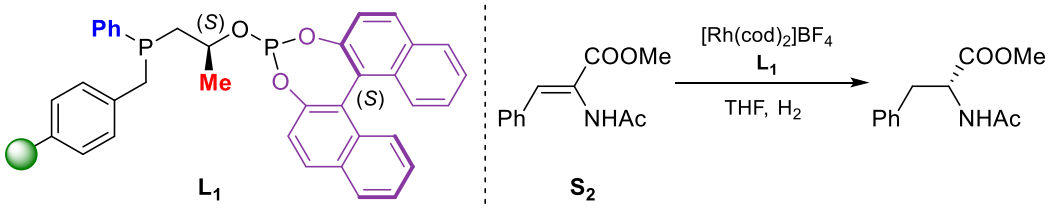

Run[a]	Conversion [%][b]	ee [%][c]	TOF [h^{-1}][d]
1	46	84 (*R*)	33,4
2	64	85 (*R*)	46,6
3	71	85 (*R*)	51,6
4	70	85 (*R*)	51,2
5	70	86 (*R*)	50,8
6	72	86 (*R*)	52,0
7	72	86 (*R*)	52,5
8	70	86 (*R*)	51,1
9	65	86 (*R*)	47,4
10	63	86 (*R*)	46,1
11	62	86 (*R*)	45,2

[a] Reaction conditions: In a Schlenk vessel under H_2 atmosphere, Rh/substrate = 1:30, $p(H_2)$ = 1 atm, T = 25 °C, t = 27.5 min, 1.5 mL of THF, all runs were performed in duplicate. [b] Conversion was determined by GC. [c] Enantiomeric excess of product determined by chiral GC (absolute configuration drawn in parenthesis). [d] Turnover frequency calculated as $n_{\mathbf{S1}}$ (mmol) x conversion / n_{Cat} (mmol) / time (h).

2.4.2 Continuous Flow Hydrogenation

Encouraged by these promising results obtained from batch recycling experiments it was decided to study the long-term performance of the previously synthesized supported P-OP ligands in a continuously operated system. One of the main advantages of continuous flow processes over batch reactors is the possibility of efficient and safe reaction parameter screening (see chapter 1.2.4). The monitoring of catalyst stabilities under various processing conditions is greatly facilitated. Both mechanical abrasion of the polymeric support as well as the introduction of air and moisture can be avoided since catalyst separation steps are not required when using a fixed bed reactor.

In a preliminary study, the resin-bound P-OP ligand **L_1** was applied in the hydrogenation of α-acetamidocinnamic acid (**S_3**) under continuous processing conditions using a custom-made reactor setup (Figure 13). Prior to preparation of the catalyst bed, pre-complexation was accomplished by treatment of supported ligand **L_1** with 1.0 equivalent of $[Rh(cod)_2]BF_4$ monitored by ^{31}P NMR to ensure full complexation as described in chapter 2.3.1. In a glove box, the reactor tube was charged with 50 mg of supported complex and plugged with glass wool at both ends prior to assembly of the reactor.

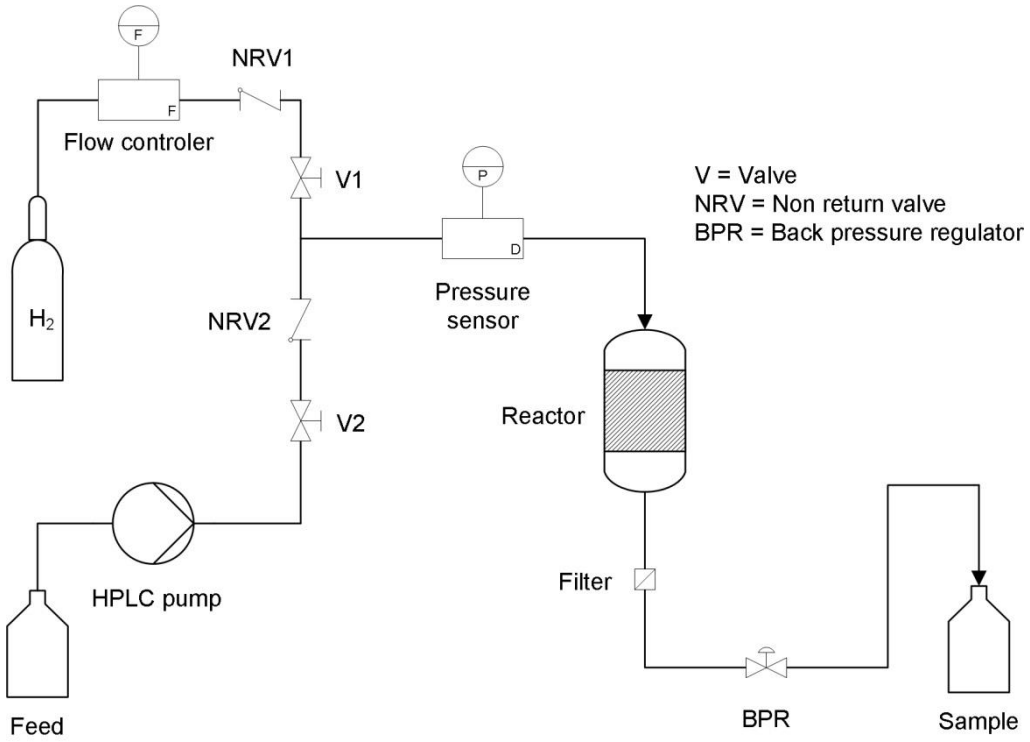

Figure 13 Flow scheme of reactor setup for continuous flow hydrogenation.

The flow rate of hydrogen gas (5 mL·min^{-1}) was controlled by a mass flow controller. The feed solution (0.05 M of **S_3** in THF) was fed into the system by a HPLC pump and mixed with hydrogen gas before entering the reactor. At room temperature the gas-liquid mixture was passed through the reactor bed at various substrate flow rates while maintaining a system pressure of 1 bar controlled by the back pressure regulator (BPR). Samples were collected down-stream and submitted to GC analysis in order to monitor substrate conversion and selectivity.

The results are of the continuous flow hydrogenation of **S_3** using the supported Rh-catalyst featuring **L_1** are shown in Figure 14. Based on previous experiments in flow it was decided to set an initial substrate flow rate of 0.1 mL·min^{-1} (Figure 14, setting 1). An increase in conversion from 79% to 95% was observed within the first hour on stream associated with slow swelling of the resin located in the reactor tube.

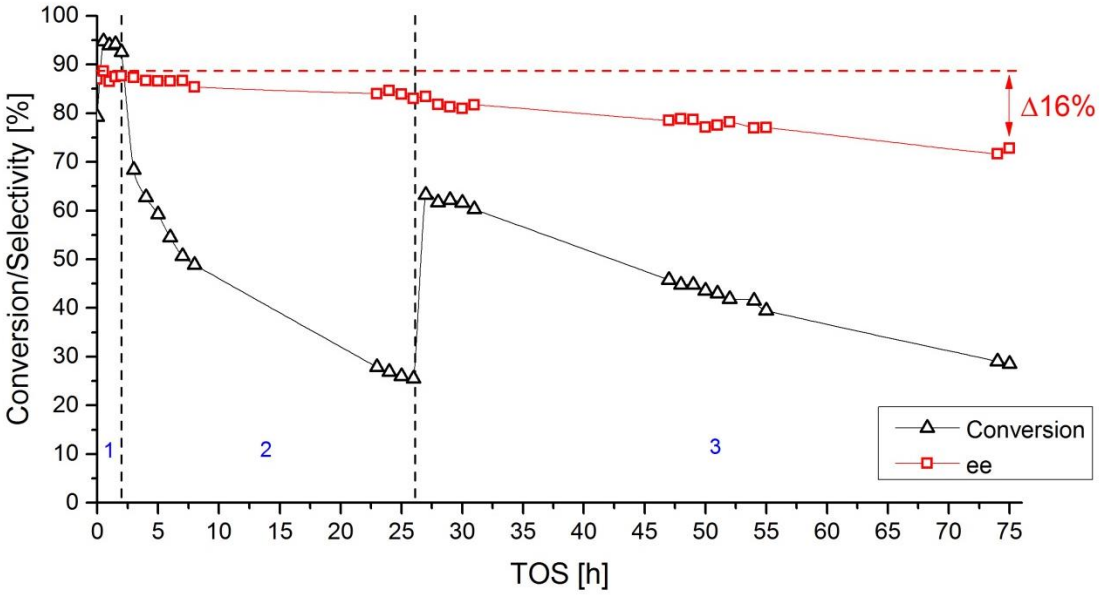

Figure 14 Continuous flow hydrogenation of **S_3** using **L_1**. Conditions: 50 mg of catalyst, 0.05 M of substrate in THF, 1.0 bar H_2 at 5 mL·min^{-1}. Setting 1: Substrate flow rate = 0.1 mL·min^{-1}. Setting 2: Substrate flow rate = 0.2 mL·min^{-1}. Setting 1: Substrate flow rate = 0.05 mL·min^{-1}. Conversion determined by GC. Selectivity determined by chiral GC.

Once the polymer was fully expanded, the immobilized catalyst provided high conversion of 94% in the following hour accompanied by 87% *ee*, which is in line with the selectivity obtained for **S_3** under batch conditions (see chapter 2.3.2, Table 1, entry 1). In order to accurately monitor the stability of the resin-bound catalyst in flow, it was decided to increase the substrate flow rate to 0.2 mL·min^{-1} to achieve moderate substrate conversion at lower residence times (Figure 14, setting 2). As expected, the

catalyst activity decreased to 68% after 3 hours but kept declining gradually reaching 26% conversion after 25 hours on stream. This is clearly indicative for a severe loss in catalyst activity under the applied conditions. Moreover, a slight decrease in selectivity from 87% to 84% occurred during this period suggesting both the decomposition of the defined diastereoisomeric catalyst geometry as well as the formation of rhodium metal capable of unselective hydrogenation of **S_3**. Next, the flow rate was reduced to 0.05 mL·min^{-1} consequently leading to an increase in conversion. This in turn enabled the monitoring of the catalyst stability for an additional time-on-stream (TOS) of 50 hours (Figure 14, setting 3). However, a constant decline in conversion from 63% to 29% after 75 hours on stream was observed together with a loss in selectivity of Δ16% over the full extent of the experiment. Upon removal of the supported catalyst from the reactor tube the deposition of black particles within the orange resin was visible pointing towards ligand degradation presumably via oxidation of the phosphine or hydrolysis of the phosphite moiety. Another explanation for the rapid catalyst decomposition could be reduction of the rhodium complex due to an excess of hydrogen gas used in this trial experiment. Unfortunately, it was impossible to employ very low flow rates of H_2 gas using the current reactor setup.

Recently, Madarász *et al.* applied structurally similar BINOL-derived P-OP ligands in the continuous flow hydrogenation of dimethyl itaconate (**S_4**) using a commercial H-Cube® reactor.[23b] In their case, the rhodium/phosphine-phosphite pre-catalyst was tethered to mesoporous Al_2O_3 using phosphotungstic acid opposed to the covalent immobilization strategy described in this chapter. In an attempt to assess the long-term stability in the continuous hydrogenation of **S_4** full conversion was maintained for 140 minutes after which the activity dropped dramatically to 41% within the following 9 hours on stream. Gradual catalyst decomposition can be assumed over the full course of the study based on the constant decline of selectivity from 95% *ee* to 83% *ee*. This result underlines the challenging task to apply intrinsically sensitive supported P-OP ligands in asymmetric hydrogenation under flow conditions.

In summary, the preliminary flow catalysis results demonstrate the general potential for application of resin-bound P-OP ligands in continuously operated processes. However, further optimizations in terms of reaction conditions and reactor equipment are required to prevent rapid catalyst degradation. The modular microreactor setup supplied by Ehrfeld Mikrotechnik BTS could offer a suitable alternative since it was successfully used in the continuous flow hydrogenation of benzonitrile (see chapter 5.5.2).

2.5 Conclusion and Outlook

The efficient and highly modular solid-phase synthetic methodology towards a large and diverse phosphine-phosphite ligand library immobilized on insoluble polymeric supports is demonstrated in this chapter. Systematic variation of four main building blocks enabled rapid access to 37 different resin-bound P-OP ligands (**L_1**-**L_{37}**) derived from regioselective ring-opening of chiral epoxides in very yields and purity. The SPS approach allowed for facile alteration of substituents **R^1**, **R^2** as well as the nature of the **–OP** moiety only requiring simple purification procedures such as filtration and decantation steps. This advantage becomes apparent when comparing this heterogeneous methodology with traditional solution-phase synthesis of homogeneous P-OP ligands often requiring tedious and low yielding workups. Moreover, SPS provides the opportunity for automated parallel synthesis of ligand libraries aiming for high throughput screening of catalysts in various applications.

A large number of high-performance ligands has been used in the homogeneous asymmetric hydrogenation of prochiral C=C and C=N compounds reaching turnover frequencies >400000 h^{-1}. Nevertheless, all members of the heterobidentate P-OP ligand library were successfully screened in Rh-catalyzed asymmetric hydrogenation of three enamide substrates. Excellent selectivities of up to 99% *ee* in case of ligand **L_{13}** were obtained demonstrating the power of screening large libraries in enantioselective transformations. Notably, the supported ligands could compete with a range of homogeneous and heterogeneous analogues and in some cases even outperform their direct counterparts. This also clearly indicates that the support does not exert a detrimental effect on the catalytic performance as often associated with heterogenized catalysts. In case of the significantly more challenging cyclic enamide **S_5**, a respectable stereoselectivity of 59% was achieved when employing **L_{13}**.

Finally, the capability for recovery and recycling of resin-bound P-OP ligands was presented. Under batch recycling conditions, **L_1** could be readily separated from the reaction mixture and reused for at least eleven consecutive runs in the asymmetric hydrogenation of methyl (*Z*)-α-acetamidocinnamate (**S_2**). No significant loss in activity could be observed over eight reaction cycles followed by a small loss of Δ8% over the subsequent three runs. High enantioselectivity could be retained over the full extent of the recycling experiments. The recyclability of the supported P-OP ligand is quite remarkable when taking the intrinsic sensitivity of this type of ligands into account.

In a preliminary attempt, the immobilized P-OP ligand **L_1** proved to be applicable in the continuously operated hydrogenation of α-acetamidocinnamic acid

(**S_3**). Although significant catalyst deactivation was observed together with a moderate decline in selectivity, the resin-bound Rh/P-OP catalyst could be used for at least 75 hours on stream. Further optimization towards process conditions as well as the use of equipment more suitable for smaller scales could improve the performance of resin-bound phosphine-phosphites under continuous flow conditions.

Combining the facile solid-phase synthetic approach with the modular nature of P-OP-type ligands would enable the rapid expansion of the immobilized library towards even more selective members. For example, the group of Vidal-Ferran found that more challenging substrates, such as cyclic enamide **S_5**, were hydrogenated with significantly higher *ee* when changing from an axially chiral BINOL group to a sterically more demanding (S_{ax})-*o*-Ph-H_8-BINOL-derived phosphite moiety (Figure 15, left).[39] Likewise, the incorporation bulky and hence less sensitive biaryl-derived phosphites lacking the possibility of atropisomer interconversion would be highly desirable especially for application in continuous flow (Figure 15, right). The solid-phase synthesis methodology for P-OP ligands could be further extended towards the preparation of resin-bound phosphine-phosphoramidite ligands, which have proven broad applicability in homogeneous catalysis.[40] Finally, the performances of these supported heterobidentate ligands could be explored in other asymmetric transformations such as hydrogenation of imines, hydroformylation and allylic substitution.

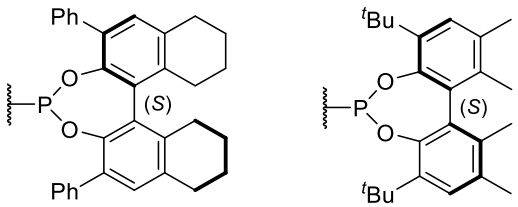

Figure 15 Representative examples of potential phosphite moieties.

2.6 Experimental

General Experimental

All reactions and manipulations were carried out using standard Schlenk techniques under inert atmosphere of purified argon or in an MBraun glovebox unless stated otherwise. All glassware was dried prior to use to remove traces of water. Toluene was distilled from sodium, THF and Et_2O from sodium sodium/benzophenone and DCM from CaH_2 under nitrogen atmosphere. Triethylamine was pre-dried over KOH and distilled from CaH_2 under argon atmosphere. All chemicals were obtained from Acros Organics, Alfa Aesar, TCI and Sigma-Aldrich and used without further purification unless otherwise stated. Novabiochem^{TM} Merrifield resin (100-200 mesh, 1.23 mmol·g^{-1}, 1% crosslinked) was obtained from EMD Millipore. ParaMax Merrifield resin (100-200 mesh, 1.2 mmol·g^{-1}, 4% crosslinked) was obtained from Advanced Chemtech. Supported secondary phosphines **1a-d** and **1a·BH$_3$**[24] as well as (*R*)-1-((*tert*-butyldimethylsilyl)oxy)propan-2-yl methanesulfonate[41] were synthesized according to literature procedures. Chlorophosphites were prepared adapting a literature procedure[42] starting from the corresponding diols: (*S*)-(−)- and (*R*)-(+)-1,1′-bi(2-naphthol) (BINOL, Sigma Aldrich), (4*R*,5*R*)-2,2-dimethyl-α, α, α′, α′-tetraphenyl-dioxolane-4,5-dimethanol (TADDOL, Sigma Aldrich), *meso*- and (*S,S*)-(−)-1,2-diphenyl-1,2-ethanediol (Sigma Aldich) and 3,3,5,5-tetra(*tert*-butyl)-2,2-biphenol[43].

NMR spectroscopic analysis was conducted using a Bruker FOURIER 300, an AVANCE II 400 or an AVANCE III 500. Gel-phase ^{31}P NMR spectra of all resins were recorded unlocked and without additional shimming in dry THF as a solvent unless mentioned otherwise. Chemical shifts for ^{31}P NMR are reported relative to 85% H_3PO_4 in water. Multiplicities are provided using the following abbreviations: s = singlet and br = broad. NMR spectra were processed using TopSpin 3.2 or MestReNova 11.0. IR spectra were recorded on a Shimadzu IRAffinity-1S spectrometer as KBr disks. Elemental analyses were measured by Mikroanalytisches Laboratorium Kolbe in Oberhausen, Germany. GC measurements were performed on a Thermo Trace GC ultra, see further experimental details for columns and conditions.

General Procedure for the Synthesis of Resin-Bound Hydoxyalkyl Phosphines

Step 1

A resin-bound phosphine (0.8 g, ~0.9 mmol, 1.0 equiv.) was swollen in THF (20 mL). Upon addition of LDA (4.5 mL, 2.0 M in THF/heptane/ethylbenzene 10 equiv.) under gentle stirring to avoid mechanical abrasion of the resin, the dark orange resin was left for 2 hours. The supernatant was removed and the resin was washed three times with THF (15 mL) followed by three times with Et_2O (15 mL). Without further purification the lithiated resin-bound phosphine (**Li·1a-d**) was used in the next step.

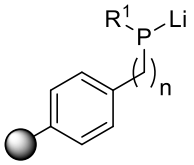

Li·1a: MF, n = 1, R^1 = Ph
Li·1b: MF 4%, n = 1, R^1 = Ph
Li·1c: MF, n = 1, R^1 = Cy
Li·1d: PS, n = 0, R^1 = ^{t}Bu

Li·1a: Dark orange resin: $^{31}P\{^1H\}$-NMR (162 MHz, THF): δ = -39.5 (br s) ppm.

Li·1b: Dark orange resin: $^{31}P\{^1H\}$-NMR (162 MHz, THF): δ = -40.3 (br s) ppm.

Li·1c: Dark orange resin: $^{31}P\{^1H\}$-NMR (121 MHz, THF): δ = -21.2 (br s) ppm.

Li·1d: Dark orange resin: $^{31}P\{^1H\}$-NMR (162 MHz, THF): δ = 4.3 (br s) ppm.

Step 2

A previously synthesized lithiated resin-bound phosphine (**Li·1a-d**, 0.8 g, ~0.9 mmol, 1.0 equiv.) was swollen in THF (20 mL). Under gentle stirring to avoid mechanical abrasion of the resin, a chiral epoxide **2a-d** (1.1 mmol, 1.2 equiv.) was added and the reaction mixture was allowed to react overnight leading to a yellow resin. The supernatant was removed and the resin was washed with THF:H_2O (1:1, 15 mL) followed by three portions of THF (15 mL) and three portions of Et_2O (15 mL). The product was dried *in vacuo* yielding a light yellow resin-bound hydoxyalkyl phosphine **3a-j** which was used in the next step without additional purification.

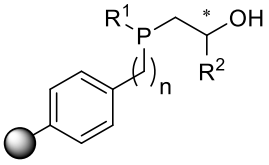

3a: MF, R^1 = Ph, R^2 = Me (S_C)
3b: MF 4%, R^1 = Ph, R^2 = Me (S_C)
3c: MF, R^1 = Ph, R^2 = Me (R_C)
3d: MF, R^1 = Ph, R^2 = Et (S_C)
3e: MF, R^1 = Ph, R^2 = Et (R_C)
3f: MF, R^1 = Cy, R^2 = Me (S_C)
3g: MF, R^1 = Cy, R^2 = Me (R_C)
3h: MF, R^1 = Cy, R^2 = Et (S_C)
3i: MF, R^1 = Cy, R^2 = Et (R_C)
3j: PS, R^1 = ^{t}Bu, R^2 = Me (S_C)

3a: Light yellow resin: $^{31}P\{^1H\}$-NMR (121 MHz, THF): δ = -25.8, -24.4 (br) ppm.

3b: Light yellow resin: $^{31}P\{^1H\}$-NMR (162 MHz, THF): δ = -18.4, -19.6 (br) ppm.

3c: Light yellow resin: $^{31}P\{^1H\}$-NMR (121 MHz, THF): δ = -25.7, -24.4 (br) ppm.

3d: Light yellow resin: $^{31}P\{^1H\}$-NMR (121 MHz, THF): δ = -26.0, -24.3 (br) ppm.

3e: Light yellow resin: $^{31}P\{^1H\}$-NMR (121 MHz, THF): δ = -26.0, -24.3 (br) ppm.

3f: Light yellow resin: $^{31}P\{^1H\}$-NMR (121 MHz, THF): δ = -18.6 (br) ppm; representative IR (KBr): $\tilde{\nu}$ = 3461 (brw), 3057 (w), 3024 (m), 2919 (s), 2848 (w), 1601 (w), 1509 (w), 1491 (m), 1451 (m), 1373 (w), 1104 (w), 1068 (w), 1026 (w), 961 (w), 841 (w), 757 (m), 698 (s) cm^{-1}; Elemental analysis calcd (%) for **3f** (1.05 $mmol \cdot g^{-1}$): P 3.26; found: P 3.22.

3g: Light yellow resin: $^{31}P\{^1H\}$-NMR (121 MHz, THF): δ = -18.1 (br) ppm.

3h: Light yellow resin: $^{31}P\{^1H\}$-NMR (121 MHz, THF): δ = -19.7, -18.4 (br) ppm.

3i: Light yellow resin: $^{31}P\{^1H\}$-NMR (162 MHz, THF): δ = -17.4 (br) ppm.

3j: Light yellow resin: $^{31}P\{^1H\}$-NMR (121 MHz, THF): δ = -5.6 (br) ppm.

Synthesis of Resin-Bound Phosphino Alcohol 5

Step 1

A previously synthesized resin-bound lithium phosphide **Li·1a** (0.15 mmol, 1.0 equiv.) was swollen in THF (10 mL). Under gentle stirring to avoid mechanical abrasion (*R*)-1-((*tert*-butyldimethylsilyl)oxy)propan-2-yl methanesulfonate (62 mg, 0.23 mmol, 1.5 equiv.) dissolved in THF (2 mL) was added at 0 °C and the reaction mixture was allowed to react overnight leading to a yellow resin. The reaction progress was monitored by ^{31}P NMR and if necessary additional equivalents of (*R*)-1-((*tert*-butyldimethylsilyl)oxy)propan-2-yl methanesulfonate were added to achieve full conversion. The supernatant was removed and the resin was washed with three portions of THF (10 mL) followed by three portions of Et_2O (10 mL). The product was

dried *in vacuo* yielding a light yellow resin-bound phosphine silylether **4** which was used in the next step without additional purification.

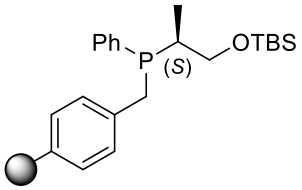

4

4: Light yellow resin: $^{31}P\{^{1}H\}$-NMR (162 MHz, THF): δ = -10.2 (**4**, br), -25.0 (10%, unknown) ppm.

Step 2

Resin-bound phosphine silylether **4** (0.15 mmol, 1.0 equiv.) prepared in the previous step was swollen in THF (10 mL). TBAF (0.76 mL, 1 m in THF, 0.76 mmol, 5.0 equiv.) was added to the resin at 0 °C under gentle stirring to avoid mechanical abrasion. The mixture was warmed to room temperature and left overnight without stirring. The supernatant was removed and the resin was washed with three portions of THF (10 mL) followed by three portions of Et_2O (10 mL). The product was dried *in vacuo* yielding a light yellow resin-bound phosphino alcohol **5**.

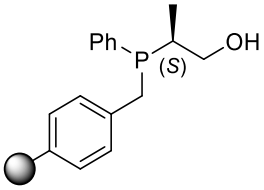

5

5: Light yellow resin: $^{31}P\{^{1}H\}$-NMR (162 MHz, THF): δ = -5.6, -8.2 (br) ppm.

Synthesis of Resin-Bound Phosphino Alcohol 3k

Step 1

Resin-bound phosphine-borane **1a·BH$_3$** (120 mg, 0.14 mmol, 1.0 equiv.) was swollen in THF (10 mL). Upon addition of LDA (0.7 mL, 1.40 mmol, 2.0 M in THF/heptane/ethylbenzene 10 equiv.) or of KHMDS (1.3 mL, 1.40 mmol, 20% in THF, 10 equiv.) under gentle stirring to avoid mechanical abrasion of the resin, the orange

resin was left for 2 hours. The supernatant was removed and the resin was washed three times with THF (10 mL) followed by three times with Et_2O (10 mL). Without further purification the lithiated resin-bound phosphine **Li·1a·BH$_3$** and the potassium phosphide **K·1a·BH$_3$** were used in the next step.

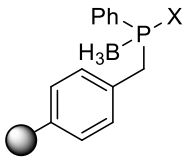

Li·1a·BH$_3$: X = Li
K·1a·BH$_3$: X = K

Li·1a·BH$_3$: Dark orange resin: $^{31}P\{^1H\}$-NMR (162 MHz, THF): δ = -39.5 (br s) ppm.

K·1a·BH$_3$: Orange resin: $^{31}P\{^1H\}$-NMR (162 MHz, THF): δ = -37.1 (br s) ppm.

Step 2

A previously synthesized resin-bound lithium or potassium phosphide (**Li·1a·BH$_3$**, **K·1a·BH$_3$**, 0.14 mmol, 1.0 equiv.) was swollen in THF (10 mL). Under gentle stirring to avoid mechanical abrasion (*S*)-styrene oxide (20 mg, 0.17 mmol, 1.2 equiv.) was added and the reaction mixture was allowed to react overnight leading to a yellow resin. The supernatant was removed and the resin was washed with THF:H_2O (1:1, 10 mL) followed by three portions of THF (10 mL) and three portions of Et_2O (10 mL). The product was dried *in vacuo* yielding a white resin-bound phosphino alcohol **3k** starting from **K·1a·BH$_3$** or a 3:1 mixture of **3k** and **3l** starting from **Li·1a·BH$_3$**.

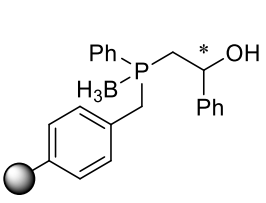

3k

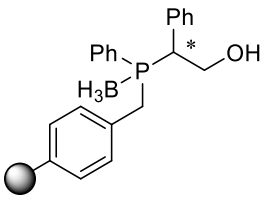

3l

3k: White resin: $^{31}P\{^1H\}$-NMR (162 MHz, THF): δ = 15.6 (br) ppm.

3l: White resin: $^{31}P\{^1H\}$-NMR (162 MHz, THF): δ = 23.2, 20.6 (br) ppm.

Synthesis of Resin-Bound Phosphine-Phosphinite 6

A previously synthesized resin-bound phosphino alcohol **3c** (278 mg, 0.29 mmol, 1.0 equiv.) was swollen in THF (20 mL) and triethylamine (0.24 mL, 1.74 mmol 6.0 equiv.) was added. Chlorodiphenylphosphine (0.16 mL, 0.87 mmol, 3.0 equiv.) was added to the reaction mixture at 0 °C under gentle stirring to avoid mechanical abrasion of the resin. Upon addition a precipitate was formed. The reaction was monitored using ^{31}P-NMR and full conversion was reached when a signal ratio of 1:1 of phosphine to phosphinite was observed (2-16 hours). The supernatant was removed and the resin was washed subsequently with three portions of DCM (15 mL), three portions of THF (15 mL) and three portions of Et_2O (15 mL). The product was dried *in vacuo* yielding an off-white resin-bound phosphine-phosphinite **6**.

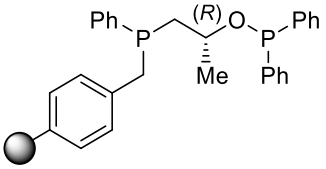

6

6: Off-white resin: $^{31}P\{^1H\}$-NMR (121 MHz, THF): δ = -26.8 (P, br s), 105.4 (–OP, br s) ppm.

General Procedure for the Synthesis of Resin-Bound Phosphine-Phosphites

A previously synthesized resin-bound phosphino alcohol (**3a-j**, 150 mg, ~0.16 mmol, 1.0 equiv.) was swollen in THF (10 mL) and triethylamine (0.96 mmol 6.0 equiv.) was added. A chlorophosphite **7a-f** (0.48 mmol, 3.0 equiv.) was dissolved in THF (5 mL) and added to the reaction mixture at 0 °C under gentle stirring to avoid mechanical abrasion of the resin. Upon addition a precipitate was formed. The reaction was monitored using ^{31}P NMR and full conversion was reached when a 1:1 ratio of signals of phosphine to phosphite was observed (6-240 hours). The supernatant was removed and the resin was washed subsequently with three portions of DCM (10 mL), three portions of THF (10 mL) and three portions of Et_2O (10 mL). The product was dried *in vacuo* yielding a light yellow resin-bound phosphine-phosphite $\mathbf{L_1}$-$\mathbf{L_{37}}$.

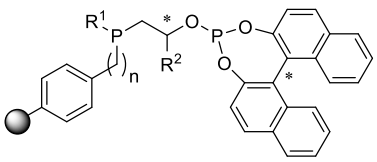

L_1: MF,n = 1, R^1 = Ph, R^2 = Me (S_C,S_{ax})
L_2: MF,n = 1, R^1 = Ph, R^2 = Me (S_C,R_{ax})
L_3: MF,n = 1, R^1 = Ph, R^2 = Me (R_C,S_{ax})
L_4: MF,n = 1, R^1 = Ph, R^2 = Me (R_C,R_{ax})
L_5: MF,n = 1, R^1 = Ph, R^2 = Et (S_C,S_{ax})
L_6: MF,n = 1, R^1 = Ph, R^2 = Et (S_C,R_{ax})
L_7: MF,n = 1, R^1 = Ph, R^2 = Et (R_C,S_{ax})
L_8: MF,n = 1, R^1 = Ph, R^2 = Et (R_C,R_{ax})
L_9: MF,n = 1, R^1 = Cy, R^2 = Me (S_C,S_{ax})
L_{10}: MF,n = 1, R^1 = Cy, R^2 = Me (S_C,R_{ax})
L_{11}: MF,n = 1, R^1 = Cy, R^2 = Me (R_C,S_{ax})
L_{12}: MF,n = 1, R^1 = Cy, R^2 = Me (R_C,R_{ax})
L_{13}: MF,n = 1, R^1 = Cy, R^2 = Et (S_C,S_{ax})
L_{14}: MF,n = 1, R^1 = Cy, R^2 = Et (S_C,R_{ax})
L_{15}: MF,n = 1, R^1 = Cy, R^2 = Et (R_C,S_{ax})
L_{16}: MF,n = 1, R^1 = Cy, R^2 = Et (R_C,R_{ax})
L_{17}: PS,n = 0, R^1 = ^{t}Bu, R^2 = Me (S_C,S_{ax})

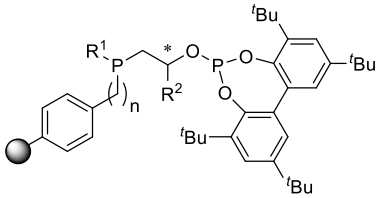

L_{18}: MF,n = 1, R^1 = Ph, R^2 = Me (S_C)
L_{19}: MF,n = 1, R^1 = Ph, R^2 = Me (R_C)
L_{20}: MF,n = 1, R^1 = Ph, R^2 = Et (S_C)
L_{21}: MF,n = 1, R^1 = Ph, R^2 = Et (R_C)
L_{22}: MF,n = 1, R^1 = Cy, R^2 = Me (S_C)
L_{23}: MF,n = 1, R^1 = Cy, R^2 = Me (R_C)
L_{24}: MF,n = 1, R^1 = Cy, R^2 = Et (S_C)
L_{25}: MF,n = 1, R^1 = Cy, R^2 = Et (R_C)

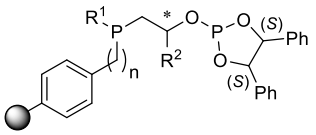

L_{35}: MF,n = 1, R^1 = Ph, R^2 = Me (R_C)
L_{36}: MF,n = 1, R^1 = Cy, R^2 = Me (S_C)
L_{37}: MF,n = 1, R^1 = Cy, R^2 = Me (R_C)

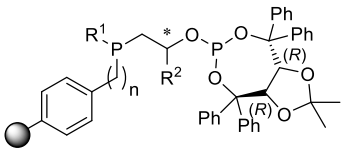

L_{26}: MF,n = 1, R^1 = Ph, R^2 = Me (S_C)
L_{27}: MF,n = 1, R^1 = Ph, R^2 = Me (R_C)
L_{28}: MF,n = 1, R^1 = Ph, R^2 = Et (S_C)
L_{29}: MF,n = 1, R^1 = Ph, R^2 = Et (R_C)
L_{30}: MF,n = 1, R^1 = Cy, R^2 = Et (S_C)

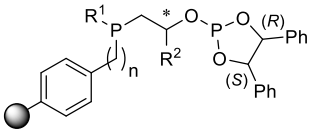

L_{31}: MF,n = 1, R^1 = Ph, R^2 = Me (S_C)
L_{32}: MF,n = 1, R^1 = Ph, R^2 = Me (R_C)
L_{33}: MF,n = 1, R^1 = Ph, R^2 = Et (S_C)
L_{34}: MF,n = 1, R^1 = Ph, R^2 = Et (R_C)

L_1: Light yellow resin: $^{31}P\{^1H\}$-NMR (162 MHz, THF): δ = -26.1 (P, br), 146.7 (–OP, br) ppm.

L_2: Light yellow resin: $^{31}P\{^1H\}$-NMR (121 MHz, THF): δ = -26.9 (P, br), 141.1, 144.3 (–OP, br) ppm.

L_3: Light yellow resin: $^{31}P\{^1H\}$-NMR (121 MHz, THF): δ = -27.1 (P, br), 141.1, 144.3 (–OP, br) ppm.

L_4: Light yellow resin: $^{31}P\{^1H\}$-NMR (121 MHz, THF): δ = -27.0 (P, br), 145.8 (–OP, br) ppm.

L_5: Light yellow resin: $^{31}P\{^1H\}$-NMR (121 MHz, THF): δ = -26.9 (P, br), 148.8 (–OP, br) ppm.

L_6: Light yellow resin: $^{31}P\{^1H\}$-NMR (162 MHz, THF): δ = -26.6 (P, br), 146.5, 148.9 (–OP, br) ppm.

L_7: Light yellow resin: $^{31}P\{^1H\}$-NMR (121 MHz, THF): δ = -27.4 (P, br), 145.7, 148.0 (–OP, br) ppm.

L_8: Light yellow resin: $^{31}P\{^1H\}$-NMR (121 MHz, THF): δ = -27.8 (P, br), 148.0 (–OP, br) ppm.

L_9: Light yellow resin: $^{31}P\{^1H\}$-NMR (162 MHz, THF): δ = -18.1 (P, br), 148.4 (–OP, br) ppm.

L_{10}: Light yellow resin: $^{31}P\{^1H\}$-NMR (162 MHz, THF): δ = -18.1 (P, br), 138.7, 145.4 (–OP, br) ppm.

L_{11}: Light yellow resin: $^{31}P\{^1H\}$-NMR (121 MHz, THF): δ = -18.6 (P, br), 138.1, 144.6 (–OP, br) ppm.

L_{12}: Light yellow resin: $^{31}P\{^1H\}$-NMR (121 MHz, THF): δ = -19.6 (P, br), 146.8 (–OP, br) ppm.

L_{13}: Light yellow resin: $^{31}P\{^1H\}$-NMR (121 MHz, THF): δ = -19.0 (P, br), 150.5 (–OP, br) ppm; representative IR (KBr): $\tilde{\nu}$ = 3057 (w), 3025 (m), 2972 (w), 2918 (m), 2848 (w), 1590 (w), 1507 (m), 1492 (m), 1452 (m), 1326 (m),1231 (m), 1201 (m), 1070 (m), 939 (s), 822 (s), 747 (s), 696 (s) cm^{-1}; Elemental analysis calcd (%) for **L_{13}** (0.78 $mmol \cdot g^{-1}$): P 4.84; found: P 4.94.

L_{14}: Light yellow resin: $^{31}P\{^1H\}$-NMR (162 MHz, THF): δ = -18.7 (P, br), 143.3, 148.0 (–OP, br) ppm.

L_{15}: Light yellow resin: $^{31}P\{^1H\}$-NMR (162 MHz, THF): δ = -18.8 (P, br), 143.2, 147.9 (–OP, br) ppm.

L_{16}: Light yellow resin: $^{31}P\{^1H\}$-NMR (121 MHz, THF): δ = -19.4 (P, br), 150.4 (–OP, br) ppm.

L_{17}: Light yellow resin: $^{31}P\{^1H\}$-NMR (121 MHz, THF): δ = -6.1 (P, br), 145.6 (–OP, br) ppm; representative IR (KBr): $\tilde{\nu}$ = 3058 (m), 3024 (m), 2922 (s), 2858 (m), 1620 (w), 1590 (m), 1508 (m), 1493 (m), 1453 (m), 1361 (m), 1326 (m), 1231 (s), 1201 (m), 1070 (m), 1014 (w), 979 (m), 938 (s), 822 (s), 748 (m), 698 (s) cm^{-1}.

L_{18}: Light yellow resin: $^{31}P\{^1H\}$-NMR (162 MHz, THF): δ = -25.2 (P, br), 145.5 (–OP, br) ppm.

L_{19}: Light yellow resin: $^{31}P\{^1H\}$-NMR (121 MHz, THF): δ = -26.0 (P, br), 144.7 (–OP, br) ppm.

L_{20}: Light yellow resin: $^{31}P\{^1H\}$-NMR (121 MHz, THF): δ = -26.9 (P, br), 144.1 (–OP, br) ppm; representative IR (KBr): $\tilde{\nu}$ = 3059 (w), 3024 (m), 2959 (s), 2922 (m), 2869 (w), 1601 (w), 1492 (m), 1454 (m), 1396 (w), 1362 (m),1229 (m), 1202 (w), 1090 (w), 960 (m), 877 (m), 846 (m), 759 (m), 697 (s) cm^{-1}; Elemental analysis calcd (%) for **L_{20}** (0.72 $mmol \cdot g^{-1}$): P 4.43; found: P 4.43.

L_{21}: Light yellow resin: $^{31}P\{^1H\}$-NMR (121 MHz, THF): δ = -26.9 (P, br), 144.1 (–OP, br) ppm.

L_{22}: Light yellow resin: $^{31}P\{^1H\}$-NMR (162 MHz, THF): δ = -17.7 (P, br), 145.2 (–OP, br) ppm.

L_{23}: Light yellow resin: $^{31}P\{^1H\}$-NMR (162 MHz, THF): δ = -16.6 (P, br), 146.2 (–OP, br) ppm.

L_{24}: Light yellow resin: $^{31}P\{^{1}H\}$-NMR (121 MHz, THF): δ = -18.9 (P, br), 144.6 (–OP, br) ppm.

L_{25}: Light yellow resin: $^{31}P\{^{1}H\}$-NMR (121 MHz, THF): δ = -19.0 (P, br), 144.5 (–OP, br) ppm.

L_{26}: Light yellow resin: $^{31}P\{^{1}H\}$-NMR (121 MHz, THF): δ = -26.6 (P, br), 134.1 (–OP, br) ppm; representative IR (KBr): $\tilde{\nu}$ = 3058 (m), 3024 (m), 2922 (s), 2850 (w), 1601 (w), 1493 (m), 1449 (m), 1374 (w), 12155 (w), 1087 (w), 958 (m), 884 (m), 830 (w), 739 (m), 697 (s) cm^{-1}.

L_{27}: Light yellow resin: $^{31}P\{^{1}H\}$-NMR (121 MHz, THF): δ = -26.5 (P, br), 134.1 (–OP, br) ppm.

L_{28}: Light yellow resin: $^{31}P\{^{1}H\}$-NMR (121 MHz, THF): δ = -26.6 (P, br), 135.4, 136.4 (–OP, br) ppm.

L_{29}: Light yellow resin: $^{31}P\{^{1}H\}$-NMR (121 MHz, THF): δ = -27.3 (P, br), 136.7 (–OP, br) ppm.

L_{30}: Light yellow resin: $^{31}P\{^{1}H\}$-NMR (121 MHz, THF): δ = -19.6 (P, br), 137.6 (–OP, br) ppm.

L_{31}: Light yellow resin: $^{31}P\{^{1}H\}$-NMR (121 MHz, THF): δ = -26.8 (P, br), 141.5 (–OP, br) ppm; representative IR (KBr): $\tilde{\nu}$ = 3059 (m), 3025 (m), 2919 (s), 2848 (w), 1601 (w), 1508 (w), 1492 (m), 1453 (m), 1205 (w), 951 (m), 824 (w), 743 (m), 697 (s) cm^{-1}.

L_{32}: Light yellow resin: $^{31}P\{^{1}H\}$-NMR (162 MHz, THF): δ = -26.4 (P, br), 140.9, 141.8 (–OP, br) ppm.

L_{33}: Light yellow resin: $^{31}P\{^{1}H\}$-NMR (162 MHz, THF): δ = -27.2 (P, br), 142.5 (–OP, br) ppm.

L_{34}: Light yellow resin: $^{31}P\{^{1}H\}$-NMR (162 MHz, THF): δ = -27.1 (P, br), 141.6, 142.4 (–OP, br) ppm.

L_{35}: Light yellow resin: $^{31}P\{^{1}H\}$-NMR (162 MHz, THF): δ = -27.0 (P, br), 142.8 (–OP, br) ppm.

L_{36}: Light yellow resin: $^{31}P\{^{1}H\}$-NMR (121 MHz, THF): δ = -18.8 (P, br), 141.9 (–OP, br) ppm.

L_{37}: Light yellow resin: $^{31}P\{^{1}H\}$-NMR (162 MHz, THF): δ = -18.3 (P, br), 142.7 (–OP, br) ppm.

In-Situ Complexation Study

Resin-bound phosphine-phosphite **L_{20}** (150 mg, 0.11 mmol, 1.0 equiv.) was swollen in DCM (5 mL) and $[Rh(cod)_2]BF_4$ dissolved in DCM (15 mL) was added to the resin under gentle stirring to avoid mechanical abrasion. The progress of the complexation was monitored using ^{31}P NMR and full consumption of the ligand was observed within 24 hours. The supernatant was removed and the orange resin was subsequently washed with three portions of DCM (10 mL), three portions of THF (10 mL) and three portions of Et_2O (10 mL). The resin-bound complex **C_1** was dried *in vacuo* yielding a bright orange resin.

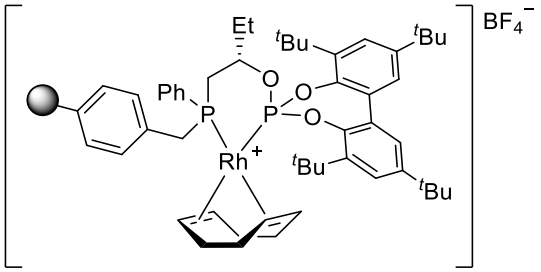

C_1

C_1: Orange resin: $^{31}P\{^1H\}$-NMR (162 MHz, THF): δ = 3.3 (P, br), 129.0 (–OP, br) ppm; IR (KBr): $\tilde{\nu}$ = 3058 (w), 3025 (w), 2961 (s), 2921 (s), 2870 (m), 1601 (w), 1492 (m), 1453 (m), 1436 (m), 1396 (m), 1362 (m), 1281 (w),1223 (m), 1204 (m), 1120 (m), 1084 (m), 1060 (m), 1027 (m), 997 (m), 879 (m), 759 (m, P-Ar), 698 (s, P-Ar) cm^{-1}.

General Procedure for Asymmetric Hydrogenation Experiments

The hydrogenation experiments were performed in a stainless steel autoclave charged with an insert suitable for 10 reaction vessels including Teflon mini stirring bars. In a typical experiment, a reaction vessel was charged with a resin-bound phosphine-phosphite (~5 mg, approximately 4.0 µmol) and a solution of $[Rh(cod)_2]X$ (0.9 equiv.) in DCM (1 mL) was added. The heterogeneous mixture was allowed to stir gently for 2 hours inside ta glove box. Upon discoloration of the solution the supernatant was removed and the resulting orange resin was washed subsequently with three 1 mL portions of THF. To the reaction vessel a solution of substrate **S_1-S_5** (0.5 mL, 0.24 M, 30 equiv.) in THF was added. Subsequently, the autoclave was purged three times with

10 bar of argon gas and the insert loaded with reaction vessels was transferred into the autoclave. Next, the autoclave was purged three times with 10 bar of H_2 and then pressurized to 1.2 bar (in case of **S_1-S_3**) or 10 bar (in case of **S_4-S_5**). The reaction mixtures were gently stirred at 25 °C. After 16 hours, the autoclave was depressurized and the reaction mixtures were filtered over a plug of silica. Prior to GC measurements substrate **S_3** and its products were derivatized using (trimethylsilyl)diazomethane (2 M in diethyl ether), in essence yielding substrate **S_2**. The conversion and the enantiomeric excess were determined by chiral GC using the following column and conditions:

Table 5 Results of Rh-catalyzed asymmetric hydrogenation using TADDOL-based ligands **L_{26}-L_{30}**.[a]

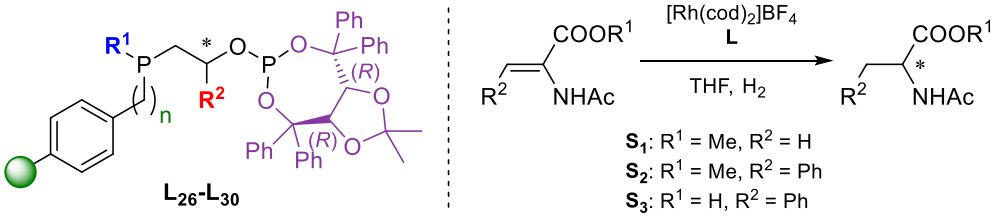

Entry	Ligand	R^1	R^2	Configuration	**S_1**	**S_2**	**S_3**
					ee [%][b]	ee [%][b]	ee [%][b]
1	**L_{26}**	Ph	Me	(S_C)	44 (*R*)	17 (*R*)	36 (*R*)
2	**L_{27}**	Ph	Me	(R_C)	63 (*S*)	51 (*S*)	62 (*S*)
3	**L_{28}**	Ph	Et	(S_C)	36 (*R*)	6 (*S*)	3 (*R*)
4	**L_{29}**	Ph	Et	(R_C)	58 (*S*)	38 (*S*)	61 (*S*)
5	**L_{30}**	Cy	Et	(S_C)	23 (*S*)	5 (*S*)	13 (*S*)

[a] Reaction conditions: Rh/substrate = 1:30, H_2 = 1.2 bar, T = 25 °C, t = 16 h, 0.5 mL of THF, quantitative conversion in all cases, conversion was determined by GC. [b] Enantiomeric excess of product determined by chiral GC (absolute configuration drawn in parenthesis).

Table 6 Results of Rh-catalyzed asymmetric hydrogenation using hydrobenzoin-based ligands $\mathbf{L_{31}}$-$\mathbf{L_{37}}$.[a]

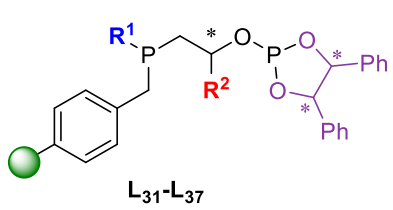

$\mathbf{L_{31}}$-$\mathbf{L_{37}}$

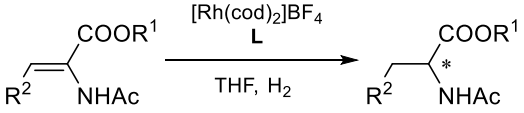

$\mathbf{S_1}$: R^1 = Me, R^2 = H
$\mathbf{S_2}$: R^1 = Me, R^2 = Ph
$\mathbf{S_3}$: R^1 = H, R^2 = Ph

Entry	Ligand	R^1	R^2	Configuration	$\mathbf{S_1}$	$\mathbf{S_2}$	$\mathbf{S_3}$
					ee [%][b]	ee [%][b]	ee [%][b]
1	$\mathbf{L_{31}}$	Ph	Me	(*S*,*R*,*S*)	30 (*R*)	9 (*R*)	33 (*R*)
2	$\mathbf{L_{32}}$	Ph	Me	(*R*,*R*,*S*)	36 (*R*)	48 (*R*)	24 (*R*)
3	$\mathbf{L_{33}}$	Ph	Et	(*S*,*R*,*S*)	32 (*R*)	11 (*R*)	35 (*R*)
4	$\mathbf{L_{34}}$	Ph	Et	(*R*,*R*,*S*)	33 (*R*)	49 (*R*)	27 (*R*)
5	$\mathbf{L_{35}}$	Ph	Me	(*R*,*S*,*S*)	59 (*R*)	41 (*R*)	37 (*R*)
6	$\mathbf{L_{36}}$	Cy	Me	(*S*,*S*,*S*)	19 (*R*)	2 (*R*)	31 (*R*)
7	$\mathbf{L_{37}}$	Cy	Me	(*R*,*S*,*S*)	65 (*R*)	46 (*R*)	40 (*R*)

[a] Reaction conditions: Rh/substrate = 1:30, H_2 = 1.2 bar, *T* = 25 °C, *t* = 16 h, 0.5 mL of THF, quantitative conversion in all cases, conversion was determined by GC. [b] Enantiomeric excess of product determined by chiral GC (absolute configuration drawn in parenthesis).

$\mathbf{S_1}$: Permabond-L-Chirasil-Val column: T_0 = 90 °C, ΔT = 8 °C min^{-1} to 170 °C, t_R ($\mathbf{S_1}$) = 2.3 min, t_R (*R*) = 3.2 min, t_R (*S*) = 3.5 min.

$\mathbf{S_2}$: Permabond-L-Chirasil-Val column: T_0 = 90 °C, ΔT = 8 °C min^{-1} to 150 °C, hold for 15 min, then ΔT = 8 °C min^{-1} to 180 °C, hold for 15 min, t_R (*R*) = 13.2 min, t_R (*S*) = 14.4 min, t_R ($\mathbf{S_2}$) = 26.3 min.

$\mathbf{S_4}$: Macherey-Nagel HYDRODEX β-TBDAc column (50 m, 0.25 mm, 0.1 µm): T_0 = 115 °C, hold for 20 min, ΔT = 6 °C min^{-1} to 180 °C, then hold for 20 min, t_R (*R*) = 7.8 min, t_R (*S*) = 8.1 min, t_R ($\mathbf{S_4}$) = 10.7 min.

$\mathbf{S_5}$: Macherey-Nagel HYDRODEX β-TBDAc column (50 m, 0.25 mm, 0.1 µm): T_0 = 120 °C, hold for 40 min, ΔT = 6 °C min^{-1} to 180 °C, then hold for 10 min, t_R (*R*) = 67.4 min, t_R (*S*) = 68.5 min, t_R ($\mathbf{S_5}$) = 76.1 min.

General Procedure for Continuously Operated Asymmetric Hydrogenation Experiments

Reactor Description

The reactor setup (chapter 2.4.2, Figure 13) is custom-made and all parts (piping, filters, connectors, valves) were purchased from Swagelok or Hoke. A stainless steel cylinder was charged with hydrogen gas with a pressure up to 290 bar. Connected to the hydrogen supply, a Bronkhorst F231-M-RAD-11-Z mass flow controller delivered a selected hydrogen flow (5 $mL \cdot min^{-1}$), which is calibrated at 0 °C and 1 bar. Equipped with a non-return valve, liquids in the gas supply piping were avoided. With a Gilson 305 HPLC pump, substrate stock solution of **S_3** in THF (0.5 M) was pumped into the piping and mixed with hydrogen gas prior entering the reactor. At room temperature, the mixture of feed solution and hydrogen passed the loaded reactor, while the system pressure of 1 bar was maintained by a Jasco BP-2080 Plus automatic back pressure regulator. An additional filter was installed behind the reactor to avoid resin and glass wool particles to pass through the back pressure regulator. The product/substrate stream was collected in vials and the conversion and selectivity was analyzed by chiral GC.

Reactor Preparation

In a glove box, one end of the stainless steel reactor tube (V = 0.65 cm^3) was plugged with glass wool and capped with a sintered filter element. The open end of the reactor was loaded with preformed resin-bound catalyst of ligand **L_1** (50 mg) and plugged with glass wool. Preformation was accomplished following the procedure for *in-situ* complexation. Prior to assembling the reactor, the reactor pipes were flushed with hydrogen gas (10 $mL \cdot min^{-1}$) for 15 minutes. The HPLC pump tubing was flushed with nitrogen for 15 minutes. Next, the reactor was assembled, the hydrogen gas flow was set to 5 $mL \cdot min^{-1}$ with the back pressure regulator set to 1 bar and a substrate flow rate of 0.05-0.2 $mL \cdot min^{-1}$ was applied.

2.7 References

[1] a) H. U. Blaser, E. Schmidt, in *Asymmetric Catalysis on Industrial Scale* (Eds.: H. U. Blaser, E. Schmidt), Wiley-VCH Verlag GmbH & Co. KGaA, Weinheim, **2004**; b) I. Ojima, *Catalytic asymmetric synthesis*, 3rd ed., John Wiley & Sons, Inc., Hoboken, **2010**; c) C. A. Busacca, D. R. Fandrick, J. J. Song, C. H. Senanayake, *Adv. Synth. Catal.* **2011**, *353*, 1825-1864.

[2] T. P. Yoon, E. N. Jacobsen, *Science* **2003**, *299*, 1691-1693.

[3] V. A. Pavlov, *Tetrahedron* **2008**, *64*, 1147-1179.

[4] a) T. G. Appleton, H. C. Clark, L. E. Manzer, *Coord. Chem. Rev.* **1973**, *10*, 335-422; b) G. Helmchen, A. Pfaltz, *Acc. Chem. Res.* **2000**, *33*, 336-345; c) J. Wassenaar, J. N. H. Reek, *Org. Biomol. Chem.* **2011**, *9*, 1704-1713.

[5] A. Börner, *Phosphorus Ligands in Asymmetric Catalysis: Synthesis and Applications*, Wiley-VCH, Weinheim, **2008**.

[6] N. Sakai, S. Mano, K. Nozaki, H. Takaya, *J. Am. Chem. Soc.* **1993**, *115*, 7033-7034.

[7] M. J. Baker, P. G. Pringle, *J. Chem. Soc., Chem. Commun.* **1993**, 314-316.

[8] H. Fernández-Pérez, P. Etayo, A. Panossian, A. Vidal-Ferran, *Chem. Rev.* **2011**, *111*, 2119-2176.

[9] N. Llorente, H. Fernández-Pérez, L. Núñez-Rico José, L. Carreras, A. Martínez-Carrión, E. Iniesta, A. Romero-Navarro, A. Martínez-Bascuñana, A. Vidal-Ferran, in *Pure Appl. Chem., Vol. 91*, **2019**, pp. 3-15.

[10] M. Diéguez, O. Pàmies, C. Claver, *Chem. Rev.* **2004**, *104*, 3189-3216.

[11] a) S. Deerenberg, P. C. J. Kamer, P. W. N. M. van Leeuwen, *Organometallics* **2000**, *19*, 2065-2072; b) S. Deerenberg, H. S. Schrekker, G. P. F. van Strijdonck, P. C. J. Kamer, P. W. N. M. van Leeuwen, J. Fraanje, K. Goubitz, *J. Org. Chem.* **2000**, *65*, 4810-4817; c) S. Deerenberg, O. Pàmies, M. Diéguez, C. Claver, P. C. J. Kamer, P. W. N. M. van Leeuwen, *J. Org. Chem.* **2001**, *66*, 7626-7631; d) H. Fernández-Pérez, M. A. Pericàs, A. Vidal-Ferran, *Adv. Synth. Catal.* **2008**, *350*, 1984-1990; e) I. Arribas, S. Vargas, M. Rubio, A. s. Suárez, C. Domene, E. Álvarez, A. Pizzano, *Organometallics* **2010**, *29*, 5791-5804; f) C. Hegedüs, H. Gulyás, Á. Szöllősy, J. Bakos, *Inorg. Chim. Acta* **2009**, *362*, 1650-1654.

[12] a) A. Suárez, M. A. Méndez-Rojas, A. Pizzano, *Organometallics* **2002**, *21*, 4611-4621; b) M. Renom-Carrasco, L. Lefort, *Chem. Soc. Rev.* **2018**, *47*, 5038-5060.

[13] T. Robert, Z. Abiri, J. Wassenaar, A. J. Sandee, S. Romanski, J.-M. Neudörfl, H.-G. Schmalz, J. N. H. Reek, *Organometallics* **2010**, *29*, 478-483.

[14] a) A. Suárez, A. Pizzano, *Tetrahedron: Asymmetry* **2001**, *12*, 2501-2504; b) S. Vargas, M. Rubio, A. Suárez, D. del Río, E. Álvarez, A. Pizzano, *Organometallics* **2006**, *25*, 961-973.

[15] H. Fernandez-Perez, S. M. Donald, I. J. Munslow, J. Benet-Buchholz, F. Maseras, A. Vidal-Ferran, *Chem. Eur. J.* **2010**, *16*, 6495-6508.

[16] M. C. Samuels, B. H. G. Swennenhuis, P. C. J. Kamer, *Solid-phase Synthesis of Ligands*, in *Phosphorus(III) Ligands in Homogeneous Catalysis: Design and Synthesis* (Eds.: P. C. J. Kamer, P. W. N. M. v. Leeuwen), John Wiley & Sons, Ltd, Chichester, **2012**, pp. 463-479.

[17] a) R. den Heeten, B. H. G. Swennenhuis, P. W. N. M. van Leeuwen, J. G. de Vries, P. C. J. Kamer, *Angew. Chem.* **2008**, *120*, 6704-6707; b) F. J. Heutz, P. C. Kamer, *Dalton Trans.* **2016**, *45*, 2116-2123.

[18] a) D. J. Cole-Hamilton, *Science* **2003**, *299*, 1702-1706; b) D. J. Cole-Hamilton, R. P. Tooze, *Homogeneous Catalysis - Advantages and Problems*, in *Catalyst*

Separation, Recovery and Recycling: Chemistry and Process Design (Eds.: D. J. Cole-Hamilton, R. P. Tooze), Springer Netherlands, Dordrecht, **2006**, pp. 1-8.
[19] a) G. Franciò, W. Leitner, *Chem. Commun.* **1999**, 1663-1664; b) G. Franciò, K. Wittmann, W. Leitner, *J. Organomet. Chem.* **2001**, *621*, 130-142.
[20] P. Kleman, P. Barbaro, A. Pizzano, *Green Chem.* **2015**, *17*, 3826-3836.
[21] a) K. Nozaki, Y. Itoi, F. Shibahara, E. Shirakawa, T. Ohta, H. Takaya, T. Hiyama, *J. Am. Chem. Soc.* **1998**, *120*, 4051-4052; b) K. Nozaki, F. Shibahara, Y. Itoi, E. Shirakawa, T. Ohta, H. Takaya, T. Hiyama, *Bull. Chem. Soc. Jpn.* **1999**, *72*, 1911-1918.
[22] a) F. M. Akwi, P. Watts, *Chem. Commun.* **2018**, *54*, 13894-13928; b) C. G. Frost, L. Mutton, *Green Chem.* **2010**, *12*, 1687-1703; c) A. Kirschning, W. Solodenko, K. Mennecke, *Chem. Eur. J.* **2006**, *12*, 5972-5990; d) S. G. Newman, K. F. Jensen, *Green Chem.* **2013**, *15*, 1456-1472; e) C. Wiles, P. Watts, *Eur. J. Org. Chem.* **2008**, *2008*, 1655-1671.
[23] a) K. Burgemeister, G. Franciò, V. H. Gego, L. Greiner, H. Hugl, W. Leitner, *Chem. Eur. J.* **2007**, *13*, 2798-2804; b) J. Madarász, B. Nánási, J. Kovács, S. Balogh, G. Farkas, J. Bakos, *Monatsh. Chem.* **2017**, *149*, 19-25.
[24] a) F. J. L. Heutz, M. C. Samuels, P. C. J. Kamer, *Catal. Sci. Technol.* **2015**, *5*, 3296-3301; b) M. C. Samuels, F. J. L. Heutz, A. Grabulosa, P. C. J. Kamer, *Top. Catal.* **2016**, *59*, 1793-1799.
[25] M. C. Samuels, P. C. J. Kamer, *PhD Thesis* **2014**.
[26] G. Muller, D. Sainz, *J. Organomet. Chem.* **1995**, *495*, 103-111.
[27] F. Fischer, *Z. Chem.* **1962**, *2*, 297-302.
[28] H. Fernández-Pérez, P. Etayo, J. L. Núñez-Rico, B. Balakrishna, A. Vidal-Ferran, *RSC Adv.* **2014**, *4*, 58440-58447.
[29] M. Rubio, S. Vargas, A. Suarez, E. Alvarez, A. Pizzano, *Chem. Eur. J.* **2007**, *13*, 1821-1833.
[30] a) Z. Hua, V. C. Vassar, I. Ojima, *Org. Lett.* **2003**, *5*, 3831-3834; b) K. N. Gavrilov, S. V. Zheglov, P. A. Vologzhanin, E. A. Rastorguev, A. A. Shiryaev, M. G. Maksimova, S. E. Lyubimov, E. B. Benetsky, A. S. Safronov, P. V. Petrovskii, V. A. Davankov, B. Schäffner, A. Börner, *Russ. Chem. Bull.* **2009**, *57*, 2311-2319.
[31] K. Burgess, M. J. Ohlmeyer, K. H. Whitmire, *Organometallics* **1992**, *11*, 3588-3600.
[32] G. Farkas, S. Balogh, Á. Szöllősy, L. Ürge, F. Darvas, J. Bakos, *Tetrahedron: Asymmetry* **2011**, *22*, 2104-2109.
[33] G. T. Whiteker, A. M. Harrison, A. G. Abatjoglou, *J. Chem. Soc., Chem. Commun.* **1995**, 1805-1806.
[34] M. T. Reetz, T. Neugebauer, *Angew. Chem.* **1999**, *38*, 179-181.
[35] G. J. H. Buisman, L. A. van der Veen, A. Klootwijk, W. G. J. de Lange, P. C. J. Kamer, P. W. N. M. van Leeuwen, D. Vogt, *Organometallics* **1997**, *16*, 2929-2939.
[36] H. Fernández-Pérez, J. R. Lao, A. Vidal-Ferran, *Org. Lett.* **2016**, *18*, 2836-2839.
[37] I. Arribas, M. Rubio, P. Kleman, A. Pizzano, *J. Org. Chem.* **2013**, *78*, 3997-4005.
[38] B. Zhang, H. Jiao, D. Michalik, S. Kloß, L. M. Deter, D. Selent, A. Spannenberg, R. Franke, A. Börner, *ACS Catal.* **2016**, *6*, 7554-7565.
[39] H. Fernández-Pérez, B. Balakrishna, A. Vidal-Ferran, *Eur. J. Org. Chem.* **2018**, *2018*, 1525-1532.
[40] X.-S. Chen, C.-J. Hou, X.-P. Hu, *Synth. Commun.* **2016**, *46*, 917-941.
[41] K. Asakawa, N. Sawada, T. Tsuritani, T. Itoh, T. Mase, K. Takahashi, F. Xu, N. Yoshikawa, *WO2009041475A1*, **2009**.

[42] J. Scherer, G. Huttner, M. Büchner, J. Bakos, *J. Organomet. Chem.* **1996**, *520*, 45-58.
[43] B. F. Straub, M. Wrede, K. Schmid, F. Rominger, *Eur. J. Inorg. Chem.* **2010**, *2010*, 1907-1911.

Chapter 3

A Supported PNP-Pincer Ligand Library for Applications in Ester Hydrogenation

Abstract: *The catalytic hydrogenation of carboxylic acid esters is a more environmentally benign alternative for the production of fine chemicals, pharmaceuticals and fragrances compared to stoichiometric hydride reductions. Usually, heterogeneous catalysts applied in industrial processes require harsh conditions (>200 °C, >100 bar) resulting in reduced selectivities. In contrast, well-defined homogeneous catalysts show much better performances but often suffer from poor reusability. Herein, we report a facile solid-phase synthesis approach towards a diverse PNP-pincer ligand library of 14 members. A series of less studied non-symmetrical ligands can be efficiently accessed in high purity requiring only simple work-up procedures. The corresponding supported ruthenium-PNP catalysts are screened in the selective hydrogenation of mono-, and diesters as well as lactones under mild conditions and compared to homogeneous analogues. Preliminary attempts towards facilitated catalyst recovery and recycling are presented.*

3.1 Introduction

Since the pioneering work of Shaw and van Koten in the 1970s,[1] terdentate pincer-type ligands have attracted tremendous attention for applications in a broad range of challenging catalytic transformations. The term pincer was initially referred to a central anionic carbon donor flanked by two lateral donor moieties in *ortho*-position enforcing a meridional coordination geometry towards the metal center.[2] The pincer terminology, however, has since been generalized referring to terdentate ligands with aromatic or aliphatic backbones commonly coordinating in a meridional fashion. In contrast to many privileged mono- and bidentate ligands, this rigid structural motif often results in high thermal and chemical robustness preventing dissociation of the metal from the ligand. Advantageously, the modular nature of pincer ligands allows for efficient fine-tuning of the electronic and steric properties (Figure 1).[3]

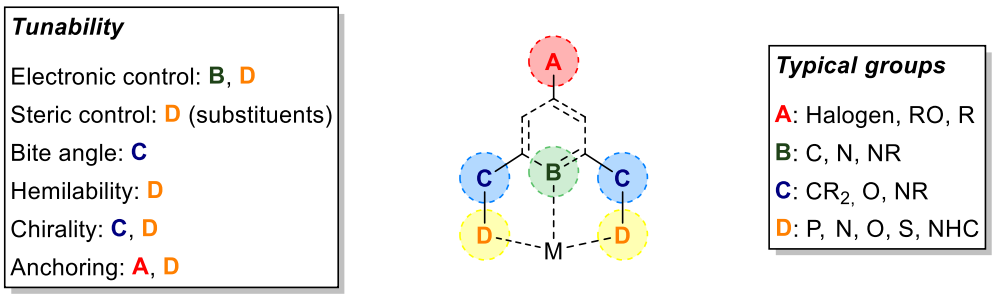

Figure 1 Modular structure and tunability of pincer-type complexes

Subtle changes in the properties of the donor atoms **B** and **D** can have a profound influence on the catalyst reactivity. Additionally, the bite angle is controlled via the size of the linkers **C**, which further enable the introduction of chirality in addition to the donor entities **D** via substituents or chiral phosphorus centers. When considering potential tethering of the molecularly defined pincer-based complex to a support, both the flanking donor atoms **D** as well as a substituent **A** located at the central aromatic ring could provide suitable anchoring groups. Moreover, the reversible dissociation of one side arm from the metal center unit, commonly referred to as hemilability,[4] can be tailored by structural modification of **D**. This in turn offers a vacant coordination site for substrate binding at the active center with the dissociated side arm remaining in close proximity opposed to mono-and bidentate ligands.[5] However, the concept of hemilability usually requires the tridentate ligand structure to be composed of two different donor moieties **D** exerting dissimilar electronic properties. Thus, non-

symmetrical PNN pincer ligands containing a hemilabile nitrogen donor atom have been widely employed for a plethora of catalytic applications.[5b,6]

Despite the modular structure of pincer-type ligands, the development and application of unsymmetrical PNP-type ligands, which occupy a central N-donor and two phosphorus moieties differing in both electronic and steric properties, remain limited to a few reports. Some representative examples are depicted in Figure 2.

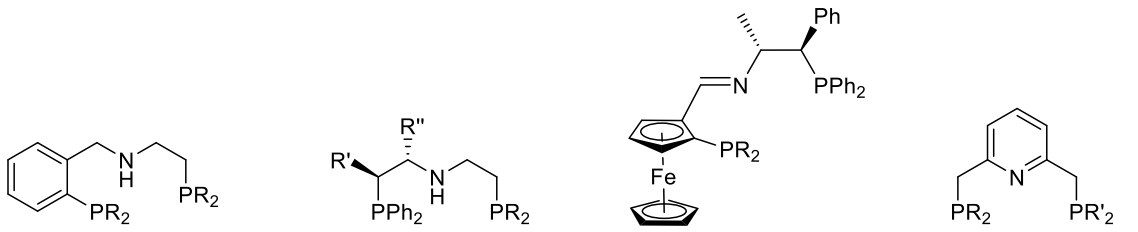

I

II: R = ^{i}Pr, R', R'' = Ph
III: R = ^{i}Pr, R' = Ph, R'' = H
IV: R = ^{i}Pr, R' = ^{i}Pr, R'' = H
V: R = Cy, R', R'' = Ph

VI: R = ^{i}Pr
VII: R = Ph
VIII: R = Cy

IX: R = ^{t}Bu, R' = Ad
X: R = Ph, R' = ^{t}Bu
XI: R = ^{t}Bu, R' = ^{i}Pr
XII: R = ^{t}Bu, R' = Cy

Figure 2 Representative examples of non-symmetrical PNP pincer ligands.

The research groups of Hayashi[7], Morris[8] and Milstein[9] reported on the non-symmetrical ligand motif **I** containing two identical phosphine moieties bound to the central NH-group via an ethylene and an *ortho*-phenylene linker. When employed as their corresponding Fe(II) complexes, high performances in reductive coupling of nitriles and terminal amines to form secondary imines were observed.[9] Chiral PNP ligands (**II**-**V**) composed of different phosphine donor groups bearing both phenyl and alkyl-based substituents resulted in high selectivity of up to 96% *ee* in Fe-catalyzed asymmetric ketone reduction.[10] Next to this motif, additional planar chirality via a ferrocene unit combined with *C*-chirality in the aliphatic imine backbone structure of ligands **VI**-**VIII** enabled selectivities of up to 86% *ee* in asymmetric ketone hydrogenation.[11] Kinoshita *et al.* employed unsymmetrical pyridine-based PNP pincer ligands **IX**-**XII** in molybdenum-catalyzed ammonia production from N_2.[12] The ligands were synthesized starting from 2,6-lutidine, which, upon lithiation, undergoes monosubstitution using a suitable chlorophosphine. The second phosphorus moiety could be introduced via substitution of the remaining methyl group. However, opposed to the straightforward disubstitution of the pyridine backbone in case of symmetrical PNP ligands, laborious and often troublesome work-up procedures are required to

isolate the air and moisture sensitive PN intermediates and final PNP ligands resulting in low overall yields. This calls for more efficient synthetic protocols to access large PNP-type ligand libraries allowing subsequent catalyst screening in various applications. Modular approaches towards symmetrical pyridine-based PNP pincer ligands have been explored by the group of Kirchner by introducing a wide range of substituted phosphorus moieties to a 2,6-diaminopyridine.[13] However, methodologies for combinatorial libraries of unsymmetrical PNP ligand-based catalysts remain elusive often due to intrinsically challenging syntheses and work-up procedures.

Solid-phase synthesis (SPS) offers an attractive alternative approach to traditional synthesis in monophasic systems (see chapter 1). When applied in a combinatorial fashion, a large PNP ligand library can be obtained in high purity and yield by allowing the use of excess reagents to ensure full conversion and requiring only simple purification steps.[14] Through systematic variation of the phosphine moieties, the electronic and steric ligand properties can be easily fine-tuned for catalyst optimization. The immobilization of a well-defined molecular catalyst on an insoluble polymeric support combines the advantages of both worlds, i.e. high activity, selectivity and tunability of homogeneous catalysts and the recoverability and recyclability of heterogeneous catalysts.[15] In particular the recycling of these expensive and often toxic transition-metals and ligands can be truly simplified when anchored to a support.

Despite the wide applicability of PNP pincer-based catalysts, approaches towards immobilization strategies remain fairly limited. In 2017, Goni *et al.* reported on a Ru-PONOP-type catalyst supported on a silica poly(allylamine) composite via a two-step Mannich reaction yielding two regioisomers covalently bound to the solid in both *ortho*- and *meta*-position of the central pyridine ring (**XIII**, Figure 3).[16] However, attempting a sequential build-up of the catalyst on the support resulted in the formation and deposition of side-products within the polyamine scaffold. When **XIII** was applied in dehydrogenative coupling of alcohols at high temperatures, moderate yields accompanied by poor recyclability due to constant metal leaching were obtained.[17] Wang *et al.* employed a ‘knitting’ strategy by anchoring the solution-phase PNP catalyst **XIV** covalently to the structure of a porous organic polymer for application in dehydrogenation of formic acid.[18] For this bottom-up approach, the external crosslinking agent dimethoxymethane was utilized to join the phenyl moieties of **XIV** with benzene molecules via a Friedel-Crafts alkylation.

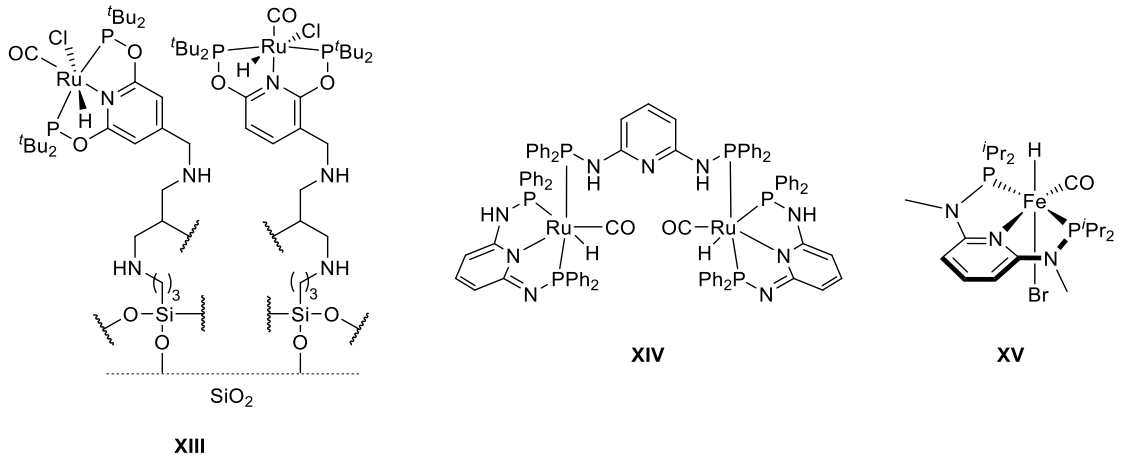

Figure 3 Representative examples of supported PNP pincer-based catalysts.

In case of the Fe(II) PNP pincer **XV** reported by Kirchner and co-workers in 2018, the homogeneous catalyst was immobilized in ionic liquids deposited on both silica[19] and polymer-based spherical activated carbon.[20] By using this supported ionic liquid phase (SILP) strategy, the immobilized catalyst was applied in the hydrogenation of aldehydes. All of the thus far reported examples of supported PNP-type ligands are cases where a single premade complex is immobilized. Hence, a more versatile and combinatorial methodology that allows for the facile synthesis of a whole library of variable PNP-type ligands would be highly desirable.

As mentioned previously, pincer-type ligands have contributed tremendously to environmentally benign, homogeneously catalyzed reductions of challenging compounds employing molecular hydrogen as an atom-economical reducing agent.[5b,21] In particular, the reduction of carboxylic acids and their ester derivatives to the corresponding alcohols represents a crucial transformation in organic synthesis for both laboratory as well as bulk and fine chemical scale in industry.[22] Common synthetic methods often rely on the use of stoichiometric amounts of metal hydrides such as $LiAlH_4$ and $NaBH_4$,[23] which is accompanied by the danger in handling as well as the generation of large amounts of inorganic waste products.[24] In industrial applications, heterogeneous catalysts require harsh reaction conditions (250-350 °C at 100-200 bar) often leading to unselective side-product formation and limiting functional group tolerance.[25] Consequently, there has been a strong drive from both academia and industry to develop molecularly well-defined homogeneous catalysts for selective catalytic hydrogenation under milder conditions.[21d]

Since the ground-breaking work of Milstein in 2006 on non-innocent dearomatized pyridine-based PNN (**XVI**) and PNP (**XVII**) ligands in Ru-catalyzed ester

hydrogenation (Figure 4),[6b] a plethora of catalysts based on pincer ligands has been developed. While most of these homogeneous catalysts commonly employ precious metals, the use of more earth-abundant metals, such as Fe, Mn and Co, has also been described in recent studies.[21b] Representative examples of PNP pincer-based catalysts used in ester hydrogenation are depicted in Figure 4. Especially aliphatic PNP ligands employed in catalysts such as the ruthenium PNP pincer complex Ru-MACHO (**XVIII**) developed at Takasago[26] and its analogues based on iron (**XIX**)[27] and cobalt (**XX**),[28] have demonstrated exceptional performances in the reduction of esters.

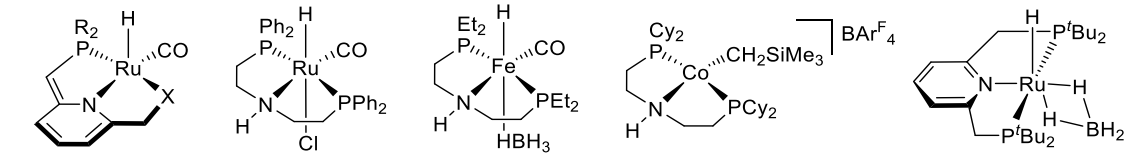

XVI: R = ^{t}Bu, X = NEt_2
XVII: R = ^{i}Pr, X = P^iPr_2

XVIII **XIX** **XX** **XXI**

Figure 4 Representative examples of pincer ligands used in catalytic ester hydrogenation.

However, catalysts derived from pyridine-based PNP pincer ligands remain limited to **XVII** and its ruthenium(II) hydrido borohydride analogue **XXI** both developed by Milstein and co-workers.[6b,29] When employed in the catalytic reduction of esters, both symmetrical catalysts revealed significantly less activity compared to their unsymmetrical PNN analogues. Consequently, this was associated with the lack of hemilability of one of the side arms due to two equally strong electron-donating phosphorus moieties present in both complexes.

In this chapter, the first facile solid-phase synthesis of a combinatorial library of non-symmetrical pyridine-based PNP pincer ligands is presented. The main goal is a systematical variation of building blocks in order to efficiently fine-tune the electronic and steric properties of the resulting ligands. Building on the previous success of immobilized PNN ligands applied in Ru-catalyzed ester reduction under very mild conditions reported by the Kamer group, the use of the corresponding resin-bound Ru-PNP catalyst library in ester hydrogenation of various lactones, mono- and diesters is described.[30] Finally, the facilitated recovery and recycling of the supported Ru-PNP catalysts will be demonstrated.

3.2 Solid-Phase Synthesis of PNP Ligand Library

In analogy to the modular solid-phase synthesis of bidentate POP ligands presented in the previous chapter 2, a combinatorial approach was chosen for the preparation of polymer supported PNP-type pincer ligands. Building on initial synthetic attempts performed within the Kamer group, the resin-bond secondary phosphine **1a·BH$_3$** was chosen as a suitable starting point for the proposed modular sequence (Scheme 1).[31]

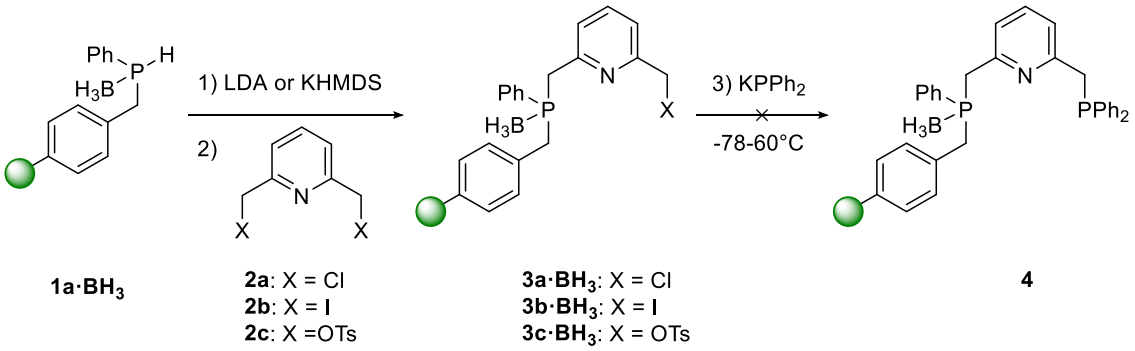

Scheme 1 Proposed modular solid-phase synthesis of supported PNP pincer ligand **4**.

Since in previous endeavors issues with overlaying signals in the gel-phase ^{31}P NMR spectra were encountered when using the free secondary phosphine **1a**, it was decided to modify the resin-bound synthon with a BH_3 group to ensure proper peak separation. Upon deprotonation of **1a·BH$_3$** using an excess of LDA or KHMDS, the corresponding resin-bound lithium or potassium phosphide (**Li·1a·BH$_3$**, **K·1a·BH$_3$**) was obtained. Next, the deprotonated species was treated with a slight excess of three different 2,6-dimethylpyridine derivatives (**2a-c**) functionalized with chloride (**2a**), iodide (**2b**) or tosylate (OTs, **2c**) leaving groups on each methyl substituent of the pyridine moiety. The successful introduction of the resin-bound PN fragments (**3a-c·BH$_3$**) could be confirmed by gel-phase ^{31}P NMR as representatively depicted in Figure 5 for **3a·BH$_3$**. Quantitative consumption of **K·1a·BH$_3$** and a significant change in chemical shift of almost $\Delta\delta = 56$ ppm was observed. In order to install the second phosphine moiety at the remaining methyl linker of the resin-bound PN fragment, **3a-c·BH$_3$** were reacted with an excess of potassium diphenylphosphide. However, when the reaction was allowed to warm up from -78 °C to room temperature, only ~10% substitution of the free methyl linker was observed for **3a·BH$_3$** (see Figure 5, top spectrum, after washing).

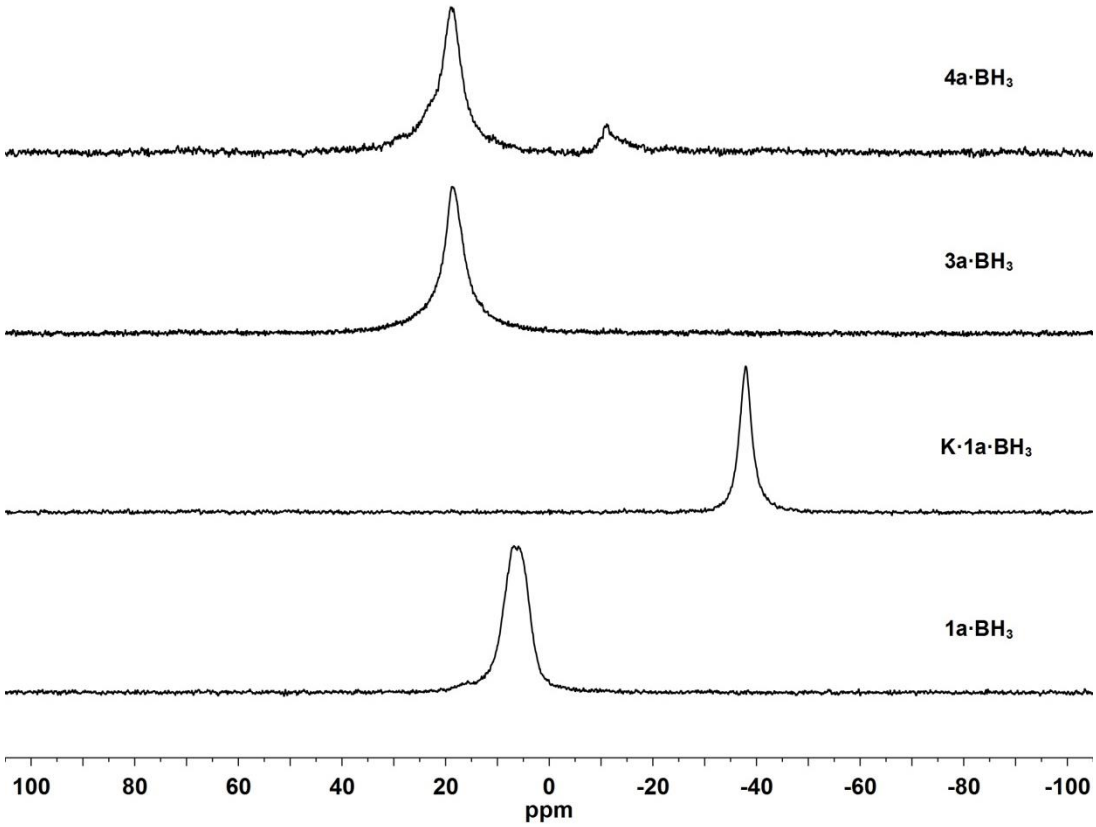

Figure 5 Attempted solid-phase synthesis of supported PNP ligand **4** monitored by ^{31}P NMR.

With additional equivalents of $KPPh_2$ as well as elevated temperatures, the reaction did not seem to proceed towards the desired resin-bound PNP ligand **4a·BH$_3$**. Instead, mainly BH_3 removal of the first phosphine moiety together with decomposition of the PN fragment was obtained. Likewise, the nature of the leaving group (I, OTs) did not lead to higher conversion.

Hence, an alternative synthetic route was chosen combining both a solid- and solution-phase strategy to access a combinatorial resin-bound PNP pincer library. Therefore, a PN building block was prepared homogeneously prior to linking it to the secondary phosphine on the support. Adapting a procedure from Gagir *et al.* gave access to eight different 2-(chloromethyl)-6-(phosphinomethyl) pyridine borane adducts (**5a-h**).[32] 2,6-bis(chloromethyl)pyridine was treated with 1.0 equivalent of a freshly prepared lithium boranyl phosphanide bearing various combinations of substituents R^2 and R^3 attached to the phosphorus moiety (Scheme 2). A series of both aromatic- (Ph, 4-MeOPh, 4-ClPh) and alkyl-based (Cy, ^{i}Bu, ^{t}Bu, Ad) substituents were employed as well as phosphine-boranes with mixed substituents (Ph and ^{t}Bu, **5g**). Table 1 summarizes the chemical shifts in the corresponding ^{31}P NMR spectra of **5a-h**.

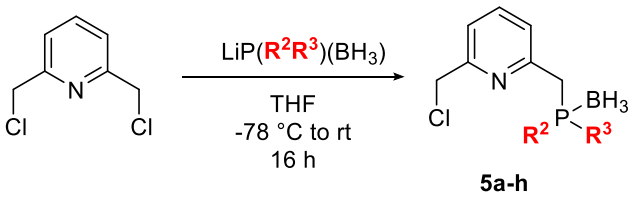

5a-h

5a: R^2 = R^3 = Ph (36%)
5b: R^2 = R^3 = 4-MeOPh (53%)
5c: R^2 = R^3 = 4-ClPh (16%)
5d: R^2 = R^3 = Cy (20%)
5e: R^2 = R^3 = ^{i}Bu (20%)
5f: R^2 = R^3 = ^{t}Bu (57%)
5g: R^2 = Ph, R^3 = ^{t}Bu (67%)
5h: R^2 = R^3 = Ad (67%)

Scheme 2 Synthesis of PN fragments **5a-h**.

This systematic variation of substituents enables an efficient tuning of the steric and electronic properties of the phosphorus donor atom. Due to the presence of mono- and di-substituted product together with unreacted starting material in the reaction mixture, which often required up to two column chromatographic work-up steps, only low to moderate yields of the desired mono-substituted phosphine boranes were obtained. Alternatively, a mixture of mono- and disubstituted products could be used in the next step as only the desired monosubstituted PN fragment reacts with the support while the unreacted by-product present in the supernatant solution can be easily filtered off. However, an optimized synthetic protocol would be still desirable, which could employ two different leaving groups on the 2,6-dimethylpyridine scaffold ensuring preferential mono-substitution.

Table 1 Summary of chemical shifts in the ^{31}P NMR spectra of compounds **5a-h**.

Compound	Substituents		$\Delta\delta$ (^{31}P NMR)
	R^2	R^2	[ppm][a]
5a	Ph	Ph	18.1
5b	4-MeOPh	4-MeOPh	15.6
5c	4-ClPh	4-ClPh	18.3
5d	Cy	Cy	28.4
5e	^{i}Bu	^{i}Bu	15.9
5f	^{t}Bu	^{t}Bu	47.3
5g	Ph	^{t}Bu	33.3
5h	Ad	Ad	38.0

[a] Recorded at 162 MHz in $CDCl_3$. Broad multiplets were obtained in all cases.

The starting synthon of the solid-phase synthesis is a secondary phosphine-borane (**1a-d·BH$_3$**) immobilized on Merrifield resin cross-linked with 1% divinylbenzene (DVB, MF, n = 1), Merrifield resin cross-linked with 4% DVB (MF 4% DVB, n = 1) and polystyrene (PS, n = 0) prepared as reported previously by our group.[31,33] The deprotonated BH$_3$-protected resin-bound potassium phosphides (**K·1a-d·BH$_3$**) were yielded as yellow-orange colored resins when using an excess of potassium bis(trimethylsilyl)amide (KHMDS) as the base of choice (Scheme 3, step 1).

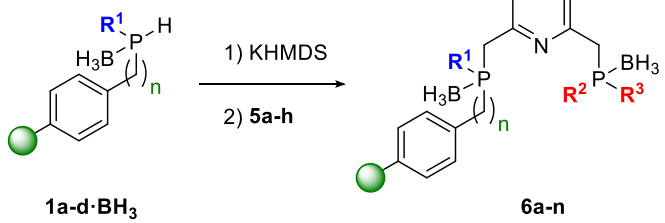

1a-d·BH$_3$ **6a-n**

1a·BH$_3$: **MF**, n = 1, **R^1** = Ph
1b·BH$_3$: **MF** 4% DVB, n = 1, **R^1** = Ph
1c·BH$_3$: **MF**, n = 1, **R^1** = Cy
1d·BH$_3$: **PS**, n = 0, **R^1** = ^{t}Bu

6a: **MF**, **R^1** = Ph, **R^2** = **R^3** = Ph
6b: **MF**, **R^1** = Ph, **R^2** = **R^3** = 4-MeOPh
6c: **MF**, **R^1** = Ph, **R^2** = **R^3** = 4-ClPh
6d: **MF**, **R^1** = Ph, **R^2** = **R^3** = Cy
6e: **MF**, **R^1** = Ph, **R^2** = **R^3** = ^{i}Bu
6f: **MF**, **R^1** = Ph, **R^2** = **R^3** = ^{t}Bu
6g: **MF** 4% DVB, **R^1** = Ph, **R^2** = **R^3** = ^{t}Bu
6h: **MF** **R^1** = Ph, **R^2** = Ph , **R^3** = ^{t}Bu
6i: **MF**, **R^1** = Ph, **R^2** = **R^3** = Ad
6j: **MF** 4% DVB, **R^1** = Ph, **R^2** = **R^3** = Ad
6k: **MF**, **R^1** = Cy, **R^2** = **R^3** = Ph
6l: **MF**, **R^1** = Cy, **R^2** = **R^3** = ^{t}Bu
6m: **PS**, **R^1** = ^{t}Bu, **R^2** = **R^3** = ^{t}Bu
6n: **PS**, **R^1** = ^{t}Bu, **R^2** = Ph , **R^3** = ^{t}Bu

Scheme 3 Solid-phase synthesis of borane protected PNP ligands **6a-n**.

The reaction proceeded quantitatively at room temperature within an hour monitored by ^{31}P NMR. **K·1a·BH$_3$** bearing a phenyl group on the phosphorus atom exhibits a broad signal at δ = -37.1 ppm (Figure 6) similar to its analogue **K·1b·BH$_3$** supported on the 4% crosslinked Merrifield resin (-39.5 ppm). In case of cyclohexyl-substituted **K·1c·BH$_3$** the spectrum shows a resonance at -34.5 ppm whereas the phosphorus attached to a ^{t}Bu group (**K·1d·BH$_3$**) exhibits a signal at -14.6 ppm. Subsequently, a premade PN fragment (**5a-h**) was added to the immobilized secondary potassium phosphide (Scheme 3, step 2). Requiring only a slight excess of **5a-h**, quantitative conversion of the supported potassium phosphides to the bench-stable borane protected PNP ligands **6a-n** was obtained. After purification of the yellow resin with several washing cycles, the successful incorporation was confirmed by gel-phase ^{31}P NMR showing a second signal in an approximate 1:1 ratio with a chemical shift of the newly appearing peak equivalent to those reported for **5a-h** (see Table 1).

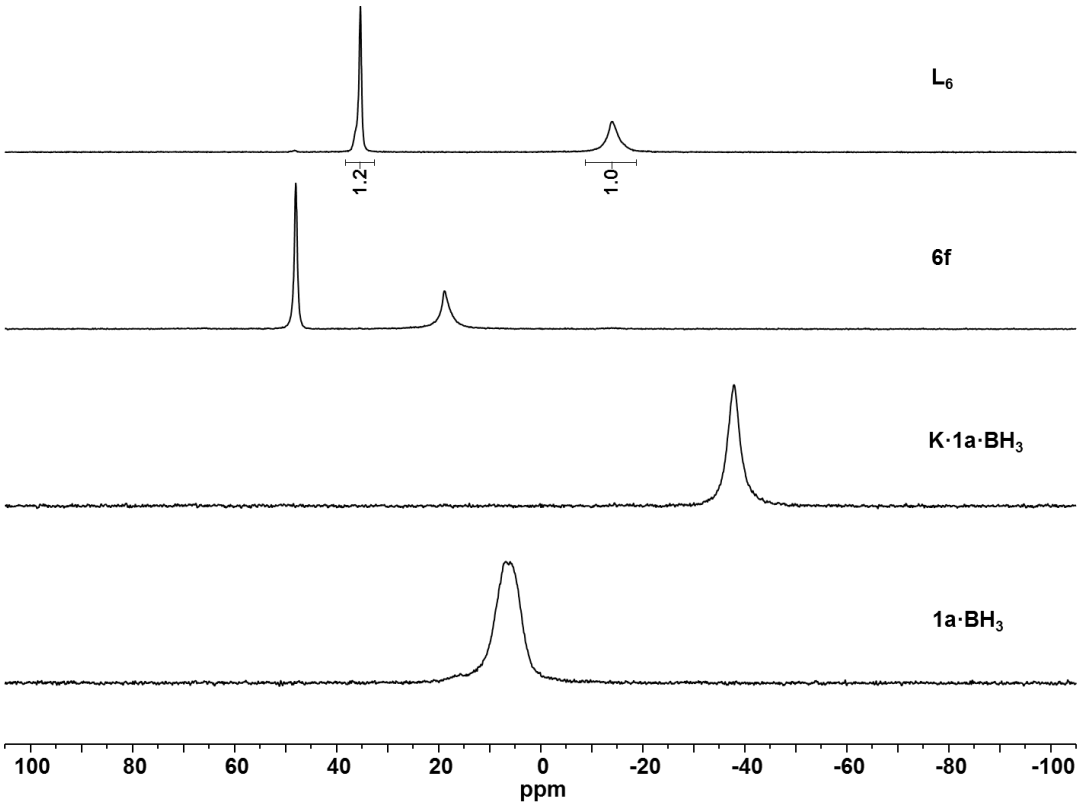

Figure 6 Solid-phase synthesis of supported PNP pincer ligand **L_6** monitored by ^{31}P NMR.

While the downfield shifted signal of the resin-bound phosphine group in close proximity to the support appears very broad, the second moiety shows a significantly sharper peak due to enhanced solution-like behavior (see Figure 6 for a representative example of **6f**). In the cases of **6a**, **6c** (Figure 7) and **6n**, similar chemical shifts for both phosphorus moieties are observed resulting in an overlap of the corresponding signals.

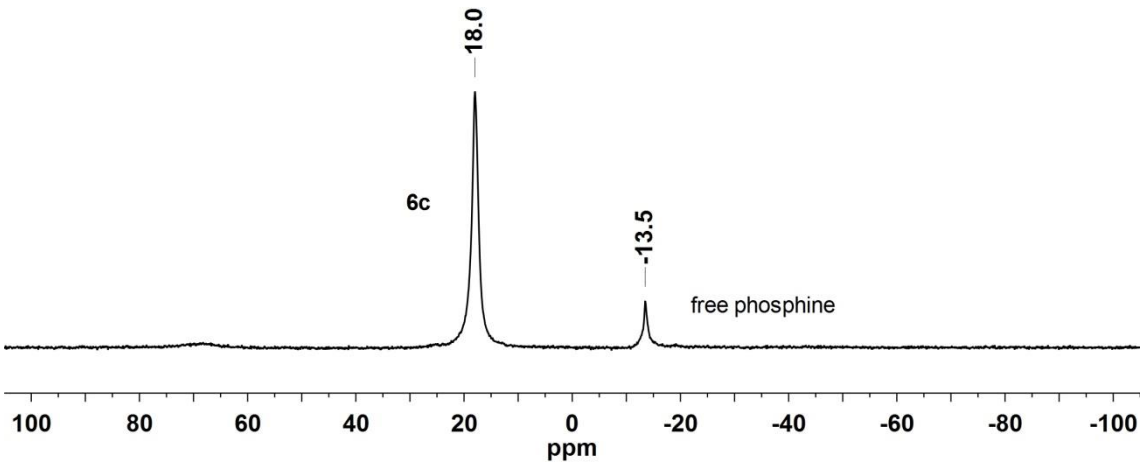

Figure 7 ^{31}P NMR spectrum of **6c** and 11% of free –P(4-ClPh)$_2$.

Furthermore, supported ligands bearing a remote PPh_2 (**6a** and **6k**) or a $P(4\text{-ClPh})_2$ moiety (**6c**) revealed a minor loss of BH_3 protection during this reaction indicated by the appearance of up to 11% of the free P-moiety at -13.5 ppm in case of **6c**. This can be attributed to the reduced basicity of the phosphorus center caused by more electron-withdrawing aryl substituents.[34]

Next, the removal of both borane groups for the synthesis of the resin-bound PNP pincer ligands $\mathbf{L_1}$-$\mathbf{L_{14}}$ was accomplished by treatment of **6a-n** with neat diethylamine at 50 °C (Scheme 4). In the presence of more bulky P^tBu_2 and PAd_2 groups, several replacements with fresh diethylamine as well as longer reaction times were required.

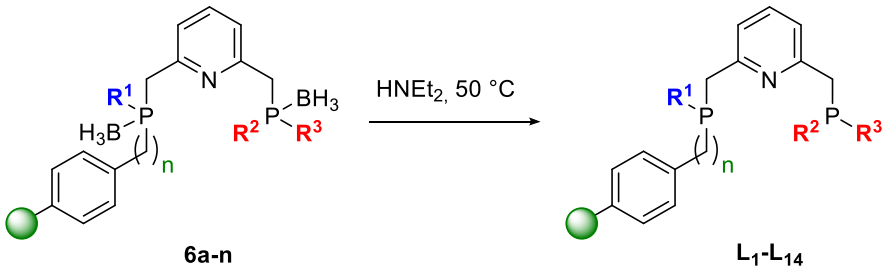

Scheme 4 Solid-phase synthesis of supported PNP pincer ligand library $\mathbf{L_1}$-$\mathbf{L_{14}}$.

Quantitative deprotection could be readily monitored and verified by ^{31}P NMR indicated by a significant upfield shift of all corresponding phosphorus signals. The representative synthesis of $\mathbf{L_6}$ followed by ^{31}P NMR is depicted in Figure 6. The chemical shifts of $\mathbf{L_1}$-$\mathbf{L_{14}}$ in the ^{31}P NMR are summarized in Table 2.

Through variation of the substituents $\mathbf{R^1}$, $\mathbf{R^2}$ and $\mathbf{R^3}$ bound to both phosphine entities as well as by employing three different types of polymeric supports, a large combinatorial library of supported PNP pincer ligands comprising 14 distinct members was achieved (Figure 8). In contrast to structurally similar homogeneous analogues, ligands $\mathbf{L_2}$-$\mathbf{L_{13}}$ represent non-symmetrical ligands which have been rarely investigated in solution-phase. However, the combination of two phosphorus moieties exhibiting different electronic and steric properties, and therefore *trans*-labilizing properties, offers great potential for efficient catalyst tuning. To date, only one unsymmetrical solution-phase analogue of $\mathbf{L_6}$ and $\mathbf{L_7}$ has been reported by Kinoshita *et al*. and applied in Mo-complexes.[12] Moreover, supported PNP ligands $\mathbf{L_1}$ and $\mathbf{L_{14}}$ represent symmetrical ligands, which can be compared to the homogeneous counterparts **XXII**[35] and **XXIII**[36] when neglecting the attachment to the polymeric support (Figure 9).

Table 2 Summary of chemical shifts in the ^{31}P NMR spectra of ligands **L_1-L_{14}**.[a]

Ligand	Substituents		^{31}P NMR (PR^1)	^{31}P NMR (PR^2R^3)
	R^1	R^2R^3	[ppm]	[ppm]
L_1	Ph	Ph	-14.0	-11.2
L_2	Ph	4-MeOPh	-14.0	-14.0
L_3	Ph	4-ClPh	-14.3	-13.3
L_4	Ph	Cy	-14.3	-13.3
L_5	Ph	^{i}Bu	-14.7	-33.4
L_6	Ph	^{t}Bu	-14.1	35.3
L_7	Ph	^{t}Bu	-14.3	35.0
L_8	Ph	Ph/^{t}Bu	-14.1	9.0
L_9	Ph	Ad	-13.9	32.1
L_{10}	Ph	Ad	-14.8	31.5
L_{11}	Cy	Ph	-4.8	-10.8
L_{12}	Cy	^{t}Bu	-4.7	35.1
L_{13}	^{t}Bu	^{t}Bu	7.2	35.2
L_{14}	^{t}Bu	Ph/^{t}Bu	8.9	8.9

[a] Recorded at 162 MHz in THF unlocked and without additional shimming or at 121 MHz in THF:C_6D_6. Broad singlets were obtained in all cases.

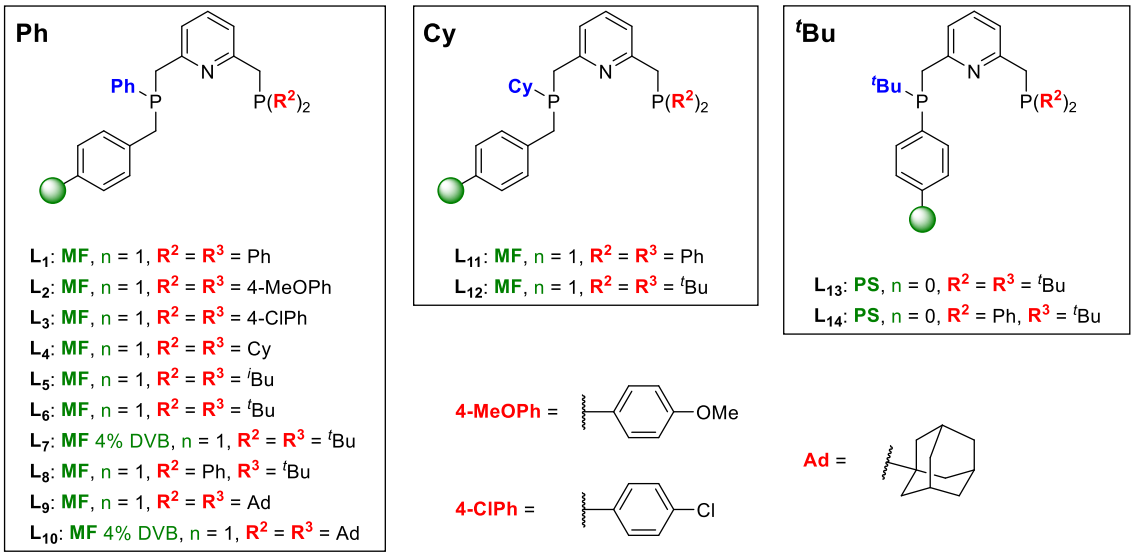

Figure 8 Complete library of supported PNP pincer ligands **L_1-L_{14}**.

The ^{31}P NMR spectra for both reported examples are well in line with those obtained for their heterogenized equivalents (see Table 2, **L_1** and **L_{14}**).

All of the 14 supported ligands were synthesized in high yield requiring only simple filtration and washing steps for purification. In addition to gel-phase ^{31}P NMR, the high purity was confirmed by FT-IR spectroscopy and elemental analysis.

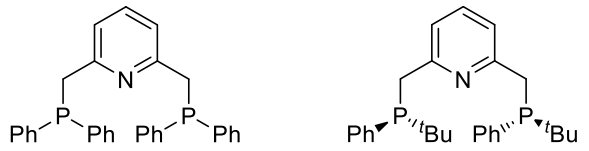

XXII: $\delta(^{31}P)$ = -9.7 ppm **XXIII**: $\delta(^{31}P)$ = 8.7 ppm

Figure 9 Symmetrical homogeneous PNP ligands **XXII**[35] and **XXIII**[36].

3.3 Synthesis of Supported Ruthenium-PNP Complexes

With a library of 14 supported PNP pincer ligands in hands the synthesis of the corresponding resin-bound ruthenium complexes was pursued. In analogy to the synthesis in monophasic systems, the resin-bound ligands were reacted with a slight excess of the ruthenium precursor [RuHCl(PPh_3)$_3$CO] at 60 °C in THF (Scheme 5).

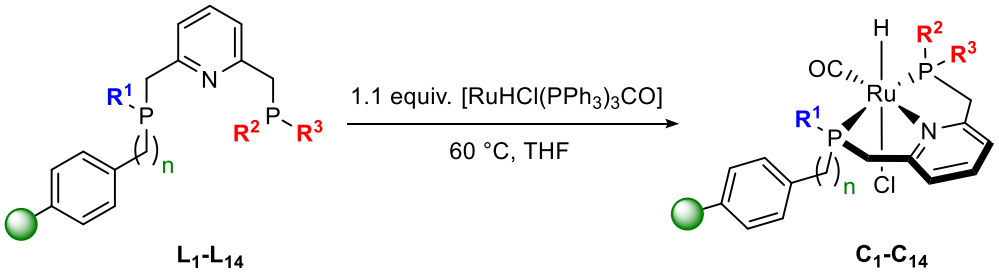

L_1-L_{14} **C_1-C_{14}**

Scheme 5 Solid-phase synthesis of resin-bound ruthenium-PNP complexes **C_1-C_{14}**.

Again, the reaction progress was monitored by ^{31}P NMR indicating full displacement of triphenylphosphine by the quantitative disappearance of the free PNP ligand signals. After removal of the supernatant, containing excess precursor and PPh_3, by filtration the yellow-brown or orange resins were thoroughly washed with THF, DCM and diethyl ether. The materials could be stored under air for a few days without any detectable decomposition. However, storage outside a glove box for more than a week led to a color change from yellow-brown or orange to green-black indicating complex

decomposition. Next, the obtained Ru-PNP complex library (**C_1-C_{14}**) was characterized using NMR and FT-IR techniques.

3.3.1 Gel-phase ^{31}P NMR

The gel-phase ^{31}P NMR spectra of complexes **C_4**, **C_6**, **C_7** and **C_9-C_{12}** reveal two new broad resonances occurring in a 1:1 ratio, which correspond to both phosphine moieties coordinating to the Ru center. Due to the lack of solvent dependent swelling properties of **C_7** and **C_{10}** immobilized on the higher cross-linked MF 4% DVB support, the signals appear significantly broadened compared to complexes immobilized on supports with 1% DVB crosslinking. A representative example of the NMR after quantitative complexation of **L_6** forming the corresponding complex **C_6** is depicted in Figure 10.

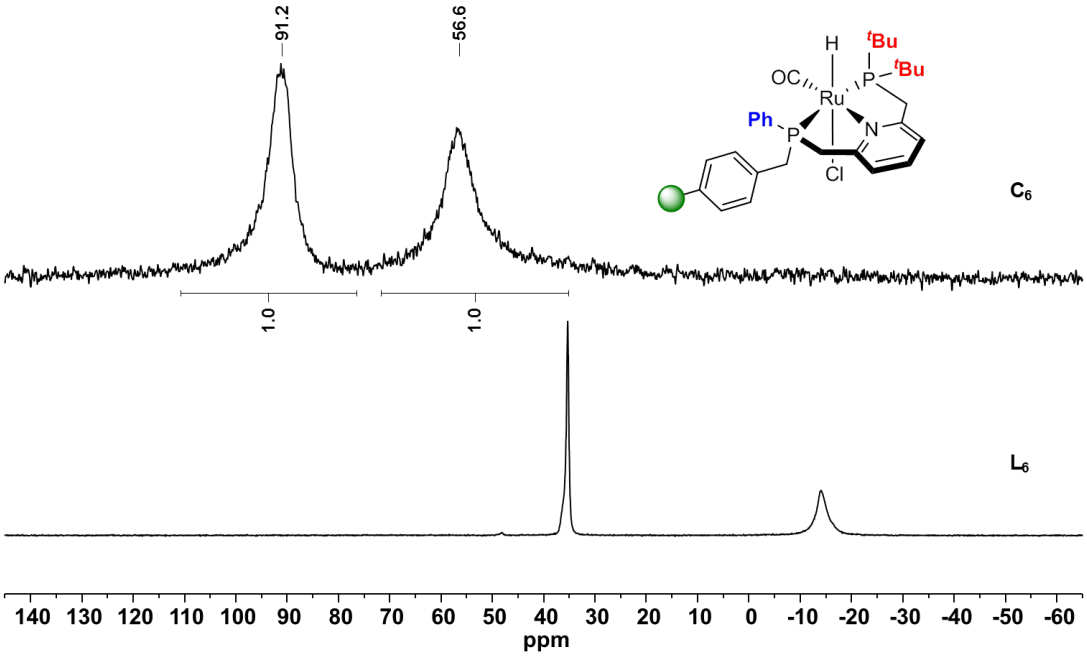

Figure 10 Solid-phase synthesis of Ru-PNP complex **C_6** monitored by ^{31}P NMR.

The signal of the remote P(^{t}Bu)$_2$ group is shifted from 35.5 ppm in **L_6** to 91.2 ppm, while the resonance of the resin-bound PPh moiety arises at 56.5 ppm in the complex opposed to -13.9 ppm for the free supported ligand. Unfortunately, due to the broad signals of the resin-bound complexes it was not possible to determine any coupling constants. Overlapping of the phosphine peaks in **C_1-C_3** and **C_5** resulted in a single broad signal for each compound whereas the ^{31}P NMR spectra for **C_8** and **C_{13}** revealed

three distinct resonances (see Figure 11 for representative example). The latter observation could be attributed to the presence of the racemic PPh^{t}Bu group in both complexes leading to a difference of up to 11-15 ppm between the corresponding signals of the stereoisomers.

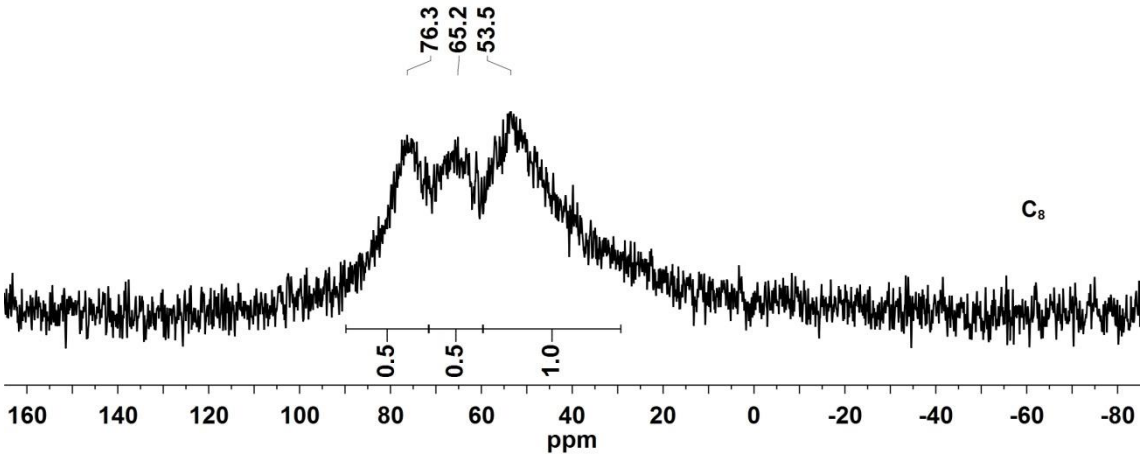

Figure 11 Gel-phase ^{31}P NMR of supported Ru-PNP complex **C$_8$**.

3.3.2 Solid-State NMR

Due to significant peak broadening in the gel-phase NMR of **C$_{14}$**, the immobilized complex was analyzed using solid-state NMR techniques. The ^{31}P MAS NMR spectrum shows two signals appearing in a ratio of 1:1 at 78.9 ppm and 65.1 ppm corresponding to the two chemically different phosphorus atoms (Figure 12a)). When compared to its homogeneous counterpart (**XXIV**) reported by Arenas *et al.*[36] (Figure 13) exhibiting two doublets at 80.3 ppm and 64.3 ppm, the chemical shifts of **C$_{14}$** are in line with those obtained in solution. In general, ^{1}H NMR spectra of immobilized compounds remain inconclusive due to broad overlapping signals belonging to the aromatic and aliphatic protons present in the polystyrene-base supports as well as to the supported species. However, in addition to these signals a single broad resonance at -13.85 ppm in the ^{1}H MAS NMR of **C$_{14}$** can be assigned to the hydride ligand bound to the Ru center (Figure 12b)). Again, no coupling constants can be determined but the chemical shift is comparable to the one observed for the symmetrical Ru-PNP **XXIV**. In the ^{13}C CP/MAS spectrum a small peak corresponding to the CO ligand can be observed at 211.0 ppm (Figure 12c)). The characteristic pyridine peaks appear at 162.1, 145.5 and 120.1 ppm overlapped by the aromatic signals belonging to the ligand phenyl group as well as to

the support. While resonances of P^{t}Bu can be observed at 35.0, 31.9 and 27.5 ppm analogous to **XXIV**, the signals corresponding to the methylene side-arms can be expected at 40.5 ppm overlapped by peaks of the support.

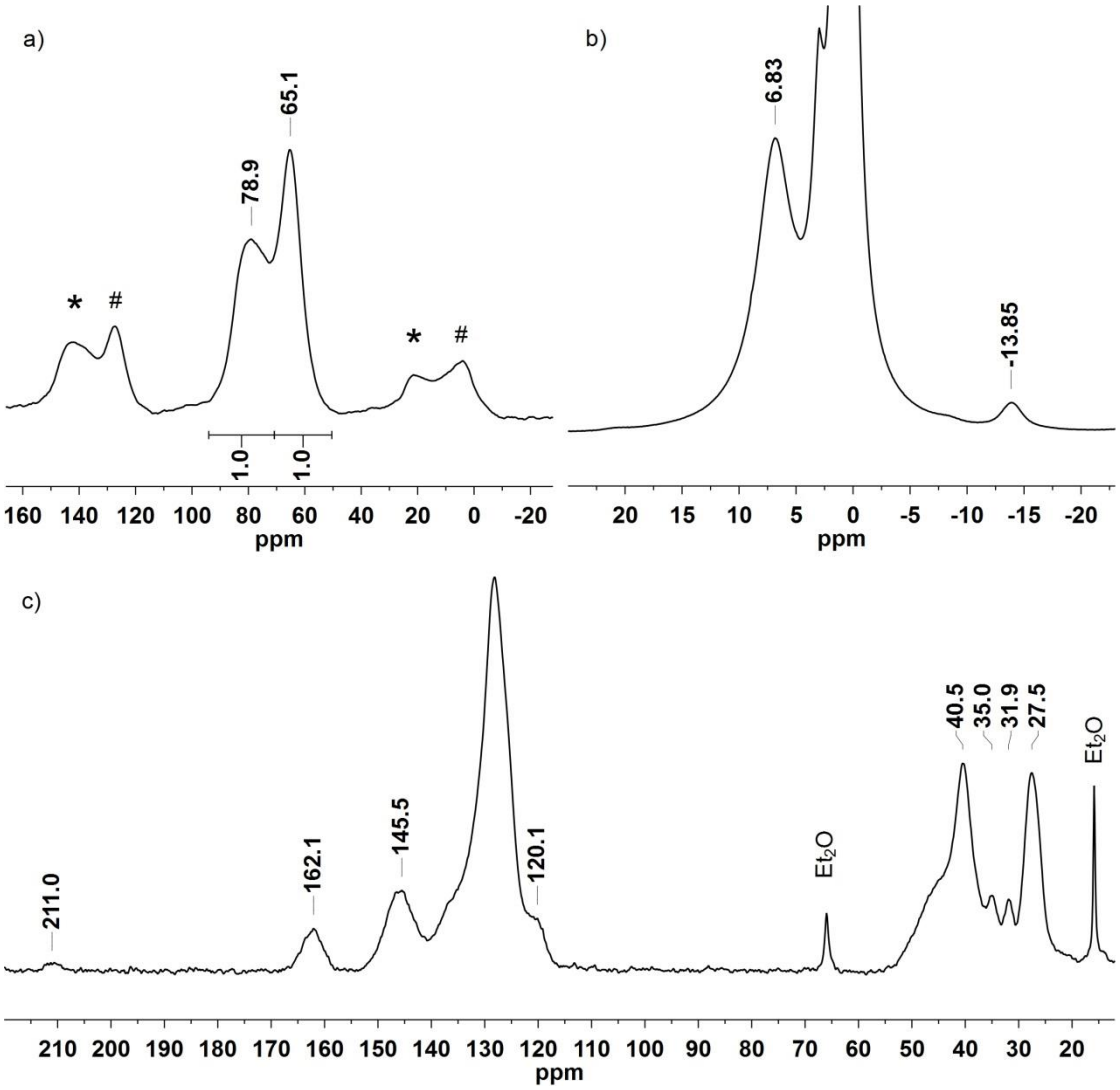

Figure 12 a) ^{31}P MAS NMR, b) ^{1}H MAS NMR and c) ^{13}C CP/MAS NMR of **C_{14}**. Rotational sidebands are denoted by asterisks (*) and (#).

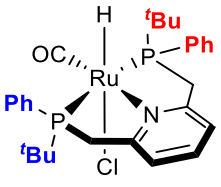

XXIV

$\delta(^{31}P)$ = 80.3, 64.3 ppm

$\delta(^{1}H, Ru\text{-}H)$ = -14.52 ppm

$\delta(^{13}C, CO)$ = 210.2 ppm

Figure 13 Molecular structure of homogeneous Ru-PNP complex **XXIV** and selected chemical shifts in ^{31}P, ^{1}H and ^{13}C NMR.[36]

3.4 Synthesis of unsymmetrical homogeneous Ru-PNP complex 8

In order to provide a direct comparison between heterogenized Ru complexes based on unsymmetrical PNP pincer ligands and a corresponding solution-phase analogue, the homogeneous complex **8** was prepared. Two different phosphorus donor moieties bearing both Ph and ^{t}Bu substituents were introduced by reacting PN fragment **5a** with one equivalent of borane protected lithium di-*tert*-butylphosphide leading to the bench-stable unsymmetrical PNP ligand **7** in 91% yield (Scheme 6, step 1).

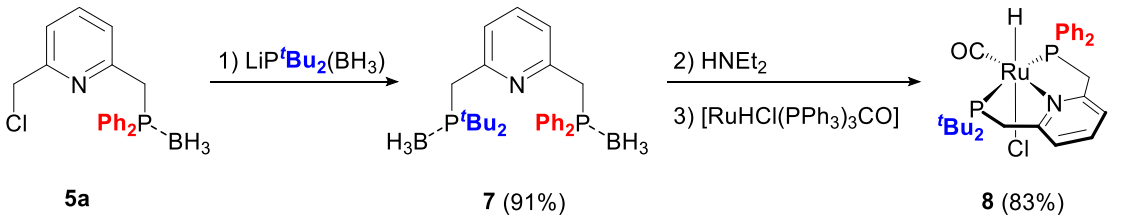

Scheme 6 Synthesis of non-symmetrical homogeneous Ru-PNP complex **8**.

Upon borane removal using diethylamine at 50 °C, the free ligand was obtained exhibiting two signals in the ^{31}P NMR at 34.9 ppm and -11.3 ppm matching with its heterogeneous counterpart **L$_6$** (see Table 2). Without further purification, the free PNP pincer was directly reacted with 0.95 equivalents of [RuHCl(PPh$_3$)$_3$CO] yielding the first non-symmetrical Ru-PNP pincer complex **8** in 83% yield (Scheme 6, step 3). Single crystals suitable for X-ray crystallography were obtained by slow diffusion of *n*-pentane into DCM. The molecular structure of **8** is depicted in Figure 14 together with selected bond distances and angles. The homogeneous complex exhibits a distorted octahedral geometry around the Ru(II) center with *trans*-coordination of the CO ligand to the nitrogen atom of pyridine and the hydride *trans* to the chloride. Hence, a meridional coordination geometry of the PNP ligand around the metal center is obtained as reported for symmetrical pyridine-based [RuHCl(PNP)CO] complexes.[37]

The hydride ligand exhibits a doublet of doublets at -14.51 ppm (J_{HP} = 17.1 and 20.5 Hz) in the ^{1}H NMR spectrum as found in similar Ru-complexes.[6a,6c,36] The protons of the PPh$_2$ methylene arm show signals at 4.89 ppm (dd, J_{HH} = 9.5 Hz, J_{PH} = 16.0 Hz) as well as at 4.12 ppm (ddd, J_{HH} = 2.6 Hz, J_{HH} = 12.1 Hz, J_{PH} = 15.9 Hz). A multiplet from 3.73-3.66 ppm and a doublet of doublets at 3.37 ppm (J_{HH} = 8.3 Hz, J_{PH} = 16.6 Hz) can be observed for both methylene protons belonging to the P^{t}Bu$_2$ arm. In the ^{13}C NMR, the CO ligand appears as a triplet resonating at 208.9 ppm (J_{PC} = 12.2 Hz).

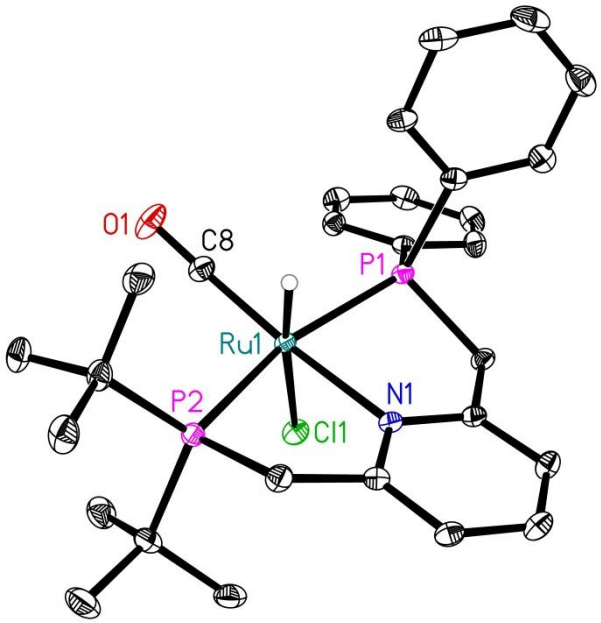

Figure 14 ORTEP representation of molecular structure of **8**. Displacement ellipsoids correspond to 30% probability. Hydrogen atoms are omitted for sake of clarity. Selected bond lengths (Å) and bond angles (°): P1–Ru1 = 2.3094(6), P2–Ru1 = 2.3357(6), N1–Ru1 = 2.1631(13), Cl1–Ru1 = 2.5183(6), C8–Ru1 = 1.830(2), C8–O1 = 1,153(3), N1–Ru1–P1 = 80.86(5), N1–Ru1–P2 = 81.75(5), N1–Ru1–C8 = 172.60(8), N1–Ru1–Cl1 = 89.17(4), P1–Ru1–P2 = 161,86(2).

Finally, the ^{31}P NMR spectrum of **8** shows two doublets corresponding to the P^{t}Bu$_2$ (δ = 90.4 ppm, J_{PP} = 266.6 Hz) and the PPh$_2$ entity (δ = 53.6 ppm, J_{PP} = 266.6 Hz) bound to the central Ru atom (Figure 15, red spectrum). These results compare well to the ^{31}P NMR resonances at 91.2 and 56.5 ppm obtained for the correlating supported Ru-complex **C$_6$**. The CO stretching band in the FT-IR spectrum was observed at 1887 cm^{-1}.

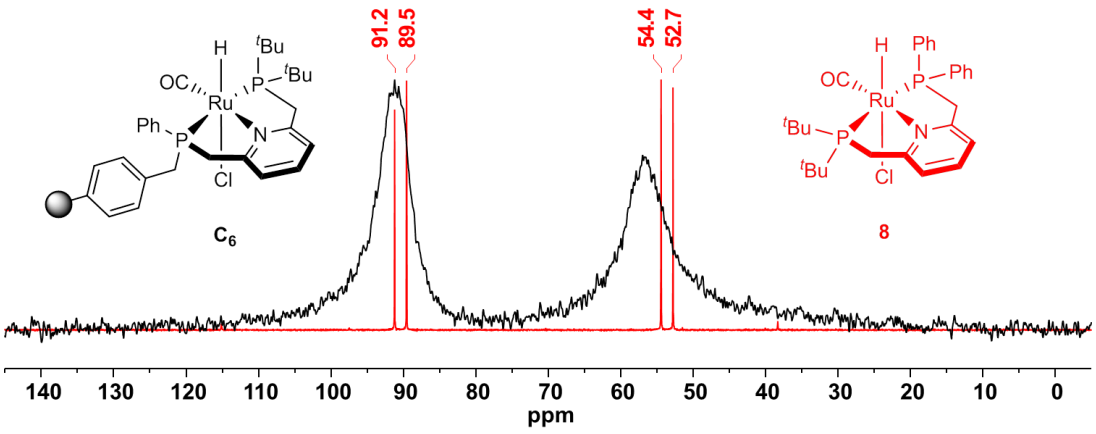

Figure 15 ^{31}P NMR spectra of supported Ru-PNP complex **C$_6$** (black) and the solution-phase analogue **8** (red).

3.5 Application in Ester Hydrogenation

3.5.1 Catalytic Screening

In recent years, extensive research effort has been devoted to the development of high performance catalysts for homogeneous hydrogenations of non-activated esters (see chapter 3.1).[5b,21] In particular, molecular Ru-catalysts featuring PNN pincer-type ligands based on a central pyridine donor moieties, such as **XVI** reported by the group of Milstein, seemed to outperform their PNP pincer analogues significantly in this transformation (see Figure 4).[6b,29] This was associated with a lack of ligand hemilability due to identical electronic properties of both phosphine donor moieties in symmetrical PNP ligands. It was anticipated that these systems could be improved by employing unsymmetrical PNP pincer ligands of various electronic and steric properties. Therefore, it was decided to apply the heterogeneous Ru-catalysts **C_1-C_{14}** in ester and lactone hydrogenation.

The Kamer group reported on an *in situ* formed supported Ru-PNN catalyst for the selective reduction of esters at room temperature.[30] Building on this work, the whole library of preformed ruthenium-PNP complexes was screened in the hydrogenation of methyl benzoate (**S_1**) as a benchmark substrate (Table 3). The catalytic reactions were performed under optimized conditions over 16 hours in THF at 80 °C and 50 bar dihydrogen pressure. Moreover, 1.0 mol% of supported catalyst was employed together with 10 mol% of KO^{t}Bu ensuring *in situ* catalyst activation. For supported catalyst **C_1**, which contains a nearly symmetrical PNP ligand bearing phenyl groups on both phosphine moieties, 84% conversion and 92% selectivity towards the desired benzyl alcohol were obtained (Table 3, entry 1). By changing to more electron-donating *para*-anisyl groups bound to the remote phosphine in **C_2** an increase in catalyst activity (97%) and selectivity (99%) was observed compared to **C_1**. Electron-withdrawing *para*-ClPh groups in **C_3** led to a reduced activity of 69% conversion and more transesterification to benzyl benzoate resulting in only 84% selectivity (Table 3, entries 2 and 3). When changing to unsymmetrical ligands carrying aromatic substituents on the resin-bound P-donor and alkyl substituents on the remote phosphine, moderate activities were obtained for **C_4** and **C_5** (Table 3, entries 4 and 5). With increasing steric demand in case of strong electron-donating ^{t}Bu moieties, catalyst **C_6**, induced excellent conversion of 98% with full selectivity towards benzyl alcohol (Table 3, entry 6). At a lower temperature of 60 °C the activity of **C_6** decreased to 82% (Table 3, entry 7). Analogously, even more bulky adamantyl groups in **C_9** led to the

best catalyst performance (Table 3, entry 10). When applying the equivalent catalysts **C$_7$** and **C$_{10}$** immobilized on the higher crosslinked resin MF 4% DVB, reduced performances (64-65% conversion, 83-84% selectivity) compared to **C$_6$** and **C$_9$** were found (Table 3, entries 6 and 10).

Table 3 Ru-catalyzed hydrogenation of **S$_1$** using supported catalysts **C$_1$-C$_{14}$**.[a]

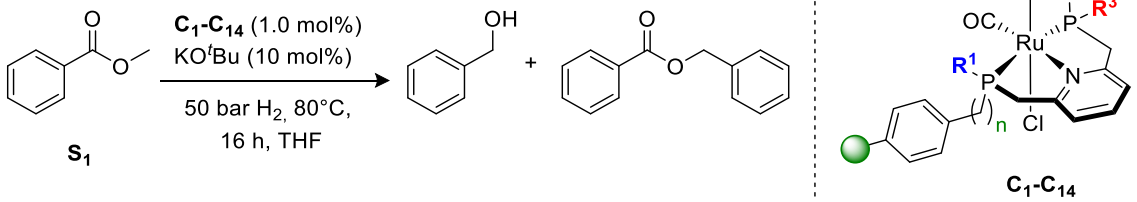

Entry	Catalyst	Substituents			Conversion	Selectivity
		R^1	R^2	R^3	[%][b]	[%][c]
1	**C$_1$**	Ph	Ph	Ph	84 (81)	92
2	**C$_2$**	Ph	4-MeOPh	4-MeOPh	97 (96)	99
3	**C$_3$**	Ph	4-ClPh	4-ClPh	69 (63)	84
4	**C$_4$**	Ph	Cy	Cy	61 (54)	83
5	**C$_5$**	Ph	^{i}Bu	^{i}Bu	58 (55)	86
6	**C$_6$**	Ph	^{t}Bu	^{t}Bu	98 (97)	99
7[d]	**C$_6$**	Ph	^{t}Bu	^{t}Bu	82 (79)	94
8	**C$_7$**	Ph	^{t}Bu	^{t}Bu	64 (58)	84
9	**C$_8$**	Ph	Ph	^{t}Bu	89 (87)	96
10	**C$_9$**	Ph	Ad	Ad	>99 (>99)	>99
11	**C$_{10}$**	Ph	Ad	Ad	65 (59)	83
12	**C$_{11}$**	Cy	Ph	Ph	72 (67)	88
13	**C$_{12}$**	Cy	^{t}Bu	^{t}Bu	94 (93)	98
14	**C$_{13}$**	^{t}Bu	^{t}Bu	^{t}Bu	80 (73)	90
15	**C$_{14}$**	^{t}Bu	Ph	^{t}Bu	70 (62)	86
16	**8**	Ph	^{t}Bu	^{t}Bu	78 (76)	94

[a] General conditions: substrate (0.5 mmol), [Ru] (1.0 mol%), KO^{t}Bu (10 mol%), THF (1 mL), 80 °C, H_2 (50 bar), 16 h. [b] Conversion of **S$_1$** determined by GC using dodecane as internal standard. The GC yield is given in parenthesis. [c] Selectivity towards the desired alcohol. [d] 60 °C.

This can be attributed to the lack of solvent dependent gel-like behavior of the higher crosslinked polymer and the consequently reduced accessibility of the catalytically active site within the support. Supported catalyst **C_8** bearing both a phenyl and ^{t}Bu substituent on the remote phosphine side arm led to 89% conversion and 96% selectivity (Table 3, entry 9). When compared to Ph-substituted **C_1** and ^{t}Bu-substituted **C_6**, this outcome confirms the trend of higher catalytic activity when the ligand shows both electron-donating sterically demanding phosphine substituents and weaker P-donor moieties. Replacing the phenyl substituent by a cyclohexyl group on the resin-bound phosphorus donor leads to slightly reduced performances for **C_{11}** and **C_{12}** opposed to the corresponding complexes **C_1** and **C_6** (Table 3, entries 12 and 13). Finally, PS-supported complex **C_{13}** carrying three bulky ^{t}Bu groups gave only 80% conversion together with 90% selectivity (Table 3, entry 14). The nearly symmetrical resin-bound catalyst **C_{14}** performed even worse compared to **C_{13}**, which could be due to equal electronic properties of the relatively strong donating phosphine side arms (Table 3, entry 15). This is in agreement with results observed for symmetrical homogeneous PNP ligands based on ^{i}Pr (**XVII**, see Figure 4, chapter 3.1) and ^{t}Bu substituents.[6b,29] Surprisingly, when the non-symmetrical solution-phase complex **8** was applied under the same conditions, only 78% conversion was achieved opposed to 98% of its heterogenized counterpart **C_6** (Table 3, entries 6 and 16).

In many examples of heterogenized molecular catalysts, the support has a detrimental effect on the performance. In this case however, the opposite outcome was found, indicating a beneficial effect of the support under the given conditions, which could be explained by an enhanced catalyst stability provided by the specific microenvironment of the polymer structure. Nevertheless, more conclusive results would be required for a profound explanation of the difference in homogeneous and heterogeneous catalyst activity. Moreover, it was found that the presence of base additive in the reaction was required unlike for homogeneous Ru-PNP catalyst **XVII**, which was applied in a base-free system as the dearomatized analogue. Unfortunately, pre-activation attempts of both, the homogeneous catalyst **8** and the solid-bound analogue **C_6** resulted in no activity. However, only poor conversion (12%) in the homogeneous reduction of ethyl benzoate employing pyridine-based PNP ligand **XVII** at 140 °C and 5 bar of H_2 was reported.[6b] In contrast to these unpromising results, the potential of the more versatile PNP ligands bound to a support in ester hydrogenation were clearly showcased.

3.5.2 Substrate Scope

Subsequently, the substrate scope was determined employing supported catalyst **C_6** in the hydrogenation of monoesters **S_1**-**S_8**, diesters **S_9**-**S_{10}** and lactones **S_{11}**-**S_{12}** (Figure 16). While the aromatic ester ethyl benzoate (**S_2**) was hydrogenated with slightly reduced conversion and selectivity compared to **S_1**, benzyl benzoate (**S_3**) proved to be more challenging (69% conversion). Similar difficulties were observed for linear alkyl esters of which methyl hexanoate (**S_4**) showed only 84% conversion and 86% selectivity to the corresponding primary alcohol. Ethyl hexanoate (**S_5**) and hexyl hexanoate (**S_6**) gave only moderate conversions together with 62% selectivity for **S_5**. However, branched alkyl esters, such as methyl isovalerate (**S_7**) and methyl cyclohexanoate (**S_8**), were converted more readily compared to their linear analogues.

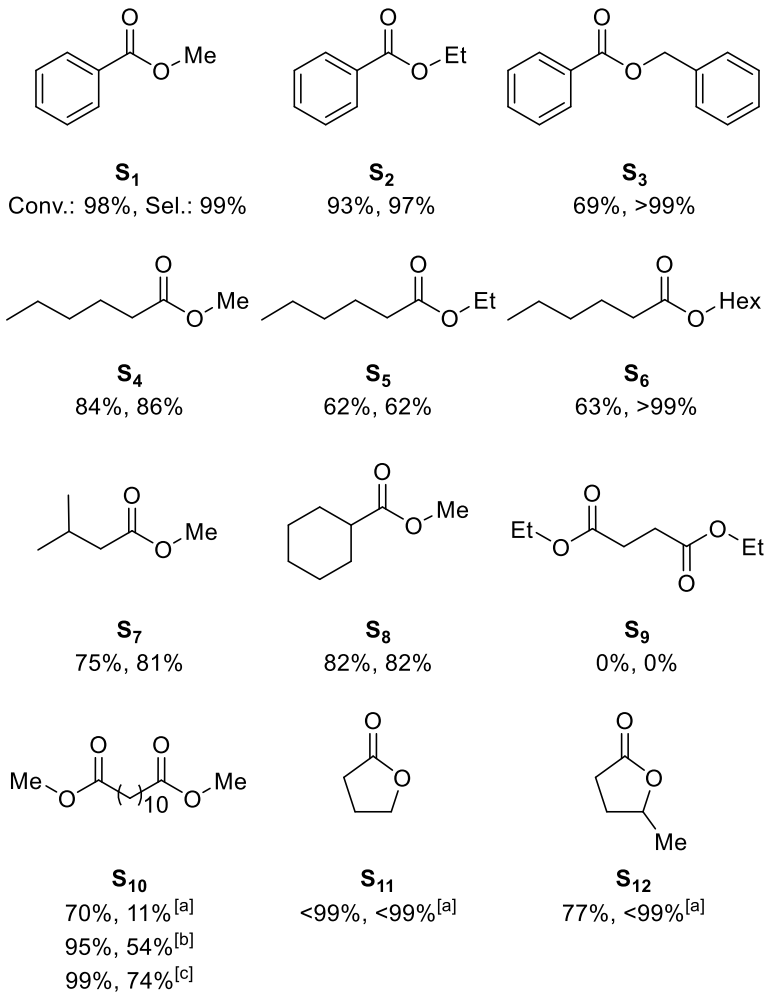

Figure 16 Substrate scope for ester hydrogenation using supported complex **C_6** (conversion and selectivity indicated below structures). For conditions see Table 3, [a] Substrate (0.25 mmol), [Ru] (1.0 mol%), KO^{t}Bu (10 mol%), THF (1 mL), 80 °C, H_2 (50 bar), 24 h, [b] [Ru] (2 mol%), 80 °C, [c] [Ru] (2 mol%), 100 °C.

In accordance to previous results obtained for supported PNN ligands, the diester diethyl succinate (**S_9**) was not reduced by **C_6** presumably attributable to the formation of a stable substrate complex via the chelating carbonyl groups.[30] However, when extending the carbon chain length by using dodecanedioate (**S_{10}**) as substrate, 70% of the diester were converted after 24 h. In this case the mono-hydrogenated product was obtained as the main product whereas the desired 1,12-dodecanediol only formed in 11% selectivity. Upon increase of the catalyst loading to 2 mol%, up to 95% conversion and 54% selectivity were achieved. At 100 °C, **S_{10}** was almost fully converted to the corresponding diol with 74% selectivity. Finally, the applicability of supported catalyst **C_6** in the reduction of lactone derivatives was examined. After 24 h, γ-butyrolactone (**S_{11}**) was selectively converted into 1,4-butanediol. For the bio-mass derived γ-valerolactone (GVL, **S_{12}**), 77% conversion and very high selectivity towards the corresponding 1,4-pentanediol was achieved underlining the versatility of the heterogenized Ru-PNP system.

3.5.3 Reaction Profile

To gain a better understanding concerning the impact of different electronic properties on the performance, as well as the catalyst stability, the reaction profile in the hydrogenation of **S_1** was investigated. The activities of two supported complexes **C_2** and **C_3**, which differ in electron-donating methoxy groups and electron-withdrawing Cl-substituents in the *para*-position of the phenyl phosphine donors, were monitored over time (Figure 17).

After 30 minutes, only 2% of the desired benzyl alcohol (BzOH) and 4% of the transester benzyl benzoate (BzBz) formed when using **C_2** (Figure 17 a) compared to 7% of each for **C_3** (Figure 17 b). This indicates an incubation time for **C_2** after which the substrate was converted at a slightly higher rate opposed to **C_3**. Thus, 18% of BzOH for **C_2** and 15% for **C_3** respectively were reached after one hour reaction time. After two hours, **C_2** yielded 34% whereas **C_3** gave 30%, respectively. In the following two hours, the reaction rate decreased significantly for both catalysts. Though, the activity of **C_2** in the simultaneous reduction of **S_1** and the transesterification product BzBz remains relatively constant over the remaining eight hours leading to an overall conversion of 97% after 16 hours. Similar to that, the reaction using **C_3** proceeded at a constant rate when reaching about 50% conversion, which resulted in 69% total conversion and a selectivity of 84% after 16 hours.

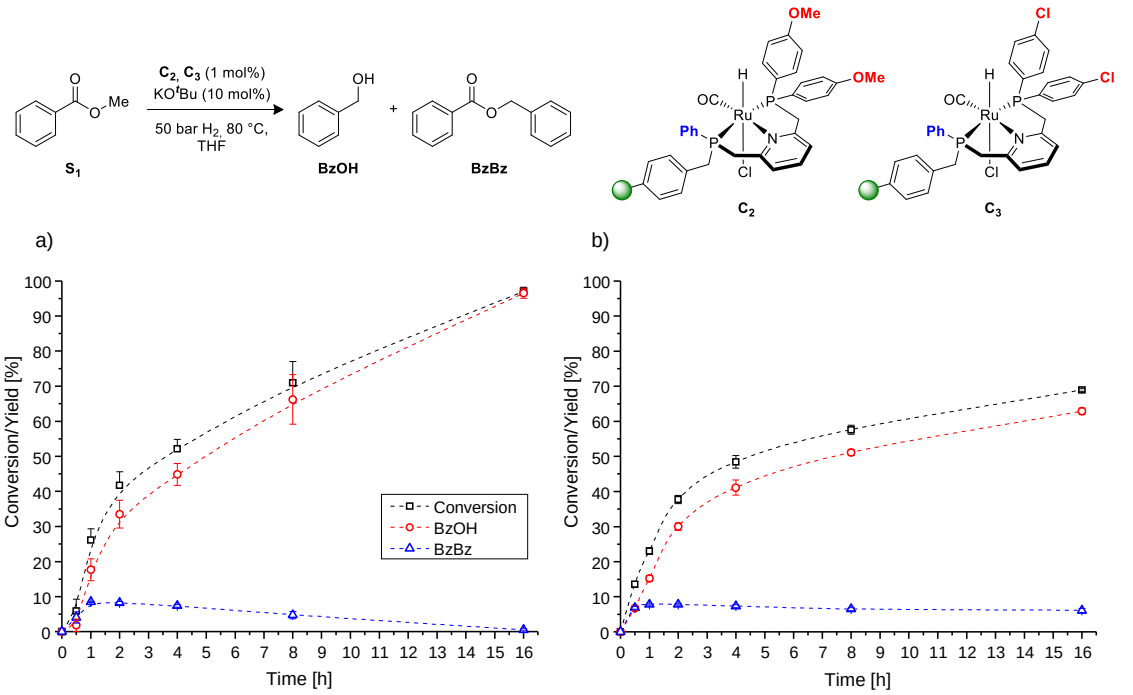

Figure 17 Reaction profile for Ru-catalyzed hydrogenation of $\mathbf{S_1}$. Reaction conditions: substrate (0.5 mmol), [Ru] (1.0 mol%), KO^{t}Bu (10 mol%), THF (1 mL), 80 °C, H_2 (50 bar). a) Conversion profile of $\mathbf{C_2}$. b) Conversion profile of $\mathbf{C_3}$. Overall conversion of $_{\mathbf{S1l}}$ (black squares) and yield of BzOH (red circles) and BzBz (blue triangles) were determined by GC using dodecane as internal standard. Error bars determined from the standard deviation of triplo experiments.

Hence, more electron-rich phosphine donor atoms, such as *para*-anisyl substituted phosphines in $\mathbf{C_2}$, lead to a slightly higher reaction rate compared to electron-withdrawing groups located in the phosphine backbone. More importantly, they seem to exhibit a beneficial influence on the catalyst lifetime for these resin-bound PNP-pincer type Ru-complexes.

3.6 Catalytic Recycling

Finally, the recovery and recyclability of the best performing supported Ru-PNP catalyst $\mathbf{C_6}$ was investigated. In contrast to reaction conditions used in the catalytic screening, it was decided to shorten the reaction time to 2 hours in order to assess any effect on the catalyst performance as a consequence of catalyst deactivation. After each cycle, the supernatant solution was filtered off followed by addition of fresh substrate and base stock solution to start a new catalytic run. The results in Table 4 show that the heterogenized catalyst could successfully be recovered and reused up to at least 4 times. However, already after the second cycle a decrease in activity of 4% together with a slight drop in selectivity was observed. While after the third run, a

similar performance was obtained compared to the previous run, the catalyst performance decreased over the following two cycles. Hence, after the 5th run, the catalyst reached only 33% conversion and 68% selectivity resulting in a total activity loss of 11% and drop in alcohol selectivity of 9% over 5 cycles.

Table 4 Batch recycling experiments using **C_6** in the hydrogenation of **S_1**.

Run	Conversion [%][b]	Selectivity [%][c]
1	44	77
2	40	75
3	40	74
4	36	70
5	33	68

[a] Conditions: substrate (0.5 mmol), [Ru] (1.0 mol%), KO^{t}Bu (10 mol%), THF (1 mL), 100 °C, H_2 (50 bar), 2 h. [b] Conversion of **S_1** determined by GC using dodecane as internal standard. The GC [c] Selectivity towards benzyl alcohol.

Potential catalyst decomposition could be caused by small amounts of air and moisture introduced during the catalyst recovery work-up. Furthermore, the hydrogen atmosphere used during the reaction cycles was replaced by argon for work-up purposes, which did not seem to have a detrimental effect on the recyclability as observed for supported PNN ligands.[30] Nevertheless, the catalyst stability may have been slightly affected by the absence of H_2. Another explanation concerning catalyst degradation could be the formation of methanol produced in the hydrogenation of methyl benzoate. Short-chain alcohols have been reported to form metal-alkoxides consequently reducing the reaction rate in ester hydrogenation, which can be restored upon addition of extra amounts of base.[38] Finally, deterioration of the polymeric support due to mechanical stirring caused finely ground particles present in the filtered supernatant solution. However, these preliminary results demonstrate the potential for recovery and recycling of supported Ru-PNP catalysts only requiring simple filtrations. As continuous flow processes in fixed bed reactors offer the opportunity to recycle under constant conditions without disruption of the catalytic system, these immobilized catalysts represent highly suitable candidates for application und flow conditions.

3.7 Conclusion and Outlook

In this chapter, the first facile synthesis of a diverse combinatorial library of supported pyridine-based PNP-type pincer ligands was presented using a solid-phase synthetic methodology. Systematic variation of substituents attached to the phosphorus donor moieties combined with employing three different types of polymeric supports led to 14 library members (**L_1-L_{14}**). The supported ligands were obtained in high purity only requiring minimal purification procedures, such as easy filtrations, opposed to typically arduous synthetic protocols for solution-phase analogues. Using this SPS approach, several non-symmetrical PNP-pincer ligands could be accessed, which remain less studied in homogeneous systems. However, unsymmetrical PNP pincer offer more variety compared to their symmetrical pendants hence providing great potential for efficient fine-tuning of the electronic and steric ligand properties. The versatile resin-bound PNP ligand library was subsequently converted into the corresponding Ru complexes **C_1-C_{14}** and compared to the solution-phase analogue **8**. The molecular structure of the complexes on support could be verified by gel-phase and solid-state NMR as well as FT-IR spectroscopy.

Subsequently, the immobilized catalyst library was screened in Ru-catalyzed hydrogenation of esters under relatively mild conditions. In comparison, typical heterogeneous catalysts applied in industrial ester hydrogenations require much harsher conditions (>200 °C and >100 bar of H_2) whereas a similar supported Ru-PNN catalyst could hydrogenate several esters at room temperature. The supported Ru-PNP catalysts demonstrated moderate to excellent activities and selectivities in the reduction of methyl benzoate **S_1** at 80 °C and 50 bar. Minor changes within the structure of the phosphine substituents led to a substantial impact on catalyst performances underlining the necessity of catalyst screening. Furthermore it showcases the power of the solid-phase synthetic approach for efficient ligand fine-tuning towards catalyst optimization. Remarkably, the supported complex **C_6** even outperformed its homogeneous counterpart **8** indicating a beneficial influence of the support on the catalyst stability rather than a detrimental effect on the performance. High to moderate activities towards various aryl and alkyl esters were achieved. Moreover, long chain C_{12}-diester **S_{10}** could be fully transferred with up to 74% selectivity towards the C_{12}-diol. Likewise, lactones, such as bio-derived GVL, could be readily converted with high selectivities towards the desired diols.

Preliminary recycling attempts employing catalyst **C_6** demonstrated the recoverability and reusability of this type of supported ester hydrogenation catalyst over

at least 5 runs accompanied by an overall activity loss of 11%. Catalyst decomposition could be attributed to the potential introduction of air and moisture during the work-up as well as to mechanical deterioration of the polymeric support. These drawbacks might be avoided by applying the supported Ru-PNP system in a continuous flow hydrogenation setup.

Regarding the modular nature of pincer-type ligands, further diversification of the PNP type ligand structure would be desirable. Introduction of other substituents bound to the phosphorus donors as well as the modification of the pyridine scaffold by installing substituents in the heterocyclic backbone would give further opportunities for catalyst tuning. However, an improved synthesis of the homogeneous PN fragments would be required in order to avoid disubstitutions on the pyridine side arms. This could be accomplished via modification of the pyridine building block with leaving groups of different reactivity.

As the versatility of homogeneous PNP-based catalysts has been demonstrated in a plethora of catalytic applications, it would be of strong interest to extend the applicability of the supported Ru-PNP system. Dehydrogenative coupling reactions, the conversion of CO_2 into methanol as well as hydrogenations of more challenging carboxylic acids derivatives might be potential applications for the heterogenized catalysts.

Finally, preliminary results towards the solid-phase synthesis of immobilized PNP-based complexes featuring earth-abundant manganese metal have been obtained. Starting from resin-bound PNP ligands **L_6** and **L_{12}**, the corresponding Mn-PNP complexes could be readily prepared using metal precursor $[Mn(CO)_5Br]$ (Scheme 7). Hence, the investigation of the catalytic activity would be highly desirable building on successful applications of similar homogeneous Mn-PNP catalysts in various catalytic transformations.[39]

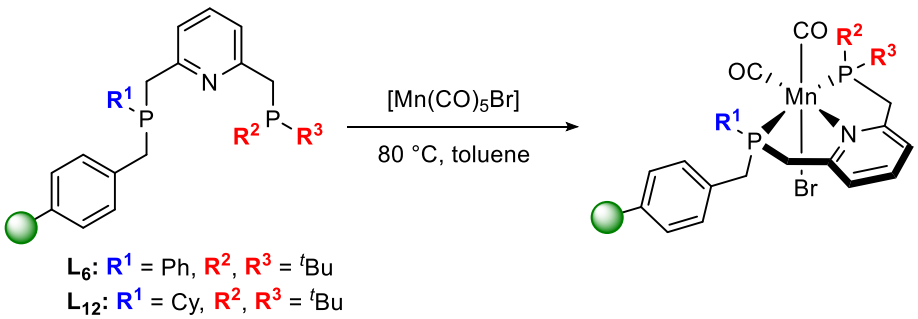

Scheme 7 Solid-phase synthesis of supported Mn-PNP complexes.

3.8 Experimental

General Experimental

All reactions and manipulations were carried out using standard Schlenk techniques under inert atmosphere of purified argon or in an MBraun glovebox unless stated otherwise. All glassware was dried prior to use to remove traces of water. All chemicals were obtained from commercial suppliers and were used as received unless otherwise stated. Diethyl ether and THF were distilled from sodium/benzophenone and toluene was distilled from sodium. Distilled THF used in catalytic reactions was additionally dried over 3 Å molecular sieves for a minimum of 72 h. DCM and diethylamine were distilled from calcium hydride. C_6D_6 was thoroughly degassed with Argon and stored over 4 Å molecular sieves. Novabiochem^{TM} Merrifield resin (100-200 mesh, 1.23 mmol·g^{-1}, 1% crosslinked) was obtained from EMD Millipore. ParaMax Merrifield resin (100-200 mesh, 1.2 mmol·g^{-1}, 4% crosslinked) was obtained from Advanced Chemtech. Supported secondary phosphines **1a-d·BH$_3$**[33,40] were synthesized according to literature. The secondary phosphine-boranes $^{i}Bu_2PH(BH_3)$, $Ad_2PH(BH_3)$ and $Ph^{t}BuPH(BH_3)$ were synthesized starting from their corresponding secondary phosphines.[41] The synthesis of (p-MeO-$C_6H_4)_2PH(BH_3)$ and (p-Cl-$C_6H_4)_2PH(BH_3)$ was adapted from literature procedure.[42]

NMR spectroscopic analysis was conducted using a Bruker FOURIER 300, an AVANCE II 400 or an AVANCE III 500. ^{1}H, ^{31}P and ^{13}C NMR experiments were recorded using standard NMR techniques and the chemical shifts (δ) are reported relative to the solvent peak. Gel-phase ^{31}P NMR spectra of all resins were recorded unlocked and without additional shimming in dry THF as a solvent unless mentioned otherwise. Chemical shifts are reported relative to 85% H_3PO_4 in water. Solid-state NMR spectra were acquired using Bruker Avance III spectrometers equipped with a 9.4 T widebore superconducting magnet operating at Larmor frequencies of 400.1 MHz for ^{1}H, 161.9 MHz for ^{31}P and 100.6 MHz for ^{13}C. Samples were packed in 4.0 mm ZrO_2 rotors and rotated at MAS rates of 14 kHz (^{1}H), 12.5 kHz (^{13}C) and 10 kHz (^{31}P). ^{13}C spectra were acquired using cross-polarization (CP), with a contact pulse (ramped for ^{1}H) between 1 and 5 ms (^{13}C) duration. Multiplicities are provided using the following abbreviations: s = singlet, d = doublet, t = triplet, m = multiplet and br = broad and the couplings (J) are reported in Hz. NMR spectra were processed using TopSpin 3.2 or MestReNova 11.0. IR spectra were recorded on a Shimadzu IRAffinity-1S spectrometer as KBr disks. Elemental analyses were measured by Mikroanalytisches

Laboratorium Kolbe in Oberhausen, Germany. GC measurements were performed on a Thermo Trace GC ultra, see further experimental details for columns and conditions.

General Procedure for the Synthesis of 2-(Chloromethyl)-6-(Phosphinomethyl) Pyridine Borane Adducts 5a-h

To a solution of secondary phosphine-borane adduct (1.0 equiv.) in dry THF at -78 °C, *n*-BuLi (2.5 M in hexanes, 1.0 equiv.) or *sec*-BuLi (1.4 M in cyclohexane, 1.0 equiv.) in case of $(Adamantyl)_2PH{\cdot}BH_3$ was added dropwise. The solution was stirred for 30 min at -78 °C and subsequently warmed to room temperature and was left for an additional amount of time until full conversion was achieved according to $^{31}P\{^1H\}$-NMR. 2,6-Bis(chloromethyl)pyridine (1.0 equiv.) was dissolved in dry THF and cooled to -78 °C. Next, the freshly prepared lithium boranyl phosphanide solution (0.28 M, 1.0 equiv.) in THF was added slowly. The mixture was allowed to warm to room temperature overnight leading to a pale yellow solution. The solvent was removed under vacuum and the yellow residue was dissolved in DCM. The organic phase was washed with water and brine and subsequently dried over $MgSO_4$. After filtration, the solvent was removed under reduced pressure. The residue was purified *via* flash chromatography (9:1 Hexanes : EtOAc) or as stated otherwise, yielding a white solid.

*2-(Chloromethyl)-6-((di-phenylphosphino)-methyl)pyridine-borane Adduct **5a***

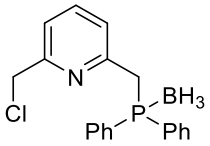

5a

The phosphine-borane adduct **5a** was obtained from 2,6-bis(chloromethyl)pyridine (2.0 g, 11.4 mmol, 1.0 equiv.) and lithium boranyl-diphenyl-phosphanide (1.0 equiv.) as a white solid after flash chromatography. Yield: 1,40 g (36%). ^1H-NMR (400 MHz, $CDCl_3$): δ = 7.76-7.71 (m, 4H, PPh), 7.58 (t, 1H, J_{HH} = 7.7 Hz, pyridine-H), 7.51-7.47 (m, 2H, PPh), 7.45-7.41 (m, 4H, PPh), 7.26 (d, 1H, J_{HH} = 7.7 Hz, pyridine-H), 7.21 (d, 1H, J_{HH} = 7.8 Hz, pyridine-H), 4.46 (s, 2H, CH_2Cl), 3.86 (d, 2H, J_{PH} = 12.0 Hz, CH_2P), 1.14 (br, 3H, BH_3) ppm, $^{13}C\{^1H\}$-NMR (101 MHz, $CDCl_3$): δ = 155.8 (s, pyridine-*C*-CH_2Cl), 153.1 (d, J_{PC} = 4.5 Hz, pyridine-*C*-CH_2P), 137.1 (s, pyridine-CH), 132.8 (d, J_{PC} = 9.3 Hz, 4xAr-CH), 131.3 (d, J_{PC} = 2.1 Hz, 2xAr-CH), 128.6 (d, J_{PC} = 55.3 Hz, 2xAr-C-P), 128.6 (d, J_{PC} = 10.1 Hz, 4xAr-CH), 124.4 (d, J_{PC} = 3.3 Hz, pyridine-CH),

120.8 (d, J_{PC} = 2.1 Hz, pyridine-CH), 46.5 (s, CH_2Cl), 36.5 (d, J_{PC} = 31.5 Hz, CH_2P) ppm. $^{31}P\{^1H\}$-NMR (162 MHz, $CDCl_3$): δ = 18.1 (m) ppm; IR (solid): $\tilde{\nu}$ = 3054 (w), 2401 (w), 2367 (m), 1584 (m, C=N), 1456 (m), 1433 (m), 1105 (m), 1061 (m), 821 (w), 740 (s, P-C), 690 (s, P-C), 596 (m), 532 (m), 493 (m), 464 (m), 418 (m) cm^{-1}; ESI-HRMS (m/z, pos): Calculated for $[C_{19}H_{20}BClNP\text{-}H]^+$ 338.1037; found: 338.1042 $[M\text{-}H]^+$; Elemental analysis calcd (%) for $[C_{19}H_{20}BClNP]$: C 67.20, H 5.94, N 4.12; found: C 67.88, H 5.93, N 4.02.

2-(Chloromethyl)-6-(bis(4-methoxy)-phenylphosphino)-methyl)pyridine-borane Adduct ***5b***

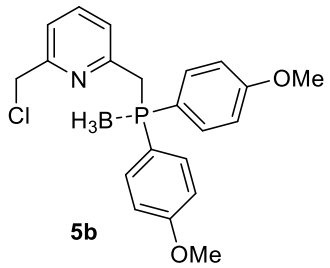

5b

The phosphine-borane adduct **5b** was obtained from 2,6-bis(chloromethyl)pyridine (0.24 g, 1.4 mmol, 1.0 equiv.) and lithium boranyl-bis(4-methoxy)phenyl-phosphanide (1.0 equiv.) as a white solid after flash chromatography. Yield: 0,30 g (53%). ^1H-NMR (400 MHz, $CDCl_3$): δ = 7.65-7.58 (m, 4H, Ar-H), 7.55 (t, 1H, J_{HH} = 7.7 Hz, pyridine-H), 7.24-7.22 (m, 1H, pyridine-H) 7.18-7.16 (m, 1H, pyridine-H), 6.93-6.90 (m, 4H, Ar-H), 4.46 (s, 2H, CH_2Cl), 3.82 (s, 6H, OCH_3), 3.76 (d, 2H, J_{PH} = 11.9 Hz, CH_2P), 1.02 (br, 3H, BH_3) ppm. $^{13}C\{^1H\}$-NMR (101 MHz, $CDCl_3$): δ = 161.9 (d, J_{PC} = 2.3 Hz 2x*C*-OCH_3), 155.7 (s, pyridine-*C*-CH_2Cl), 153.5 (d, J_{PC} = 4.7 Hz, pyridine-*C*-CH_2P), 137.0 (s, pyridine-CH), 134.4 (d, J_{PC} = 10.5 Hz, 4xAr-CH), 124.4 (d, J_{PC} = 3.2 Hz, pyridine-CH), 120.8 (d, J_{PC} = 2.0 Hz, pyridine-CH), 119.5 (d, J_{PC} = 60.3 Hz, 2xAr-C-P), 114.2 (d, J_{PC} = 11.0 Hz, 4xAr-CH), 55.3 (s, 2xOCH_3), 46.6 (s, CH_2Cl), 37.1 (d, J_{PC} = 32.0 Hz, CH_2P) ppm. $^{31}P\{^1H\}$-NMR (162 MHz, $CDCl_3$): δ = 15.6 (m) ppm; IR (solid): $\tilde{\nu}$ = 2962 (w), 2903 (m), 2841 (w), 2382 (m), 2345 (w), 1593 (m, C=N), 1569 (m), 1500 (m), 1452 (m), 1410 (w), 1293 (m), 1250 (s), 1180 (m), 1109 (m), 1064 (m), 1022 (m), 819 (s), 807 (s), 765 (m), 740 (m), 689 (w), 619 (m), 587 (m), 525 (s) cm^{-1}; ESI-HRMS (m/z, pos): Calculated for $[C_{21}H_{24}BClNO_2P\text{-}H]^+$ 398.1248; found: 398.1252 $[M\text{-}H]^+$; Elemental analysis calcd (%) for $[C_{21}H_{24}BClNO_2P]$: C 63.11, H 6.05, N 3.50; found: C 63.79, H 6.08, N 3.37.

2-(Chloromethyl)-6-(bis(4-chloro)-phenylphosphino)-methyl)pyridine-borane Adduct ***5c***

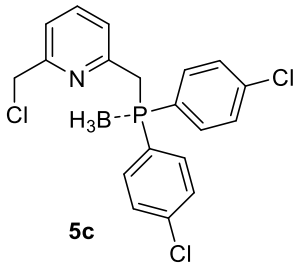

5c

The phosphine-borane adduct **5c** was obtained from 2,6-bis(chloromethyl)pyridine (0.24 g, 1.4 mmol, 1.0 equiv.) and lithium boranyl-bis(4-chloro)phenyl-phosphanide (1.0 equiv.) as an off-white solid after flash chromatography (DCM). Yield: 65.3 mg (16%). ^{1}H-NMR (300 MHz, $CDCl_3$): δ = 7.67-7.61(m, 4H, 4xAr-H), 7.58 (t, 1H, J_{HH} = 7.2 Hz, pyridine-H), 7.42-7.38 (m, 4H, Ar-H) 7.26-7.23 (m, 1H, pyridine-H), 7.19-7.15 (m, 1H, pyridine-H), 4.45 (s, 2H, CH_2Cl), 3.80 (d, 2H, J_{PH} = 11.8 Hz, CH_2P), 1.07 (br, 3H, BH_3) ppm. ^{13}C{^{1}H}-NMR (75 MHz, $CDCl_3$): δ = 156.1 (s, pyridine-*C*-CH_2Cl), 152.6 (d, J_{PC} = 4.9 Hz, pyridine-*C*-CH_2P), 138.4 (d, J_{PC} = 2.7 Hz 2x*C*-Cl), 137.5 (s, pyridine-CH), 134.2 (d, J_{PC} = 10.2 Hz, 4xAr-CH), 129.2 (d, J_{PC} = 10.6 Hz, 4xAr-CH), 126.7 (d, J_{PC} = 55.7 Hz, 2xAr-C-P) 124.6 (d, J_{PC} = 3.7 Hz, pyridine-CH), 121.3 (d, J_{PC} = 2.3 Hz, pyridine-CH), 46.5 (s, CH_2Cl), 36.4 (d, J_{PC} = 31.3 Hz, CH_2P) ppm. ^{31}P{^{1}H}-NMR (121 MHz, $CDCl_3$): δ = 18.3 (m) ppm; IR (solid): $\tilde{\nu}$ = 2962 (w), 2379 (m), 2347 (m), 1574 (m, C=N), 1482 (m), 1451 (m), 1388 (m), 1297 (w), 1262 (w), 1083 (s), 1058 (s), 1012 (2), 813 (s), 768 (s), 744 (s), 701 (m), 615 (s), 543 (m), 489 (s) cm^{-1}; ESI-HRMS (m/z, pos): Calculated for $[C_{19}H_{18}BCl_3NP\text{-}H]^+$ 406.0257; found: 406.0261 $[M\text{-}H]^+$; Elemental analysis calcd (%) for $[C_{19}H_{18}BCl_3NP]$: C 55.87, H 4.44, N 3.43; found: C 54.86, H 4.26, N 3.05.

2-(Chloromethyl)-6-((di-cyclohexylphosphino)-methyl)pyridine-borane Adduct ***5d***

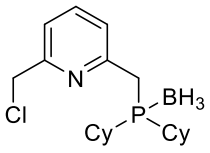

5d

The phosphine-borane adduct **5d** was obtained from 2,6-bis(chloromethyl)pyridine (0.64 g, 3.6 mmol, 1.0 equiv.) and lithium boranyl-di-cyclohexyl-phosphanide (1.0 equiv.) as an clear oil after flash chromatography. Yield: 0,25 g (20%). ^{1}H-NMR (300 MHz, $CDCl_3$): δ = 7.64 (app. t, 1H, J_{HH} = 7.7 Hz, pyridine-H), 7.31-7.26 (m, 2H, pyridine-H), 4.60 (s, 2H, CH_2Cl), 3.22 (d, 2H, J_{PH} = 11.2 Hz, CH_2P), 1.87-1.77 (m, 12H,

Cy-H), 1.38-1.17 (m, 10H, Cy-H), 0.34 (br, 3H, BH_3) ppm. $^{13}C\{^1H\}$-NMR (100 MHz, $CDCl_3$): δ = 156.0 (d, J_{PC} = 1.6 Hz, pyridine-*C*-CH_2Cl), 155.1 (d, J_{PC} = 5.6 Hz, pyridine-*C*-CH_2P), 137.4 (d, J_{PC} = 1.8 Hz, pyridine-CH), 124.5 (d, J_{PC} = 3.1 Hz, pyridine-CH), 120.9 (d, J_{PC} = 2.0 Hz, pyridine-CH), 46.9 (s, CH_2Cl), 35.3 (d, J_{PC} = 5.0 Hz, CH_2P), 31.7 (d, J_{PC} = 31.1 Hz, PCH_2), 30.4 (d, J_{PC} = 26.4 Hz, CH_2PCH), 27.1 (d, J_{PC} = 4.4 Hz, Cy-CH_2), 27.0 (d, J_{PC} = 5.1 Hz, Cy-CH_2), 26.9 (s, Cy-CH_2), 26.8 (d, J_{PC} = 2.1 Hz, Cy-CH_2), 26.1 (d, J_{PC} = 1.5 Hz, Cy-CH_2) ppm. $^{31}P\{^1H\}$-NMR (121 MHz, $CDCl_3$): δ = 28.4 (m) ppm; IR (solid): $\tilde{\nu}$ = 2926 (s), 2851 (s), 2368 (s, B–H), 1591 (m, C=N), 1574 (m, C=N), 1451 (s), 1404 (w), 1274 (w), 1062 (s), 1004 (w), 995 (w), 891 (w), 855 (s), 827 (m), 745 (s, P–C), 595 (m), 579 (m), 525 (w) cm^{-1}; ESI-HRMS (m/z, pos): Calculated for $[C_{19}H_{32}BClNP\text{-}H]^+$ 350.1976; found: 350.1979 $[M\text{-}H]^+$; Elemental analysis calcd (%) for $[C_{19}H_{32}BClNP]$: C 64.89, H 9.17, N 3.98; found: C 64.83, H 9.04, N 3.98.

2-(Chloromethyl)-6-((di-iso-butylphosphino)-methyl)pyridine-borane Adduct ***5e***

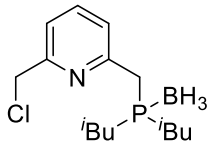

5e

The phosphine-borane adduct **5e** was obtained from 2,6-bis(chloromethyl)pyridine (0.29 g, 1.7 mmol, 1.0 equiv.) and lithium boranyl-di-*iso*-butyl-phosphanide (1.0 equiv.) as a white solid after flash chromatography. Yield: 0,10 g (20%). ^1H-NMR (500 MHz, $CDCl_3$): δ = 7.67 (t, 1H, J_{HH} = 7.7 Hz, pyridine-H), 7.33 (d, 1H, J_{HH} = 7.7 Hz, pyridine-H) 7.19 (d, 1H, J_{HH} = 7.8 Hz, pyridine-H), 4.62 (s, 2H, CH_2Cl), 3.22 (d, 2H, J_{PH} = 10.5 Hz, CH_2P), 2.02 (m, 2H, C*H*$(CH_3)_2$), 1.67 (ddd, 2H, J_{HH} = 14.7, 12.0, 6.0 Hz, C*H*HCH$(CH_3)_2$), 1.48 (ddd, 2H, J_{HH} = 14.8, 10.1, 7.0 Hz, CH*H*CH$(CH_3)_2$), 1.01 (dd, 12H, J_{HH} = 12.1, 6.6 Hz, 4xCH_3), 0.54 (br, 3H, BH_3) ppm. $^{13}C\{^1H\}$-NMR (126 MHz, $CDCl_3$): δ = 156.1 (s, pyridine-*C*-CH_2Cl), 154.4 (d, J_{PC} = 7.3 Hz, pyridine-*C*-CH_2P), 137.5 (s, pyridine-CH), 124.1 (d, J_{PC} = 3.3 Hz, pyridine-CH), 120.9 (s, pyridine-CH), 46.7 (s, CH_2Cl), 35.3 (d, J_{PC} = 5.0 Hz, CH_2P), 33.1 (d, J_{PC} = 31.2 Hz, PCH_2), 24.8 (dd, J_{PC} = 18.1, 7.3 Hz, CH_3), 24.3 (s, *C*$(CH_3)_2$) ppm. $^{31}P\{^1H\}$-NMR (202 MHz, $CDCl_3$): δ = 15.9 (m) ppm; IR (solid): $\tilde{\nu}$ = 2958 (m), 2926 (w), 2872 (w), 2380 (s), 1583 (m, C=N), 1456 (s), 1403 (w), 1282 (w), 1250 (w), 1139 (w), 1056 (s), 993 (w), 826 (s), 749 (s, P-C), 711 (w), 631 (w), 574 (m), 520 (w) cm^{-1}; ESI-HRMS (m/z, pos): Calculated for

$[C_{15}H_{28}BClNP\text{-}H]^+$ 298.1663; found: 298.1664 $[M\text{-}H]^+$; Elemental analysis calcd (%) for $[C_{15}H_{28}BClNP]$: C 60.13, H 9.42, N 4.67; found: C 60.41, H 9.59, N 4.59.

2-(Chloromethyl)-6-((di-tert-butylphosphino)-methyl)pyridine-borane Adduct ***5f***

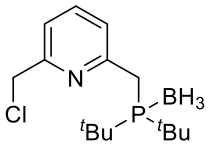

5f

The phosphine-borane adduct **5f** was obtained from 2,6-bis(chloromethyl)pyridine (1.0 g, 5.7 mmol, 1.0 equiv.) and lithium boranyl-di-*tert*-butyl-phosphanide (1.0 equiv.) as a white solid after flash chromatography. Yield: 0,97 g (57%). NMR data matches literature values.[32] ^{1}H-NMR (400 MHz, $CDCl_3$): δ = 7.67 (t, 1H, J_{HH} = 7.7 Hz, pyridine-H), 7.58 (d, 1H, J_{HH} = 7.9 Hz, pyridine-H), 7.31 (d, 1H, J_{HH} = 7.6 Hz, pyridine-H), 4.63 (s, 2H, CH_2Cl), 3.38 (d, 2H, J_{PH} = 12.1 Hz, CH_2P), 1.29 (d, 18H, J_{PH} = 12.7 Hz, 6xCH_3) 0.62 (br, 3H, BH_3) ppm. $^{31}P\{^1H\}$-NMR (162 MHz, $CDCl_3$): δ = 47.3 (m) ppm; IR (solid): $\tilde{\nu}$ = 2904 (s), 2849 (w), 2384 (s), 2347 (w), 1575 (m, C=N), 1453 (s), 1069 (m), 993 (w), 971 (w), 823 (s), 744 (s, P-C), 681 (w), 625 (m), 600 (m), 522 (w), 432 (s) cm^{-1}, Elemental analysis calcd (%) for $[C_{15}H_{28}BClNP]$: C 60.13, H 9.42, N 4.67; found: C 60.26, H 9.30, N 4.48.

2-(Chloromethyl)-6-((tert-butylphenyl-phosphino)-methyl)pyridine-borane Adduct ***5g***

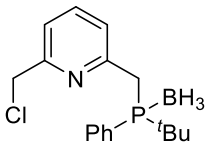

5g

The phosphine-borane adduct **5g** was obtained from 2,6-bis(chloromethyl)pyridine (0.65 g, 3.7 mmol, 1.0 equiv.) and lithium boranyl-*tert*-butylphenyl-phosphanide (1.0 equiv.) as a white solid after flash chromatography. Yield: 0,79 g (67%). ^{1}H-NMR (400 MHz, $CDCl_3$): δ = 7.88-7.83 (m, 2H, PPh), 7.57 (t, 1H, J_{HH} = 7.6 Hz, pyridine-H), 7.49-7.40 (m, 5H, pyridine-H, PPh) 7.23 (d, 1H, J_{HH} = 7.6 Hz, pyridine-H), 4.53 (s, 2H, CH_2Cl), 3.78 (app. t, 1H, J_{PH} = 13.7 Hz, J_{HH} = 13.7 Hz, C*H*HP) 3.64 (dd, 1H, J_{PH} = 9.6 Hz, J_{HH} = 13.7 Hz, CH*H*P), 1.18 (d, 9H, J_{PH} = 14.0 Hz, 3xCH_3) 0.89 (br, 3H, BH_3) ppm. $^{13}C\{^1H\}$-NMR (101 MHz, $CDCl_3$): δ = 155.4 (s, pyridine-C-CH_2Cl), 153.8 (d, J_{PC} = 2.8 Hz, pyridine-C-CH_2P), 137.0 (s, pyridine-CH), 134.2 (d, J_{PC} = 8.2 Hz, 2xphenyl-CH), 131.2 (d, J_{PC} = 2.4 Hz, phenyl-CH), 127.9 (d, J_{PC} = 9.5 Hz, 2xphenyl-

CH), 124.8 (d, J_{PC} = 2.5 Hz, pyridine-CH), 120.8 (d, J_{PC} = 2.3 Hz, pyridine-CH), 46.7 (s, CH_2Cl), 30.2 (d, J_{PC} = 2.8 Hz, P-*C*$(CH_3)_3$), 29.9 (d, J_{PC} = 5.0 Hz, CH_2P), 25.6 (d, J_{PC} = 2.1 Hz, P-C(*C*$H_3)_3$) ppm. $^{31}P\{^1H\}$-NMR (162 MHz, $CDCl_3$): δ = 33.3 (m) ppm; IR (solid): $\tilde{\nu}$ = 3054 (w), 2401 (w), 2367 (m), 1584 (m, C=N), 1456 (m), 1433 (m), 1105 (m), 1061 (m), 821 (w), 740 (s, P-C), 690 (s, P-C), 596 (m), 532 (m), 493 (m), 464 (m), 418 (m) cm^{-1}; ESI-HRMS (m/z, pos): Calculated for $[C_{17}H_{24}BClNP\text{-}H]^+$ 318.1350; found: 318.1354 $[M\text{-}H]^+$; Elemental analysis calcd (%) for $[C_{17}H_{24}BClNP]$: C 63.88, H 7.57, N 4.38; found: C 63.95, H 7.25, N 4.29.

2-(Chloromethyl)-6-((di-adamantylphosphino)-methyl)pyridine-borane Adduct ***5h***

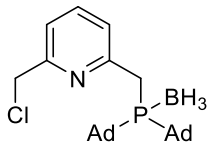

5h

The phosphine-borane adduct **5h** was obtained from 2,6-bis(chloromethyl)pyridine (0.22 g, 1.3 mmol, 1.0 equiv.) and lithium boranyl-di-adamantyl-phosphanide (1.0 equiv.) as a white solid after flash chromatography. Yield: 0,38 g (67%). ^1H-NMR (400 MHz, $CDCl_3$): δ = 7.62 (t, 1H, J_{HH} = 7.7 Hz, pyridine-H), 7.53 (d, 1H, J_{HH} = 7.9 Hz, pyridine-H) 7.28 (m, 1H, pyridine-H), 4.61 (s, 2H, CH_2Cl), 3.31 (d, 2H, J_{PH} = 12.1 Hz, CH_2P), 2.15-1.70 (m, 30H, adamantyl-H), 0.41 (br, 3H, BH_3) ppm. $^{13}C\{^1H\}$-NMR (101 MHz, $CDCl_3$): δ = 156.2 (d, J_{PC} = 2.0 Hz, pyridine-*C*-CH_2P), 155.2 (s, pyridine-*C*-CH_2Cl), 136.8 (s, pyridine-CH), 125.5 (s, pyridine-CH), 120.7 (s, pyridine-CH), 46.8 (s, CH_2Cl), 38.0 (s, adamantyl-CH_2) 37.6 (d, J_{PC} = 23.8 Hz, adamantyl-C-P), 36.5 (s, adamantyl-CH_2), 28.3 (d, J_{PC} = 7.9 Hz, adamantyl-CH), 26.8 (d, J_{PC} = 23.4 Hz, CH_2P) ppm. $^{31}P\{^1H\}$-NMR (202 MHz, $CDCl_3$): δ = 38.0 (m) ppm; IR (solid): $\tilde{\nu}$ = 2905 (s), 2849 (m), 2368 (w), 1581 (m, C=N), 1451 (m), 1067 (m), 970 (w), 837 (w), 744 (w, P-C), 685 (w, P-C), 596 (m), 527 (w), 413 (s) cm^{-1}; ESI-HRMS (m/z, pos): Calculated for $[C_{27}H_{40}BClNP\text{-}H]^+$ 454.2602; found: 454.2610 $[M\text{-}H]^+$; Elemental analysis calcd (%) for $[C_{27}H_{40}BClNP]$: C 71.14, H 8.84, N 3.07; found: C 72.04, H 9.32, N 3.25.

General Procedure for the Synthesis of Resin-Bound Pyridine-based PNP-Pincer Ligands L_1-L_{14}

Step 1

A resin-bound phosphine-borane (**1a·BH_3**, 0.32 g, 0.36 mmol, 1.0 equiv.), (**1b·BH_3**, 0.22 g, 0.24 mmol, 1.0 equiv.), (**1c·BH_3**, 0.25 g, 0.28 mmol, 1.0 equiv.) or (**1d·BH_3**,

0.12 g, 0.22 mmol, 1.0 equiv.) was swollen in THF (20 mL). After addition of KHMDS (20% in THF, 10 equiv.) under gentle stirring to avoid mechanical abrasion of the resin, the orange resin was allowed to react for 2 hours at room temperature. The supernatant was removed and the resin was washed three times with THF (15 mL) followed by three times with Et_2O (15 mL). Without further purification the BH_3-protected resin-bound potassium phosphides were used in the next step.

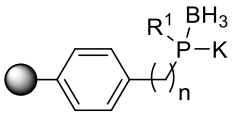

K·1a·BH$_3$: MF, n = 1, R^1 = Ph
K·1b·BH$_3$: MF 4% DVB, n = 1, R^1 = Ph
K·1c·BH$_3$: MF, n = 1, R^1 = Cy
K·1d·BH$_3$: PS, n = 0, R^1 = ^{t}Bu

K·1a·BH$_3$: Orange resin: $^{31}P\{^1H\}$-NMR (162 MHz, THF): δ = -37.1 (br s) ppm.

K·1b·BH$_3$: Yellow resin: $^{31}P\{^1H\}$-NMR (121 MHz, THF:C_6D_6 6:1): δ = -39.5 (br s) ppm.

K·1c·BH$_3$: Orange resin: $^{31}P\{^1H\}$-NMR (162 MHz, THF): δ = -34.5 (br s) ppm.

K·1d·BH$_3$: Orange resin: $^{31}P\{^1H\}$-NMR (162 MHz, THF): δ = -14.6 (br s) ppm.

Step 2

A previously synthesized BH_3-protected resin-bound potassium phosphide (**K·1a·BH$_3$**, 0.36 mmol, 1.0 equiv.), (**K·1b·BH$_3$**, 0.24 mmol, 1.0 equiv.), (**K·1c·BH$_3$**, 0.28 mmol, 1.0 equiv.) or (**K·1d·BH$_3$**, 0.22 mmol, 1.0 equiv.) was swollen in THF (10 mL) and cooled to -78 °C. A member of the series of 2-(chloromethyl)-6-(phosphinomethyl)pyridine-boranes **5a-h** (1.1 equiv.) was azeotropically dried with toluene (3x5 mL), dissolved in 10 mL THF and added to the resin at -78 °C under gentle stirring to avoid mechanical abrasion. The mixture was left with occasional stirring and warmed up to room temperature overnight. The reaction was monitored using gel-phase $^{31}P\{^1H\}$-NMR and was allowed to react until full conversion was observed. Next, the supernatant was removed and the resin was washed three times with THF (10 mL) followed by three times with Et_2O (10 mL) and dried *in vacuo* yielding a pale yellow resin-bound PNP borane adduct (**6a-n**).

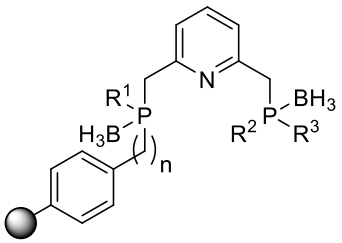

6a: MF, n = 1, R^1 = Ph, R^2 = R^3 = Ph
6b: MF, n = 1, R^1 = Ph, R^2 = R^3 = 4-MeOPh
6c: MF, n = 1, R^1 = Ph, R^2 = R^3 = 4-ClPh
6d: MF, n = 1, R^1 = Ph, R^2 = R^3 = Cy
6e: MF, n = 1, R^1 = Ph, R^2 = R^3 = ^{i}Bu
6f: MF, n = 1, R^1 = Ph, R^2 = R^3 = ^{t}Bu
6g: MF 4% DVB, n = 1, R^1 = Ph, R^2 = R^3 = ^{t}Bu
6h: MF, n = 1, R^1 = Ph, R^2 = Ph, R^3 = ^{t}Bu
6i: MF, n = 1, R^1 = Ph, R^2 = R^3 = Ad
6j: MF 4% DVB, n = 1, R^1 = Ph, R^2 = R^3 = Ad
6k: MF, n = 1, R^1 = Cy, R^2 = R^3 = Ph
6l: MF, n = 1, R^1 = Cy, R^2 = R^3 = ^{t}Bu
6m: PS, n = 0, R^1 = ^{t}Bu, R^2 = R^3 = ^{t}Bu
6n: PS, n = 0, R^1 = ^{t}Bu, R^2 = Ph, R^3 = ^{t}Bu

6a: Pale yellow resin: $^{31}P\{^1H\}$-NMR (162 MHz, THF): δ = 18.4 (br s, -*P*Ph_2-BH_3 and -MF-*P*Ph-BH_3), –11.1 (s, free -*P*Ph_2) ppm.

6b: Yellow resin: $^{31}P^1H\}$-NMR (162 MHz, THF): δ = 18.5 (br s, -MF-*P*Ph-BH_3), 14.9 (br, -*P*(4-MeOPh)$_2$-BH_3 and ppm.

6c: Pale yellow resin: $^{31}P^1H\}$-NMR (121 MHz, THF:C_6D_6 6:1): δ = 18.0 (br s, -*P*(4-ClPh)$_2$-BH_3 and -MF-*P*Ph-BH_3), –13.5 (s, free -*P*(4-ClPh)$_2$) ppm.

6d: Pale yellow resin: $^{31}P\{^1H\}$-NMR (121 MHz, THF:C_6D_6 6:1): δ = 28.9 (br s, -PCy_2-BH_3), 18.4 (br s, -MF-*P*Ph-BH_3) ppm.

6e: Pale yellow resin: $^{31}P\{^1H\}$-NMR (162 MHz, THF): δ = 21.3 (br s, -MF-*P*Ph-BH_3), 18.4 (s, -*P*^{i}Bu_2-BH_3) ppm.

6f: Pale yellow resin: $^{31}P\{^1H\}$-NMR (162 MHz, THF): δ = 48.0 (s, -*P*^{t}Bu_2-BH_3), 18.8 (br s, -MF-*P*Ph-BH_3) ppm.

6g: Yellow resin: $^{31}P\{^1H\}$-NMR (121 MHz, THF:C_6D_6 6:1): δ = 47.6 (s, -*P*^{t}Bu_2-BH_3), 18.3 (br s, -MF-*P*Ph-BH_3) ppm.

6h: Pale yellow resin: $^{31}P\{^1H\}$-NMR (162 MHz, THF): δ = 33.8 (s, -*P*Ph^{t}Bu-BH_3), 18.6 (br s, -MF-*P*Ph-BH_3) ppm.

6i: Pale yellow resin: $^{31}P\{^1H\}$-NMR (162 MHz, THF): δ = 38.9 (s, -*P*Ad_2-BH_3), 18.8 (br s, -MF-*P*Ph-BH_3) ppm.

6j: Yellow resin: $^{31}P\{^1H\}$-NMR (121 MHz, THF:C_6D_6 2:1): δ = 38.5 (s, -*P*Ad_2-BH_3), 18.2 (br s, -MF-*P*Ph-BH_3) ppm.

6k: Pale orange resin: $^{31}P\{^1H\}$-NMR (162 MHz, THF): δ = 25.8 (br s, -MF-*P*Cy-BH_3), 18.1 (s, -*P*Ph_2-BH_3), –11.1 (s, free -*P*Ph_2) ppm.

6l: Pale orange resin: $^{31}P\{^{1}H\}$-NMR (162 MHz, THF): δ = 48.2 (s, -*P*^{t}Bu$_2$-BH$_3$), 25.9 (br s, -MF-*P*Cy-BH$_3$) ppm.

6m: Pale yellow resin: $^{31}P\{^{1}H\}$-NMR (162 MHz, THF): δ = 48.3 (s, -*P*^{t}Bu$_2$-BH$_3$), 32.6 (br s, -PS-*P*^{t}Bu-BH$_3$) ppm.

6n: Pale yellow resin: $^{31}P\{^{1}H\}$-NMR (162 MHz, THF): δ = 33.5 (br s, -*P*Ph^{t}Bu-BH$_3$), 32.0 (br s, -PS-*P*^{t}Bu-BH$_3$) ppm.

Step 3

A resin-bound PNP borane adduct **6a-n** synthesized in the last step was swollen in 10 mL of diethyl amine and heated to 50 °C overnight with occasional stirring to avoid mechanical abrasion of the resin. The reaction was monitored using gel-phase $^{31}P\{^{1}H\}$-NMR and was allowed to react until full conversion was observed. Next, the mixture was cooled to room temperature and the supernatant was removed. The resin was washed with three portions of THF (10 mL) followed by three portions of Et$_2$O (10 mL) and dried *in vacuo* yielding a pale yellow resin-bound PNP pincer ligand (**L$_1$**-**L$_{14}$**).

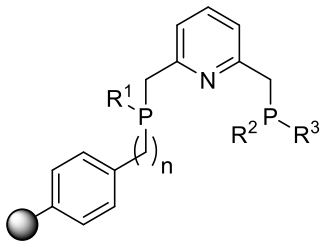

L$_1$: MF, n = 1, R^1 = Ph, R^2 = R^3 = Ph
L$_2$: MF, n = 1, R^1 = Ph, R^2 = R^3 = 4-MeOPh
L$_3$: MF, n = 1, R^1 = Ph, R^2 = R^3 = 4-ClPh
L$_4$: MF, n = 1, R^1 = Ph, R^2 = R^3 = Cy
L$_5$: MF, n = 1, R^1 = Ph, R^2 = R^3 = ^{i}Bu
L$_6$: MF, n = 1, R^1 = Ph, R^2 = R^3 = ^{t}Bu
L$_7$: MF 4% DVB, n = 1, R^1 = Ph, R^2 = R^3 = ^{t}Bu
L$_8$: MF, n = 1, R^1 = Ph, R^2 = Ph, R^3 = ^{t}Bu
L$_9$: MF, n = 1, R^1 = Ph, R^2 = R^3 = Ad
L$_{10}$: MF 4% DVB, n = 1, R^1 = Ph, R^2 = R^3 = Ad
L$_{11}$: MF, n = 1, R^1 = Cy, R^2 = R^3 = Ph
L$_{12}$: MF, n = 1, R^1 = Cy, R^2 = R^3 = ^{t}Bu
L$_{13}$: PS, n = 0, R^1 = ^{t}Bu, R^2 = R^3 = ^{t}Bu
L$_{14}$: PS, n = 0, R^1 = ^{t}Bu, R^2 = Ph, R^3 = ^{t}Bu

L$_1$: Pale yellow resin (288 mg, 0.245 mmol, 99%): $^{31}P\{^{1}H\}$-NMR (162 MHz, THF): δ = -11.2 (s, -*P*Ph$_2$), -14.0 (br s, -MF-*P*Ph) ppm; IR (KBr): $\tilde{\nu}$ = 3056 (m), 3024 (m), 2918 (m), 2849 (m), 1578 (m), 1487 (m, C=C), 1445 (m), 1110 (w), 1071 (w), 838 (w), 743 (m, P-Ar), 697 (s, P-Ar) cm^{-1}; Elemental analysis calcd (%) for **L$_1$** (0.82 mmol·g^{-1}): P 5.08, N 1.15; found: P 4.98, N 0.97.

L$_2$: Pale yellow resin (322 mg, 0.260 mmol, 90%): $^{31}P\{^{1}H\}$-NMR (162 MHz, THF): δ = -14.0 (br, -*P*(4-MeOPh)$_2$ and -MF-*P*Ph) ppm; IR (KBr): $\tilde{\nu}$ = 3057 (m), 3023

(m), 2919 (m), 2845 (m), 1592 (s), 1497 (s, C=C), 1448 (s), 1282 (w), 1246 (m, C-O), 1177 (m), 1102 (w), 824 (w), 750 (m, P-Ar), 698 (s, P-Ar) cm^{-1}; Elemental analysis calcd (%) for **L_2** (0.81 $mmol \cdot g^{-1}$): P 5.01, N 1.13; found: P 5.55, N 0.84.

L_3: Pale yellow resin (322 mg, 0.260 mmol, 90%): $^{31}P\{^1H\}$-NMR (121 MHz, THF:C_6D_6 6:1): δ = -13.3 (br, -*P*(4-ClPh)$_2$), -14.3 (br, -MF-*P*Ph) ppm; IR (KBr): $\tilde{\nu}$ = 3056 (w), 3022 (m), 2917 (m), 2850 (m), 1583 (s), 1495 (m, C=C), 1445 (s), 1384 (m), 1081 (w), 1013 (m), 838 (m), 812 (m), 743 (s, P-Ar), 697 (s, P-Ar), 498 (s) cm^{-1}; Elemental analysis calcd (%) for **L_3** (0.77 $mmol \cdot g^{-1}$): P 4.78, N 1.08, Cl 5.47; found: P 6.41, N 0.75, Cl 5.41.

L_4: Pale yellow resin (195 mg, 0.164 mmol, 97%): $^{31}P\{^1H\}$-NMR (121 MHz, THF:C_6D_6 6:1): δ = 3.0 (s, -*P*Cy$_2$), -14.5 (br s, -MF-*P*Ph) ppm; IR (KBr): $\tilde{\nu}$ = 3056 (w), 3024 (m), 2919 (m), 2855 (m), 1578 (m), 1495 (m, C=C), 1446 (s), 1179 (w), 845 (w), 752 (m, P-Ar), 698 (s, P-Ar) cm^{-1}.

L_5: Pale yellow resin (401 mg, 0.356 mmol, 99%): $^{31}P\{^1H\}$-NMR (162 MHz, THF): δ = -14.7 (br s, -MF-*P*Ph), -33.4 (s, -*P*^{i}Bu$_2$), ppm; IR (KBr): 3057 (w), 3024 (m), 2919 (s), 2868 (m), 1578 (m), 1495 (m; C=C), 1448 (s), 1162 (w), 845 (w), 752 (m, P-Ar), 697 (s, P-Ar), 514 (w) cm^{-1}; Elemental analysis calcd (%) for **L_5** (0.84 $mmol \cdot g^{-1}$): P 5.18, N 1.17; found: P 7.26, N 1.03.

L_6: Pale yellow resin (401 mg, 0.356 mmol, 99%): $^{31}P\{^1H\}$-NMR (162 MHz, THF): δ = 35.5 (s, -*P*^{t}Bu$_2$), -13.9 (br s, -MF-*P*Ph) ppm; IR (KBr): $\tilde{\nu}$ = 3057 (m), 3024 (m), 2920 (m), 2857 (m), 1578 (m), 1497 (m, C=C), 1448 (m), 1179 (w), 1111 (w), 1073 (w), 831 (w), 746 (m, P-Ar), 698 (s, P-Ar), 539 (w) cm^{-1}; Elemental analysis calcd (%) for **L_6** (0.84 $mmol \cdot g^{-1}$): P 5.18, N 1.17; found: P 4.30, N 0.98.

L_7: Yellow resin (200 mg, 0.231 mmol, 96%): $^{31}P\{^1H\}$-NMR (121 MHz, THF:C_6D_6 6:1): δ = 35.0 (s, -*P*^{t}Bu$_2$), -14.3 (br s, -MF-*P*Ph) ppm; IR (KBr): $\tilde{\nu}$ = 3056 (w), 3024 (w), 2919 (m), 2856 (w), 1577 (m), 1497 (m, C=C), 1445 (m), 1111 (w), 1071 (w), 833 (w), 745 (m, P-Ar), 697 (s, P-Ar) cm^{-1}; Elemental analysis calcd (%) for **L_7** (0.87 $mmol \cdot g^{-1}$): P 5.36; found: P 6.42.

L_8: Pale yellow resin (132 mg, 0.114 mmol, 96%): $^{31}P\{^1H\}$-NMR (162 MHz, THF): δ = 9.0 (s, -*P*Ph^{t}Bu), -14.1 (br s, -MF-*P*Ph) ppm; IR (KBr): $\tilde{\nu}$ = 3056 (w), 3024 (m), 2921 (m), 2853 (m), 1578 (m), 1496 (m, C=C), 1448 (m), 1180 (w), 1107 (w), 1072 (w), 837 (w), 746 (m, P-Ar), 697 (s, P-Ar) cm^{-1}; Elemental analysis calcd (%) for **L_8** (0.82 $mmol \cdot g^{-1}$): P 5.08, N 1.15; found: P 4.51, N 1.08.

L_9: Pale yellow resin (338 mg, 0.262 mmol, 91%): $^{31}P\{^1H\}$-NMR (162 MHz, THF): δ = 32.1 (s, -*P*Ad$_2$), -13.9 (br s, -MF-*P*Ph) ppm; IR (KBr): $\tilde{\nu}$ = 3056 (m), 3024

(m), 2901 (s), 2847 (m), 1578 (m, C=N), 1496 (m, C=C), 1446 (m, P-C), 1111 (w), 835 (w), 746 (m, P-Ar), 697 (s, P-Ar) cm^{-1}; Elemental analysis calcd (%) for **L_9** (0.74 $mmol \cdot g^{-1}$): P 4.60, N 1.04; found: P 3.57, N 0.86.

L_{10}: Pale yellow resin (320 mg, 0.244 mmol, 95%): $^{31}P\{^1H\}$-NMR (121 MHz, THF:C_6D_6 6:1): δ = 31.5 (s, -*P*Ad_2), -14.9 (br s, -MF-*P*Ph) ppm; IR (KBr): $\tilde{\nu}$ = 3057 (w), 3024 (w), 2899 (m), 2848 (w), 1578 (m), 1495 (m, C=C), 1445 (m), 1111 (w), 837 (w), 746 (m, P-Ar), 696 (s, P-Ar) cm^{-1}; Elemental analysis calcd (%) for **L_{10}** (0.66 $mmol \cdot g^{-1}$): P 4.72; found: P 8.18.

L_{11}: Pale yellow resin (324 mg, 0.274 mmol, 99%): $^{31}P\{^1H\}$-NMR (162 MHz, THF): δ = -4.8 (br s, -MF-*P*Cy), -10.8 (s, -*P*Ph_2) ppm; IR (KBr): $\tilde{\nu}$ = 3057 (w), 3024 (m), 2920 (m), 2848 (m), 1577 (m), 1490 (m, C=C), 1449 (m), 1070 (w), 837 (w), 745 (m, P-Ar), 698 (s, P-Ar) cm^{-1}; Elemental analysis calcd (%) for **L_{11}** (0.85 $mmol \cdot g^{-1}$): P 5.24, N 1.19; found: P 5.32, N 1.11.

L_{12}: Pale yellow resin (276 mg, 0.242 mmol, 88%): $^{31}P\{^1H\}$-NMR (162 MHz, THF): δ = 35.1 (s, -*P*^{t}Bu_2), -4.7 (br s, -MF-*P*Cy) ppm; IR (KBr): $\tilde{\nu}$ = 3057 (m), 3025 (m), 2922 (s), 2852 (m), 1578 (m), 1497 (m, C=C), 1448 (m), 1179 (w), 1072 (w), 822 (w), 753 (m, P-Ar), 698 (s, P-Ar) cm^{-1}; Elemental analysis calcd (%) for **L_{12}** (0.88 $mmol \cdot g^{-1}$): P 5.42, N 1.23; found: P 5.02, N 1.09.

L_{13}: Pale yellow resin (125 mg, 0.159 mmol, 98%): $^{31}P\{^1H\}$-NMR (162 MHz, THF): δ = 35.2 (s, -*P*^{t}Bu_2), 7.2 (br s, -PS-*P*^{t}Bu) ppm; IR (KBr): $\tilde{\nu}$ = 3059 (m), 3026 (m), 2928 (s), 2860 (m), 1578 (m), 1495 (m, C=C), 1452 (m), 1179 (w), 822 (m), 754 (m, P-Ar), 699 (s, P-Ar) cm^{-1}; Elemental analysis calcd (%) for **L_{13}** (1.20 $mmol \cdot g^{-1}$): P 7.47, N 1.69; found: P 5.78, N 1.36.

L_{14}: Pale yellow resin (177 mg, 0.220 mmol, 99%): $^{31}P\{^1H\}$-NMR (162 MHz, THF): δ = 8.9 (br s, -*P*Ph^{t}Bu and -PS-*P*^{t}Bu) ppm; IR (KBr): $\tilde{\nu}$ = 3059 (m), 3025 (m), 2926 (m), 2857 (m), 1579 (m), 1495 (w, C=C), 1451 (m), 1180 (w), 825 (w), 749 (m, P-Ar), 698 (s, P-Ar) cm^{-1}; Elemental analysis calcd (%) for **L_{14}** (1.18 $mmol \cdot g^{-1}$): P 7.29, N 1.65; found: P 5.49, N 1.19.

General Procedure for the Synthesis of Resin-Bound complexes C_1-C_{14}

A previously synthesized resin-bound PNP pincer ligand (**L_1-L_{14}**, ~80-170 mg, 1.0 equiv.) and [Ru(HCl(PPh_3)$_3$CO] (1.1 equiv.) were weighed into a Schlenk tube. The mixture was suspended in THF (10 mL) and heated to 60 °C under gentle stirring. The reaction mixture was left at 60 °C with occasional stirring to avoid mechanical abrasion of the resin and the progress of the reaction was monitored by gel-phase $^{31}P\{^1H\}$-NMR.

Once full complexation of the resin-bound PNP ligand was observed, the mixture was cooled to room temperature and the supernatant was removed. The resin-bound complex was washed with three portions of THF (10 mL), three portions of DCM (10 mL) followed by three portions of Et_2O (10 mL). After drying *in vacuo* a yellow to brown resin-bound RuPNP complex (**C_1**-**C_{14}**) was obtained.

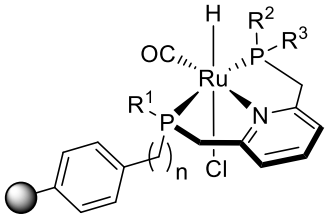

C_1: MF, n = 1, R^1 = Ph, R^2 = R^3 = Ph
C_2: MF, n = 1, R^1 = Ph, R^2 = R^3 = 4-MeOPh
C_3: MF, n = 1, R^1 = Ph, R^2 = R^3 = 4-ClPh
C_4: MF, n = 1, R^1 = Ph, R^2 = R^3 = Cy
C_5: MF, n = 1, R^1 = Ph, R^2 = R^3 = ^{i}Bu
C_6: MF, n = 1, R^1 = Ph, R^2 = R^3 = ^{t}Bu
C_7: MF 4% DVB, n = 1, R^1 = Ph, R^2 = R^3 = ^{t}Bu
C_8: MF, n = 1, R^1 = Ph, R^2 = Ph, R^3 = ^{t}Bu
C_9: MF, n = 1, R^1 = Ph, R^2 = R^3 = Ad
C_{10}: MF 4% DVB, n = 1, R^1 = Ph, R^2 = R^3 = Ad
C_{11}: MF, n = 1, R^1 = Cy, R^2 = R^3 = Ph
C_{12}: MF, n = 1, R^1 = Cy, R^2 = R^3 = ^{t}Bu
C_{13}: PS, n = 0, R^1 = ^{t}Bu, R^2 = R^3 = ^{t}Bu
C_{14}: PS, n = 0, R^1 = ^{t}Bu, R^2 = Ph, R^3 = ^{t}Bu

C_1: Yellow-brown resin (85 mg, 0.063 mmol, 93%): $^{31}P\{^1H\}$-NMR (162 MHz, THF): δ = 51.6 (br s, 2P) ppm; IR (KBr): $\tilde{\nu}$ = 3054 (m), 3024 (m), 2917 (m), 2850 (w), 1926 (s, CO), 1598 (w), 1485 (m, C=C), 1443 (m), 1099 (m), 746 (m, P-Ar), 696 (s, P-Ar) cm^{-1}.

C_2: Yellow-orange resin (161 mg, 0.115 mmol, 95%): $^{31}P\{^1H\}$-NMR (162 MHz, THF): δ = 49.7 (br s, 2P) ppm; IR (KBr): $\tilde{\nu}$ = 3055 (w), 3024 (m), 2918 (m), 2846 (w), 1926 (s, CO), 1594 (m), 1497 (s, C=C), 1453 (m), 1286 (w), 1250 (m, C-O), 1180 (m), 1102 (m), 750 (m, P-Ar), 697 (s, P-Ar) cm^{-1}.

C_3: Yellow-orange resin (85 mg, 0.063 mmol, 93%): $^{31}P\{^1H\}$-NMR (121 MHz, THF:C_6D_6 6:1): δ = 50.8 (br s, 2P) ppm; IR (solid): $\tilde{\nu}$ = 3055 (w), 3023 (m), 2917 (m), 2850 (w), 1927 (s, CO), 1599 (m), 1570 (w), 1485 (m), 1450 (s), 1384 (m), 1183 (w), 1081 (m), 1011 (m), 965 (w), 839 (m), 815 (m), 741 (s, P-Ar), 694 (s, P-Ar), 494 (s) cm^{-1}.

C_4: Yellow-brown resin (123 mg, 0.094 mmol, 84%): $^{31}P\{^1H\}$-NMR (121 MHz, THF:C_6D_6 6:1): δ = 66.8 (br s, -*P*Cy_2) and 50.0 (br s, -MF-*P*Ph) ppm; IR (KBr): $\tilde{\nu}$ = 3056 (w), 3024 (m), 2918 (m), 2856 (w), 1920 (s, CO), 1596 (w), 1487 (w, C=C), 1450 (m), 752 (m, P-Ar), 698 (s, P-Ar) cm^{-1}.

C_5: Yellow-brown resin (171 mg, 0.131 mmol, 91%): $^{31}P\{^1H\}$-NMR (162 MHz, THF): δ = 46.5 (br s, 2P) ppm; IR (KBr): $\tilde{\nu}$ = 3024 (w), 2918 (m), 2863 (w), 1921 (s, CO), 1599 (w), 1494 (w, C=C), 1453 (m), 842 (w), 751 (m, P-Ar), 698 (s, P-Ar) cm^{-1}.

C_6: Yellow-brown resin (175 mg, 0.134 mmol, 93%): $^{31}P\{^1H\}$-NMR (162 MHz, THF): δ = 91.2 (br s, -*P*^{t}Bu$_2$), 56.5 (br s, -MF-*P*Ph) ppm; IR (KBr): $\tilde{\nu}$ = 3024 (w), 2918 (m), 2866 (w), 1921 (s, CO), 1599 (w), 1496 (w, C=C), 1454 (m), 842 (w), 750 (m, P-Ar), 698 (s, P-Ar) cm^{-1}.

C_7: Yellow-brown resin (218 mg, 0.165 mmol, 71%): $^{31}P\{^1H\}$-NMR (162 MHz, THF): δ = 91.3 (br s, -*P*^{t}Bu$_2$), 56.4 (br s, -MF-*P*Ph) ppm; IR (solid): $\tilde{\nu}$ = 3024 (w), 2917 (m), 2852 (w), 1918 (s, CO), 1599 (m), 1492 (w, C=C), 1451 (m), 835 (w), 744 (m, P-Ar), 695 (s, P-Ar) cm^{-1}.

C_8: Orange-brown resin (88 mg, 0.076 mmol, 88%): $^{31}P\{^1H\}$-NMR (162 MHz, THF): δ = 76.3 (br s, -*P*Ph^{t}Bu), 65.2 (br s, -*P*Ph^{t}Bu), 53.5 (br s, -MF-*P*Ph) ppm; IR (KBr): $\tilde{\nu}$ = 3055 (w), 3024 (w), 2918 (m), 2855 (m), 1921 (s, CO), 1600 (w), 1497 (w, C=C), 1450 (m), 1105 (w), 750 (m, P-Ar), 697 (s, P-Ar) cm^{-1}.

C_9: Yellow resin (203 mg, 0.139 mmol, 92%): $^{31}P\{^1H\}$-NMR (162 MHz, THF): δ = 83.7 (br s, -*P*Ad$_2$), 56.5 (br s, -MF-*P*Ph), 31.0 (-*P*Ad$_2$ of free ligand) ppm; IR (KBr): $\tilde{\nu}$ = 3056 (w), 3024 (m), 2903 (s), 2849 (m), 1920 (s, CO), 1597 (s), 1490 (w, C=C), 1449 (m), 1109 (w), 967 (w), 748 (m, P-Ar), 697 (s, P-Ar) cm^{-1}.

C_{10}: Yellow-brown resin (325 mg, 0.220 mmol, 90%): $^{31}P\{^1H\}$-NMR (162 MHz, THF): δ = 86.9 (br s, -*P*Ad$_2$), 58.8 (br s, -MF-*P*Ph) ppm; IR (solid): $\tilde{\nu}$ = 3055 (w), 3024 (m), 2902 (m), 1918 (s, CO), 1595 (m), 1487 (w, C=C), 1448 (m), 1105 (w) 746 (m, P-Ar), 695 (s, P-Ar) cm^{-1}.

C_{11}: Yellow-brown resin (111 mg, 0.086 mmol, 93%): $^{31}P\{^1H\}$-NMR (162 MHz, THF): δ = 61.0 (br s, -*P*Cy), 51.5 (br s, -MF-*P*Ph$_2$) ppm; IR (KBr): $\tilde{\nu}$ = 3055 (w), 3024 (w), 2920 (m), 2850 (m), 1924 (s, CO), 1598 (w), 1494 (m, C=C), 1450 (m), 1105 (m), 750 (m, P-Ar), 697 (m, P-Ar) cm^{-1}.

C_{12}: Yellow-brown resin (129 mg, 0.099 mmol, 90%): $^{31}P\{^1H\}$-NMR (162 MHz, THF): δ = 90.7 (br s, -*P* ^{t}Bu$_2$), 66.8 (br s, -MF-*P*Cy) ppm; IR (KBr): $\tilde{\nu}$ = 3024 (w), 2921 (m), 2852 (m), 1919 (s, CO), 1598 (w), 1497 (w, C=C), 1451 (m), 1179 (w), 752 (m, P-Ar), 698 (m, P-Ar) cm^{-1}.

C_{13}: Orange resin (113 mg, 0.119 mmol, 94%): $^{31}P\{^1H\}$-NMR (162 MHz, THF): δ = 90.7 (br s, -*P* ^{t}Bu$_2$), 79.8 (br s, -*P*Ph^{t}Bu), 64.9 (br s, -*P*Ph^{t}Bu) ppm; IR (KBr):

$\tilde{\nu}$ = 3024 (w), 2926 (m), 2864 (m), 1916 (s, CO), 1598 (w), 1458 (m), 1178 (w), 1107 (w), 836 (w), 752 (m, P-Ar), 698 (m, P-Ar) cm^{-1}.

C_{14}: Orange resin (110 mg, 0.107 mmol, 94%): ^{1}H MAS NMR (400 MHz): δ = –13.85 (s, Ru-H) ppm; ^{13}C CP-MAS NMR (101 MHz): δ = 211.0 (CO), 162.1 (pyridine-*C*), 145.5 (pyridine-*C*), 128.1 (PS-*C*, P-Ph), 120.8 (pyridine-*C*), 40.5 (PS-*C*, *C*H_2P), 35.0 (P-*C*$(CH_3)_3$), 31.9 (P-*C*$(CH_3)_3$), 27.5 (P-C(*C*$H_3)_3$) ppm; ^{31}P MAS NMR (400 MHz): δ = 78.9 (br s), 65.1 (br s) ppm; IR (KBr): $\tilde{\nu}$ = 3056 (w), 3025 (w), 2926 (m), 2861 (m), 1917 (s, CO) 1597 (w), 1456 (m), 1106 (w), 750 (m, P-Ar), 698 (m, P-Ar) cm^{-1}.

2-(Di-*tert*-butylphosphino)methyl-6-(diphenylphosphino)methylpyridine-diborane Adduct 7

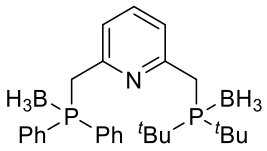

7

To a solution of di-*tert*-butylphosphino-borane adduct (100 mg, 0.62 mmol, 1.2 equiv.) in dry THF at -78 °C, *n*-BuLi (0.25 mL, 0.62 mmol, 2.5 M in hexanes, 1.2 equiv.) was added dropwise. The solution was stirred for 30 min at –78 °C and subsequently warmed to room temperature and was left for an additional amount of time until full conversion was achieved according to ^{31}P{^{1}H}-NMR. **5a** (156 mg, 0.52 mmol, 1.0 equiv.) was dissolved in dry THF and cooled to -78 °C. Next, the freshly prepared lithium boranyl phosphanide solution in THF was added. The mixture was allowed to warmed to room temperature overnight leading to a yellow solution. The solvent was removed under vacuum and the yellow residue was dissolved in DCM. The organic phase was washed with water and brine and subsequently dried over $MgSO_4$. After filtration, the solvent was removed under reduced pressure. The residue was purified *via* flash chromatography (1:4 Hexanes : CH_2Cl_2) yielding **7** as a white solid (220 mg, 91% yield). ^{1}H-NMR (300 MHz, $CDCl_3$): δ = 7.74-7.68 (m, 4H, PPh), 7.46-7.41 (m, 8H, PPh and pyridine-H), 6.96 (app. d, 1H, J_{HH} = 6.7 Hz, pyridine-H), 3.78 (d, 2H, J_{HH} = 12.0 Hz, C*H*$_2$PPh), 3.11 (d, 2H, J_{HH} = 12.2 Hz, C*H*$_2$P^{t}Bu), 1.18 (d, 18H, J_{HH} = 12.7 Hz, C$(CH_3)_3$) , 1.49-0.00 (br, 6H, BH_3) ppm. ^{13}C{^{1}H}-NMR (101 MHz, $CDCl_3$): δ = 155.1 (s, pyridine-*C*-CH_2P), 152.3 (d, J_{PC} = 3.2 Hz, pyridine-*C*-CH_2P), 136.2 (s, pyridine-CH), 132.8 (d, J_{PC} = 9.3 Hz, 4xAr-CH), 131.3 (s, 2xAr-CH), 129.2 (d,

J_{PC} = 55.0 Hz, 2xAr-C-P), 128.7 (d, J_{PC} = 10.0 Hz, 4xAr-CH), 124.0 (s, pyridine-CH), 123.0 (s, pyridine-CH), 36.2 (d, J_{PC} = 32.3 Hz, CH_2PPh), 32.8 (d, J_{PC} = 25.3 Hz, 2xP-*C*$(CH_3)_3$), 28.9 (d, J_{PC} = 23.3 Hz, CH_2P^tBu), 28.2 (s, 2xP-C(*C*$H_3)_3$) ppm. $^{31}P\{^1H\}$-NMR (202 MHz, $CDCl_3$): δ = 47.0-46.4 (m, P^tBu_2), 18.4-17.9 (m, PPh_2) ppm; IR (solid): $\tilde{\nu}$ = 2965 (w), 2902 (w), 2403 (m), 2373 (m), 2348 (m), 1588 (w), 1571 (m, C=N), 1478 (w), 1451 (s), 1434 (s), 1391 (w), 1367 (m), 1276 (w), 1231 (w), 1185 (w), 1158 (w), 1132 (w), 1104 (m), 1059 (s), 1024 (m), 948 (w), 837 (w), 810 (m), 740 (s), 723 (m), 690 (s), 627 (m), 577 (m), 490 (m), 469 (m), 436 (m) cm^{-1}; ESI-HRMS (m/z, pos): Calculated for $[C_{27}H_{41}B_2NP_2+H]^+$ 464.2973; found: 464.2998 $[M+H]^+$; Elemental analysis calcd (%) for $[C_{27}H_{41}B_2NP_2]$: C 70.01, H 8.92, N 3.02; found: C 70.34, H 9.13, N 3.46.

Synthesis of homogeneous complex 8

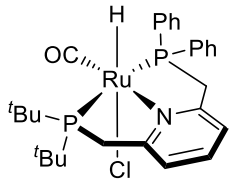

8

Step1

The phosphine-borane **7** (188 mg, 0.41 mmol, 1.0 equiv.) was dissolved in 10 mL of diethyl amine and stirred overnight at 50 °C. After cooling to room temperature the excess diethyl amine was removed. The remaining oil was dried *in vacuo* at 40 °C overnight and analyzed by $^{31}P\{^1H\}$-NMR (162 MHz, C_6D_6): δ = 34.9 (s, P^tBu_2), –11.3 (s, PPh_2) ppm. The ligand was used in the next step without further purification.

Step 2

15 ml of THF were added to the colorless oil of the freshly prepared PNP ligand and $[Ru(HCl(PPh_3)_3CO]$ (387 mg, 0.41 mmol, 1.0 equiv.). The suspension was heated to 60 °C and the resulting yellow solution was stirred for 5 hours. All volatiles were removed *in vacuo*. Next the yellow residue was dissolved in 1 mL of THF and 10 mL of *n*-pentane were added to precipitate the pale yellow solid. After filtration, the solid was washed with *n*-pentane (3x5 mL) and dried *in vacuo* yielding Ru-complex **8** (202 mg, 83%). Crystals suitable for X-ray diffraction could be obtained through vapor diffusion of *n*-pentane into a solution of **8** in dichloromethane over two days at room temperature. ^1H-NMR (400 MHz, CD_2Cl_2): δ = 7.88-7.83 (m, 2H, phenyl-CH), 7.60-7.58 m, 3H, 2xphenyl-CH, 1xpyridine-H), 7.46-7.45 (m, 3H, phenyl-CH), 7.35-7.27 (m, 5H,

3xphenyl-CH, 2xpyridine-H), 4.89 (dd, 1H, J_{HH} = 9.5 Hz, J_{PH} = 15.9 Hz, C*H*HPPh$_2$), 4.12 (ddd, 1H, J_{HH} = 2.6 Hz, J_{HH} = 12.1 Hz, J_{PH} = 15.9 Hz, CH*H*PPh$_2$), 3.73-3.66 (m, 1H, C*H*HP^{t}Bu$_2$), 3.37 (dd, 1H, J_{HH} = 8.3 Hz, J_{PH} = 16.6 Hz, CH*H*P^{t}Bu$_2$), 1.42 (d, 9H, J_{HP} = 9.2 Hz, PC(CH$_3$)$_3$), 1.39 (d, 9H, J_{HP} = 9.0 Hz, PC(CH$_3$)$_3$), –14.51 (dd, 1H, J_{HP} = 17.1 Hz, J_{HP} = 20.5 Hz, Ru-H) ppm. ^{1}H-NMR (300 MHz, C$_6$D$_6$): δ = 8.26-8.19 (m, 2H, phenyl-CH), 7.64-7.54 m, 2H, phenyl-CH), 7.13-7.04 (m, 3H, phenyl-CH), 6.94-6.86 (m, 3H, phenyl-CH), 6.75 (t, 1H, J_{HH} = 7.7 Hz, pyridine-H), 6.52 (d, 1H, J_{HH} = 7.7 Hz, pyridine-H) 6.37 (d, 1H, J_{HH} = 7.8 Hz, pyridine-H), 5.15 (dd, 1H, J_{HH} = 9.5 Hz, J_{PH} = 15.9 Hz, C*H*HPPh$_2$), 3.65 (ddd, 1H, J_{HH} = 2.9 Hz, J_{HH} = 12.2 Hz J_{PH} = 15.5 Hz, CH*H*PPh$_2$), 3.11-3.02 (m, 1H, C*H*HP^{t}Bu$_2$), 2.70 (dd, 1H, J_{HH} = 7.8 Hz, J_{PH} = 16.5 Hz, CH*H*P^{t}Bu$_2$), 1.45 (d, 9H, J_{HP} = 13.2 Hz, PC(CH$_3$)$_3$), 1.21 (d, 9H, J_{HP} = 12.8 Hz, PC(CH$_3$)$_3$), –13.87 (dd, 1H, J_{HP} = 17.5 Hz, J_{HP} = 20.4 Hz, Ru-H) ppm. ^{13}C{^{1}H}-NMR (101 MHz, CD$_2$Cl$_2$): δ = 208.5 (t, J_{PC} = 12.2 Hz, Ru-CO), 163.6 (s, pyridine-*C*-CH$_2$P), 160.9 (dd, J_{PC} = 3.0 Hz, 7.8 Hz, pyridine-*C*-CH$_2$P), 138.5 (dd, J_{PC} = 1.6 Hz, 41.5 Hz Ar-C-P), 137.4 (s, pyridine-CH), 133.4 (dd, J_{PC} = 1.4 Hz, 11.5 Hz, 2xAr-CH), 133.4 (dd, J_{PC} = 2.6 Hz, 39.6 Hz, Ar-C-P), 132.3 (d, J_{PC} = 12.1 Hz, 2xAr-CH), 130.5 (d, J_{PC} = 2.2 Hz, Ar-CH), 130.1 (d, J_{PC} = 2.0 Hz, Ar-CH), 128.7 (d, J_{PC} = 9.8 Hz, 4xAr-CH), 120.9 (d, J_{PC} = 10.3 Hz, pyridine-CH), 120.2 (d, J_{PC} = 9.3 Hz, pyridine-CH), 44.3 (d, J_{PC} = 24.2 Hz, CH$_2$PPh), 38.4 (d, J_{PC} = 16.3 Hz, CH$_2$P^{t}Bu), 37.8 (dd, J_{PC} = 5.4 Hz, 8.2 Hz, P-*C*(CH$_3$)$_3$), 34.6 (d, J_{PC} = 24.2 Hz, P-*C*(CH$_3$)$_3$), 30.1 (d, J_{PC} = 4.0 Hz, 2xP-C(*C*H$_3$)$_3$), 29.3 (d, J_{PC} = 4.6 Hz, 2xP-C(*C*H$_3$)$_3$) ppm. ^{31}P{^{1}H}-NMR (162 MHz, CD$_2$Cl$_2$): δ = 90.4 (d, J_{PP} = 266.6 Hz, P^{t}Bu$_2$) 53.6 (d, J_{PP} = 266.6 Hz, PPh$_2$) ppm; IR (solid): $\tilde{\nu}$ = 2953 (w), 2895 (w), 2863 (w), 2034 (w, Ru-H), 1887(s, CO), 1597 (w), 1584 (w, C=N), 1458 (m), 1433 (m), 1386 (w), 1366 (w), 1281 (w), 1179 (w), 1187 (m), 1018 (w), 962 (w), 837 (m), 814 (m), 780 (w), 751 (m), 713 (w), 693 (s), 623 (m), 511 (m), 474 (m), 457 (m) cm^{-1}, Elemental analysis calcd (%) for [C$_{28}$H$_{36}$ClNOP$_2$Ru]: C 55.95, H 6.04, N 2.33; found: C 54.56, H 6.28, N 2.93.

General Procedure for Batch-wise operated Ester Hydrogenation Experiments

The hydrogenation experiments were performed in a stainless steel autoclave charged with an insert suitable for up to 12 reaction vessels (2 mL) including Teflon mini stirring bars. Inside a glove box, a reaction vessel was charged with a resin-bound Ru-PNP complex **C$_1$-C$_{14}$** (~3-7 mg, 2.5-5.0 µmol). To the reaction vessel 0.5 mL of a stock solution of KO^{t}Bu (5-10 mol%) in THF was added and the mixture was stirred for 5 minutes. Next, 0.5 mL of the substrates **S$_1$-S$_{12}$** (0.25-0.50 mmol) and the internal

standard dodecane (50 mol%) dissolved in THF were added. Subsequently, the autoclave was purged three times with 10 bar of argon gas and the insert loaded with reaction vessels was transferred into the autoclave. Next, the autoclave was purged three times with 10 bar of H_2 and then pressurized (30-50 bar) and heated to the desired temperature. The reaction mixtures were gently stirred at 400 rpm for 2-24 hours. The autoclave was cooled to room temperature, depressurized and the conversion was determined by GC-FID measurements using the following column and conditions:

Restek RTX-1 Agilent HP-5 column (30 m, 0.25 mm, 0.1 µm): T_0 = 50 °C, ΔT = 8 °Cmin^{-1} to 180 °C, then hold for 2 min.

SI: t_r (ester) = 3.70 min, t_r (alcohol) = 5.65 min, t_r (transester) = 22.00 min.
SII: t_r (ester) = 4.75 min, t_r (alcohol) = 5.67 min, t_r (transester) = 13.83 min.
SIII: t_r (ester) = 13.78 min, t_r (alcohol) = 5.73 min.
SIV: t_r (ester) = 1.86 min, t_r (alcohol) = 2.83 min, t_r (transester) = 7.87 min
SV: t_r (ester) = 2.47 min, t_r (alcohol) = 2.83 min, t_r (transester) = 7.87 min.
SVI: t_r (ester) = 7.87 min, t_r (alcohol) = 2.90 min.
SVII: t_r (ester) = 1.81 min, t_r (alcohol) = 1.64 min, t_r (transester) = 6.45 min.
SVIII: t_r (ester) = 3.15 min, t_r (alcohol) = 4.62 min, t_r (transester) = 12.46 min.
SIX: t_r (ester) = 5.13 min.

Restek Agilent HP-5 column (30 m, 0.25 mm, 0.1 µm): T_0 = 50 °C, ΔT = 8 °Cmin^{-1} to 180 °C, then hold for 2 min.

SX: t_r (diester) = 21.08 min, t_r (diol) = 19.91 min, t_r (monoester) = 20.52 min.
SXI: t_r (lactone) = 5.89 min, t_r (diol) = 6.28 min.
SXII: t_r (diester) = 6.54 min, t_r (diol) = 6.81 min.

General Procedure for Batch Recycling Experiments

The first ester hydrogenation cycle was performed as described above using **C_6** (5 µmol, 1.0 mol%), 1.0 mL of a stock solution of **S_1** (0.5 M), KO^{t}Bu (10 mol%) and the internal standard dodecane (50 mol%) in THF at 100 °C and 50 bar H_2. After 2 hours the autoclave was cooled and depressurized and the reaction vessel was removed. Keeping the catalyst under a argon atmosphere the supernatant was removed. Next,

new stock solution of **S_1** (0.5 M, 1.0 mL) was added to the reaction vessel and the autoclave was then charged with the reaction vessel and a new reaction cycle was started. The supernatant was submitted for GC-FID analysis.

X-Ray Crystallographic Data of 8

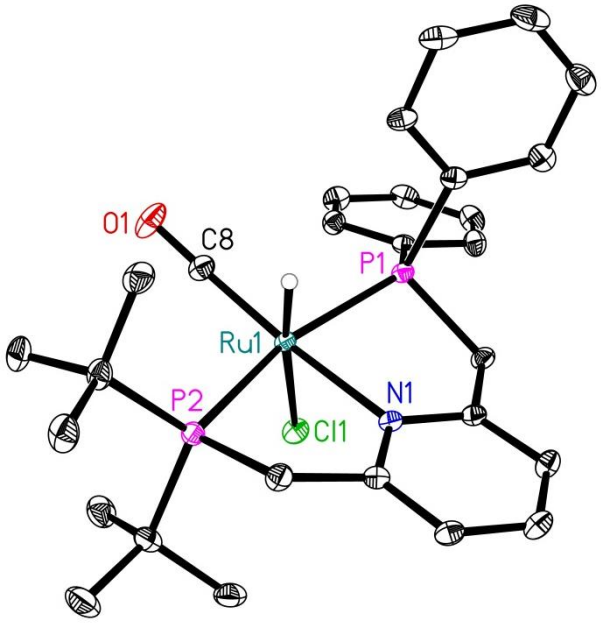

Figure 18 Figure 19 ORTEP representation of molecular structure of **8**. Displacement ellipsoids correspond to 30% probability. Hydrogen atoms are omitted for clarity.

Empirical formula:	$C_{28}H_{36}ClNOP_2Ru$
Formula Weight:	601.04 g·mol^{-1}
Temperature:	150.2 K
Wave length:	0.71073 Å
Crystal System:	monoclinic
Space group:	$P2_1/n$
Unit cell:	a = 16.732(3) Å, b = 11.269(2) Å, c = 29.356(5) Å
	α = 90 °, β = 100.462(3) °, γ = 90 °
Volume	5443.2(2) Å^3
Z	8
Density (calculated)	1.467 mg/m^3
Absorption coefficient	0.813
F(000)	2480
Crystal size	0.378 x 0.145 x 0.098 mm^3
Theta range	2.19 to 30.52°

Index ranges	-21<=h<=21, -14<=k<=14, -37<=l<=34
Reflexes collected	11889
Independent reflections	10134
Absorption correction	multi-scan
Refinement method	Full matrix least-squares on F^2
Data/restraints/parameters	11889/2/633
Goodness-of-fit on F^2	1.046
Final R indices [I>2sigma(I)]	R1 = 0.0266, wR2 = 0.0660
R indices (all data)	R1 = 0.0340, wR2 = 0.0707
Extinction coefficient	n.d.
Largest diff. Peak and hole	1.059 and -0.312 e.$Å^{-3}$

3.9 References

[1] a) C. J. Moulton, B. L. Shaw, *J. Chem. Soc., Dalton Trans.* **1976**, 1020-1024; b) G. van Koten, K. Timmer, J. G. Noltes, A. L. Spek, *J. Chem. Soc., Chem. Commun.* **1978**, 250-252.

[2] M. Albrecht, G. van Koten, *Angew. Chem. Int. Ed.* **2001**, *40*, 3750-3781.

[3] E. Peris, R. H. Crabtree, *Chem. Soc. Rev.* **2018**, *47*, 1959-1968.

[4] J. C. Jeffrey, T. B. Rauchfuss, *Inorg. Chem.* **1979**, *18*, 2658-2666.

[5] a) H. Grützmacher, *Angew. Chem. Int. Ed.* **2008**, *47*, 1814-1818; b) C. Gunanathan, D. Milstein, *Chem. Rev.* **2014**, *114*, 12024-12087.

[6] a) J. Zhang, G. Leitus, Y. Ben-David, D. Milstein, *J. Am. Chem. Soc.* **2005**, *127*, 10840-10841; b) J. Zhang, G. Leitus, Y. Ben-David, D. Milstein, *Angew. Chem. Int. Ed.* **2006**, *45*, 1113-1115; c) B. Gnanaprakasam, J. Zhang, D. Milstein, *Angew. Chem. Int. Ed.* **2010**, *49*, 1468-1471.

[7] K. Kenjiro, F. Hitomi, H. Masahiko, *Bull. Chem. Soc. Jpn.* **2011**, *84*, 640-647.

[8] J. F. Sonnenberg, A. J. Lough, R. H. Morris, *Organometallics* **2014**, *33*, 6452-6465.

[9] S. Chakraborty, G. Leitus, D. Milstein, *Angew. Chem. Int. Ed.* **2017**, *56*, 2074-2078.

[10] S. A. M. Smith, P. O. Lagaditis, A. Lupke, A. J. Lough, R. H. Morris, *Chem. Eur. J.* **2017**, *23*, 7212-7216.

[11] A. Zirakzadeh, K. Kirchner, A. Roller, B. Stöger, M. Widhalm, R. H. Morris, *Organometallics* **2016**, *35*, 3781-3787.

[12] E. Kinoshita, K. Arashiba, S. Kuriyama, Y. Miyake, R. Shimazaki, H. Nakanishi, Y. Nishibayashi, *Organometallics* **2012**, *31*, 8437-8443.

[13] D. Benito-Garagorri, E. Becker, J. Wiedermann, W. Lackner, M. Pollak, K. Mereiter, J. Kisala, K. Kirchner, *Organometallics* **2006**, *25*, 1900-1913.

[14] a) K. Burgess, *Solid-Phase Organic Synthesis*, John Wiley & Sons, Inc., New York, **2002**; b) D. Obrecht, J. M. Villalgordo, *Introduction, Basic Concepts and Strategies*, in *Solid-Supported Combinatorial and Parallel Synthesis of Small-Molecular-Weight Compound Libraries*, Elsevier Science ltd., Oxford, **1998**, pp. 1-184; c) M. C. Samuels, B. H. G. Swennenhuis, P. C. J. Kamer, *Solid-phase Synthesis of Ligands*, in *Phosphorus(III) Ligands in Homogeneous Catalysis: Design and Synthesis* (Eds.: P. C. J. Kamer, P. W. N. M. v. Leeuwen), John Wiley & Sons, Ltd, Chichester, **2012**, pp. 463-479.

[15] a) D. J. Cole-Hamilton, R. P. Tooze, *Homogeneous Catalysis — Advantages and Problems*, in *Catalyst Separation, Recovery and Recycling: Chemistry and Process Design* (Eds.: D. J. Cole-Hamilton, R. P. Tooze), Springer Netherlands, Dordrecht, **2006**, pp. 1-8; b) A. E. C. Collis, I. T. Horváth, *Cat. Sci. Technol.* **2011**, *1*, 912-919; c) R. Konrath, F. J. L. Heutz, P. C. J. Kamer, D. Vogt, *Catalyst Separation*, in *Contemporary Catalysis* (Eds.: P. C. J. Kamer, D. Vogt, J. W. Thybaut), The Royal Society of Chemistry, **2017**, pp. 711-747.

[16] M. A. Goni, E. Rosenberg, S. Meregude, G. Abbott, *J. Organomet. Chem.* **2016**, *807*, 1-10.

[17] M. A. Goni, E. Rosenberg, R. Gobetto, M. Chierotti, *J. Organomet. Chem.* **2017**, *845*, 213-228.

[18] X. Wang, E. A. P. Ling, C. Guan, Q. Zhang, W. Wu, P. Liu, N. Zheng, D. Zhang, S. Lopatin, Z. Lai, K.-W. Huang, *ChemSusChem* **2018**, *11*, 3591-3598.

[19] J. Brünig, Z. Csendes, S. Weber, N. Gorgas, R. W. Bittner, A. Limbeck, K. Bica, H. Hoffmann, K. Kirchner, *ACS Catal.* **2018**, *8*, 1048-1051.

[20] R. Castro-Amoedo, Z. Csendes, J. Brünig, M. Sauer, A. Foelske-Schmitz, N. Yigit, G. Rupprechter, T. Gupta, A. M. Martins, K. Bica, H. Hoffmann, K. Kirchner, *Cat. Sci. Technol.* **2018**, *8*, 4812-4820.

[21] a) P. A. Dub, T. Ikariya, *ACS Catal.* **2012**, *2*, 1718-1741; b) G. A. Filonenko, R. van Putten, E. J. M. Hensen, E. A. Pidko, *Chem. Soc. Rev.* **2018**, *47*, 1459-1483; c) H. Valdés, M. A. García-Eleno, D. Canseco-Gonzalez, D. Morales-Morales, *ChemCatChem* **2018**; d) S. Werkmeister, K. Junge, M. Beller, *Org. Process Res. Dev.* **2014**, *18*, 289-302.

[22] P. G. Andersson, I. J. Munslow, *Modern Reduction Methods*, Wiley-VCH: Weinheim, Germany, **2008**.

[23] a) J. Seyden-Penne, *Reductions by the Allumino- and Borohydride in Organic Synthesis*, 2 ed., Wiley-VCH, New York, **1997**; b) G. W. Gribble, *Chem. Soc. Rev.* **1998**, *27*, 395-404.

[24] a) P. Urben, *Bretherick's Handbook of Reactive Chemical Hazards*, 6 ed., Academic Press, **2006**; b) A. M. Smith, R. Whyman, *Chem. Rev.* **2014**, *114*, 5477-5510.

[25] a) R. D. Rieke, D. S. Thakur, B. D. Roberts, G. T. White, *J. Am. Oil Chem. Soc.* **1997**, *74*, 333-339; b) R. D. Rieke, D. S. Thakur, B. D. Roberts, G. T. White, *J. Am. Oil Chem. Soc.* **1997**, *74*, 341-345; c) Y. Pouilloux, F. Autin, J. Barrault, *Catal. Today* **2000**, *63*, 87-100.

[26] W. Kuriyama, T. Matsumoto, O. Ogata, Y. Ino, K. Aoki, S. Tanaka, K. Ishida, T. Kobayashi, N. Sayo, T. Saito, *Org. Process Res. Dev.* **2011**, *16*, 166-171.

[27] S. Elangovan, B. Wendt, C. Topf, S. Bachmann, M. Scalone, A. Spannenberg, H. Jiao, W. Baumann, K. Junge, M. Beller, *Adv. Synth. Catal.* **2016**, *358*, 820-825.

[28] J. Yuwen, S. Chakraborty, W. W. Brennessel, W. D. Jones, *ACS Catal.* **2017**, *7*, 3735-3740.

[29] J. Zhang, E. Balaraman, G. Leitus, D. Milstein, *Organometallics* **2011**, *30*, 5716-5724.

[30] F. J. L. Heutz, C. Erken, M. J. B. Aguila, L. Lefort, P. C. J. Kamer, *ChemCatChem* **2016**, *8*, 1896-1900.

[31] F. J. Heutz, P. C. Kamer, *Dalton Trans.* **2016**, *45*, 2116-2123.

[32] M. Gargir, Y. Ben-David, G. Leitus, Y. Diskin-Posner, L. J. W. Shimon, D. Milstein, *Organometallics* **2012**, *31*, 6207-6214.

[33] M. C. Samuels, F. J. L. Heutz, A. Grabulosa, P. C. J. Kamer, *Top. Catal.* **2016**, *59*, 1793-1799.

[34] A. Staubitz, A. P. M. Robertson, M. E. Sloan, I. Manners, *Chem. Rev.* **2010**, *110*, 4023-4078.

[35] G. Müller, M. Klinga, M. Leskelä, B. Rieger, *Z. Anorg. Allg. Chem.* **2002**, *628*, 2839-2846.

[36] I. Arenas, O. Boutureira, M. I. Matheu, Y. Díaz, S. Castillón, *Eur. J. Org. Chem.* **2015**, *2015*, 3666-3669.

[37] H. Salem, L. J. W. Shimon, Y. Diskin-Posner, G. Leitus, Y. Ben-David, D. Milstein, *Organometallics* **2009**, *28*, 4791-4806.

[38] a) S. Takebayashi, S. H. Bergens, *Organometallics* **2009**, *28*, 2349-2351; b) R. van Putten, E. A. Uslamin, M. Garbe, C. Liu, A. Gonzalez-de-Castro, M. Lutz, K. Junge, E. J. M. Hensen, M. Beller, L. Lefort, E. A. Pidko, *Angew. Chem. Int. Ed.* **2017**, *56*, 7531-7534; c) B. M. Stadler, P. Puylaert, J. Diekamp, R. van Heck, Y. Fan, A. Spannenberg, S. Hinze, J. G. de Vries, *Adv. Synth. Catal.* **2018**, *360*, 1151-1158.

[39] a) A. Mukherjee, A. Nerush, G. Leitus, L. J. Shimon, Y. Ben David, N. A. Espinosa Jalapa, D. Milstein, *J. Am. Chem. Soc.* **2016**, *138*, 4298-4301; b) A. Nerush, M. Vogt, U. Gellrich, G. Leitus, Y. Ben-David, D. Milstein, *J. Am. Chem.*

Soc. **2016**, *138*, 6985-6997; c) M. Glatz, B. Stöger, D. Himmelbauer, L. F. Veiros, K. Kirchner, *ACS Catal.* **2018**, *8*, 4009-4016; d) Y.-Q. Zou, S. Chakraborty, A. Nerush, D. Oren, Y. Diskin-Posner, Y. Ben-David, D. Milstein, *ACS Catal.* **2018**, *8*, 8014-8019.

[40] F. J. L. Heutz, M. C. Samuels, P. C. J. Kamer, *Catal. Sci. Technol.* **2015**, *5*, 3296-3301.

[41] G. P. Elsbeth, J. Xiao-Bin, K. Mark, L. Renske, V. L. P. W. N. M., R. J. N. H., *Eur. J. Org. Chem.* **2008**, *2008*, 6079-6092.

[42] A. Panossian, H. Fernández-Pérez, D. Popa, A. Vidal-Ferran, *Tetrahedron: Asymmetry* **2010**, *21*, 2281-2288.

Chapter 4

Supported Chiral PNP-Pincer Ligands in Asymmetric Ketone Hydrogenation

Abstract: *Transition-metal catalyzed enantioselective hydrogenations are commonly applied in the synthesis of enantiopure alcohols from prochiral ketones leading to building blocks for fine-chemical industries as well as pharmaceuticals. In homogeneous catalysis, chiral pincer-type ligands have demonstrated excellent enantioselectivities in this transformation. However, the discovery of high performance catalysts still relies heavily on trial-and-error methodologies calling for more efficient synthetic approaches towards ligand libraries. In this chapter, a facile and highly modular solid-phase synthesis towards a resin-bound chiral PNP-type ligand library is presented. Systematic variation of building blocks allows for an efficient introduction of multiple stereogenic centers into the aliphatic and heteroaromatic ligand structures. The corresponding resin-bound ruthenium-PNP complexes are screened in the asymmetric hydrogenation of several aromatic and aliphatic ketones.*

4.1 Introduction

The ever-growing demand of optically pure alcohol building blocks in the production of agrochemicals, pharmaceuticals, fragrances, flavors and other fine chemicals has called for sophisticated synthetic solutions in the last few decades. One of the most efficient organic synthesis approaches towards chiral alcohols employs the reduction of carbonyl compounds.[1] In the past, the chemoselective reduction of a C=O bond heavily relied on the stoichiometric use of metal hydride reagents, such as $LiAlH_4$ and $NaBH_4$,[2] accompanied by the formation of large quantities of metal salt waste and the inherent danger of the reducing agents. Stereoselective reductions of prochiral carbonyl compounds were accomplished using stoichiometric amounts of chiral reducing reagents including BINOL-based BINAL-H[3] or boron-derived DIP-Cl™,[4] CBS[5] and further oxazaborolidines.[6]

Catalytic enantioselective hydrogenation of achiral carbonyl substrates offers a more environmentally benign and atom-economical approach to chiral target alcohols using inexpensive H_2 gas as the reducing agent. Since the pivotal work of Nobel laureate Ryōji Noyori in the 1990s[7], the asymmetric reduction of ketones employing molecular hydrogen as well as the asymmetric transfer hydrogenation using hydrogen sources derived from secondary alcohols have emerged as powerful tools for the production of chiral alcohols.[8] Since then, a plethora of molecularly well-defined catalysts has been developed over the last decades. Highly efficient and selective Noyori-type catalysts applicable for a broad range of ketone substrates are typically composed of a combination of chiral diphosphines and diamines bound to a ruthenium metal center. For instance, ruthenium (*S*)-TolBINAP/(*S*,*S*)-DPEN complex **I** provided a rapid productivity in the asymmetric reduction of acetophenone with over 2.400.000 turnovers and a TOF of 63 s^{-1} at 30% conversion (Figure 1).

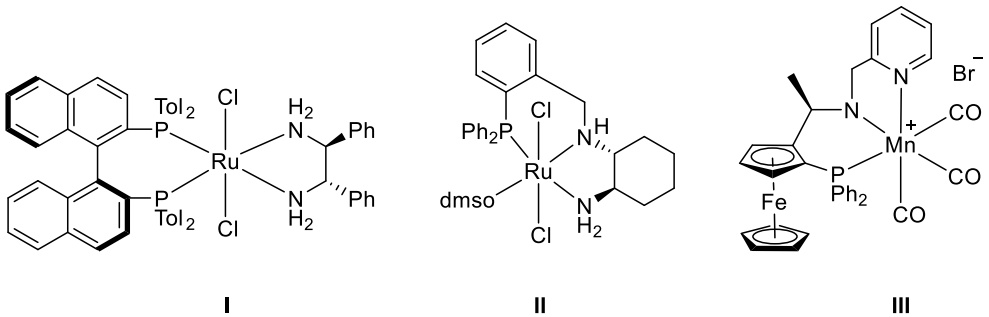

I **II** **III**

Figure 1 Representative examples of stereoselective ketone hydrogenation catalysts.

Over 600 g of the corresponding secondary alcohol was produced in 80% *ee* using only 2.2 mg of the Ru-catalyst. Insufficient selectivities of Noyori's catalysts in the hydrogenation of tetralones, dialkyl, bulky, and some heterocyclic ketones combined with the desire to merge both the phosphine and the amine ligand in order to prevent ligand leaching have led to the development of many chiral tri- and tetradentate ligands.[9] Clarke *et al.* reported on the chiral PNN pincer-type Ru-catalysts capable of reducing challenging bulky *tert*-butyl aryl ketones with up to 94% *ee* (**II**, Figure 1).[10] In many recent studies, the often expensive and toxic precious metals have been replaced by more earth-abundant and environmentally benign first-row transition metals such as Fe, Mn and Co.[11] Widegren *et al.* employed the PNN-based Mn-catalyst **III** introducing planar chirality via a ferrocene moiety in addition to *C*-chirality in the ligand backbone reaching up to 97% *ee* for aromatic mono- and diketones.[12]

Surprisingly, examples of chiral PNP pincer-type ligands employed in asymmetric ketone reduction remain scarce despite their versatile applicability reported for various reductive transformations.[13] In case of the aliphatic PNP ligand **IV** reported by Garbe *et al.*, chirality was installed in the backbone of the phosphorus donor moieties using (2*R*,5*R*)-2,5-dimethylphospholane groups (Figure 2).[14]

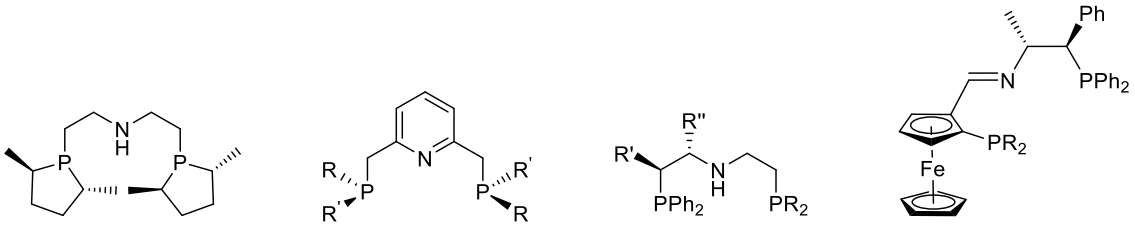

Figure 2 Chiral PNP ligands applied in asymmetric ketone reduction.

Moderate to good enantioselectivities of up to 84% *ee* were obtained preferentially for aliphatic ketones when using the corresponding Mn-complex of **IV**. *P*-stereogenic PNP pincer ligand **V** prepared by Arenas *et al.* containing two (S_P)-phosphorus donor atoms was applied in Ru-catalyzed ketone hydrogenation reaching up to 95% *ee* for aromatic substrates at -40 °C.[15] The related ligand **VI** employing (S_P)-cycloheyxlmethylphosphine moieties led to moderate enantioselectivities when used in the Fe-catalyzed reduction of acetophenone.[16] Moreover, the solution-phase synthesis of the borane adduct of this *P*-stereogenic ligand proved to be arduous relying on

multiple crystallization and chromatography purification steps resulting in an overall yield of 4%. For a small library of non-symmetrical PNP pincer ligands carrying *C*-chirality in the aliphatic backbone (**VII**-**X**) more promising results of up to 96% *ee* were observed when used as their Fe-complexes.[17] Due to a key-role of the NH donor group in the reaction mechanism, highest enantioselectivities were obtained for ligands bearing chiral phenyl substituents adjacent to the PPh_2 moiety providing backbone rigidity and accessibility of the nitrogen.[18] PNP ligands based on planar as well as *C*-chirality (**XI**-**XIII**) could achieve up to 86% *ee* when employed as their manganese complexes.[19]

Despite the modular nature of aromatic and aliphatic PNP-type ligands, combinatorial synthetic approaches towards chiral ligands remain scarce.[20] A small ligand library in case of aliphatic ligands **VII**-**X** was modularly accessed by employing a reductive amination strategy.[17] Merging air- and moisture-stable phosphonium dimers[21] with a series of chiral β-aminophosphines derived from natural amino acids and chiral amino alcohols gave the corresponding chiral ligands in 54-75% yield (Scheme 1, Strategy A).

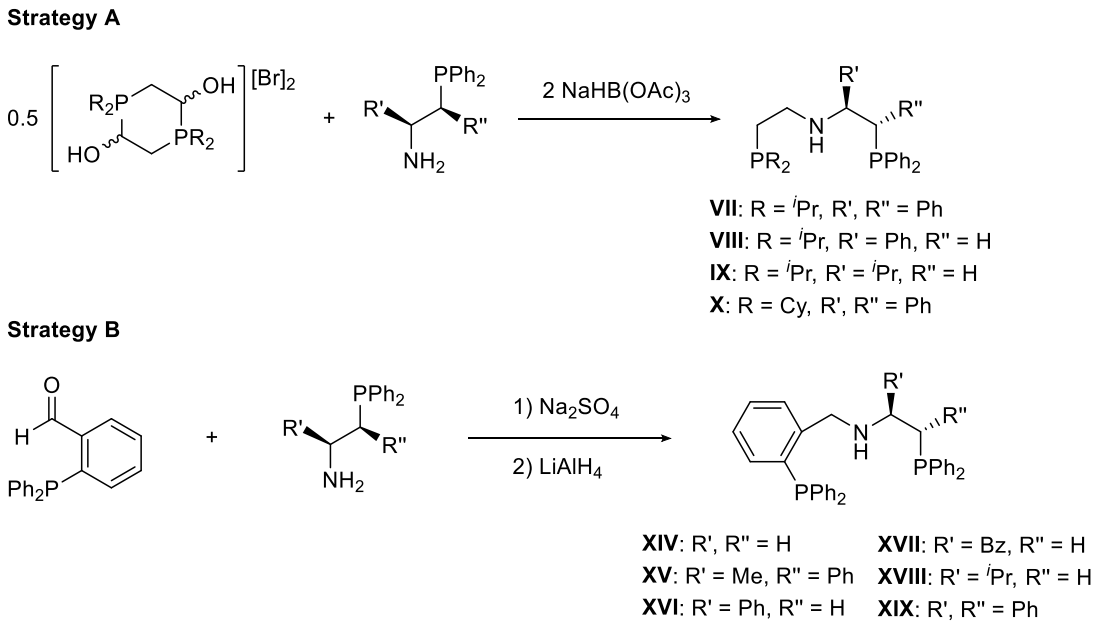

Scheme 1 Modular strategies A and B towards chiral PNP pincer-type ligands.

Another modular route regarding the solution-phase synthesis of chiral PNP ligands reported by Morris and co-workers involves the condensation of β-aminophosphines and *o*-(diphenylphosphino)benzaldehyde in the presence of a water scavenger (Scheme 1, Strategy B).[18,22] This led to a small library of Schiff base-type

ligands containing more flexible *o*-phenylene linkers, which were subsequently reduced to the chiral aliphatic ligands **XIV**-**XIX**. The formation of the corresponding iron carbonyl complexes of the chiral ligands **XV**-**XIX** proved to be troublesome as complex decomposition was observed upon removal from CO atmosphere. Hence, these catalysts were not tested in asymmetric ketone reduction.

Inspired by modular approaches developed for chiral homogeneous PNP ligands, it was decided to adapt and expand this methodology by using a solid-phase synthetic approach for the development of the first polymer-supported chiral PNP ligands and their application in Ru-catalyzed asymmetric ketone hydrogenation. Solid-phase synthesis offers the opportunity to obtain the desired ligands in high yield only requiring simple purification procedures such as filtration and decantation steps (see chapter 1.3).[23] Systematic variation of the three main building blocks **A**, **B** and **C** throughout the solid-phase synthetic sequence provides an efficient tool to access a large and diverse PNP ligand library bound to polymeric supports (Figure 3).

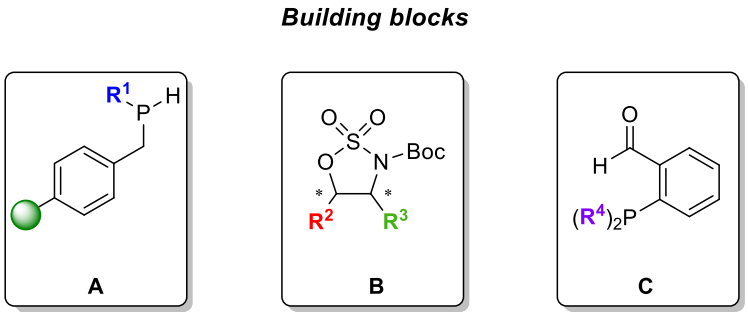

Figure 3 Main building blocks applied in the solid-phases synthetic route.

Building on previous work within the Kamer group, various secondary phosphines (**A**) immobilized on different types of polymeric supports are readily available.[24] Moreover, N-protected cyclic sulfamidates (**B**) have proven to be valuable synthetic modules for the synthesis of chiral aminophosphines via highly selective nucleophilic ring-opening.[18,25] Derived from natural and unnatural amino acids, chiral information can be conveniently installed in the aliphatic backbone of **B**. Finally, the second phosphorus moiety bearing various substituents R^4 in order to tune the electronic and steric donor properties can be introduced via building block **C** in analogy to the homogeneous synthesis strategy B (see Scheme 1). Subsequently, the impact of the combination of chiral centers in the aliphatic backbone on the asymmetrical induction in Ru-catalyzed ketone reduction will be presented.

4.2 Solid-Phase Synthesis

Again, the solid-phase synthetic route towards aliphatic resin-bound PNP ligands starts from supported secondary phosphine synthons (building block **A**) as previously established in the modular synthesis of immobilized P-OP (see chapter 2), PNP (see chapter 3) and diphosphine ligands.[24a,24c] Several electrophiles have been employed in homogeneous as well as heterogeneous strategies to introduce chirality into the ligand backbone such as epoxides and cyclic sulfates. In order to access chiral PN ligands, the compound classes of N-protected cyclic sulfamidates (**B**) as well as tosylated aminoalcohols was found to serve as promising modular building blocks.

4.2.1 Synthesis of Cyclic Sulfamidates

Beneficially, a broad range of aminoalcohols bearing a single *C*-chiral center can be derived from abundant and inexpensive natural and artificial amino acids. Commercially available Boc-protected derivatives of L-alanine (**1a**), L-*tert*-leucine (**1c**) and L-phenylalanine (**1d**) could be readily reduced to the corresponding Boc-protected aminoalcohols using a solution of BH_3 in THF (Scheme 2, step 1).[26] In case of Boc-L-valine (**1b**), the starting material was first derivatized using isobutyl chloroformate and subsequently reduced with $NaBH_4$.[27] Two adjacent *C*-chiral centers were provided by (1*R*,2*S*)-1,2-diphenyl-2-aminoethanol (**2a**), L-Norephedrin (**2b**) and both (1*R*,2*S*) and (1*S*,2*R*) stereoisomers of 1-amino-2-indanol (**2c-d**), which were Boc-protected to obtain the corresponding Boc-amino alcohols (Scheme 2, step 2). Having prepared the unsubstituted achiral derivative **3a** as well as a series of eight different chiral aminoalcohols (**3b-i**), it was decided to follow two different strategies, the tosylate substitution[28] and the sulfamidate route,[25] reported for the access to bidentate aminophosphine ligands. Hence, (*S*)-Boc phenylalaninol (**3e**) was treated with 4-toluenesulfonyl chloride under basic conditions to achieve the tosylated Boc-aminoalcohol **4** (Scheme 2, step 3).[29] Following reported protocols for the sulfamidate approach, **3a-i** were first reacted with thionyl chloride ($SOCl_2$) in the presence of triethylamine to form the corresponding cyclic sulfamidites (Scheme 2, step 4).[25,30] These intermediates were subsequently oxidized using catalytic amounts of $RuCl_3 \cdot xH_2O$ and oxidizing reagent $NaIO_4$ leading to the desired (a)chiral Boc-protected cyclic sulfamidates **5a-i** in moderate to high yields after recrystallization (Scheme 2, step 5).

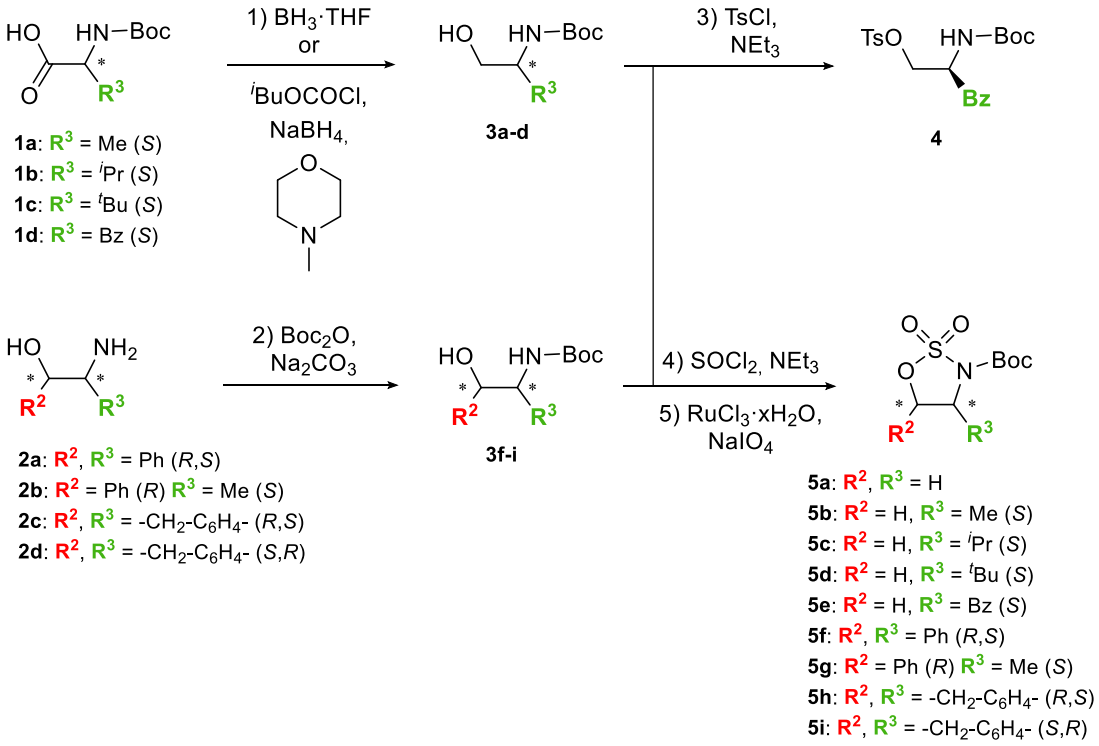

Scheme 2 Synthesis of tosylated Boc-aminoalcohol **4** and cyclic Boc-sulfamidates **5a-5i**.

4.2.2 Synthesis of Supported PN Ligands

In the next step, both building blocks, **A** and **B**, were merged to gain access to resin-bound (a)chiral PN sulfamates **7a-l** to continue the modular solid-phase synthetic approach. In analogy to the report of Guo *et al.*, who synthesized a range of chiral aminophosphines via rapid and highly selective ring-opening of cyclic sulfamidates by using suitable phosphides as nucleophiles. Lithiated supported secondary phosphide **Li·6** was prepared following a procedure previously described within the Kamer group (Scheme 3, step 1).[24a] Upon addition of a slight excess (1.5 equiv.) of an azeotropically dried cyclic sulfamidate **5a-i** to the resin at 0 °C, a resin color change from orange-brown to light yellow for **5a-g** and to dark green for **5h-i** was observed overnight (Scheme 3, step 2). Due to *N*-protection and *O*-activation of the cyclic sulfamidates, the ring-opening proceeded regioselectively with full inversion at the stereogenic center.[31] The formation of the desired resin-bound (a)chiral PN sulfamates **7a-i** could be monitored by using gel-phase ^{31}P NMR (see Figure 4 for representative example **7i**).

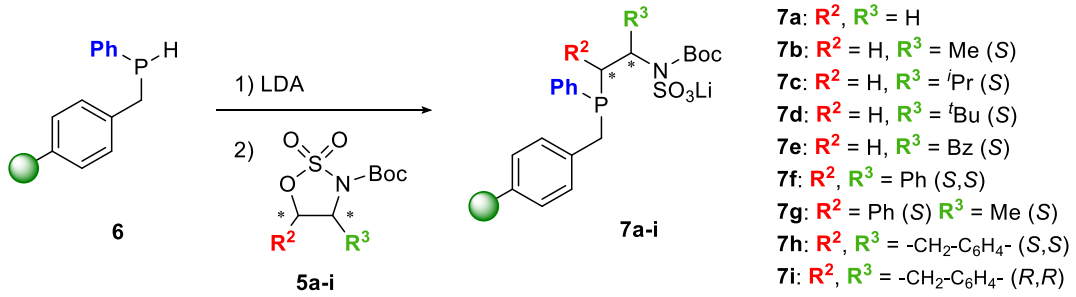

Scheme 3 Solid-phase synthesis of *N*-protected resin-bound aminophosphines **7a-i**.

In most cases, the reaction seemed to proceed quantitatively indicated by a significant chemical shift between $\Delta\delta$ = 15 and 35 ppm when compared to the lithiated secondary phosphide **Li·6**. In case of indane-based sulfamidate **5i**, a single resonance appeared at δ = -5.6 ppm in the ^{31}P NMR belonging to the resin-bound PN intermediate **7i** (Figure 4). Furthermore, the formation of the lithium sulfamate group could also be observed using ^{7}Li NMR.

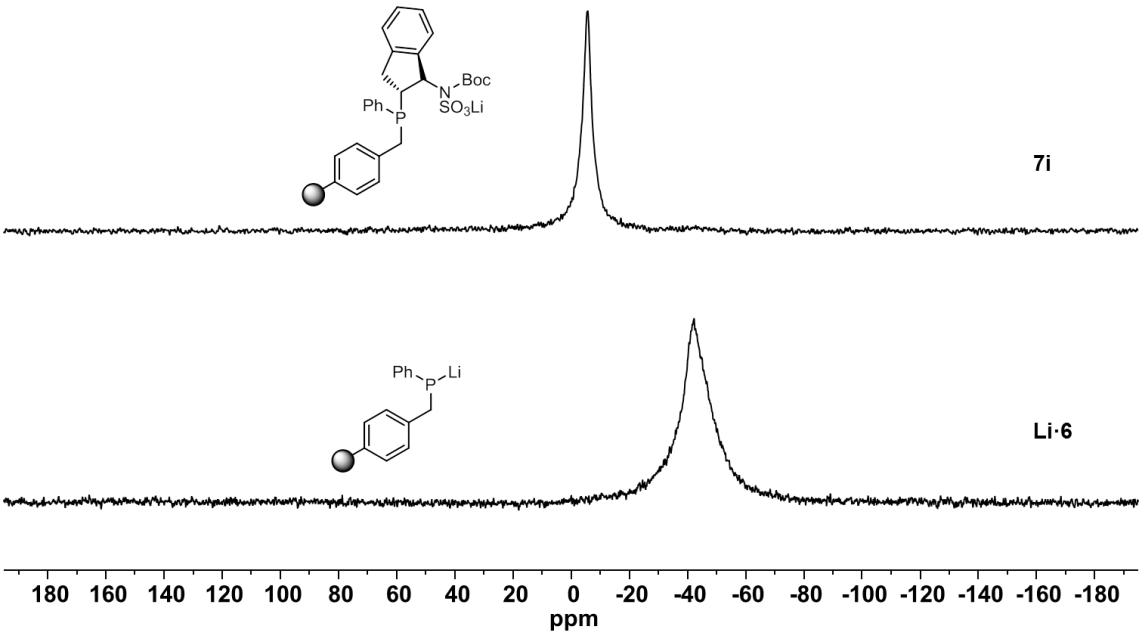

Figure 4 Solid-phase synthesis of supported PN intermediate **7i** monitored by ^{31}P NMR.

For sulfamidates **5f** and **5g** bearing a Ph group at the electrophilic carbon center, incomplete conversion towards the corresponding PN intermediates **7f** and **7g** resulted in a mixture containing up to 20% of resin-bound starting material (**6**). However, after removal of excess material in solution, relithiation followed by the addition of 0.5 equivalents of the respective sulfamidate enabled nearly quantitative substitution of the

phosphorus moiety bound to the support. Interestingly, for **7c-e** carrying a more bulky substituent (^{i}Pr, ^{t}Bu and Bz) adjacent to the PN nitrogen atom, two resonances could be observed in the ^{31}P NMR spectra. In case of **7c** (Figure 5, left) and **7d**, the peak splitting of the resin-bound phosphorus atom occurring in a 1:1 ratio can be attributed to the presence of a mixture of two epimers. **7e** bearing a benzyl group revealed a 2:1 splitting of the signal, which could be due to the significant overlay of the broad resonances and hence challenging integration (Figure 5, right).

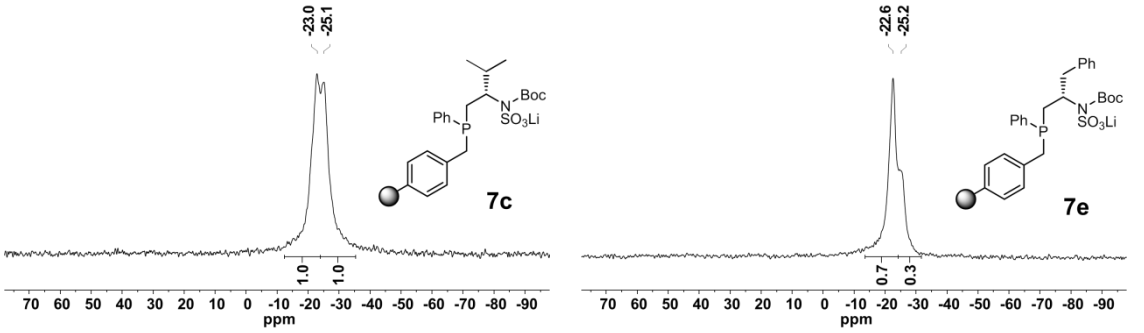

Figure 5 Gel-phase ^{31}P NMR spectra of supported PN intermediate **7c** (left) and **7e** (right).

In contrast to the successful incorporation of a chiral ligand backbone following the sulfamidate route, severe problems were encountered when employing the tosylated Boc-aminoalcohol **4**. Predominantly starting material **6** was recovered when treating lithium phosphide **Li·6** with **4** accompanied by the formation of an unidentified side-product remaining covalently bound to the support. Similar issues have been reported for solution-phase approaches referring to the undesired conversion of tosylated aminoalcohols to aziridines in the presence of potassium diphenylphosphine.[28c] Consequently, the tosylate route was not further investigated.

Analogous to the solid-phase synthetic route described for Merrifield resin-based compounds **7a-i**, it was decided to apply this methodology to ligands supported on polystyrene resin (PS). Thus, the immobilized derivatives **7j-l** bearing a ^{t}Bu substituent on the first phosphorus atom were synthesized accordingly. Synthetic work was conducted in cooperation with visiting student Sven Wendholt. The preparation of the borane-protected secondary phosphine and the subsequent deprotonation using excess amounts of LDA were performed following a procedure previously reported by the Kamer group (Scheme 4, step 1).[24c] Upon addition of 1.5 equivalents of an achiral (**5a**) or chiral (**5c,f**) cyclic sulfamidate to **Li·8** at room temperature, a resin color change from dark orange to light yellow was observed overnight (Scheme 4, step 2).

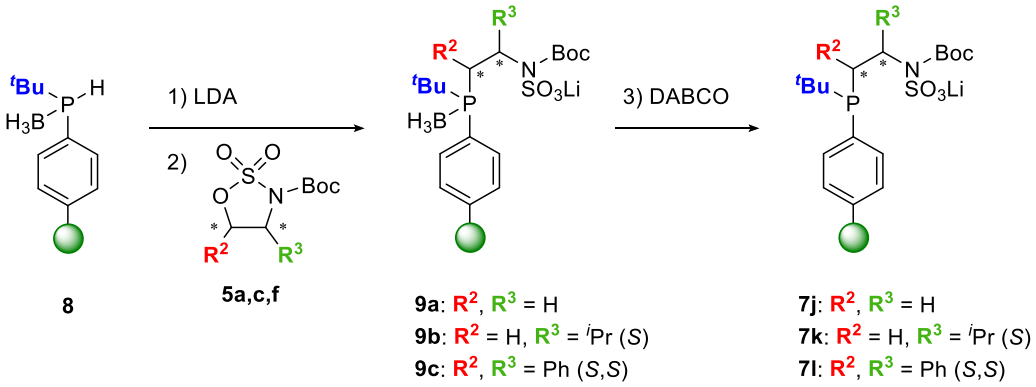

Scheme 4 Solid-phase synthesis of PS-supported aminophosphines **7j-7l**.

Again, the progress of the formation of borane-protected PN intermediates **9a-c** was monitored by ^{31}P NMR showing a significant downfield shift between $\Delta\delta$ = 42 and 64 ppm when compared to the lithiated secondary phosphide **Li·8** (see Figure 6 for representative example **9a**). Removal of the borane group was required in the following step as problems concerning intramolecular borane adduct formation involving the free amine group were encountered later in the sequence.

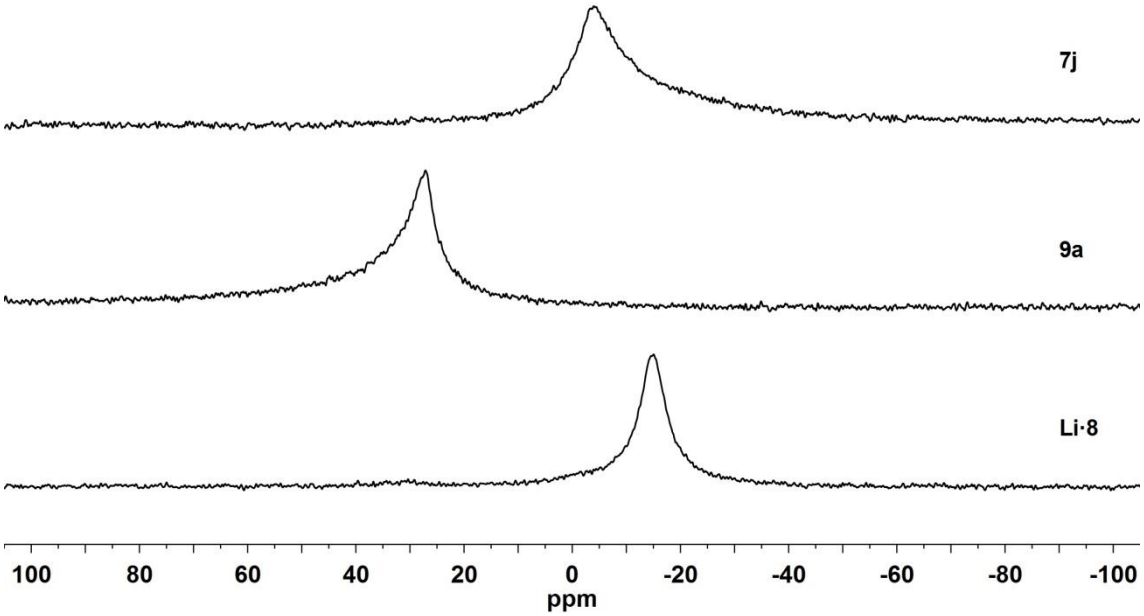

Figure 6 Solid-phase synthesis of supported PN intermediate **7j** monitored by ^{31}P NMR.

Hence, **9a-c** were treated with a large excess of 1 M 1,4-diazabicyclo [2.2.2]octane (DABCO) in THF at 50 °C leading to the deprotected resin-bound PN

sulfamates **7j-l** (Scheme 4, step 3). The deprotection proceeded readily overnight and could be monitored by ^{31}P NMR. In case of polystyrene-based PN intermediate **7j**, the sharp signal of **9a** at δ = 27.1 ppm is shifted upfield to δ = -4.1 ppm (see Figure 6).

Next, both the Boc protecting group and the SO_3Li moiety bound to the ligand nitrogen donor were removed in one reaction step. Opposed to a consecutive approach reported for homogeneous systems, which employ a hydrolysis step to form the free carbamate prior to cleavage of the Boc group,[18,25] it was found that both steps proceed simultaneously when using a 3:1 mixture of DCM and trifluoroacetic acid (TFA) at 0 °C. Under these strongly acidic conditions followed by neutralization with an aqueous 2 M NaOH solution, the supported bidentate PN-ligands **10a-l** could be obtained overnight in high yield and purity in most cases (Scheme 5). Light yellow resins were isolated in all cases except for **10h** and **10i**, which changed to a brown (**10h**) and an intensive purple color (**10i**).

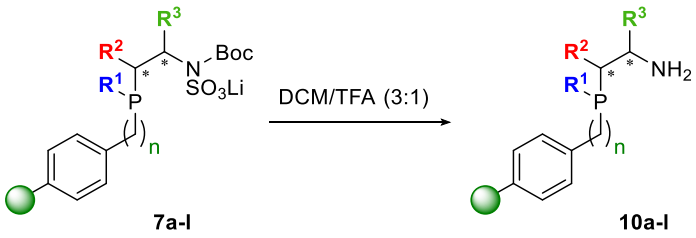

10a: n = 1, R^1 = Ph, R^2, R^3 = H
10b: n = 1, R^1 = Ph, R^2 = H, R^3 = Me (*S*)
10c: n = 1, R^1 = Ph, R^2 = H, R^3 = ^{i}Pr (*S*)
10d: n = 1, R^1 = Ph, R^2 = H, R^3 = ^{t}Bu (*S*)
10e: n = 1, R^1 = Ph, R^2 = H, R^3 = Bz (*S*)
10f: n = 1, R^1 = Ph, R^2, R^3 = Ph (*S,S*)
10g: n = 1, R^1 = Ph, R^2 = Ph (*S*) R^3 = Me (*S*)
10h: n = 1, R^1 = Ph, R^2, R^3 = -CH_2-C_6H_4- (*S,S*)
10i: n = 1, R^1 = Ph, R^2, R^3 = -CH_2-C_6H_4- (*R,R*)
10j: n = 0, R^1 = ^{t}Bu, R^2, R^3 = H
10k: n = 0, R^1 = ^{t}Bu, R^2 = H, R^3 = ^{i}Pr (*S*)
10l: n = 0, R^1 = ^{t}Bu, R^2, R^3 = Ph (*S,S*)

Scheme 5 Solid-phase synthesis of supported PN ligands **10a-10l**.

The successful solid-phase synthesis of the resin-bound PN ligands was confirmed by gel-phase ^{31}P NMR as well as by the quantitative disappearance of the signal belonging to the lithium sulfamate group in the corresponding ^{7}Li NMR spectra. A representative ^{31}P NMR spectrum of **10i** is depicted in Figure 7 (red spectrum) showing the slight upfield shift ($\Delta\delta$ = 3 ppm) of the single resonance compared to **7i** (black spectrum). The chemical shifts of Merrifield supported (a)chiral PN ligands **10a-i** in the ^{31}P NMR are in agreement with those obtained for solution-phase counterparts (see Table 1), which structurally differ solely in the additional methylene bridge belonging to the Merrifield resin.[25,32] Consequently, a difference in chemical shift of $\Delta\delta$ = 2-4 ppm is observed between heterogeneous and homogeneous aminophosphines.

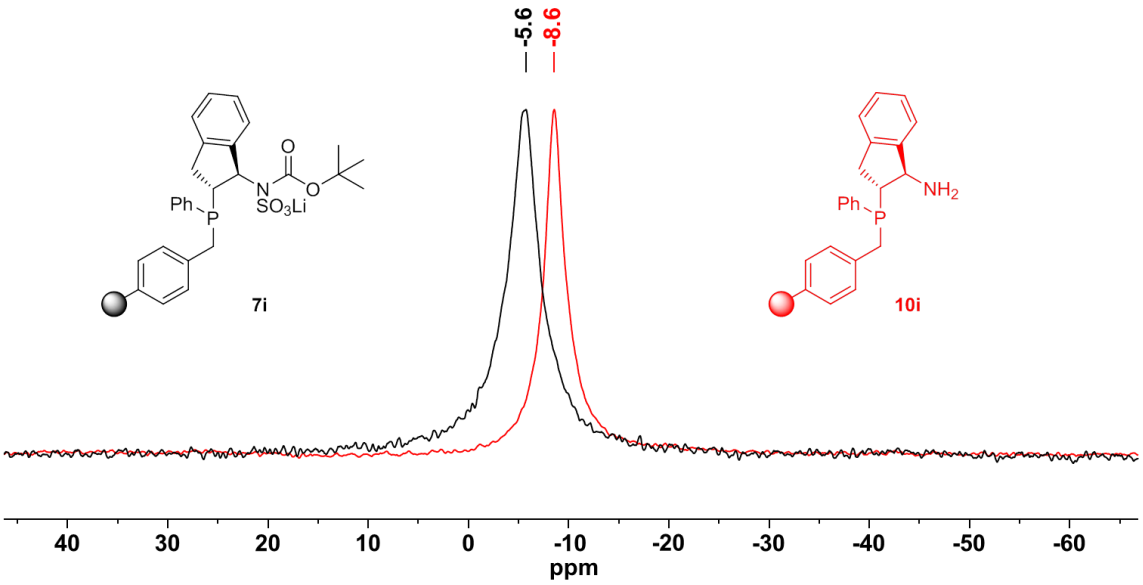

Figure 7 Overlaid ^{31}P NMR spectra of supported compounds **7i** (black) and **10i** (red).

Table 1 Summary of chemical shifts in the ^{31}P NMR spectra of PN-ligands **10a-l**.[a]

PN	Substituents			^{31}P NMR	^{31}P NMR (reference)
	R^1	R^2	R^3	[ppm]	[ppm][b,c]
10a	Ph	H	H	-24.0	-21.4[b]
10b	Ph	H	Me	-25.5	-21.5[b]
10c	Ph	H	^{i}Pr	-23.8	-20.2[c]
10d	Ph	H	^{t}Bu	-21.8	-18.3[c]
10e	Ph	H	Bz	-26.3	-22.0[b]
10f	Ph	Ph	Ph	-10.7	-7.2[c]
10g	Ph	Ph	Me	-11.3	-8.7[c]
10h	Ph	-CH_2-C_6H_4- (*S*,*S*)		-8.1	-5.8[c]
10i	Ph	-CH_2-C_6H_4- (*R*,*R*)		-8.6	-5.8[c]
10j	^{t}Bu	H	H	-4.5	-
10k	^{t}Bu	H	^{i}Pr	-5.5	-
10l	^{t}Bu	Ph	Ph	12.6	-

[a] Recorded at 162 MHz in THF unlocked and without additional shimming or at 121 MHz in THF:C_6D_6. Broad singlets were obtained in all cases. [b] Data taken from reference [32]. [c] Data taken from reference [25].

Furthermore, the two phosphorus signals corresponding to the presence of epimers in compounds **7c-e** merged to a single broad resonance in **10c-e** most likely due to enhanced rotational freedom upon removal of the Boc group.

4.2.3 Synthesis of Supported (a)chrial PNP Ligands

In order to access a large and diverse ligand library of supported (a)chiral PNP-type pincer ligands, the incorporation of the second phosphorus moiety into the desired ligand structure was required. Following a synthetic protocol reported by Morris and co-workers,[18] *o*-(diphenylphosphino)benzaldehyde was employed in a condensation reaction with previously prepared resin-bound aminophosphines **10a-l** to form the corresponding Schiff base PNP ligands **11a-l** (Scheme 6).

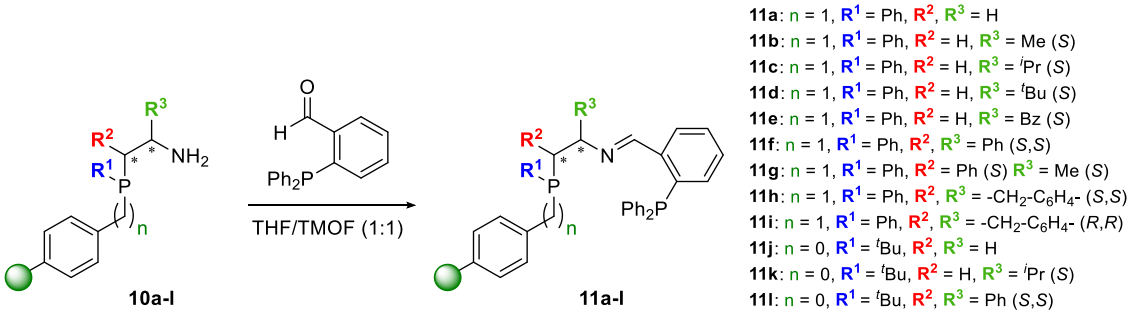

Scheme 6 Solid-phase synthesis of resin-bound PNP Schiff bases **11a-11l**.

Due to the water produced in this reaction, the presence of a suitable drying agent was required to ensure full conversion of the starting material. Commonly, inorganic salts, such as $MgSO_4$ or Na_2SO_4, as well as molecular sieves have been used in both homogeneous and solid-phase synthetic approaches. However, in the final condensation step in the solid-phase synthesis of supported PNN ligands reported by the Kamer group, the separation of insoluble $MgSO_4$ from the solid-supported compound proved to be troublesome.[33] Hence, it was decided to employ the water scavenger trimethyl orthoformate (TMOF)[34] in this reaction step present in a 1:1 mixture with THF to ensure sufficient resin swelling properties. At 50 °C using 1.5 equivalents of the *ortho*-aldehyde, the reaction proceeded slowly often requiring additional amounts of reagent to drive the reaction to completion. Especially in the presence of more sterically demanding substituents in the aliphatic ligand backbone close to the nitrogen atom, prolonged reaction times of up to 3 days were needed. The reaction progress was monitored by gel-phase ^{31}P NMR as depicted in Figure 8 for

supported PNP imine **11i**. After 24 hours, a second phosphorus signal belonging to a resin-bound species emerges at δ = -14.6 ppm next to the peak of the *ortho*-aldehyde at δ = -12.7 ppm. Over the course of 3 days, two signals were obtained after removal of excess reagents. The signals, occurring in a ratio of 1:1, can be assigned to the resin-bound phosphorus atom at δ = -7.7 ppm and the remote PPh_2 group at δ = -13.6 ppm.

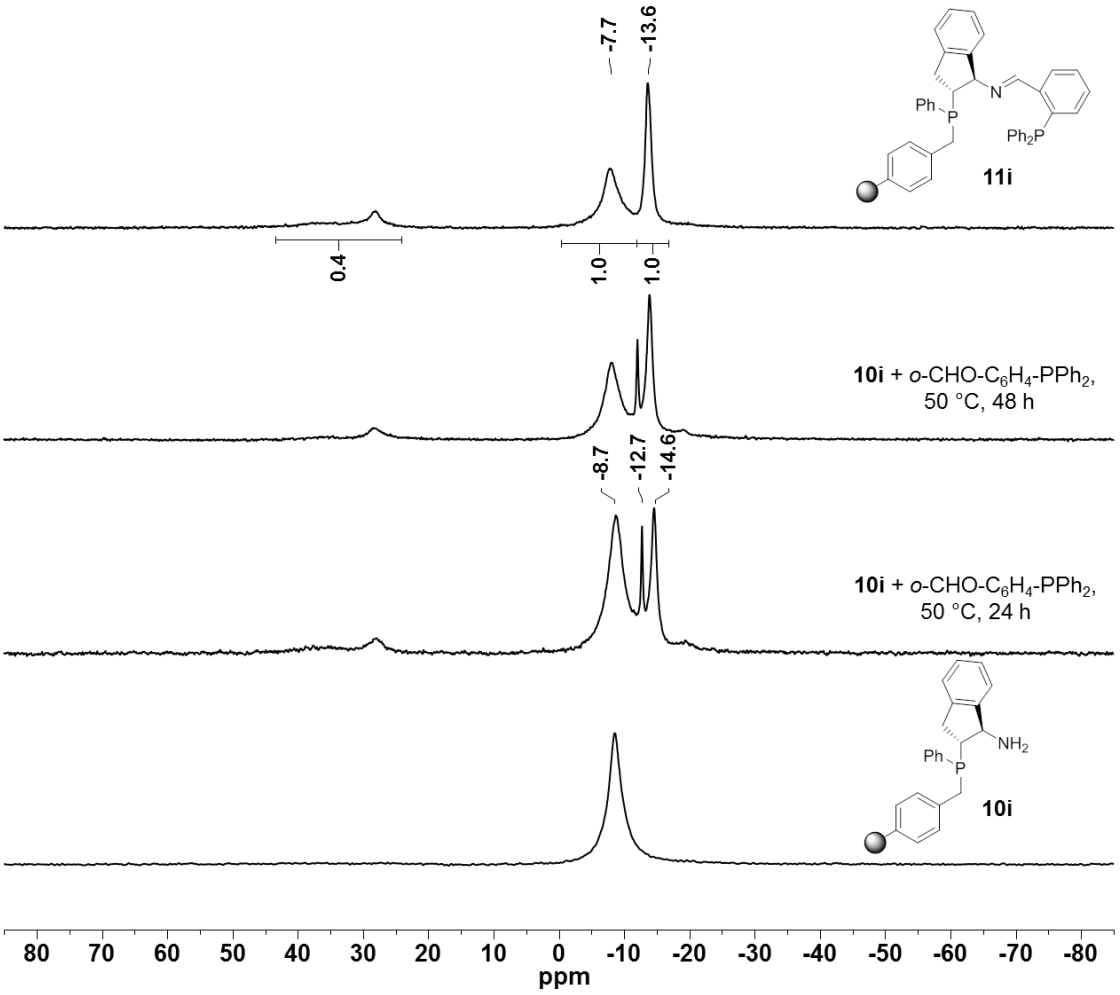

Figure 8 Solid-phase synthesis of supported PNP intermediate **11i** monitored by ^{31}P NMR.

Unfortunately, the simultaneous formation of the corresponding phosphine oxides exhibiting broad signals at δ = 37-28 ppm was observed. This may be attributed to side-reactions involving both phosphines and the drying agent TMOF as well as the degradation species formed upon reaction with water. It was found that the amount of phosphine oxides remaining covalently bound to the support depends on the time required for the condensation step. In the case of **11d** bearing a bulky ^{t}Bu group near the nucleophilic nitrogen, up to 40% of oxidized by-products were obtained. Despite the

facilitated work-up procedure requiring only a simple filtration step when employing TMOF, an optimized synthetic protocol would be highly desirable in order to yield the supported imine-based PNP ligands in high purity. In fact, homogeneous Schiff base-type PNP ligands bearing an imine functionality instead of the free amine have proven to be suitable ligands for application in asymmetric (transfer)hydrogenation.[19] In all cases of supported imine intermediates **11a-l**, a slight chemical shift of up to $\Delta\delta$ = 2 ppm for the resin-bound phosphorus atoms compared to their PN starting materials was observed together with a signal belonging to the PPh_2 entity at δ = -11.8--15.1 ppm. Furthermore, imine formation in case of **11e** could also be confirmed using gel-phase ^{13}C NMR showing a distinctive signal assigned to the C=N carbon at δ = 158.5 ppm as well as a peak belonging to the chiral *C*HBz carbon at δ = 71.2 ppm.

The supported intermediates **11a-l** were used as received in the subsequent reduction of the imine to the free secondary amine to access the desired immobilized (a)chiral PNP ligands. Building on the successful application of diisobutylaluminum hydride (DIBAL-H) serving as reducing agent in the solid-phase synthesis of PNN ligands,[33] the protocol was adapted in the next reaction step. When using an excess of 10 equivalents of a 1 M solution of DIBAL-H in toluene at 70 °C, the reduction proceeded smoothly within 2 hours leading to the supported PNP ligands $\mathbf{L_1}$-$\mathbf{L_{12}}$ (Scheme 7).

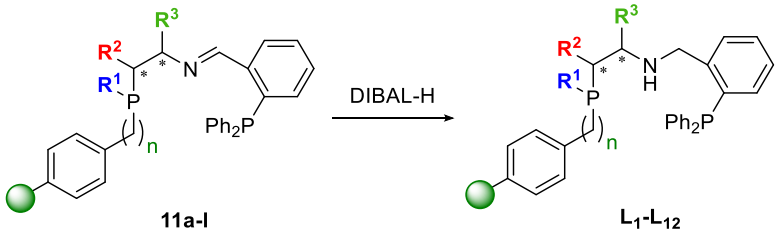

Scheme 7 Solid-phase synthesis of supported (a)chiral PNP ligands $\mathbf{L_1}$-$\mathbf{L_{12}}$.

Upon reduction of the C=N functionality, a small change in chemical shift of $\Delta\delta$ = 1.7 ppm was observed for the remote PPh_2 moiety in $\mathbf{L_9}$ (red spectrum, Figure 9) whereas the signal of the resin-bound phosphorus atom remained unaffected when compared to **11i** (black spectrum). Similar results were obtained for the whole PNP ligand library. Gratifyingly, covalently-bound oxidized phosphorus impurities could be simultaneously reduced back to the desired P(III) species in all cases indicated by the disappearance of the P(V) oxide species at δ = 37-28 ppm.

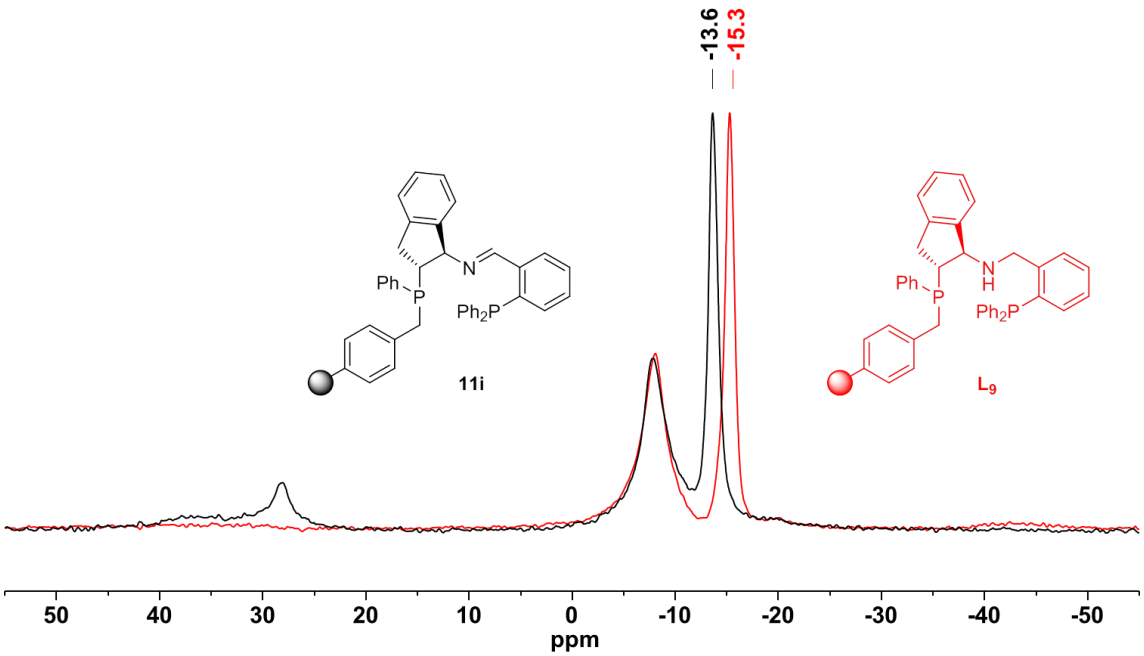

Figure 9 ^{31}P NMR spectra of supported imine **11i** (black) and PNP ligand **L$_9$** (red).

Moreover, the quantitative reduction of the imine group could also be verified using gel-phase ^{13}C NMR of **L$_5$** bearing a benzyl substituent in the aliphatic backbone. The disappearance of the signal belonging to the C=N carbon at δ = 158.5 ppm and the formation of a new resonance corresponding to the N–CH_2–Ph carbon at δ = 49.7 ppm was observed. In addition, the peak of the *C*HBz carbon at δ = 71.2 ppm of **11e** shifted to δ = 56.8 ppm upon reduction. These results for **L$_5$** as well as the ^{31}P NMR spectra of supported ligands **L$_1$**, **L$_3$**, **L$_5$** and **L$_7$** are well in line with those reported for their homogeneous analogues.[18] Interestingly, in case of PS-supported PNP ligand **L$_{12}$**, a splitting of the signal belonging to the first P-nucleus was detected (δ = 12.7 and 8.4 ppm, Figure 10), which again is attributable to the presence two epimers in the supported species. Furthermore, a minor impurity bound to the support (~5%) is observed at δ = -6.8 ppm, which could not be avoided during the synthetic sequence. Finally, the reduction of the imine moiety could also be confirmed using FT-IR spectroscopy. The immobilized (a)chiral PNP ligand library was obtained in high yield by applying a highly modular solid-phase synthetic methodology requiring only minimal work-up procedures.

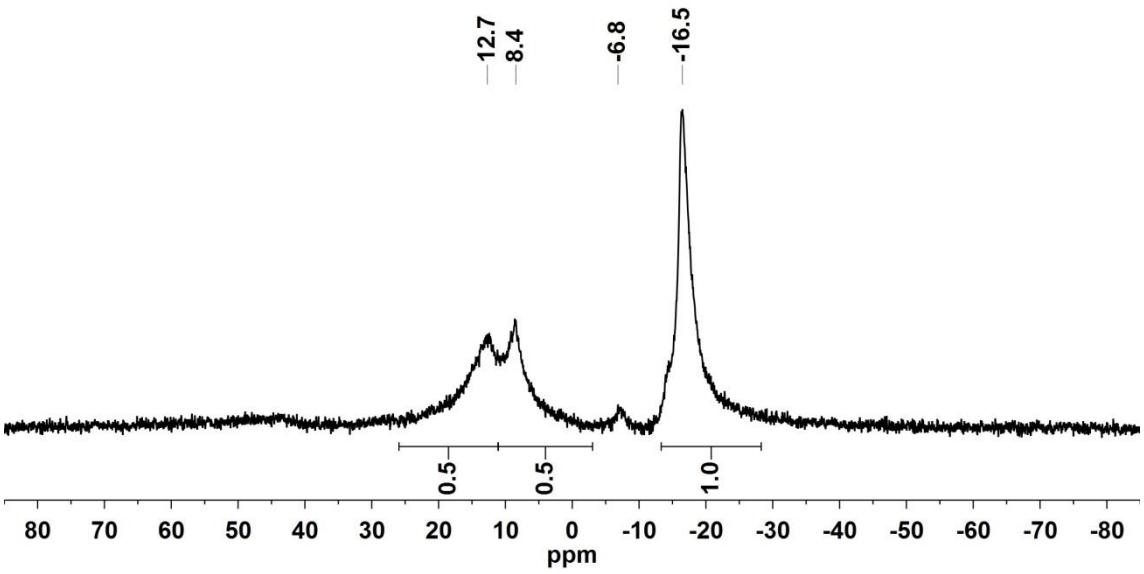

Figure 10 Gel-phase ^{31}P NMR spectrum of supported PNP ligand $\mathbf{L_{12}}$.

The entire resin-bound library of 12 aliphatic PNP pincer-type ligands is depicted in Figure 11. $\mathbf{L_1}$ and $\mathbf{L_{10}}$ (grey box) represent achiral ligand structures differing in the substituent attached to the first phosphorus atom (Ph and ^{t}Bu) as well as in the type of polymeric support, i.e. Merrifield and polystyrene. A second subgroup of ligands ($\mathbf{L_2}$-$\mathbf{L_5}$ and $\mathbf{L_{11}}$) carries a single chiral center adjacent to the nitrogen donor atom (Figure 11, green box). By employing substituents such as Me, ^{i}Pr, ^{t}Bu or Bz, the steric environment in close proximity to the ligand donor atoms was efficiently altered. Finally, 5 members of supported PNP ligands were synthesized bearing two chiral centers in the aliphatic backbone (Figure 11, red box), which in turn allows for investigation of the effects of the number of chiral centers in catalysis. While ligands $\mathbf{L_6}$ and $\mathbf{L_{12}}$ provide two phenyl groups adjacent to both P and N donor atoms, $\mathbf{L_7}$ carries a less sterically demanding Me group next to the NH moiety. In case of $\mathbf{L_8}$ and $\mathbf{L_9}$, the (*R*,*R*)- and the (*S*,*S*)-enantiomer of a bicyclic indane-based backbone were prepared. All supported ligands were obtained as off-white resins except for $\mathbf{L_8}$ and $\mathbf{L_9}$, which appear as pale orange to light brown materials.

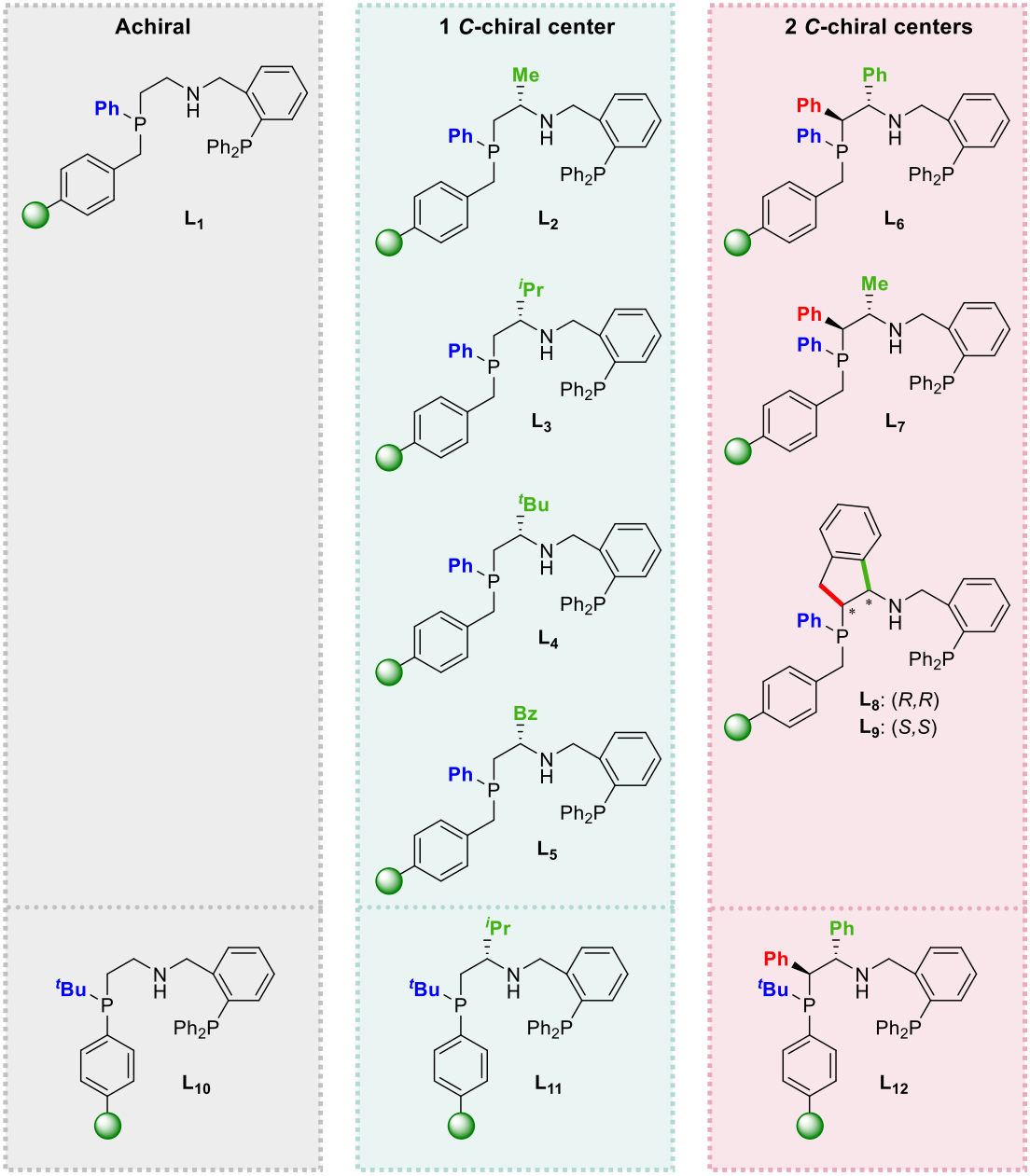

Figure 11 Supported ligand library of (a)chiral PNP ligands **L_1-L_{12}**.

4.2.4 Synthesis of Supported Chiral Pyridine-based PNP Ligand L_{13}

In recent studies towards catalytic applications of tridentate PNN and PNP pincer ligands, structural motifs based on chiral phospholane moieties have demonstrated high enantioselectivities when employed in asymmetric hydrogenation of ketones. In the Mn-catalyzed ketone reduction using aliphatic PNP ligand **IV** equipped with two (2*R*,5*R*)-2,5-dimethylphospholane donor moieties (see Figure 2, chapter 4.1), aliphatic

ketones were converted with up to 84% *ee*.[14] More recently, Ding *et al.* reported on a manganese-based PNN complex introducing a chiral and sterically more demanding (2*R*,5*R*)-2,5-diphenylphospholane.[35] In the screening of over 80 ketone substrates, up to 98% *ee* was achieved.

Building on these promising results from homogeneous systems, it was decided to employ chirality via a phospholane moiety into a supported PNP-type ligand by using a solid-phase synthetic approach. Following a synthetic route, which has been established for the synthesis of supported pyridine-based PNP ligands described in chapter 3, the preparation of the resin-bound chiral ligand **L_{13}** was attempted accordingly. Therefore, 2,6-bis(chloromethyl)pyridine was monosubstituted with borane-protected lithiated (2*R*,5*R*)-2,5-dimethylphospholane in order to obtain the PN fragment **12** in 53% yield by following an adapted literature protocol.[36] Upon deprotonation of supported secondary phosphine **6·BH_3** using an excess of KHMDS, the PN fragment **12** (1.2 equiv.) was introduced into the solid-phase synthetic sequence (Scheme 8, steps 1 and 2). After addition at -78 °C, the mixture was warmed to room temperature overnight showing a resin color change from yellow-orange to yellow.

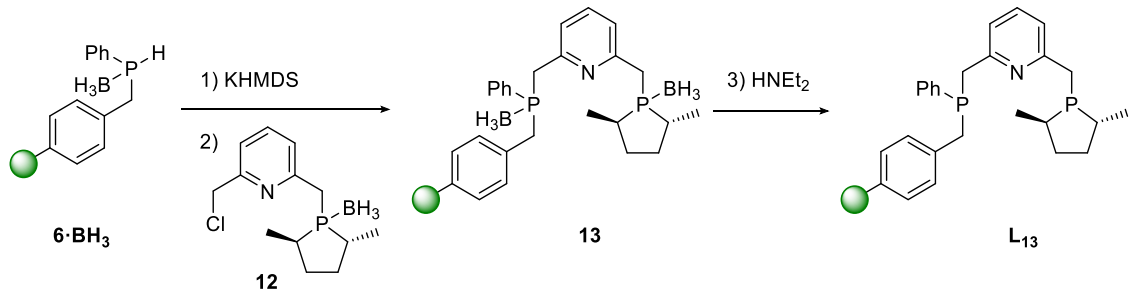

Scheme 8 Solid-phase synthesis of resin-bound pyridine-based PNP pincer ligand **L_{13}**.

Quantitative formation of the bench-stable chiral PNP precursor **13** was confirmed by ^{31}P NMR. The spectrum exhibits a broad signal at δ = 18.6 ppm belonging to the resin-bound phenylphosphine borane adduct next to a sharper peak at δ = 40.0 ppm assigned to the borane-protected phospholane moiety both appearing in a 1:1 ratio (Figure 12, middle spectrum). Subsequent removal of the BH_3 groups upon treatment with diethylamine at 50 °C led to the immobilized pyridine-based PNP ligand **L_{13}** (Scheme 8, step 3). The product was obtained as a pale yellow resin in high yield and purity. Again, full borane removal overnight was verified by an upfield shift of both

phosphorus resonances to δ = 6.5 ppm for the phospholane and -14.2 ppm for the –PPh group in the corresponding ^{31}P NMR spectrum (Figure 12, top spectrum).

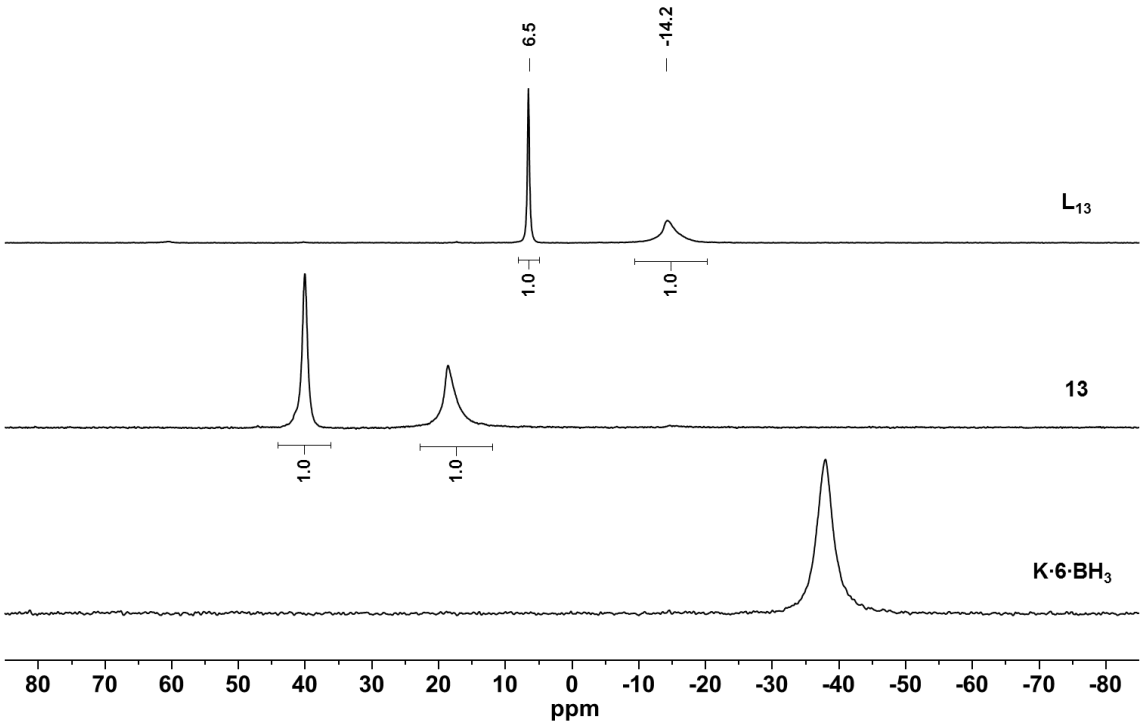

Figure 12 Solid-phase synthesis of supported PNP ligand **L_{13}** monitored by ^{31}P NMR.

4.3 Application in Asymmetric Ketone Hydrogenation

4.3.1 Synthesis of Supported Ru-PNP Complexes

Subsequent to the successful preparation of a diverse resin-bound (a)chiral PNP pincer ligand library, the synthesis of the corresponding Ru pre-catalysts (**C_1-C_{12}**) was attempted. Adapting the protocol established for the synthesis of pyridine-based Ru-PNP complexes (see chapter 3), ligands **L_1-L_{12}** were treated with a stoichiometric amount of Ru precursor [$RuHCl(PPh_3)_3CO$] in THF and heated to 60 °C (Scheme 9). The complexation progress was followed by ^{31}P NMR as depicted in Figure 13 for the preparation of representative compound **C_4**. After 1.5 hours, both signals corresponding to the free ligand **L_4** had gradually disappeared accompanied by the appearance of a signal at δ = -5.0 ppm belonging to liberated triphenylphosphine. Full conversion of **L_4** was observed after 24 hours indicated by the disappearance of the ligand signals.

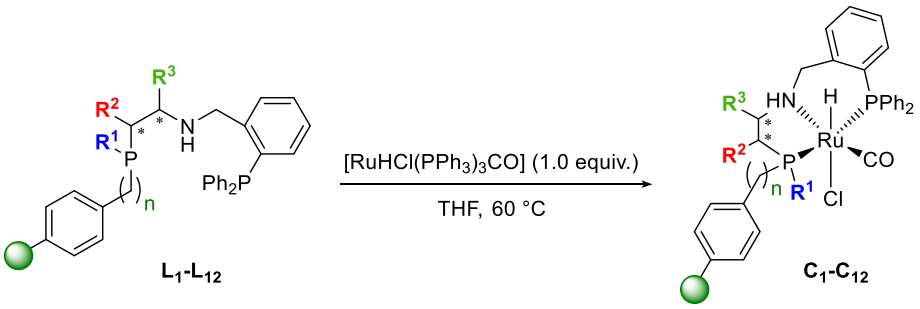

Scheme 9 Solid-phase synthesis of resin-bound ruthenium-PNP complexes **C_1-C_{12}**.

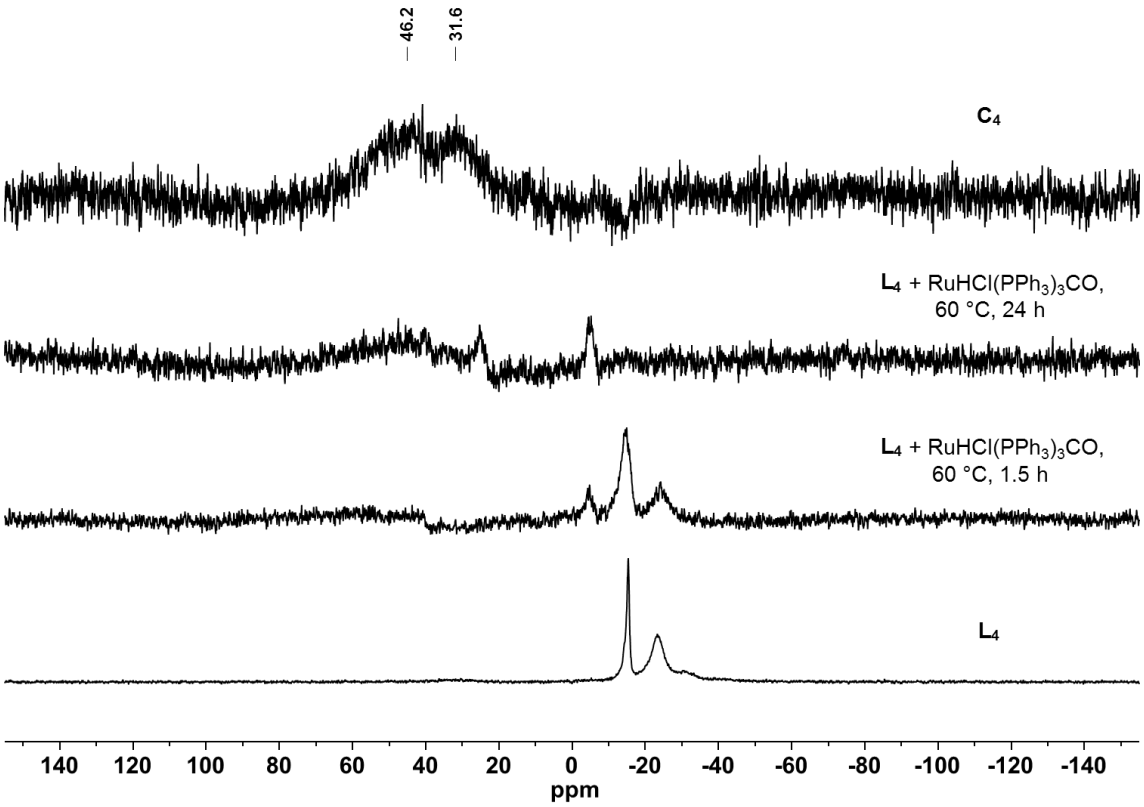

Figure 13 Solid-phase synthesis of supported Ru-PNP complex **C_4** monitored by ^{31}P NMR.

After washing the brown resin, the ^{31}P NMR spectrum showed two new but very broad peaks at about δ = 46.2 and 31.6 ppm corresponding to the chemically different phosphorus donor atoms bound to the Ru metal center. However, due to significant peak broadening, determination of coupling constants as well as the peak integration ratio proved to be troublesome. Hence, a meridional coordination geometry of the supported PNP ligand to the ruthenium center, as found in most homogeneous systems, can only be assumed. Moreover, the presence of isomeric Ru-complexes on

the support cannot be excluded. Comparable chemical shifts of δ = 49.6 and 41.3 ppm were observed for a structurally similar unsymmetrical PNP ligand employed in a solution-phase Fe(II) complex.[18] In case of all remaining PN(H)P ligand library members full consumption of the ligand signals was observed. Unfortunately, no corresponding complex resonances could be detected most likely due to their disappearance in the baseline. Similar broad peaks have been observed for immobilized Ru-PNN complexes developed within the Kamer group.[37] Nevertheless, analysis by FT-IR spectroscopy indicated successful incorporation of ruthenium precursor in all cases showing distinct stretching bands at 1918-1928 cm^{-1} corresponding to the CO ligand bound to the metal center. The presence of a P:Ru ratio of 2:1 in case of **C_1** was confirmed by elemental analysis. However, for further characterization, the use of solid-state NMR techniques would be required to determine the distinctive chemical shifts of the immobilized Ru-PNP complexes.

Complexation of **L_{13}** was achieved by following a synthetic protocol used for the preparation of resin-bound pyridine-based Ru-PNP complexes (see chapter 3). Treatment with a slight excess of [$RuHCl(PPh_3)_3CO$] at 60 °C led to the chiral Ru-catalyst **C_{13}** as a brown-orange resin (Scheme 10). Again, the progress was monitored by gel-phase ^{31}P NMR showing full complexation of ligand **L_{13}** overnight (Figure 14).

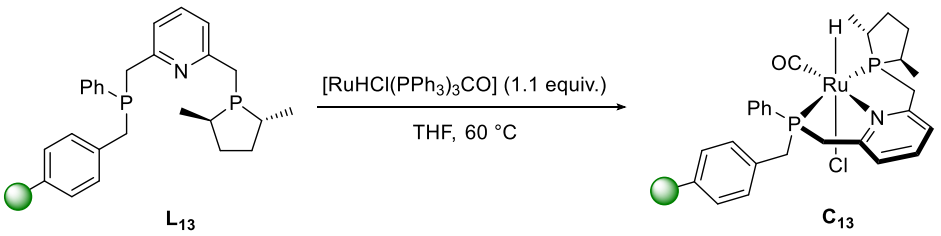

Scheme 10 Solid-phase synthesis of resin-bound Ru-PNP complex **C_{13}**.

While the signals of the free ligand disappeared quantitatively, two new broad resonances at δ = 77.9 and 51.9 ppm emerged in a 1:1 ratio corresponding to both phosphorus nuclei coordinated to the ruthenium metal. The successful introduction of the metal center is supported by the IR spectrum showing a strong band at 1919 cm^{-1} belonging to the CO ligand. In analogy to similar homogeneous ruthenium complexes (see chapter 3), a meridional coordination geometry of the supported Ru-PNP complex **C_{13}** and its isomeric structures can be assumed.

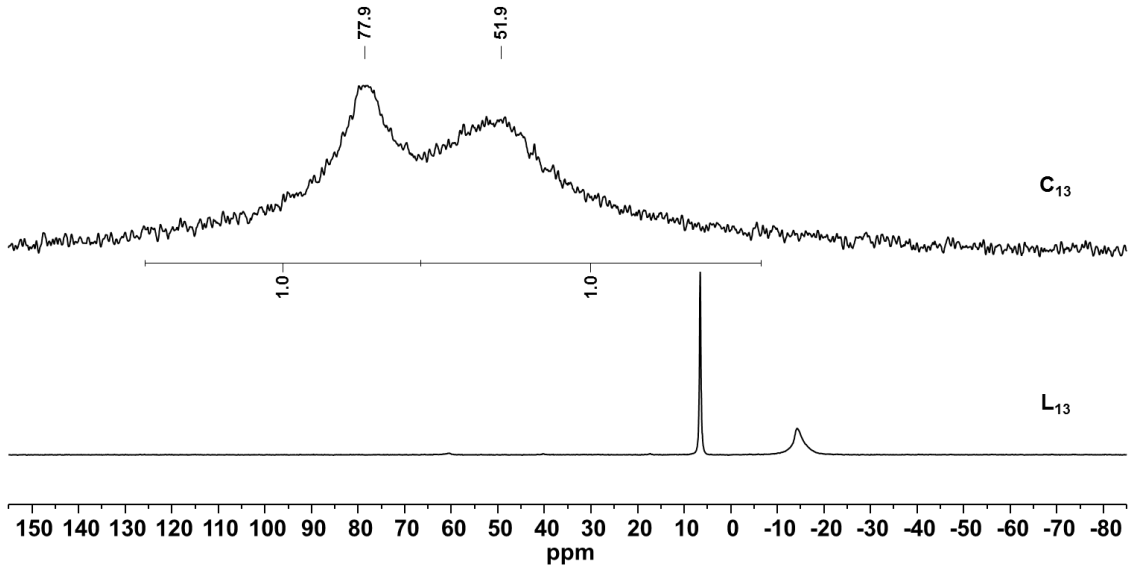

Figure 14 Solid-phase synthesis of supported Ru-PNP complex **C_{13}** monitored by ^{31}P NMR.

4.3.2 Catalytic Screening

The entire immobilized library of (a)chiral PNP-type pincer ligands was applied in the Ru-catalyzed (asymmetric) hydrogenation of various ketones. Acetophenone (**S_1**), representing one of the simplest aromatic ketones, was chosen as a benchmark substrate for catalyst library screening. The results for the supported catalysts **C_1-C_{13}** are summarized in Table 2.

Initially, the achiral PS-supported complex **C_{10}** was examined in the hydrogenation of **S_1** under basic conditions in THF at 30 bar H_2 and room temperature. When using 1 mol% of **C_{10}** and 5 mol% of KO^{t}Bu full conversion towards 1-phenyethanol was obtained within 4 hours (Table 2, entry 1). Lowering the amount of base to 2 mol% gave the same result whereas with 1 mol% no activity was observed (Table 2, entries 2 and 3). In analogy to that, the Merrifield-supported achiral equivalent **C_1** carrying a phenyl substituent on the first phosphorus showed a similar performance in the presence of 2 mol% of base (Table 2, entry 4).

Next, the influence of a chiral substituent adjacent to the NH donor moiety was examined. Supported complex **C_2** carrying an (*S*)-configured methyl substituent in the backbone gave full conversion of **S_1** along with a low enantiomeric excess of 10% towards the (*S*)-product (Table 2, entry 5). Increasing the steric bulk by employing an ^{i}Pr group in the same positon in **C_3** resulted in 47% conversion to the racemic alcohol (Table 2, entry 6). Even less activity was obtained for the sterically more demanding

^{t}Bu analogue **C$_4$** (12% conversion, Table 2, entry 7). Mechanistic studies for similar Ru, Mn and Fe-based solution-phase systems involving a NH donor moiety have shown that the hydrogenation of ketones proceeds most likely in the outer-sphere of the catalyst via a metal-ligand bifunctional process.[14,38]

Table 2 Ru-catalyzed (asymmetric) hydrogenation of **S$_1$** using supported catalysts **C$_1$-C$_{13}$**.

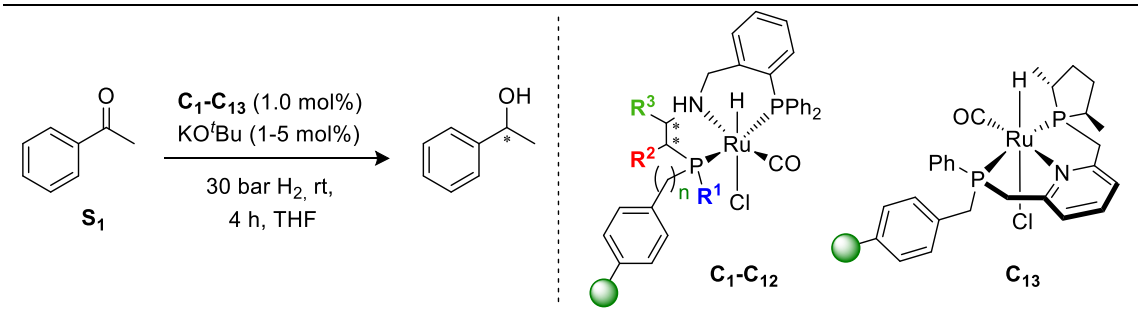

Entry	Catalyst	Substituents			KO^{t}Bu	Conversion	ee
		R^1	R^2	R^3	[mol%]	[%][b]	[%][c]
1	**C$_{10}$**	^{t}Bu	H	H	5	>99	0
2	**C$_{10}$**	^{t}Bu	H	H	2	>99	0
3	**C$_{10}$**	^{t}Bu	H	H	1	1	0
4	**C$_1$**	Ph	H	H	2	>99	0
5	**C$_2$**	Ph	H	Me	2	>99	10 (*S*)
6	**C$_3$**	Ph	H	^{i}Pr	2	47	0
7	**C$_4$**	Ph	H	^{t}Bu	5	12	0
8	**C$_5$**	Ph	H	Bz	2	>99	22 (*S*)
9	**C$_6$**	Ph	Ph	Ph	2	>99	4 (*S*)
10	**C$_7$**	Ph	Ph	Me	5	>99	4 (*S*)
11	**C$_8$**	Ph	indane (*S*,*S*)		5	>99	0
12	**C$_9$**	Ph	indane (*R*,*R*)		2	96	0
13	**C$_{11}$**	^{t}Bu	H	^{i}Pr	5	>99	0
14	**C$_{11}$**	^{t}Bu	H	^{i}Pr	2	45	14 (*R*)
15	**C$_{12}$**	^{t}Bu	Ph	Ph	5	>99	43 (*S*)
16	**C$_{13}$**	Ph	phospholane		5	>99	26 (*S*)

[a] General conditions: substrate (0.5 mmol), [Ru] (1.0 mol%), THF (1 mL), H_2 (30 bar), 4 h. [b] Conversion towards the secondary alcohol determined by GC using. [c] Enantiomeric excess of product determined by chiral GC (absolute configuration drawn in parenthesis).

As the access of the carbonyl compound to the nitrogen functionality plays a crucial role in this mechanism, the participation may be hindered in presence of bulky substituents in close proximity.[18] Full conversion was obtained again when employing a less bulky and more flexible benzyl substituent in **C_5** (Table 2, entry 8). Moreover, the supported catalyst achieved 22% *ee* towards the (*S*)-alcohol, which exceeds the selectivity of 13% *ee* reported for a similar homogeneous Fe-based analogue carrying a benzyl group adjacent to the nitrogen atom.[18] No further improvements on the enantioselectivity were accomplished when employing other base additives such as KHMDS, NaO^{i}Pr and NaOEt. Changing to alcohols as reaction media had a detrimental effect on both activity and selectivity due to the poor swelling properties of the polymeric supports in protic solvents.

The presence of 1:1 mixtures of epimers at the resin-bound phosphine did not have an impact on the stereoselective outcomes in previously described asymmetric hydrogenation reactions using supported phosphine-phosphite ligands (see chapter 2). In the case of supported chiral PNP ligands, however, the chiral induction solely relies on the stereocenter(s) located in the aliphatic backbone. Hence, a detrimental effect on the enantioselectivities due to the presence of an epimeric mixture cannot be excluded. In order to determine the overall influence of the *P*-stereogenic center, the selective synthesis of a single epimer on the support would be required.

Next, the effect on the stereoselective outcome upon installation of an additional center of chirality in α-position to the resin-bound phosphorus was investigated. Solution-phase studies by Morris and co-workers showed the importance of a second stereocenter to provide a rigid, asymmetric ligand structure, which had a positive effect on the chiral induction.[17] When the resin-bound catalyst **C_6** bearing two phenyl groups in (*S*,*S*)-configuration was employed in the hydrogenation of **S_1**, nearly a racemic mixture of 1-phenylethanol was obtained (Table 2, entry 9). The same result was obtained for Ru-catalyst **C_7** when replacing the Ph substituent next to the NH group with a Me group (Table 2, entry 10). Likewise, the racemic alcohol was yielded in cases of supported catalysts **C_8** and **C_9** based on a chiral bicyclic and hence less flexible indane backbones (Table 2, entries 11 and 12).

Subsequently, PS-supported **C_{11}** carrying a single ^{i}Pr substituent was employed resulting in quantitative hydrogenation to the racemic alcohol (Table 2, entry 13). Reducing the amount of KO^{t}Bu from 5 to 2 mol% led to only 45% conversion of **S_1**, which is comparable to the Merrifield-supported analogue **C_3** (Table 2, entry 6 versus 14) In this case, however, 14% *ee* of the (*R*)-alcohol were obtained opposed to a

racemic mixture for **C_3**. Interestingly, up to 43% *ee* towards the (*S*)-alcohol were achieved when employing immobilized catalyst **C_{12}** carrying two chiral phenyl substituents in contrast to only 4% *ee* for the Merrifield-bound analogue **C_6** (Table 2, entry 9 versus 15). Both ligands differ in the **R^1** substituent attached to the resin-bound phosphorus moiety as well as the type of support linker. The PNP ligand in **C_6** contains a phenyl substituent bound to the first phosphorus moiety and is linked to the Merrifield support via a flexible methylene bridge. The first phosphine in **C_{12}**, however, is bound to a sterically more demanding ^{t}Bu substituent as well as directly bound to an aryl group of the polystyrene support. This in turn enforces a stronger ligand rigidity in the supported complex **C_{12}** potentially locking the asymmetric structure into position, which could be one explanation for the higher *ee*. Similar trends were observed by Morris and co-workers in case of their Fe-PNP catalysts **XI**-**XIII** (see Figure 2, chapter 4.1). All three homogeneous examples resemble the same ligand backbone structure containing two chiral substituents (Me and Ph) but differed in the substituents (^{i}Pr, Ph and Cy) bound to one of the phosphorus donor atoms. In the asymmetric reduction of various aromatic ketones, a slightly lower *ee* was obtained for the Ph substituted complex **XII** when compared to catalyst **XI** bearing a more sterically demanding ^{i}Pr substituent (74% *ee* versus 81% *ee* for **S_1**).[19a,38f] Moreover, the homogeneous ferrocene-based catalysts **XI**-**XIII** contain an additional, planar chiral stereocenter, which played a key role in the chiral induction.[19a] Consequently, it seems likely that an epimeric mixture of phosphines present in the polymer-bound PNP ligands causes a detrimental effect on the enantioselectivity.

In case of the resin-bound Ru-PNP complex **C_{13}** providing a chiral phospholane at the remote pyridine side arm, acetophenone was fully converted affording (*S*)-1-phenylethanol in 26% *ee* (Table 2, entry 15). A similar selectivity of only 18% *ee* was reported by Garbe *et al.* for the Mn-PNP catalysts featuring aliphatic diphospholane pincer ligand **IV** (see Figure 2, chapter 4.1).[14] An increase in steric demand by replacing the chiral Me-phospholane groups by Ph substituents could lead to significantly improved stereoselectivity as demonstrated recently for corresponding Mn-PNN complexes.[35]

Finally, the substrate scope was expanded towards a small variety of aromatic and aliphatic ketones. Due to availability reasons, the second best performing aliphatic Ru-PN(H)P complex **C_5** was employed in the screening of substrates **S_2**-**S_{13}** and compared to the supported pyridine-based catalyst **C_{13}** (Figure 15).

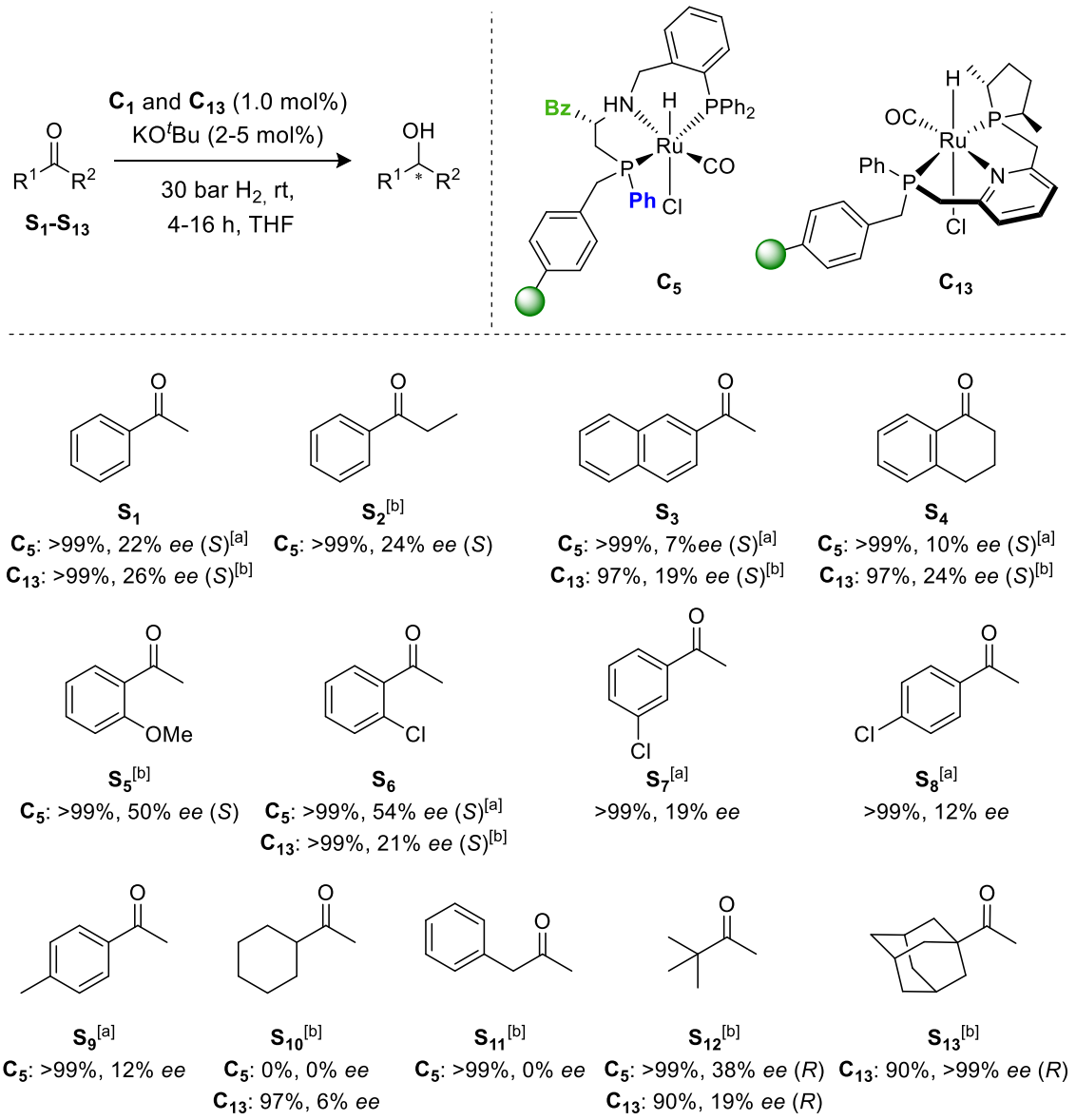

Figure 15 Substrate scope for asymmetric ketone hydrogenation (conversion and enantiomeric excess indicated below structures). General conditions: [a]: [Ru] (1.0 mol%), KO^{t}Bu (2 mol%), THF (1 mL), 25 °C, H_2 (30 bar), 4 h. [b]: KO^{t}Bu (5 mol%), 16 h. Percentage conversion determined by GC. Enantiomeric excess of product determined by chiral GC or HPLC (absolute configuration drawn in parenthesis).

The aromatic substrate propiophenone (**S$_2$**) was hydrogenated with similar enantioselectivity compared to **S$_1$** (22 % *ee* versus 24% *ee*) but required increased amounts of base (5 mol%) and longer reaction time (16 h). 2-acetonaphthone (**S$_3$**) and α-tetralone (**S$_4$**) were fully converted to the corresponding alcohols when using **C$_5$**. However, enantiomeric excesses towards the (*S*)-products remained low. Slightly increased *ee*s for substrate **S$_4$** were produced achieving up to 24% in case of phospholane-based catalyst **C$_{13}$**. However, homogeneous systems providing two chiral

phospholane donor groups (**IV**, see section 4.1, Figure 2) instead of one, as it is the case for $\mathbf{C_{13}}$, were able to induce *ee*s of up to 84%.[14]

Next, steric effects were investigated by employing *ortho*-, *meta*- and *para*-substituted acetophenones. Substrate $\mathbf{S_5}$ bearing a methoxy group in *ortho*-position was hydrogenated to the (*S*)-product in 50% *ee* after 16 hours. Slightly electron-withdrawing 1-(2-chlorophenyl)ethanone ($\mathbf{S_6}$) was converted to the desired alcohol in 54% *ee* within 4 hours. Similar enantioselectivities (56-61% *ee*) for $\mathbf{S_6}$ but lower activities (60-62% conversion after 16 hours) were obtained with solution-phase Fe-PNP analogues.[19a] In contrast to immobilized catalyst $\mathbf{C_5}$, a substituent in *ortho*-position of the substrate did not seem to improve the selectivity of supported catalyst $\mathbf{C_{13}}$ (21% *ee* for $\mathbf{S_6}$). A gradual decline in *ee* was observed for substrates providing a substituent in *meta*- or *para*-position. While *meta*-substituted substrate $\mathbf{S_7}$ led to 19% *ee*, *para*-functionalized acetophenones $\mathbf{S_8}$ and $\mathbf{S_9}$ resulted in even lower enantioselectivity of 12%.

Aliphatic ketones proved to be even more challenging. Surprisingly, no activity in the reduction of 1-cyclohexylethanone ($\mathbf{S_{10}}$) was obtained in case of $\mathbf{C_5}$, whereas $\mathbf{C_{13}}$ resulted in 97% conversion to the racemic 1-cyclohexylethanol under the same conditions. The less sterically hindered 1-phenyl-2-butanone ($\mathbf{S_{11}}$) was quantitatively converted to the racemic alcohol when using $\mathbf{C_5}$. 3,3-dimethyl-2-butanone ($\mathbf{S_{12}}$) was fully hydrogenated to the (*R*)-alcohol with up to 38% *ee*. This result seems quite remarkable since chiral solution-phase Fe- and Mn-PNP catalysts showed either no or low activity towards $\mathbf{S_{12}}$ with *ee*s between 25% and 33%.[14,17,39] $\mathbf{C_{13}}$ gave a slightly reduced catalyst performance with 19% *ee*. Finally, 90% of the very bulky substrate adamantyl methyl ketone ($\mathbf{S_{13}}$) were hydrogenated with excellent enantioselectivity towards the (*R*)-product (>99%) in case of the phospholane-based Ru-catalyst $\mathbf{C_{13}}$. A similar boost in enantioselectivity from 19% *ee* in case of the bulky ^{t}Bu-functionalized substrate $\mathbf{S_{12}}$ to >99% *ee* for adamantyl-substituted substrate $\mathbf{S_{13}}$ was observed for homogeneous Mn and Fe catalysts based on the bisphospholane PNP ligand **IV** (see section 4.1, Figure 2).[39]

4.4 Conclusion and Outlook

In this chapter a new modular solid-phase synthetic protocol was presented that enables the first efficient synthesis of immobilized chiral PNP-type pincer ligands. Using this methodology by applying the three main building blocks **A**, **B** and **C** in a combinatorial fashion, a diverse ligand library of 13 supported PNP ligands could be readily accessed. Chirality was installed into the aliphatic ligand backbone via selective ring-opening of Boc-protected sulfamidates, which, in some cases, could be derived from natural and unnatural amino acids. In case of resin-bound pyridine-based PNP ligand $\mathbf{L_{13}}$, the chiral information could be incorporated via a phospholane moiety linked to a pyridine side arm. Moreover, only simple purification steps were required during the reaction sequence comprising easy filtration and washing procedures. In the solution-phase synthesis of similar homogenous analogues often laborious and hence low yielding workup procedures are necessary.

The entire supported ligand library was transferred into the corresponding ruthenium-PNP complexes. The successful formation of the desired transition-metal complexes bound to the support is supported by gel-phase ^{31}P NMR and FTIR spectroscopy. However, additional analytical efforts, such as solid-state NMR spectroscopy, are required in order to gain more information on the molecularly defined catalyst structure.

Yet, the supported Ru-PNP complexes were successfully screened in the Ru-catalyzed (asymmetric) hydrogenation of acetophenone ($\mathbf{S_1}$). Although only low to moderate enantioselectivities of up to 43% were obtained in case of $\mathbf{C_{12}}$, important trends concerning the amount of stereocenters as well as ligand rigidity could be extracted. Moreover, immobilized catalysts $\mathbf{C_5}$ and $\mathbf{C_{13}}$ were tested in a range of aromatic and more challenging aliphatic ketones. Supported catalyst $\mathbf{C_5}$ achieved up to 54% *ee* in case of the aromatic *ortho*-substituted substrate $\mathbf{S_6}$, whereas $\mathbf{C_{13}}$ led to excellent stereoselectivity of >99% when employed in the hydrogenation of the bulky adamantyl methyl ketone $\mathbf{S_{13}}$.

Some preliminary results in Ru-catalyzed (asymmetric) transfer hydrogenation and more challenging reduction of esters have shown great potential for expanding the applicability of the supported ligands.

When compared to similar homogeneous Fe and Mn-based catalysts, generally lower enantioselectivities were obtained for the supported chiral Ru-PNP complexes. This could be due to the presence of epimers at the resin-bound phosphorus atom in all cases. In order to examine the impact of a racemic phosphorus donor atom on the

stereoselective outcome the preparation of a single resin-bound epimer would be desirable. Furthermore, the introduction of additional stereocenters into the ligand structure could result in enhanced enantioinduction when applied in ketone hydrogenation. The *ortho*-aldehyde building block **C** offers the possibility for both the fine-tuning of the electronic and steric properties of the remote phosphine as well as the incorporation of extra chirality. Following an adapted synthetic procedure reported by the groups of Walter[40] and Milstein,[41] *ortho*-aldehyde derivatives bearing a diisopropylphosphine or a chiral phospholane moiety could be prepared via treatment of a lithiated dioxolane or its corresponding Grignard species with a suitable chlorophosphine (Scheme 11 a). Subsequent removal of the acetal protection using *p*-toluenesulfonic acid (PTSA) affords the desired *ortho*-aldehyde which can be employed in the condensation step of the solid-phase synthetic sequence. Alternatively, planar chirality could be introduced via an *ortho*-substituted ferrocene carboxaldehyde to achieve supported PNP ligand (S_{Fc})-**14** as reported by Morris and co-workers (Scheme 11 b).[19a] Finally, the replacement of the Me groups by more bulky Et or Ph groups in case of phospholane-base PNP ligand **L_{13}** could lead to improved stereoselectivities.

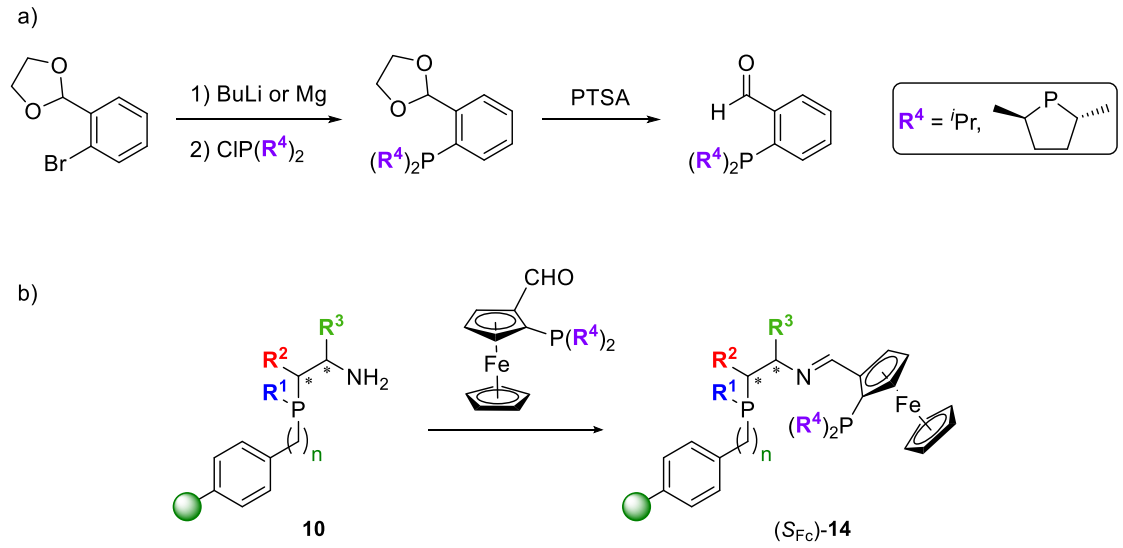

Scheme 11 Proposed synthetic route towards *ortho*-aldehydes and planar chiral ligand (S_{Fc})-**14**.

4.5 Experimental

General Experimental

All reactions and manipulations were carried out using standard Schlenk techniques under inert atmosphere of purified argon or in an MBraun glovebox unless stated otherwise. All glassware was dried prior to use to remove traces of water. All chemicals were obtained from commercial suppliers and were used as received unless stated otherwise. Diethyl ether and THF were distilled from sodium/benzophenone and toluene was distilled from sodium. Distilled THF used in catalytic reactions was additionally dried over 3 Å molecular sieves for a minimum of 72 h. DCM, diethylamine and triethylamine were distilled from calcium hydride. C_6D_6, TFA and TMOF were thoroughly degassed with Argon. C_6D_6 was stored over 4 Å molecular sieves. Supported secondary phosphines **6** and **8** as well as the lithiated species **Li·6** and **Li·8** were synthesized according to literature.[24a,24c] Boc-protected amino alcohols **3b-i** were prepared via reduction of Boc-amino acids **1a-d**[26-27] and Boc protected amino alcohols **2a-d**.[25] **4**[29] and **5a-i**[25,30] were prepared according to literature. (2*R*,5*R*)-2,5-dimethylphospholane-borane was provided by Dr. Marcel Garbe and Dr. Kathrin Junge from the Leibniz Institut für Katalyse in Rostock, Germany.

NMR spectroscopic analysis was conducted using a Bruker FOURIER 300, an AVANCE II 400 or an AVANCE III 500. ^{1}H, ^{31}P and ^{13}C NMR experiments were recorded using standard NMR techniques and the chemical shifts (δ) are reported relative to the solvent peak. Gel-phase ^{31}P and ^{13}C NMR spectra of all resins were recorded unlocked and without additional shimming in dry THF as a solvent unless stated otherwise. Chemical shifts are reported relative to 85% H_3PO_4 in water. Multiplicities are provided using the following abbreviations: s = singlet, d = doublet, t = triplet, m = multiplet and br = broad and the couplings (*J*) are reported in Hz. NMR spectra were processed using TopSpin 3.2 or MestReNova 11.0. IR spectra were recorded on a Shimadzu IRAffinity-1S spectrometer as KBr disks or on a Bruker Alpha ATR-FT-IR spectrometer. Elemental analyses were measured by Mikroanalytisches Laboratorium Kolbe in Oberhausen, Germany. GC-FID measurements were performed on a HP 6890; see further experimental details for columns and conditions.

General Procedure for the Synthesis of Merrifield-Bound PN Sulfamates 7a-i

A previously synthesized lithiated resin-bound phosphine (**6·Li**, 0.35 mmol, 1.0 equiv.) was swollen in THF (20 mL). A cyclic Boc-protected sulfamidate **5a-i** (0.53 mmol, 1.5 equiv.) was azeotropically dried three times with 5 mL portions of toluene, dissolved in 5 mL THF and added to the resin at 0 °C under gentle stirring to avoid mechanical abrasion. The reaction mixture was left without stirring and was allowed to warm to room temperature overnight. The supernatant was removed and the resin was washed three times with THF (15 mL) followed by three times with Et_2O (15 mL). The product was dried *in vacuo* and used in the next step without additional purification.

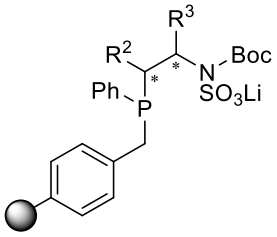

7a: R^2, R^3 = H
7b: R^2 = H, R^3 = Me (*S*)
7c: R^2 = H, R^3 = ^{i}Pr (*S*)
7d: R^2 = H, R^3 = ^{t}Bu (*S*)
7e: R^2 = H, R^3 = Bz (*S*)
7f: R^2, R^3 = Ph (*S*,*S*)
7g: R^2 = Ph (*S*) R^3 = Me (*S*)
7h: R^2, R^3 = -CH_2-C_6H_4- (*S*,*S*)
7i: R^2, R^3 = -CH_2-C_6H_4- (*R*,*R*)

7a: Pale yellow resin: ^{31}P-NMR (162 MHz, THF): δ = -23.8 (s) ppm.

7b: Pale yellow resin: ^{31}P-NMR (162 MHz, THF): δ = -22.6 (s) ppm.

7c: Pale yellow resin: ^{31}P-NMR (162 MHz, THF): δ = -23.0, -25.1 ppm.

7d: Pale yellow resin: ^{31}P-NMR (162 MHz, THF): δ = -21.5, -23.9 ppm.

7e: Pale yellow resin: ^{31}P-NMR (121 MHz, THF): δ = -22.6, -25.2 ppm; ^{7}Li-NMR (117 MHz, THF): δ = -1.1 (br s) ppm.

7f: Pale yellow resin: ^{31}P-NMR (162 MHz, THF): δ = -14.0 (br s) ppm.

7g: Pale yellow resin: ^{31}P-NMR (121 MHz, THF:C_6D_6 6:1): δ = -11.6 (br s) ppm.

7h: Dark green resin: ^{31}P-NMR (162 MHz, THF): δ = -5.5 (s) ppm.

7i: Dark green resin: ^{31}P-NMR (162 MHz, THF): δ = -5.6 (s) ppm; ^{7}Li-NMR (156 MHz, THF): δ = 0.0 (s) ppm.

General Procedure for the Synthesis of Polystyrene-Bound PN Sulfamates 7j-l

Step 1

A previously synthesized lithiated resin-bound phosphine borane (**Li ·8**, 0.33 mmol, 1.0 equiv.) was swollen in THF (20 mL). A cyclic Boc-protected sulfamidate (**5a**, **5c** and **5f**) (0.50 mmol, 1.5 equiv.) was azeotropically dried three times with 5 mL portions of toluene, dissolved in 5 mL THF and added to the resin at room temperature under gentle stirring to avoid mechanical abrasion. The reaction mixture was left overnight without stirring. The supernatant was removed and the resin was washed three times with THF (15 mL) followed by three times with Et_2O (15 mL). The borane protected products **9a-c** were dried *in vacuo* and used in the next step without additional purification.

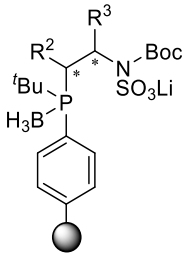

9a: R^2, R^3 = H
9b: R^2 = H, R^3 = ^{i}Pr (*S*)
9c: R^2, R^3 = Ph (*S*,*S*)

9a: Pale yellow resin: ^{31}P-NMR (162 MHz, THF): δ = 27.1 (br s) ppm.

9b: Pale yellow resin: ^{31}P-NMR (162 MHz, THF): δ = 33.1 (br s) ppm.

9c: Pale yellow resin: ^{31}P-NMR (162 MHz, THF): δ = 47.3 (br s) ppm.

Step 2

A resin-bound PN sulfamate borane adduct (**9a-c**, 0.33 mmol, 1.0 equiv.) was suspended in THF (5 mL) and a solution of 1,4-diazabicyclo[2.2.2]octane (0.5 M in THF, 20 eq.) was added. The reaction was heated to 40 °C and was left overnight without stirring to avoid mechanical abrasion. After complete deprotection was confirmed by ^{31}P NMR, the supernatant was removed and the resin was subsequently washed three times with THF (15 mL) followed by three times with Et_2O (15 mL). The product was dried *in vacuo* yielding a pale-yellow deprotected resin−bound PN sulfamate. The product was used directly in the next step without further purification.

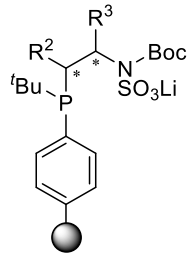

7j: R^2, R^3 = H
7k: R^2 = H, R^3 = ^{i}Pr (*S*)
7l: R^2, R^3 = Ph (*S*,*S*)

7j: Pale yellow resin: ^{31}P-NMR (162 MHz, THF): δ = -4.1 (br s) ppm.

7k: Pale yellow resin: ^{31}P-NMR (162 MHz, THF): δ = -3.8 (br s) ppm.

7l: Pale yellow resin: ^{31}P-NMR (162 MHz, THF): δ = 12.0 (br s) ppm.

General Procedure for the Synthesis of Resin-Bound Aminophosphines 10a-l

To a previously synthesized Boc-protected resin-bound PN sulfamate (**7a-j**, 0.13 mmol, 1.0 equiv.) suspended in DCM (4.5 mL) degassed trifluoroacetic acid (1.5 mL) was added at 0 °C under gentle stirring to avoid mechanical abrasion. After 0.5 h the mixture was warmed to room temperature and left for another 2 h. The supernatant was removed and the resin was washed with DCM (5 mL). A 1:1 mixture of an aqueous solution of 2 M NaOH (2.5 mL) and THF (2.5 mL) was added and the multiphasic mixture was stirred vigorously for 20 minutes. Next, three portions of degassed H_2O (5 mL) were added followed by three portions of THF (5 mL) and three portions of Et_2O (5 mL). The product was dried *in vacuo* yielding a resin-bound aminophosphine (**10a-l**).

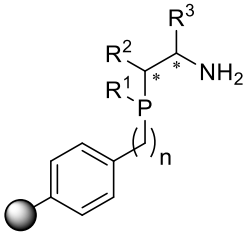

10a: n = 1, R^1 = Ph, R^2, R^3 = H
10b: n = 1, R^1 = Ph, R^2 = H, R^3 = Me (*S*)
10c: n = 1, R^1 = Ph, R^2 = H, R^3 = ^{i}Pr (*S*)
10d: n = 1, R^1 = Ph, R^2 = H, R^3 = ^{t}Bu (*S*)
10e: n = 1, R^1 = Ph, R^2 = H, R^3 = Bz (*S*)
10f: n = 1, R^1 = Ph, R^2, R^3 = Ph (*S*,*S*)
10g: n = 1, R^1 = Ph, R^2 = Ph (*S*) R^3 = Me (*S*)
10h: n = 1, R^1 = Ph, R^2, R^3 = -CH_2-C_6H_4- (*S*,*S*)
10i: n = 1, R^1 = Ph, R^2, R^3 = -CH_2-C_6H_4- (*R*,*R*)
10j: n = 0, R^1 = ^{t}Bu, R^2, R^3 = H
10k: n = 0, R^1 = ^{t}Bu, R^2 = H, R^3 = ^{i}Pr (*S*)
10l: n = 0, R^1 = ^{t}Bu, R^2, R^3 = Ph (*S*,*S*)

10a: Pale yellow resin: ^{31}P-NMR (162 MHz, THF): δ = -24.4 (s) ppm.

10b: Pale yellow resin: ^{31}P-NMR (162 MHz, THF): δ = -25.5 (s) ppm.

10c: Pale yellow resin: ^{31}P-NMR (162 MHz, THF): δ = -23.8 (s) ppm.

10d: Pale yellow resin: ^{31}P-NMR (162 MHz, THF): δ = -21.8 (s) ppm; ^{13}C NMR (101 MHz, C_6D_6): δ = 58.4, 40.6, 35.2 ($C(CH_3)_3$), 25.9 ($C(CH_3)_3$) ppm.

10e: Pale yellow resin: ^{31}P-NMR (162 MHz, THF): δ = -26.3 (s) ppm.

10f: Pale yellow resin: ^{31}P-NMR (162 MHz, THF): δ = -10.7 (br s), -42.0 (5%, MF–PPhH) ppm.

10g: Pale yellow resin: ^{31}P-NMR (121 MHz, THF:C_6D_6 6:1): δ = -11.3 (br s), ppm.

10h: Brown resin: ^{31}P-NMR (162 MHz, THF): δ = -8.1 (br s) ppm.

10i: Purple resin: ^{31}P-NMR (162 MHz, THF): δ = -8.6 (s) ppm; IR (KBr): $\tilde{\nu}$ = 3058 (w), 3024 (w), 2918 (m), 2847 (w), 1601 (w), 1492 (w), 1452 (m), 1153 (m), 1028 (w), 744 (m, P-Ar), 697 (s, P-Ar) cm^{-1}.

10j: Pale yellow resin: ^{31}P-NMR (162 MHz, THF): δ = -4.5 (s) ppm; IR (KBr): $\tilde{\nu}$ = 3059 (w), 3025 (w), 2923 (m), 2858 (m), 1601 (w), 1493 (m), 1452 (m), 1362 (w), 1155 (m), 1036 (m), 758 (m, P-Ar), 698 (s, P-Ar) cm^{-1}.

10k: Pale yellow resin: ^{31}P-NMR (162 MHz, THF): δ = -4.2 (br s) ppm.

10l: Pale yellow resin: ^{31}P-NMR (162 MHz, THF): δ = 10.8 (br s) ppm.

General Procedure for the Synthesis of Resin-Bound PNP Ligands L_1-L_{12}

Step 1

A previously synthesized resin-bound aminophosphine (**10a-j**, 0.13 mmol, 1.0 equiv.) was suspended in trimethyl orthoformate (3.0 mL) and *o*-(diphenylphosphino)-benzaldehyde (0.19 mmol, 54.5 mg, 1.5 equiv.) dissolved in THF (3 mL) was added at room temperature under gentle stirring to avoid mechanical abrasion of the resin. The mixture was heated to 50 °C and left over night without stirring. The reaction was monitored using ^{31}P NMR and full conversion was reached after 24-72 h when a 1:1 ratio of both phosphine moieties was observed. In some cases, additional equivalents of *o*-(diphenylphosphino)benzaldehyde were required. The supernatant was removed and the resin was subsequently washed three times with THF (5 mL) followed by three times with Et_2O (5 mL). The resin was dried *in vacuo* yielding a resin-bound Schiff base (**11a-l**). The product was directly used in the next step without further purification.

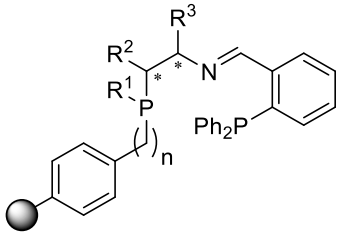

11a: n = 1, R^1 = Ph, R^2, R^3 = H
11b: n = 1, R^1 = Ph, R^2 = H, R^3 = Me (*S*)
11c: n = 1, R^1 = Ph, R^2 = H, R^3 = ^{i}Pr (*S*)
11d: n = 1, R^1 = Ph, R^2 = H, R^3 = ^{t}Bu (*S*)
11e: n = 1, R^1 = Ph, R^2 = H, R^3 = Bz (*S*)
11f: n = 1, R^1 = Ph, R^2, R^3 = Ph (*S*,*S*)
11g: n = 1, R^1 = Ph, R^2 = Ph (*S*) R^3 = Me (*S*)
11h: n = 1, R^1 = Ph, R^2, R^3 = -CH_2-C_6H_4- (*S*,*S*)
11i: n = 1, R^1 = Ph, R^2, R^3 = -CH_2-C_6H_4- (*R*,*R*)
11j: n = 0, R^1 = ^{t}Bu, R^2, R^3 = H
11k: n = 0, R^1 = ^{t}Bu, R^2 = H, R^3 = ^{i}Pr (*S*)
11l: n = 0, R^1 = ^{t}Bu, R^2, R^3 = Ph (*S*,*S*)

11a: Pale yellow resin: ^{31}P-NMR (162 MHz, THF): δ = 34.7-28.0 (30% P=O), -13.5 (s, PPh_2), -24.2 (br s, MF–PPh) ppm.

11b: Pale yellow resin: ^{31}P-NMR (162 MHz, THF): δ = 33.8-28.3 (11% P=O), -12.4 (s, PPh_2), -25.3 (br s, MF–PPh) ppm.

11c: Pale yellow resin: ^{31}P-NMR (162 MHz, THF): δ = 33.5-28.1 (22% P=O), -12.6 (s, PPh_2), -25.1 (br s, MF–PPh) ppm.

11d: Pale yellow resin: ^{31}P-NMR (162 MHz, THF): δ = 34.7-27.8 (19% P=O), -12.3 (s, PPh_2), -23.6 (br s, MF–PPh) ppm.

11e: Pale yellow resin: ^{31}P-NMR (162 MHz, THF): δ = 32.7-28.1 (12% P=O), -13.2 (s, PPh_2), -25.5 (br s, MF–PPh) ppm; ^{13}C-NMR (101 MHz, C_6D_6): δ = 158.1 (C=N), 71.3 (CH–N) ppm.

11f: Pale yellow resin: ^{31}P-NMR (162 MHz, THF): δ = 38.0 (7% P=O), -8.4 (br s, MF–PPh), -14.7 (br s, PPh_2), -20.0 (12%, unknown) ppm.

11g: Pale yellow resin: ^{31}P-NMR (121 MHz, THF:C_6D_6 6:1): δ = 36.6 (9% P=O), -9.1 (br s, MF–PPh), -14.3 (br s, PPh_2), -19.4 (9%, unknown) ppm.

11h: Brown resin: ^{31}P-NMR (162 MHz, THF): δ = 36.0-28.0 (6% P=O), -7.8 (br s, MF–PPh), -13.6 (s, PPh_2) ppm.

11i: Dark red resin: ^{31}P-NMR (162 MHz, THF): δ = 37.0-28.1 (16% P=O), -7.7 (br s, MF–PPh), -13.6 (s, PPh_2) ppm.

11j: Pale yellow resin: ^{31}P-NMR (162 MHz, THF): δ = -2.8 (br s, PS–P^{t}Bu), -13.1 (s, PPh_2) ppm; IR (KBr): $\tilde{\nu}$ = 3057 (w), 3024 (w), 2922 (m), 2857 (m), 1670 (s, C=N), 1600 (w), 1492 (w), 1452 (m), 1362 (w), 1154 (w), 1116 (w), 1040 (w), 826 (w), 758 (m, P-Ar), 697 (s, P-Ar) cm^{-1}.

11k: Pale yellow resin: ^{31}P-NMR (162 MHz, THF): δ = 28.0 (8% P=O), -5.1 (br s, PS–P^{t}Bu), -12.1 (br s, PPh_2) ppm.

11l: Pale yellow resin: ^{31}P-NMR (162 MHz, THF): δ = 57.1-48.4 (17% P=O), 16.9, 8.4 (PS–P^{t}Bu), -14.2, -15.1 (PPh_2) ppm.

Step 2

To a previously synthesized resin-bound Schiff base (**11a-l**, 0.13 mmol, 1.0 equiv.) suspended in toluene 5.0 mL of a DIBAL-H solution in toluene (1.25 mL, 1.0 M, 10.0 equiv.) was added at room temperature under gentle stirring to avoid mechanical abrasion of the resin. The mixture was heated to 70 °C and left for 2 h with occasional stirring. In case no further gas evolution was observed, the mixture was cooled to room temperature and the supernatant was removed. The resin was washed with THF (5.0 mL), a 1:1 mixture of an aqueous solution of 2 M NaOH and THF (5 mL), three portions of degassed H_2O (5 mL), three portions of THF (5 mL) followed by three portions of Et_2O (5 mL). The product was dried *in vacuo* yielding the resin-bound PNP ligands **L_1-L_{12}**.

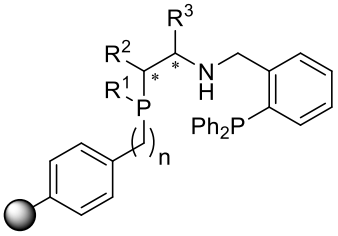

L_1: n = 1, R^1 = Ph, R^2, R^3 = H
L_2: n = 1, R^1 = Ph, R^2 = H, R^3 = Me (*S*)
L_3: n = 1, R^1 = Ph, R^2 = H, R^3 = ^{i}Pr (*S*)
L_4: n = 1, R^1 = Ph, R^2 = H, R^3 = ^{t}Bu (*S*)
L_5: n = 1, R^1 = Ph, R^2 = H, R^3 = Bz (*S*)
L_6: n = 1, R^1 = Ph, R^2, R^3 = Ph (*S*,*S*)
L_7: n = 1, R^1 = Ph, R^2 = Ph (*S*) R^3 = Me (*S*)
L_8: n = 1, R^1 = Ph, R^2, R^3 = -CH_2-C_6H_4- (*S*,*S*)
L_9: n = 1, R^1 = Ph, R^2, R^3 = -CH_2-C_6H_4- (*R*,*R*)
L_{10}: n = 0, R^1 = ^{t}Bu, R^2, R^3 = H
L_{11}: n = 0, R^1 = ^{t}Bu, R^2 = H, R^3 = ^{i}Pr (*S*)
L_{12}: n = 0, R^1 = ^{t}Bu, R^2, R^3 = Ph (*S*,*S*)

L_1: Pale yellow resin: ^{31}P-NMR (162 MHz, THF): δ = -16.1 (s, PPh_2), -20.6 (br s, MF–PPh) ppm; IR (KBr): $\tilde{\nu}$ = 3057 (w), 3024 (w), 2918 (m), 2847 (w), 1601 (w), 1492 (w), 1452 (m), 1434 (m), 1155 (w), 1028 (w), 744 (m, P-Ar), 697 (m, P-Ar) cm^{-1}, Elemental analysis calcd (%) for **L_1** (0.83 mmol·g^{-1}): P 5.14; found: P 3.76.

L_2: White resin: ^{31}P-NMR (162 MHz, THF): δ = -15.7 (s, PPh_2), -25.6 (br s, MF–PPh) ppm; IR (KBr): $\tilde{\nu}$ = 3057 (w), 3024 (w), 2919 (m), 2847 (w), 1601 (w), 1492 (w), 1452 (m), 1434 (m), 1151 (w), 1027 (w), 744 (m, P-Ar), 697 (m, P-Ar) cm^{-1}.

L_3: Pale brown resin: ^{31}P-NMR (162 MHz, THF): δ = -15.7 (s, PPh_2), -25.2 (br s, MF–PPh) ppm; IR (KBr): $\tilde{\nu}$ = 3057 (w), 3024 (w), 2920 (m), 2848 (w), 1601 (w), 1492 (w), 1452 (m), 1434 (m), 1153 (w), 1028 (w), 744 (m, P-Ar), 697 (m, P-Ar) cm^{-1}.

L_4: White resin: ^{31}P-NMR (162 MHz, THF): δ = -15.4 (s, PPh_2), -23.3 (br s, MF–PPh) ppm; IR (KBr): $\tilde{\nu}$ = 3057 (w), 3024 (w), 2919 (m), 2848 (w), 1601 (w), 1492 (w), 1452 (m), 1434 (m), 1152 (w), 1028 (w), 744 (m, P-Ar), 697 (m, P-Ar) cm^{-1}.

L_5: Pale yellow resin: ^{31}P-NMR (162 MHz, THF): δ = -15.7 (s, PPh_2), -26.5 (br s, MF–PPh) ppm; ^{13}C NMR (101 MHz, C_6D_6): δ = 56.8 (CH–N), 49.7 (N–CH_2) ppm; IR (KBr): $\tilde{\nu}$ = 3024 (w), 2918 (w), 2847 (w), 1601 (w), 1492 (w), 1452 (m), 1435 (m), 1029 (w), 745 (m, P-Ar), 697 (m, P-Ar) cm^{-1}.

L_6: Pale yellow resin: ^{31}P-NMR (162 MHz, THF): δ = -10.1 (br s, MF–PPh), -15.9 (s, PPh_2), -19.7 (12%, unknown) ppm; IR (KBr): $\tilde{\nu}$ = 3057 (w), 3024 (w), 2915 (m), 2847 (w), 1600 (w), 1492 (w), 1451 (m), 1434 (m), 1153 (w), 1027 (w), 744 (m, P-Ar), 697 (m, P-Ar) cm^{-1}.

L_7: Pale yellow resin: ^{31}P-NMR (162 MHz, THF:C_6D_6 6:1): δ = -11.4 (br s, MF–PPh), -16.0 (br s, PPh_2), -42.0 (3%, MF–PPhH) ppm.

L_8: Pale orange resin: ^{31}P-NMR (162 MHz, THF): δ = -10.2 (br s, MF–PPh), -17.1 (s, PPh_2) ppm; IR (KBr): $\tilde{\nu}$ = 3056 (w), 3024 (w), 2918 (m), 2847 (w), 1601 (w), 1492 (w), 1452 (m), 1434 (m), 1148 (w), 1120 (w), 1027 (w), 744 (m, P-Ar), 697 (m, P-Ar) cm^{-1}.

L_9: Red resin: ^{31}P-NMR (162 MHz, THF): δ = -8.0 (br s, MF–PPh), -15.3 (s, PPh_2) ppm; IR (KBr): $\tilde{\nu}$ = 3057 (w), 3024 (w), 2916 (m), 2846 (w), 1601 (w), 1492 (w), 1452 (m), 1433 (m), 1027 (w), 743 (m, P-Ar), 697 (m, P-Ar) cm^{-1}.

L_{10}: Pale yellow resin: ^{31}P-NMR (162 MHz, THF): δ = -3.4 (br s, PS–P^{t}Bu), -15.9 (s, PPh_2) ppm; IR (KBr): $\tilde{\nu}$ = 3057 (w), 3024 (w), 2922 (m), 2857 (w), 1600 (w), 1492 (w), 1453 (m), 1435 (m), 1362 w), 1155 (w), 1040 (m), 746 (m, P-Ar), 698 (s, P-Ar) cm^{-1}.

L_{11}: Pale yellow resin: ^{31}P-NMR (162 MHz, THF): δ = -4.9 (br s, PS–P^{t}Bu), -16.2 (br s, PPh_2) ppm; IR (KBr): $\tilde{\nu}$ = 3059 (w), 3025 (w), 2924 (m), 2859 (w), 1601 (w), 1491 (w), 1456 (m), 1362 (w), 1181 (m), 1115 (m), 1030 (m), 757 (m, P-Ar), 698 (s, P-Ar) cm^{-1}.

L_{12}: Pale yellow resin: ^{31}P-NMR (162 MHz, THF): δ = 12.7, 8.4 (PS–P^{t}Bu), -6.8 (5% unknown), -16.5 (PPh_2) ppm; IR (KBr): $\tilde{\nu}$ = 3057 (w), 3025 (w), 2922 (m), 2857

(w), 1600 (w), 1492 (w), 1453 (m), 1362 (w), 1115 (m), 1028 (w), 756 (m, P-Ar), 698 (s, P-Ar) cm^{-1}.

Preparation of 2-(Chloromethyl)-6-((2*R*,5*R*)-2,5-dimethylphospholanemethyl) Pyridine Borane Adduct 12

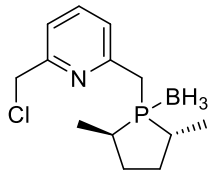

12

To a solution of (2*R*,5*R*)-2,5-dimethylphospholane-borane (412 mg, 3.17 mmol, 1.0 equiv.) in dry THF (20 mL) at -78 °C, *n*-BuLi (1.3 mL, 3.17 mmol, 2.5 M in hexanes, 1.0 equiv.) was added dropwise. The pale yellow solution was stirred for 30 min at -78 °C and subsequently warmed to room temperature and was stirred for another 2 h. 2,6-bis(chloromethyl)pyridine (669 mg, 3.8 mmol, 1.2 equiv.) was dissolved in dry THF (10 mL) and cooled to -78 °C. Next, the freshly prepared lithiated phospholane borane adduct solution (0.16 M) in THF was added slowly. The mixture was allowed to warm to room temperature overnight leading to a pale yellow solution. Upon addition of water (15 mL) the mixture was extracted with EtOAc (3x20 mL). The organic phase was washed with water and brine and subsequently dried over $MgSO_4$. After filtration, the solvent was removed under reduced pressure. The residue was purified *via* flash chromatography (9:1 Hexanes : EtOAc) yielding a colorless oil of **12**. Yield: 450 mg (53%). ^{1}H-NMR (400 MHz, $CDCl_3$): δ = 7.68 (t, 1H, J_{HH} = 7.5 Hz, pyridine-H), 7.34-7.31 (m, 2H, pyridine-H), 4.65-4.59 (m, 2H, CH_2Cl), 3.24-3.10 (m, 2H, CH_2P), 2.62-2.49 (m. 1H, C*H*CH_3), 2.25-2.06 (m, 3H, C*H*CH_3 and CH_2CH_2), 1.51-1.25 (m, 2H, CH_2CH_2), 1.29 (dd, 3H, J_{HH} = 7.0, 13.5 Hz, CH_3), 0.90 (dd, 3H, J_{HH} = 7.0, 16.5 Hz, CH_3), 0.38 (br, 3H, BH_3) ppm, ^{13}C-NMR (101 MHz, $CDCl_3$): δ = 155.9 (s, pyridine-*C*-CH_2Cl), 154.0 (d, J_{PC} = 5.0 Hz, pyridine-*C*-CH_2P), 137.6 (s, pyridine-CH), 124.7 (s, pyridine-CH), 121.0 (s, pyridine-CH), 46.5 (s, CH_2Cl), 34.7 (d, J_{PC} = 3.6 Hz, *C*H_2CH_2), 34.4 (s, CH_2CH_2) 34.3 (d, J_{PC} = 35.2 Hz, P*C*HCH_3), 31.4 (d, J_{PC} = 21.6 Hz, CH_2P), 30.6 (d, J_{PC} = 32.8 Hz, P*C*HCH_3), 15.1 (d, J_{PC} = 4.6 Hz, CH_3), 13.5 (d, J_{PC} = 2.9 Hz, CH_3) ppm. ^{31}P-NMR (162 MHz, $CDCl_3$): δ = 40.0 (m) ppm; ESI-HRMS (m/z, pos): Calculated for $[C_{13}H_{22}BClNP\text{-}H]^+$ 268.1193; found: 268.1198 $[M\text{-}H]^+$; Elemental analysis calcd (%) for $[C_{13}H_{22}BClNP]$: C 57:93, H 8:23, N 5:20; found: C 58.05, H 7:99, N 5:10.

Synthesis of Resin-Bound Pyridine-based PNP-Pincer Ligand L_{13}

Step 1

Resin-bound phosphine-borane **6·BH$_3$** (0.19 g, 0.22 mmol, 1.0 equiv.) was swollen in THF (10 mL). After addition of KHMDS (2.0 mL, 2.17 mmol, 20% in THF, 10 equiv.) under gentle stirring to avoid mechanical abrasion of the resin, the orange resin was allowed to react for 2 hours at room temperature. The supernatant was removed and the resin was washed three times with THF (10 mL) followed by three times with Et_2O (10 mL). Without further purification the BH_3-protected resin-bound potassium phosphide **K·6·BH$_3$** was used in the next step.

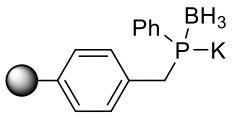

K·6·BH$_3$

K·6·BH$_3$: Orange resin: ^{31}P-NMR (162 MHz, THF): δ = -37.1 (br s) ppm.

Step 2

The previously synthesized BH_3-protected resin-bound potassium phosphide **K·6·BH$_3$** (0.22 mmol, 1.0 equiv.) was suspended in THF (10 mL). PN fragment **12** (73 mg, 0.27 mmol, 1.25 equiv.) was azeotropically dried with three 5 mL portions of toluene and dissolved in THF (5 mL). The solution was added to the resin at -78 °C under gentle stirring to avoid mechanical abrasion. The mixture was left with occasional stirring and allowed to warm to room temperature overnight. The reaction was monitored by gel-phase ^{31}P-NMR and was allowed to react until full conversion was observed. Next, the supernatant was removed and the resin was washed three times with THF (10 mL) followed by three times with Et_2O (10 mL) and dried *in vacuo* yielding a yellow resin-bound PNP borane adduct (**13**).

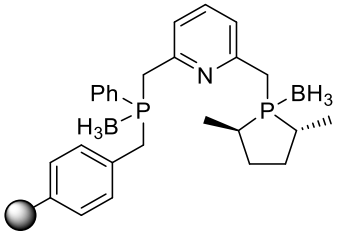

13

13: Yellow resin: ^{31}P-NMR (162 MHz, THF:C_6D_6 6:1): δ = 40.0 (s, P–BH_3-phospholane), 18.6 (br s, MF–*P*Ph–BH_3) ppm.

Step 3

Resin-bound PNP borane adduct **13** synthesized in the last step was swollen in 10 mL of diethyl amine and heated to 50 °C overnight with occasional stirring to avoid mechanical abrasion of the resin. The reaction was monitored using gel-phase ^{31}P-NMR and was allowed to react until full conversion was observed. Next, the mixture was cooled to room temperature and the supernatant was removed. The resin was washed with three portions of THF (10 mL) followed by three portions of Et_2O (10 mL) and dried *in vacuo* yielding a pale yellow resin-bound PNP pincer ligand (**L_{13}**).

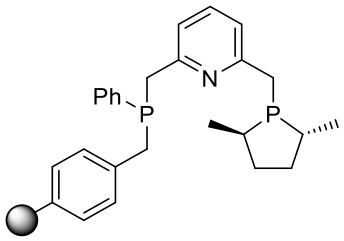

L_{13}

L_{13}: Pale yellow resin (221 mg, 0,20 mmol, 92%): ^{31}P-NMR (162 MHz, THF:C_6D_6 6:1): δ = 6.5 (s, P-phospholane), -14.4 (br s, MF–*P*Ph) ppm.

General Procedure for the Synthesis of Resin-Bound complexes C_1-C_{13}

A previously synthesized resin-bound PNP pincer ligand (**L_1**-**L_{13}**, ~90-160 mg, 1.0 equiv.) and [Ru(HCl(PPh_3)$_3$CO] (1.0-1.1 equiv.) were weighed into a Schlenk tube. The mixture was suspended in THF (10 mL) and heated to 60 °C under gentle stirring. The reaction mixture was left at 60 °C with occasional stirring to avoid mechanical abrasion of the resin and the progress of the reaction was monitored by gel-phase ^{31}P NMR. Once full disappearance of the resin-bound PNP ligand signals was observed, the mixture was cooled to room temperature and the supernatant was removed. The resin-bound complex was washed with three portions of THF (10 mL), three portions of DCM (10 mL) followed by three portions of Et_2O (10 mL). After drying *in vacuo* a brown resin-bound Ru-PNP complex (**C_1**-**C_{13}**) was obtained.

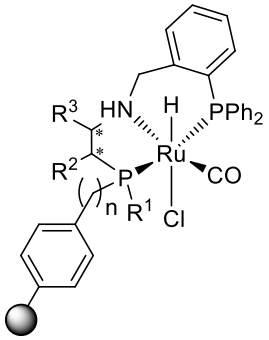

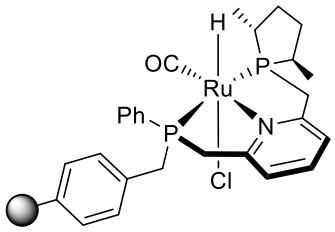

C₁₃

C₁: n = 1, R^1 = Ph, R^2, R^3 = H
C₂: n = 1, R^1 = Ph, R^2 = H, R^3 = Me (*S*)
C₃: n = 1, R^1 = Ph, R^2 = H, R^3 = ^{i}Pr (*S*)
C₄: n = 1, R^1 = Ph, R^2 = H, R^3 = ^{t}Bu (*S*)
C₅: n = 1, R^1 = Ph, R^2 = H, R^3 = Bz (*S*)
C₆: n = 1, R^1 = Ph, R^2, R^3 = Ph (*S*,*S*)
C₇: n = 1, R^1 = Ph, R^2 = Ph (*S*) R^3 = Me (*S*)
C₈: n = 1, R^1 = Ph, R^2, R^3 = -CH_2-C_6H_4- (*S*,*S*)
C₉: n = 1, R^1 = Ph, R^2, R^3 = -CH_2-C_6H_4- (*R*,*R*)
C₁₀: n = 0, R^1 = ^{t}Bu, R^2, R^3 = H
C₁₁: n = 0, R^1 = ^{t}Bu, R^2 = H, R^3 = ^{i}Pr (*S*)
C₁₂: n = 0, R^1 = ^{t}Bu, R^2, R^3 = Ph (*S*,*S*)

C₁: Brown resin (179 mg, 0.111 mmol, 89%): ^{31}P-NMR (162 MHz, THF): no signal was obtained; IR (KBr): $\tilde{\nu}$ = 3057 (w), 3023 (w), 2914 (m), 2848 (m), 1924 (s, CO), 1600 (w), 1492 (w), 1451 (m), 1434 (m), 746 (m, P-Ar), 697 (m, P-Ar) cm^{-1}; Elemental analysis calcd (%) for **C₁** (0.73 mmol·g^{-1}): P 4.52, Ru 7.38; found: P 4.12, Ru 6.79.

C₂: Brown resin (35 mg, 0,025 mmol, 87%): ^{31}P-NMR (121 MHz, THF:C_6D_6 6:1): no signal was obtained; IR (solid): $\tilde{\nu}$ = 3057 (w), 3024 (w), 2920 (m), 2847 (w), 1923 (s, CO), 1600 (w), 1492 (m), 1451 (m), 1434 (m), 1112 (w), 1026 (m), 840 (m), 743 (m, P-Ar), 693 (s, P-Ar) cm^{-1}.

C₃: Brown resin (135 mg, 0,096 mmol, 98%): ^{31}P-NMR (121 MHz, THF:C_6D_6 6:1): no signal was obtained; IR (solid): $\tilde{\nu}$ = 3057 (w), 3024 (w), 2920 (m), 2847 (w), 1923 (m, CO), 1600 (w), 1492 (m), 1451 (m), 1434 (m), 1113 (w), 1027 (w), 840 (m), 743 (m, P-Ar), 694 (s, P-Ar) cm^{-1}.

C₄: Brown resin (112 mg): ^{31}P-NMR (162 MHz, THF): δ = 46.2, 31.6 (br, 2P); IR (KBr): $\tilde{\nu}$ = 3057 (w), 3024 (w), 2916 (m), 2847 (m), 1923 (s, CO), 1601 (w), 1491 (m), 1452 (m), 1435 (m), 1028 w), 745 (m, P-Ar), 697 (s, P-Ar) cm^{-1}.

C₅: Pale brown resin (118 mg, 0,077 mmol, 91%): ^{31}P-NMR (162 MHz, THF): δ = 45.3, 36.0 (br, 2P) ppm; IR (KBr): $\tilde{\nu}$ = 3056 (w), 3024 (w), 2912 (m), 2845

(w), 1923 (s, CO), 1601 (w), 1491 (w), 1453 (m), 1435 (m), 745 (m, P-Ar), 698 (m, P-Ar) cm^{-1}.

C_6: Brown resin (56 mg, 0,37 mmol, 92 %): ^{31}P-NMR (121 MHz, THF:C_6D_6 6:1): no signal was obtained; IR (solid): $\tilde{\nu}$ = 3057 (w), 3024 (w), 2920 (m), 2847 (w), 1935 (m, CO), 1600 (w), 1492 (m), 1451 (m), 1434 (m), 1115 (w), 1027 (w), 839 (m), 744 (m, P-Ar), 694 (s, P-Ar) cm^{-1}.

C_7: Brown resin (195 mg, 0.134 mmol, 80%): ^{31}P-NMR (162 MHz, THF): 121 MHz, THF:C_6D_6 6:1): no signal was obtained; IR (solid): $\tilde{\nu}$ = 3056 (w), 3024 (w), 2917 (m), 2849 (w), 1937 (m, CO), 1600 (w), 1492 (m), 1451 (m), 1435 (m), 1093 (w), 1027 (w), 839 (m), 744 (m, P-Ar), 694 (s, P-Ar) cm^{-1}.

C_8: Dark brown resin (34 mg, 0,023 mmol, 90 %): ^{31}P-NMR (121 MHz, THF:C_6D_6 6:1): no signal was obtained; IR (solid): $\tilde{\nu}$ = 3057 (w), 3024 (w), 2919 (m), 2847 (w), 1926 (s, CO), 1600 (w), 1492 (m), 1451 (m), 1434 (m), 1093 (w), 1026 (w), 840 (w), 744 (m, P-Ar), 693 (s, P-Ar) cm^{-1}.

C_9: Dark brown resin (51 mg, 0,035 mmol, 87 %): ^{31}P-NMR (162 MHz, THF): δ = 45.1 (br, 2P) ppm; IR (KBr): $\tilde{\nu}$ = 3056 (w), 3023 (w), 2912 (m), 2847 (w), 1928 (s, CO), 1601 (w), 1492 (w), 1451 (m), 1434 (m), 1027 (w), 744 (m, P-Ar), 697 (m, P-Ar) cm^{-1}.

C_{10}: Dark brown resin (121 mg): ^{31}P-NMR (162 MHz, THF): no signal was obtained; IR (KBr): $\tilde{\nu}$ = 3056 (w), 3024 (w), 2921 (m), 2860 (m), 1922 (s, CO), 1600 (w), 1491 (w), 1454 (m), 1435 (m), 1184 (w), 1094 (m), 1028 (w), 751 (m, P-Ar), 698 (m, P-Ar) cm^{-1}.

C_{11}: Dark brown resin (138 mg): ^{31}P-NMR (162 MHz, THF): no signal was obtained; IR (KBr): $\tilde{\nu}$ = 3057 (w), 3024 (w), 2923 (m), 2866 (m), 1922 (s, CO), 1601 (w), 1492 (w), 1456 (m), 1435 (m), 1182 (m), 1095 (w), 1029 (m), 756 (m, P-Ar), 698 (m, P-Ar) cm^{-1}.

C_{12}: Dark brown resin (98 mg): ^{31}P-NMR (162 MHz, THF): no signal was obtained; IR (KBr): $\tilde{\nu}$ = 3056 (w), 3024 (w), 2920 (m), 2856 (m), 1923 (s, CO), 1600 (w), 1491 (m), 1452 (m), 1435 (m), 1115 (m), 1028 (w), 756 (m, P-Ar), 698 (s, P-Ar) cm^{-1}.

C_{13}: Brown-orange resin (179 mg, 0.139 mmol, 95%): ^{31}P-NMR (162 MHz, THF:C_6D_6 6:1): δ = 77.9 (br s, *–P*-phospholane), 51.9 (br s, MF*–P*Ph); IR (KBr): $\tilde{\nu}$ = 3055 (w), 3024 (w), 2920 (m), 2853 (w), 1919 (s, CO), 1599 (w), 1489 (m), 1450 (m), 1376 (w), 1096 (w), 1023 (w), 838 (m), 746 (m, P-Ar), 694 (s, P-Ar) cm^{-1}.

General Procedure for Ru-catalyzed (A)symmetric Ketone Hydrogenation

The hydrogenation experiments were performed in a stainless steel autoclave charged with an insert suitable for up to 12 reaction vessels (2 mL) including Teflon mini stirring bars. Inside a glove box, a reaction vessel was charged with a resin-bound Ru-PNP complex **C_1-C_{13}** (~3-7 mg, 2.5-5.0 µmol). To the reaction vessel 0.5 mL of a stock solution of KO^{t}Bu (1-5 mol%) in THF was added and the mixture was stirred for 5 minutes. Next, substrates **S_1-S_{13}** (0.25-0.50 mmol) dissolved in 0,5 mL of THF were added. Subsequently, the autoclave was purged three times with 10 bar of argon gas and the insert loaded with reaction vessels was transferred into the autoclave. Next, the autoclave was purged three times with 10 bar of H_2 and then pressurized (30 bar). The reaction mixtures were gently stirred at 450 rpm at 25 °C for 4-16 hours. The autoclave was depressurized and the reaction mixtures were filtered over a plug of silica. The conversion was determined by GC-FID using an Agilent HP-5 column. The *ee* was determined by chiral GC-FID or HPLC using the following column and conditions:

Macherey-Nagel LIPODEX A column (25 m, 0.25 mm, 0.1 µm): T_0 = 85 °C, hold for 35 min, ΔT = 8 °C min^{-1} to 180 °C, then hold for 20 min.
S_1: t_r (*S*) = 14.78 min, t_r (*R*) = 15.42 min.

Macherey-Nagel HYDRODEX β-TBDAc column (50 m, 0.25 mm, 0.1 µm): T_0 = 120 °C, hold for 40 min, ΔT = 6 °C min^{-1} to 180 °C, then hold for 10 min.
S_2: t_r (enantiomer 1) = 23.08 min, t_r (enantiomer 2) = 23.96 min.
S_6: t_r (*R*) = 24.46 min, t_r (*S*) = 25.71 min.
S_7: t_r (enantiomer 1) = 48.14 min, t_r (enantiomer 2) = 48.66 min.
S_8: t_r (enantiomer 1) = 49.69 min, t_r (enantiomer 2) = 49.96 min.
S_9: t_r (enantiomer 1) = 14.32 min, t_r (enantiomer 2) = 15.51 min.
S_{10}: t_r (*S*) = 48.12 min, t_r (*R*) = 48.78 min.
S_{11}: t_r (enantiomer 1) = 22.53 min, t_r (enantiomer 2) = 23.39 min.

Macherey-Nagel LIPODEX E column (25 m, 0.25 mm, 0.1 µm): T_0 = 35 °C, hold for 35 min, ΔT = 10 °C min^{-1} to 180 °C, then hold for 10 min.
S_{12}: t_r (*S*) = 22.43 min, t_r (*R*) = 23.80 min.
HPLC Amylose column, heptane:EtOH = 99:1: flow = 1.0 mL·min^{-1}.
S_3: t_r (enantiomer 1) = 10.64 min, t_r (enantiomer 2) = 11.52 min.

HPLC Cellulose column, heptane:EtOH = 90:10: flow = 1.0 mL·min^{-1}.

S$_4$: t_r (enantiomer 1) = 6.10 min, t_r (enantiomer 2) = 7.16 min.

S$_5$: t_r (enantiomer 1) = 11.56 min, t_r (enantiomer 2) = 12.42 min.

Derivatization of 1-(1-adamantyl)ethanol

The enantiomeric ratio was determined by HPLC after labeling of the alcohol with 3,5-dinitrobenzoyl chloride.

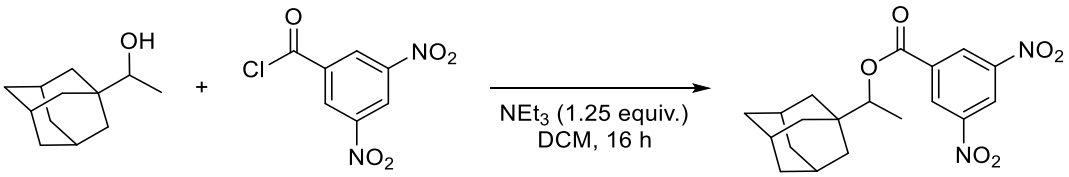

1.25 equivalents of NEt_3 were added to 3,5-dinitrobenzoyl chloride (1.0 equiv.) dissolved in 10 mL of DCM. Upon substrate addition the solution was stirred for 16 h. The suspension was dissolved in additional 10 mL of DCM. The solution was washed with H_2O, HCl (10%) and a saturated aqueous solution of $NaHCO_3$. The collected organic layer was dried with $MgSO_4$ and after filtration the solvent was evaporated.

HPLC ReproSil column, heptane:EtOH = 98:2: flow = 0.5 mL·min^{-1}.

S$_{13}$: t_r (*R*) = 14.70 min, t_r (*S*) = 21.11 min.

4.6 References

[1] C. Hedberg, *Carbonyl Hydrogenation*, in *Modern Reduction Methods* (Eds.: P. G. Andersson, I. J. Munslow), Wiley-VCH, **2008**, pp. 363-385.

[2] a) H. C. Brown, H. I. Schlesinger, I. Sheft, D. M. Ritter, *J. Am. Chem. Soc.* **1953**, *75*, 192-195; b) H. C. Brown, S. Krishnamurthy, *Tetrahedron* **1979**, *35*, 567-607.

[3] R. Noyori, I. Tomino, Y. Tanimoto, M. Nishizawa, *J. Am. Chem. Soc.* **1984**, *106*, 6709-6716.

[4] R. K. Dhar, *Aldrichimica Acta* **1994**, *27*, 43-51.

[5] E. J. Corey, R. K. Bakshi, S. Shibata, *J. Am. Chem. Soc.* **1987**, *109*, 5551-5553.

[6] R. Berenguer, J. Garcia, J. Vilarrasa, *Tetrahedron: Asymmetry* **1994**, *5*, 165-168.

[7] a) T. Ohkuma, H. Ooka, S. Hashiguchi, T. Ikariya, R. Noyori, *J. Am. Chem. Soc.* **1995**, *117*, 2675-2676; b) R. Noyori, *Angew. Chem. Int. Ed.* **2002**, *41*, 2008-2022.

[8] a) R. Noyori, T. Ohkuma, *Angew. Chem. Int. Ed.* **2001**, *40*, 40-73; b) T. Ikariya, A. J. Blacker, *Acc. Chem. Res.* **2007**, *40*, 1300-1308.

[9] a) M. Yoshimura, S. Tanaka, M. Kitamura, *Tetrahedron Lett.* **2014**, *55*, 3635-3640; b) J.-H. Xie, D.-H. Bao, Q.-L. Zhou, *Synthesis* **2015**, *47*, 460-471.

[10] a) M. L. Clarke, M. B. Díaz-Valenzuela, A. M. Z. Slawin, *Organometallics* **2007**, *26*, 16-19; b) M. B. Díaz-Valenzuela, S. D. Phillips, M. B. France, M. E. Gunn, M. L. Clarke, *Chem. Eur. J.* **2009**, *15*, 1227-1232.

[11] a) L. Alig, M. Fritz, S. Schneider, *Chem. Rev.* **2018**; b) G. A. Filonenko, R. van Putten, E. J. M. Hensen, E. A. Pidko, *Chem. Soc. Rev.* **2018**, *47*, 1459-1483.

[12] M. B. Widegren, G. J. Harkness, A. M. Z. Slawin, D. B. Cordes, M. L. Clarke, *Angew. Chem. Int. Ed.* **2017**, *56*, 5825-5828.

[13] a) P. A. Dub, T. Ikariya, *ACS Catal.* **2012**, *2*, 1718-1741; b) S. Werkmeister, K. Junge, M. Beller, *Org. Process Res. Dev.* **2014**, *18*, 289-302; c) C. Gunanathan, D. Milstein, *Chem. Rev.* **2014**, *114*, 12024-12087; d) H. Valdés, M. A. García-Eleno, D. Canseco-Gonzalez, D. Morales-Morales, *ChemCatChem* **2018**.

[14] M. Garbe, K. Junge, S. Walker, Z. Wei, H. Jiao, A. Spannenberg, S. Bachmann, M. Scalone, M. Beller, *Angew. Chem. Int. Ed.* **2017**, *56*, 11237-11241.

[15] I. Arenas, O. Boutureira, M. I. Matheu, Y. Díaz, S. Castillón, *Eur. J. Org. Chem.* **2015**, *2015*, 3666-3669.

[16] R. Huber, A. Passera, A. Mezzetti, *Organometallics* **2018**, *37*, 396-405.

[17] S. A. M. Smith, P. O. Lagaditis, A. Lupke, A. J. Lough, R. H. Morris, *Chem. Eur. J.* **2017**, *23*, 7212-7216.

[18] J. F. Sonnenberg, A. J. Lough, R. H. Morris, *Organometallics* **2014**, *33*, 6452-6465.

[19] a) A. Zirakzadeh, K. Kirchner, A. Roller, B. Stöger, M. Widhalm, R. H. Morris, *Organometallics* **2016**, *35*, 3781-3787; b) A. Zirakzadeh, S. R. M. M. de Aguiar, B. Stöger, M. Widhalm, K. Kirchner, *ChemCatChem* **2017**, *9*, 1744-1748.

[20] E. Peris, R. H. Crabtree, *Chem. Soc. Rev.* **2018**, *47*, 1959-1968.

[21] P. E. Sues, A. J. Lough, R. H. Morris, *Organometallics* **2011**, *30*, 4418-4431.

[22] M. E. Bluhm, O. Walter, M. Döring, *J. Organomet. Chem.* **2005**, *690*, 713-721.

[23] a) K. Burgess, *Solid-Phase Organic Synthesis*, John Wiley & Sons, Inc., New York, **2002**; b) D. Obrecht, J. M. Villalgordo, *Introduction, Basic Concepts and Strategies*, in *Solid-Supported Combinatorial and Parallel Synthesis of Small-*

Molecular-Weight Compound Libraries, Elsevier Science ltd., Oxford, **1998**, pp. 1-184.

[24] a) F. J. L. Heutz, M. C. Samuels, P. C. J. Kamer, *Cat. Sci. Technol.* **2015**, *5*, 3296-3301; b) F. J. Heutz, P. C. Kamer, *Dalton Trans.* **2016**, *45*, 2116-2123; c) M. C. Samuels, F. J. L. Heutz, A. Grabulosa, P. C. J. Kamer, *Top. Catal.* **2016**, *59*, 1793-1799.

[25] R. Guo, S. Lu, X. Chen, C.-W. Tsang, W. Jia, C. Sui-Seng, D. Amoroso, K. Abdur-Rashid, *J. Org. Chem.* **2010**, *75*, 937-940.

[26] M. D. Mertens, M. Gütschow, *Synthesis* **2014**, *46*, 2191-2200.

[27] S. Rapireddy, L. Nhon, R. E. Meehan, J. Franks, D. B. Stolz, D. Tran, M. E. Selsted, D. H. Ly, *J. Am. Chem. Soc.* **2012**, *134*, 4041-4044.

[28] a) A. Saitoh, T. Uda, T. Morimoto, *Tetrahedron: Asymmetry* **1999**, *10*, 4501-4511; b) M. Quirmbach, J. Holz, V. I. Tararov, A. Börner, *Tetrahedron* **2000**, *56*, 775-780; c) J. C. Anderson, R. J. Cubbon, J. D. Harling, *Tetrahedron: Asymmetry* **2001**, *12*, 923-935.

[29] P. Kaur, A. R. Chamberlin, T. L. Poulos, I. F. Sevrioukova, *J. Med. Chem.* **2016**, *59*, 4210-4220.

[30] T. A. Moss, D. M. Barber, A. F. Kyle, D. J. Dixon, *Chem. Eur. J.* **2013**, *19*, 3071-3081.

[31] P. Rönnholm, M. Södergren, G. Hilmersson, *Org. Lett.* **2007**, *9*, 3781-3783.

[32] M. Ito, A. Osaku, C. Kobayashi, A. Shiibashi, T. Ikariya, *Organometallics* **2009**, *28*, 390-393.

[33] F. J. L. Heutz, C. Erken, M. J. B. Aguila, L. Lefort, P. C. J. Kamer, *ChemCatChem* **2016**, *8*, 1896-1900.

[34] G. Kesslin, R. Bradshaw, *Ind. Eng. Chem. Prod. Res. Dev.* **1966**, *5*, 27-29.

[35] L. Zhang, Y. Tang, Z. Han, K. Ding, *Angew. Chem. Int. Ed.* **2019**, *58*, 4973-4977.

[36] a) M. Gargir, Y. Ben-David, G. Leitus, Y. Diskin-Posner, L. J. W. Shimon, D. Milstein, *Organometallics* **2012**, *31*, 6207-6214; b) R. Sablong, C. Newton, P. Dierkes, J. A. Osborn, *Tetrahedron Lett.* **1996**, *37*, 4933-4936.

[37] F. J. L. Heutz, P. C. J. Kamer, *PhD Thesis* **2016**.

[38] a) K. Abdur-Rashid, A. J. Lough, R. H. Morris, *Organometallics* **2000**, *19*, 2655-2657; b) K. Abdur-Rashid, S. E. Clapham, A. Hadzovic, J. N. Harvey, A. J. Lough, R. H. Morris, *J. Am. Chem. Soc.* **2002**, *124*, 15104-15118; c) S. E. Clapham, A. Hadzovic, R. H. Morris, *Coord. Chem. Rev.* **2004**, *248*, 2201-2237; d) R. Abbel, K. Abdur-Rashid, M. Faatz, A. Hadzovic, A. J. Lough, R. H. Morris, *J Am Chem Soc* **2005**, *127*, 1870-1882; e) A. Hadzovic, D. Song, C. M. MacLaughlin, R. H. Morris, *Organometallics* **2007**, *26*, 5987-5999; f) J. F. Sonnenberg, K. Y. Wan, P. E. Sues, R. H. Morris, *ACS Catal.* **2016**, *7*, 316-326.

[39] M. Garbe, Z. Wei, B. Tannert, A. Spannenberg, H. Jiao, S. Bachmann, M. Scalone, K. Junge, M. Beller, *Adv. Synth. Catal.* **2019**, *361*, 1913-1920.

[40] M. Ahlmann, O. Walter, *J. Organomet. Chem.* **2004**, *689*, 3117-3131.

[41] S. Chakraborty, G. Leitus, D. Milstein, *Angew. Chem. Int. Ed.* **2017**, *56*, 2074-2078.

Chapter 5

Heterogenized Ruthenium Triphos Catalysts for Applications in Nitrile Hydrogenation

Abstract: *The selective catalytic hydrogenation of nitriles remains an important but challenging transformation for many homogeneous and heterogeneous catalysts. Herein, we report the efficient and modular solid-phase synthesis of immobilized Triphos-type ligands in very high yields, involving only minimal work-up procedures. The corresponding supported ruthenium-Triphos catalysts are tested in the hydrogenation of various nitriles. Under mild conditions and without the requirement of additives, the tunable supported catalyst library provides selective access to both primary amines and secondary imines. Moreover, the first application of a Triphos-type catalyst in a continuous flow process is presented demonstrating high catalyst life-time over at least 195 hours without significant activity loss.*

5.1 Introduction

Amines represent an essential class of compounds prevalent in both naturally occurring nitrogen compounds and synthetic products. Especially in bulk and fine chemical industries as well as for pharmaceuticals, amines are produced on vast scale and used in detergents, agrochemicals, polymers and drugs.[1] On the one hand, terminal amines are of great importance due to the possibility of versatile modifications.[2] On the other hand however, the selective synthesis of primary amines proves to be challenging due to their relatively high reactivity. Common routes towards primary amines include catalytic aminations of alcohols with ammonia,[3] reductive aminations of aldehydes[4] and hydrogenations of amides[5] as well as nitro compounds.[6] Processes involving atom-economical hydrogenations of abundant nitriles using inexpensive molecular hydrogen can offer an alternative approach to terminal amines. On laboratory scale, nitriles are conventionally reduced by employing stoichiometric amounts of metal hydrides (e.g. $NaBH_4$, $LiAlH_4$). Although these reducing reagents are applicable for a wide range of substrates, stoichiometric amounts of waste metal salts are produced during the reaction and precautions are required when handling highly reactive reagents. Heterogeneous catalysts applied in this transformation are often based on Raney®-Ni and -Co catalysts[7] as well as noble metals such as palladium.[8] As an example of these processes, hexamethylenediamine as key constituent of nylon 6,6 is produced on large industrial scale via selective hydrogenation of adiponitrile.[9] Furthermore, fatty acid based nitriles are converted into their amine derivatives, which are used as components for surfactants.[10]

Heterogeneous systems often suffer from reduced selectivity combined with limited functional group tolerance. Typically harsh reaction conditions are required (up to 180 °C and 250 bar) and selectivity enhancing additives, such as ammonia or hydrochloric acid, are used to suppress side products.[7a,9a] The catalytic hydrogenation of nitriles (**A**) to primary amines (**B**) proceeds via a reactive aldimine intermediate, which can undergo transamination through condensation with the nucleophilic amine product **B** (Scheme 1). Under elimination of NH_3, the secondary imine **C** is formed enabling further reduction to secondary amines (**D**) and tertiary amines (**E**). In order to overcome the limitations associated with heterogeneous catalysts, there has been a growing interest in homogeneous catalysts from both academia and industry to develop efficient protocols for nitrile hydrogenations under very mild conditions.

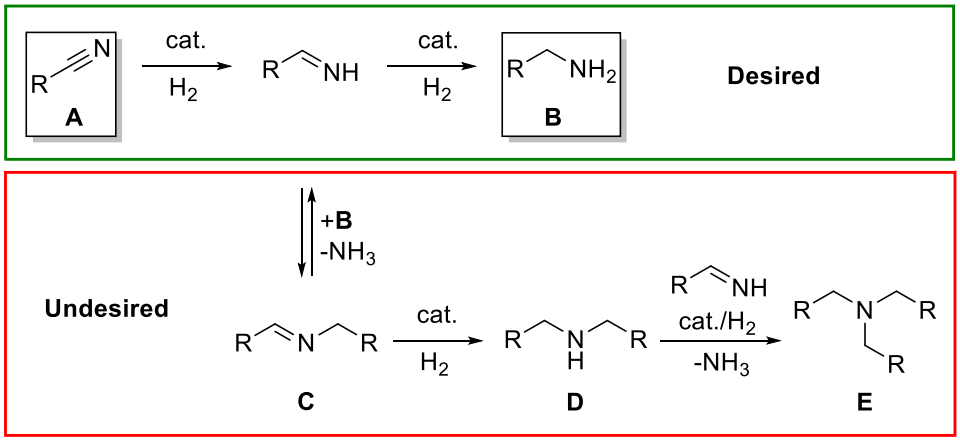

Scheme 1 Catalytic hydrogenation of nitriles (**A**) to primary amines (**B**) and potential formation of secondary imines (**C**), amines (**D**) and tertiary amines (**E**).

A broad variety of transition-metal complexes has been studied in this transformation and most of them are based on precious metals, such as Ru and Rh.[7a,11] More recently also base metals have been employed.[12] Although many examples display exceptional catalyst performances in the reduction of nitrile compounds, the addition of bases is almost exclusively required. Surprisingly, tripodal phosphorus-based ligands, such as the well-known Triphos ligand (Figure 1, **I**), are less studied in the reduction of nitriles to primary amines, despite having been successfully applied in challenging hydrogenations of amides to primary amines in combination with a ruthenium center.[13]

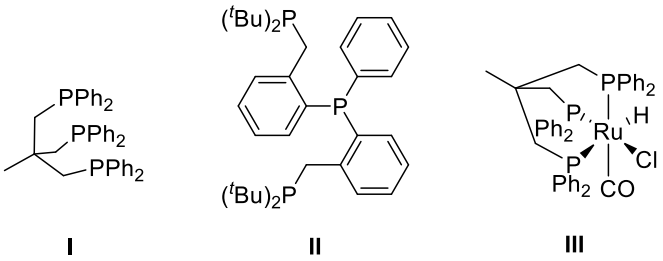

Figure 1 Tripodal phosphorus ligands **I** and **II** and [RuHCl(Triphos)CO] complex **III**.

The first examples of a Triphos-based catalyst applied in the hydrogenation of pure benzonitrile was reported by Suarez and Fontal employing [$RuCl_2$(Triphos)], which led to an unselective mixture of amines **B** (34%), **D** (27%) and **E** (39%).[14] In 2016, Beller and co-workers reported on ligand **I** and its better performing and more bulky tripodal analogue **II**, when employed in combination with a Ru-source, were able to achieve high selectivities for a range of aliphatic and aromatic monoamines under mild

and additive-free conditions, starting from their corresponding nitriles.[15] However, no reactivity in this reaction was observed for the *in situ* generated $Co(acac)_3$/Triphos system.[16] When the homogeneous ruthenium-Triphos complex **III** was employed in the deaminative hydrogenation of *n*-octanenitrile to the corresponding primary alcohol **G** in the presence of water, 73% product selectivity was obtained accompanied by the formation of **D** (3%), **E** (23%) and 1% of the primary amide **H** (Scheme 2).[17]

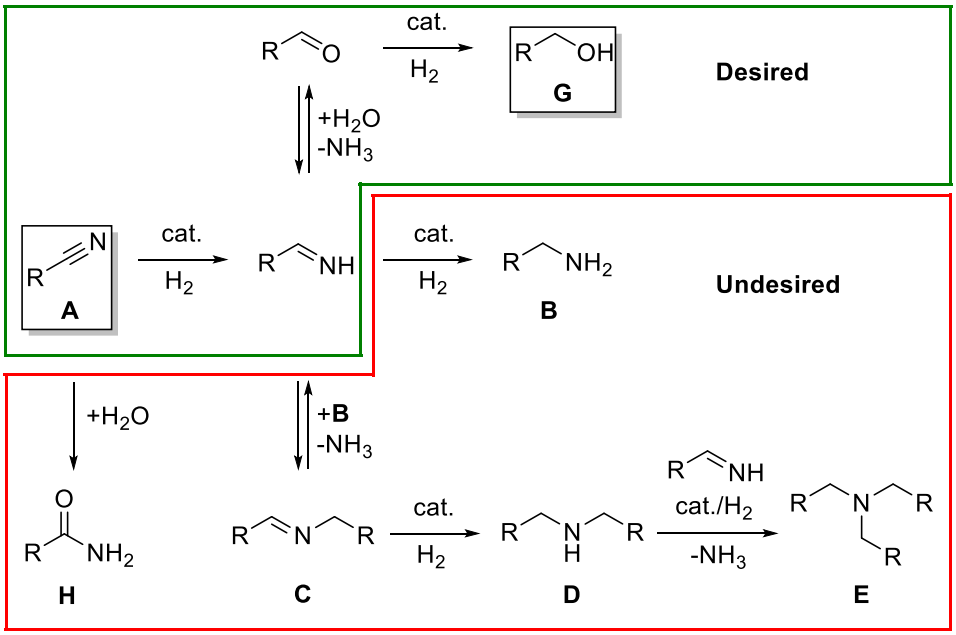

Scheme 2 Catalytic deaminative hydrogenation of nitriles (**A**) to primary alcohols (**G**) and potential formation of primary amines (**B**), secondary imines (**C**), amines (**D**), tertiary amines (**E**) and primary amides (**H**).

Despite the advantages of versatile homogeneous catalysts based on tripodal ligand structures, applications are often limited by intrinsic separation and recycling issues associated with catalysts situated in monophasic systems. To overcome these drawbacks, a tremendous research effort has been devoted to heterogenization of homogeneous catalysts in the past 40 years (see chapter 1.2).[18] The ideal hybrid catalyst combines the advantages of both fields, i.e. high activity, selectivity and tunability of molecular catalysts and ease of separation and recycling of heterogeneous catalysts.[19] However, metal leaching from the support into the product phase as well as catalyst degradation remain prevailing problems associated with immobilized catalysts.[20] Although tripodal ligands offer great potential to provide highly stable transition-metal complexes on a support, only a few research accounts have focused on approaches towards heterogenization of Triphos-based complexes. Inorganic

supports were employed by Bianchini *et al.* reporting on silica-grafted rhodium- and ruthenium-Triphos complexes (**IV**, see Figure 2) via supported hydrogen bonding between silanol groups on the surface and the sulphonate moiety of a modified Triphos ligand.[21] In particular SiO_2-bound Ru-Triphos complex **IV** was applied in the hydrogenation of benzonitrile leading selectively to the secondary imine (**C**).[21b]

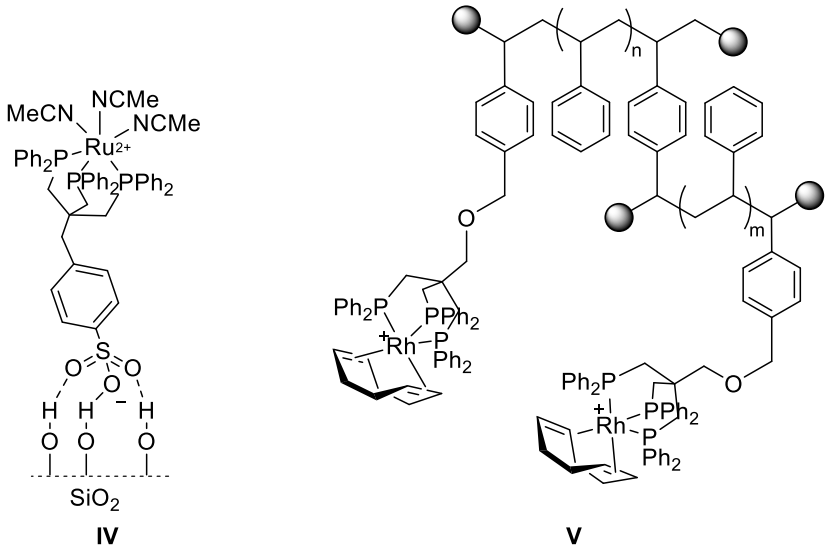

Figure 2 Representative examples of immobilized metal Triphos complexes on silica (**IV**)[21b] and polystyrene (**V**).[22]

Organic supports have been used to immobilize Rh-Triphos complexes following a bottom-up approach (**V**, see Figure 2).[22] The Triphos structure modified with a *para*-styrenyl moiety was incorporated into the polystyrene scaffold via copolymerization. Further immobilization strategies have employed tripodal ligand-based catalysts supported on dendrimers,[23] in ionic liquids[24] and aqueous biphasic systems.[25] However, all methodologies mentioned above require inefficient and often troublesome modifications of the pre-made tripodal ligand structure. This often results in low yields and functional group incompatibilities which in turn hamper the creation of ligand diversity on the support. Moreover, tuning ligand properties by modifying the phosphorus donor moieties remains challenging. Opposed to the uncomplicated synthesis of C_{3V} symmetrical arylphosphine tripods,[26] unsymmetrical, mixed phosphorus donor ligands rely on less straightforward synthetic protocols.[3d,27] Different leaving groups bound to the tripodal backbone to facilitate selective phosphine substitution as well as additional phosphorus borane protection and removal steps are often necessary. This in turn calls for a more efficient modular approach.

Solid-phase synthesis (SPS) could provide a more efficient alternative for the combinatorial synthesis of tripodal ligands and their corresponding complexes on a support in high yields requiring only minimal workup procedures (see chapter 1.3).[28]

Since the obtained heterogenized complexes are covalently bound to the polymeric support, recovery and recycling in catalytic processes could be greatly facilitated. Particularly with regard to continuous flow hydrogenations, these systems could represent suitable candidates for application in fixed bed reactors avoiding potential mechanical degradation of the support in stirred batch processes. Moreover, catalytic reactions performed in continuous flow enable the determination of the long-term catalyst performance. They also offer environmentally benign and safe processing, facile process optimization for scale-up and high process reliability for multiphasic hydrogenation reactions.[29] Despite the many advantages though, Triphos-based catalysts have not been employed in continuous flow hydrogenations to date.

In this chapter, the solid-phase synthesis of five Ru-Triphos complexes immobilized on three different polymeric supports is presented as well as their characterization using various analytical techniques. The application of this small catalyst library in the selective hydrogenolysis and hydrogenation of nitriles under mild and additive-free conditions is demonstrated. Finally, the facile recovery and recycling of the heterogeneous catalyst is showcased highlighting in particular the long-term performance and robustness of the catalyst under continuous flow conditions.

5.2. Solid-Phase Synthesis of Supported Triphos Derivatives

The modular solid-phase synthesis of the Triphos-type ligands **L_1-L_5** immobilized on three different insoluble polymeric supports was established previously by Dr. Frank J. L. Heutz. As the small but diverse supported ligand library forms the basis of the research presented in this chapter, the solid-phase synthetic access is described briefly. A detailed discussion can be found in the corresponding PhD thesis.[30]

The solid-phase synthesis of supported tripodal phosphorus ligands was adapted from literature procedures in solution-phase.[26,27b,31] As described for the preparation of supported P-OP and PNP-type ligands in the previous chapters, secondary phosphines **1a-d** immobilized on Merrifield resin cross-linked with 1% divinylbenzene (DVB, MF), JandaJel™ resin (JJ), Merrifield resin cross-linked with 4% DVB (MF 4% DVB) and polystyrene (PS) were deprotonated using an excess of lithium diisopropylamide (LDA, Scheme 3, step 1). The corresponding lithium phosphides **Li·1a-d** were reacted with a small excess of 1,1,1-tris(chloromethyl)ethane, readily proceeding to the supported phosphine dichloride intermediates **2a-d** (Scheme 3, step 2). The successful introduction of the ligand backbone was confirmed by gel-phase ^{31}P NMR showing the appearance of a single peak at around δ = -30 ppm in cases of **2a-c** and -11.4 ppm for **2d**, respectively. Quantitative conversion and high purity of representative compound **2a** was confirmed by determination of phosphorus and chlorine loading by elemental analysis.

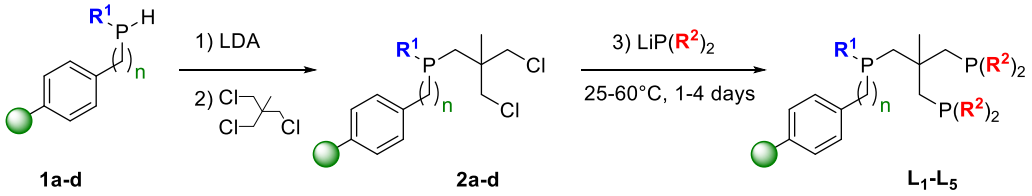

1a: **MF** 1% DVB, n = 1, R^1 = Ph
1b: **JJ**, n = 1, R^1 = Ph
1c: **MF** 4% DVB, n = 1, R^1 = Ph
1d: **PS**, n = 0, R^1 = ^{t}Bu

L_1: **MF** 1%, R^1 = Ph, R^2 = Ph
L_2: **JJ**, R^1 = Ph, R^2 = Ph
L_3: **MF** 4% , R^1 = Ph, R^2 = Ph
L_4: **PS**, R^1 = ^{t}Bu, R^2 = Ph
L_5: **MF**, R^1 = Ph, R^2 = *o*-Tol

Scheme 3 Solid-phase synthetic approach towards supported Triphos ligands **L_1-L_5**.[30]

The resin-bound phosphine intermediates **2a-d** were subsequently treated with a large excess of a secondary lithium phosphide (20-30 equiv.) in order to obtain the desired supported Triphos ligand derivatives **L_1-L_5**. Both, lithium diphenylphosphide (for **L_1-L_4**) and lithium di(*o*-tolyl)phosphide (for **L_5**) at 60 °C, delivered full conversions to the

corresponding resin-bound ligands within 1-4 days (Scheme 3, step 3). In case of the representative Triphos analogue **L_1** supported on Merrifield resin, two single resonances at δ = -25.4 and -28.1 ppm were observed in the ^{31}P NMR spectrum occurring in an expected 2:1 ratio. Variation of the type of polymeric support as well as the introduction of different substituents **R^1** and **R^2** bound to the phosphine moieties led to a small but diverse library of five supported Triphos-type ligands (**L_1-L_5**, Figure 3), which was used in the following sections.

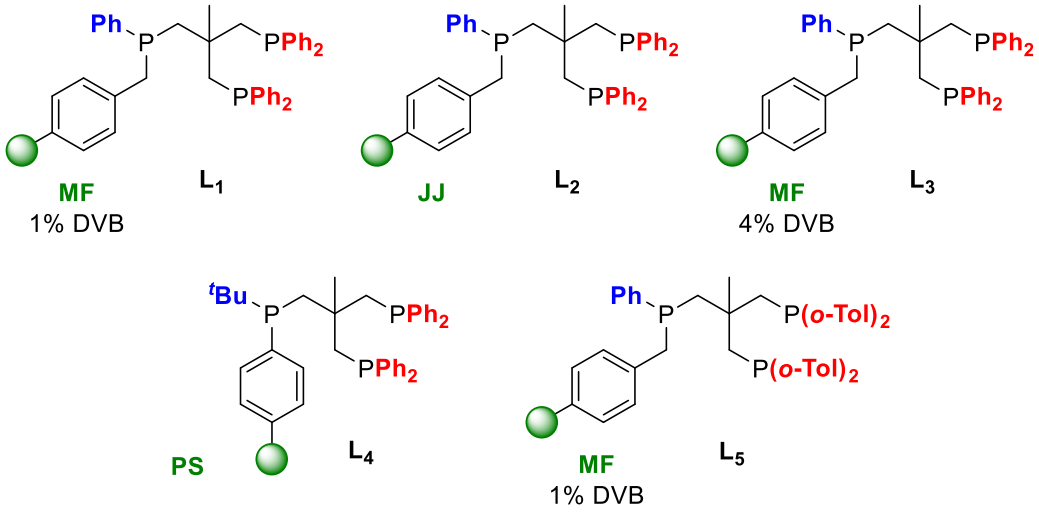

Figure 3 Supported Triphos-based ligand library **L_1-L_5**.

5.3. Solid-Phase Synthesis of Supported Ruthenium-Triphos Complexes

In previous attempts, the resin-bound Triphos ligand **L_1** was treated with [Ru(cod)(methallyl)$_2$] (cod = cyclooctadiene) in order to form the supported analogue **Ru·L_1** of the well-defined and stable [Ru(Triphos)(methallyl)] complex **VI** reported by vom Stein *et al* (Figure 4).[30,32] Unfortunately, the formation of the supported complex **Ru·L_1** was accompanied by deposition of Ru metal within the polymeric scaffold. Numerous washing steps did not lead to a satisfying purification of the entirely black polymer. When **Ru·L_1** was employed in the hydrogenation of benchmark esters, severe activity and selectivity problems were encountered. This can be attributed to the slow formation of the active catalyst as well as the embedded catalytically active Ru nanoparticles.

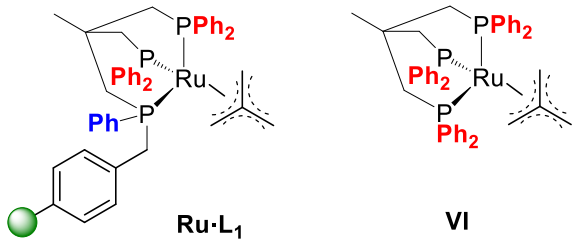

Figure 4 Structures of attempted resin-bound Ru-Triphos complex **Ru·L_1** and homogeneous analogue **VI**.

To avoid the troublesome deposition of Ru metal, an alternative strategy employing a different ruthenium precursor was chosen. The resin-bound ligand library **L_1-L_5** was treated with 1.1 equivalent of [RuHCl(PPh$_3$)$_3$CO] in toluene at 80 °C (Scheme 4). The displacement of PPh$_3$ as well as the quantitative disappearance of the free ligand peaks were monitored by gel-phase ^{31}P NMR. When nearly full complexation was achieved, the resins could be decanted yielding yellow to orange materials of resin-bound ruthenium-Triphos complexes **C_1-C_5**.

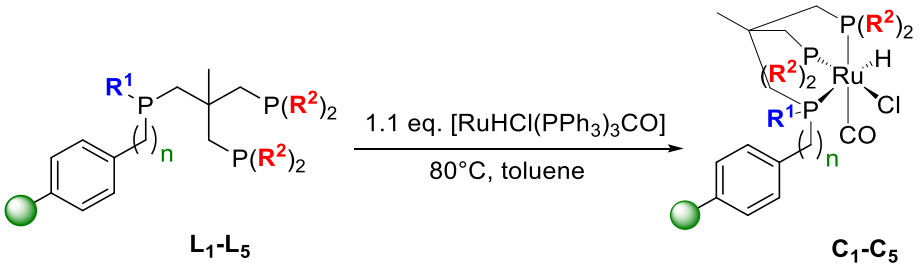

Scheme 4 Synthesis of supported complexes **C_1-C_5**.

Next, the resins were purified by filtration and washing with DCM, THF and diethyl ether to ensure quantitative removal of excess Ru-precursor. Satisfyingly, no visible formation of Ru nanoparticles occurred in solution or on the support. However, when stored under air instead of inside a glovebox, the color of the resins changed over the period of a week from yellow/orange to green/black indicating slow decomposition of the Ru(II) species. Next, the supported ruthenium-Triphos complexes **C_1-C_5** were characterized using various analytical techniques.

5.3.1 Gel-phase ^{31}P NMR

In the gel-phase ^{31}P NMR spectrum of **C_1**, three new broad signals appear in an approximate ratio of 1:1:1 corresponding to the three Ru–P moieties while sharp signals of the free ligand **L_1** disappeared (Figure 5).

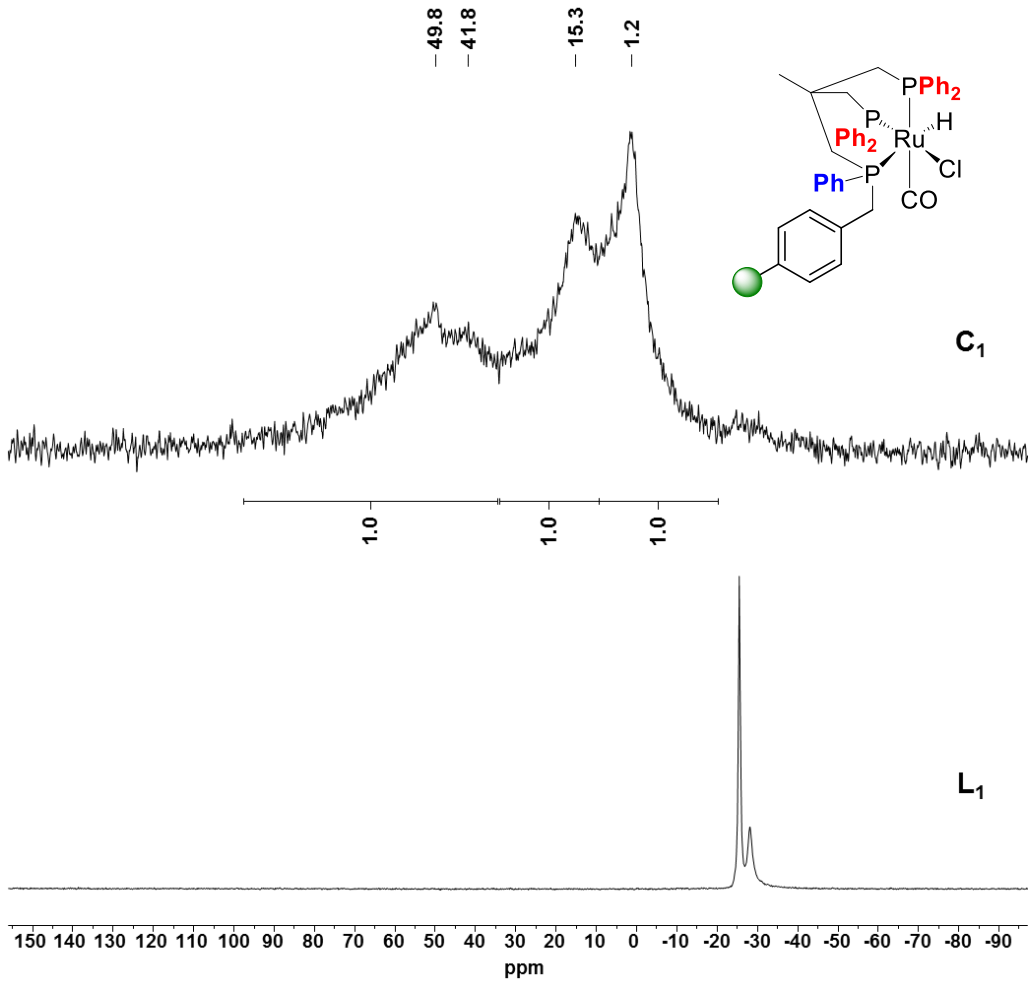

Figure 5 Representative solid-phase synthesis of supported Ru-Triphos complex **C_1** monitored by gel-phase ^{31}P NMR.

For the two PPh_2 moieties, two sharper resonances are observed at δ = 15.3 and 1.2 ppm whereas the broader signal of the P-atom in close proximity to the polymeric support exhibits a splitting (δ = 49.8 and 41.8 ppm). This could be attributed to the presence of isomeric Ru-complexes as observed in homogeneous systems employing unsymmetrical Triphos ligands.[3d] Unfortunately, coupling constants cannot be assigned due to significant peak broadening.

For a direct comparison, the solution-phase analogue **III** (see Figure 1, chapter 5.1) was prepared according to literature procedure.[33] The molecular structure of **III** only differs in a phenyl group attached to the phosphorus instead of the Merrifield methylene linker in $\mathbf{C_1}$. The ^{31}P NMR spectrum of **III** shows three double doublets at δ = 48.9, 12.2 and -0.4 ppm (Figure 6, red spectrum). The chemical shifts of the homogeneous complex are well in line with those obtained for $\mathbf{C_1}$ indicating the formation of three different Ru–P bonds on the support. Analogous to $\mathbf{C_1}$, the spectrum of $\mathbf{C_2}$ immobilized on JandaJel™ resin exhibits signals at δ = 51.0, 14.4 and 0.8 ppm.

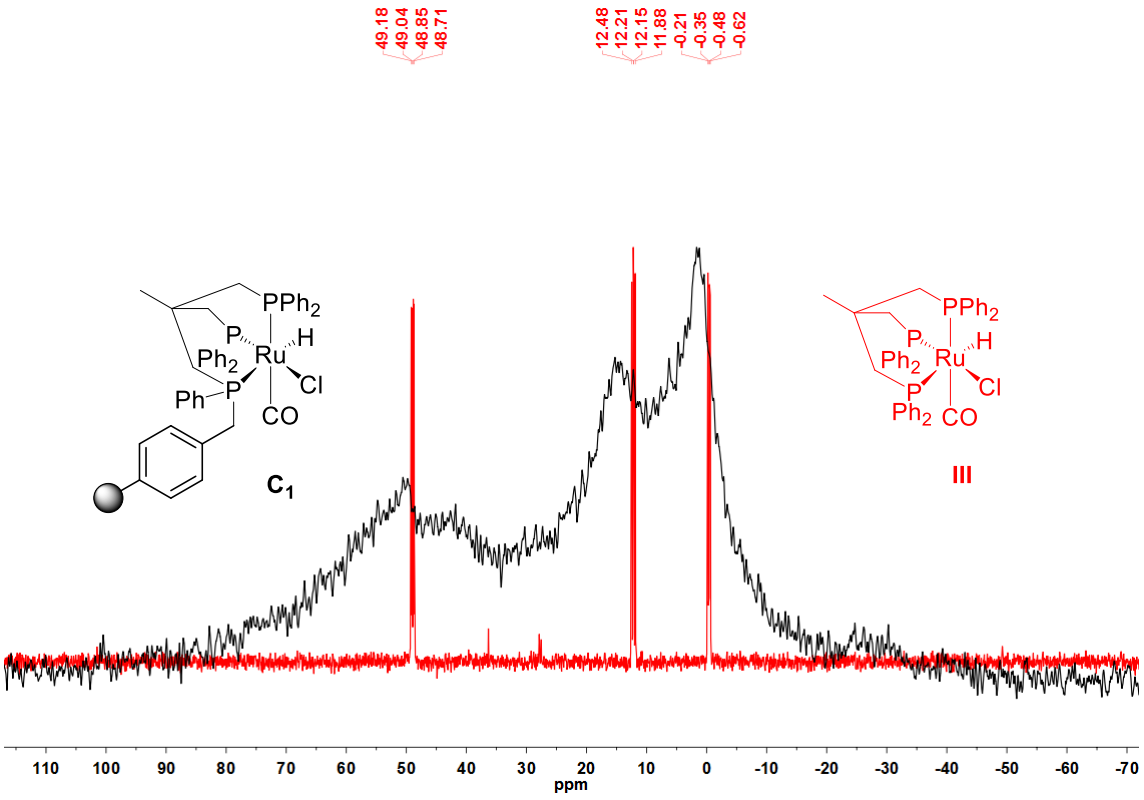

Figure 6 ^{31}P NMR spectra of supported Ru-Triphos complex $\mathbf{C_1}$ (black) and the solution-phase analogue **III** (red).

These are accompanied by minor signals at 43.8 and 5.4 ppm which could be attributed again to the presence of an isomeric mixture. Unfortunately, no signals were observed for **C_3** supported on the 4% cross-linked Merrifield resin probably due to the more heterogeneous nature of the polymer and hence reduced swelling properties in solvents like THF and 1,4-dioxane. However, the complete disappearances of the ligand signals as well as observation of PPh_3 in the supernatant solution indicated full complexation. Likewise, the gel-phase NMR spectra obtained for **C_4** and **C_5** were of no use due to very broad resonances. Hence, solid-state NMR techniques were utilized for further analysis of the supported materials.

5.3.2 Solid-State NMR

In case of **C_1** bound to MF and JJ-supported complex **C_2**, similar ^{31}P MAS NMR spectra were recorded and compared to those in solution-phase. Furthermore, distinctive signals in the ^{1}H MAS NMR spectrum of **C_1** expected for protons located in the ligand backbone, i.e. the CH_3 bridge head as well as the CH_2–P linkers, are mainly superimposed by broad signals belonging to the polymeric support (Figure 7). However, a small shoulder at -5.80 ppm could indicate the presence of the hydride bound to Ru, which is well in line with the *ddd* at -5.90 ppm obtained for the homogeneous counterpart **III**.

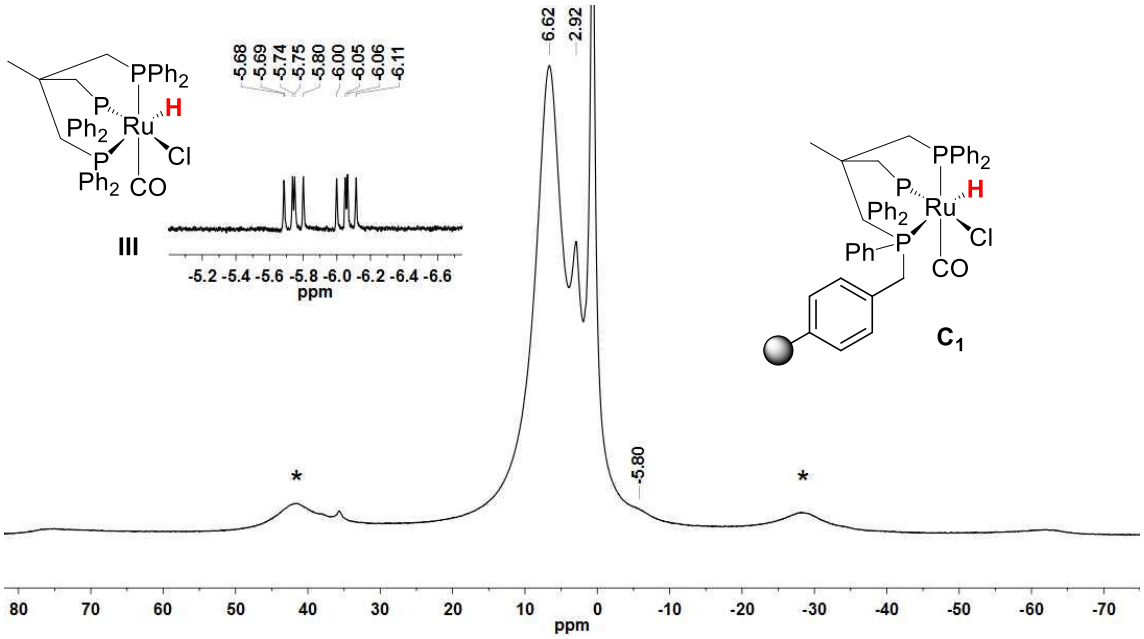

Figure 7 ^{1}H MAS NMR spectrum of **C_1** (spinning rate 14 kHz) and hydride region of solution phase ^{1}H NMR spectrum of **III** (top left). Rotational sidebands are denoted by asterisks (*).

In case of PS-immobilized complex **C_4**, three broad multiplets at about δ = 47.0, 17.0 and -6.0 ppm are observed in an approximate 1:1:1 ratio in ^{31}P MAS NMR (Figure 8, left spectrum). As mentioned above, the occurrence of multiple resonances can be attributed to the presence of isomeric Ru-complexes on the support. Moreover, distinct resonances for the *tert*-butyl group bound to the phosphorus atom are observed in the ^{13}C MAS NMR spectrum at δ = 32.7 and 28.4 ppm next to a range of signals in the aromatic and aliphatic region belonging to the support (Figure 8, right spectrum). Unfortunately, a signal for the CO ligand could not be unambiguously assigned.

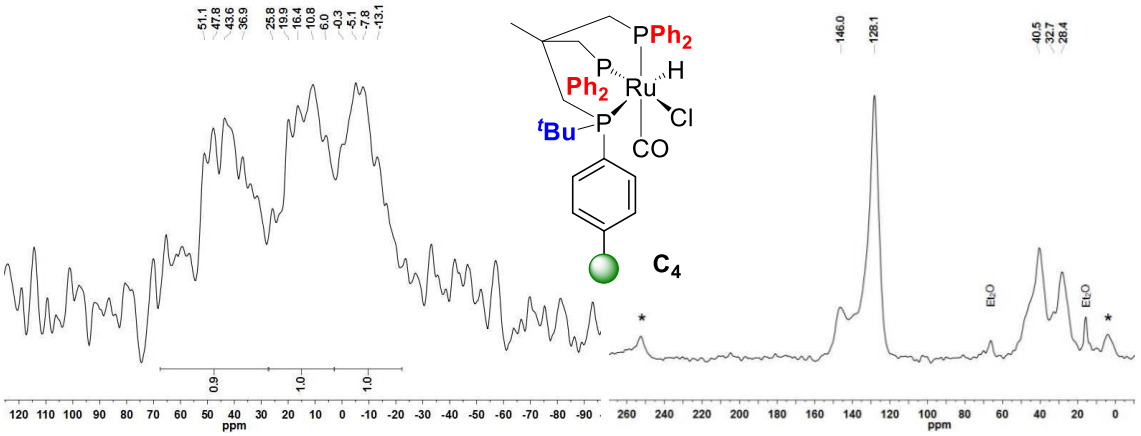

Figure 8 Left spectrum: ^{31}P MAS NMR spectrum of **C_4** (spinning rate 14 kHz). Right spectrum: ^{13}C MAS NMR spectrum of **C_4** (spinning rate 12.5 kHz). Rotational sidebands are denoted by asterisks (*).

The ^{31}P MAS NMR spectra of the solid-supported complexes **C_3** and **C_5** reveal very broad multiplets (from δ = 51.8 to 5.7 ppm for **C_3** and δ = 57.3 to -2.5 ppm for **C_5**), which are not suitable for conclusive statements about the tridentate coordination of the Triphos-based ligand to the Ru center.

5.3.3 ATR-FTIR Spectroscopy

Additionally, all materials were analyzed by ATR-FTIR spectroscopy. A comparison of the IR spectra of the non-complexated Triphos ligand **L_2** supported on JandaJel™ (red spectrum) with its corresponding Ru-complex **C_2** (blue spectrum) is depicted in Figure 9. In order to confirm the molecular structure of the complex on the support, the spectrum of resin-bound **C_2** is compared to its homogeneous counterpart **III** (green spectrum). In the area from 2100-1500 cm^{-1} (Figure 9, light green box), no bands are observed for **L_2** whereas complex **C_2** shows two bands appearing at 1974 cm^{-1} and 1925 cm^{-1}. The band at 1974 cm^{-1} corresponds to the vibration of the CO ligand bound

to the Ru center roughly in line with both the vibration at 1965 cm^{-1} obtained for **III** and data in literature reported for structurally similar complexes.[3c,3d,33] The band at 1925 cm^{-1} for $\mathbf{C_2}$ can be attributed to Ru–H, which is in agreement with the band exhibited by **III** at 1921 cm^{-1}. The third band for **III**, at 1896 cm^{-1}, could origin from a C–H deformation vibration also found in $[RuCl_2(PPh_3)_3]$.[34] The area from 1650-1400 cm^{-1} (Figure 9, light orange box) predominantly contains bands belonging to aromatic C–C vibration of arene rings attached to phosphorus atoms.[34] Especially the bands at 1450 cm^{-1} and 1433 cm^{-1} in $\mathbf{L_2}$ and $\mathbf{C_2}$ are also present in the spectrum of **III**. Similar results can be concluded from P-aromatic C–C vibrations at 841-838 cm^{-1}, 738-740 cm^{-1} and 693-695 cm^{-1} (Figure 9, light blue box), which are present in both heterogeneous compounds and the homogeneous complex. Resembling IR spectra were obtained for the supported complexes $\mathbf{C_1}$ and $\mathbf{C_3}$-$\mathbf{C_5}$.

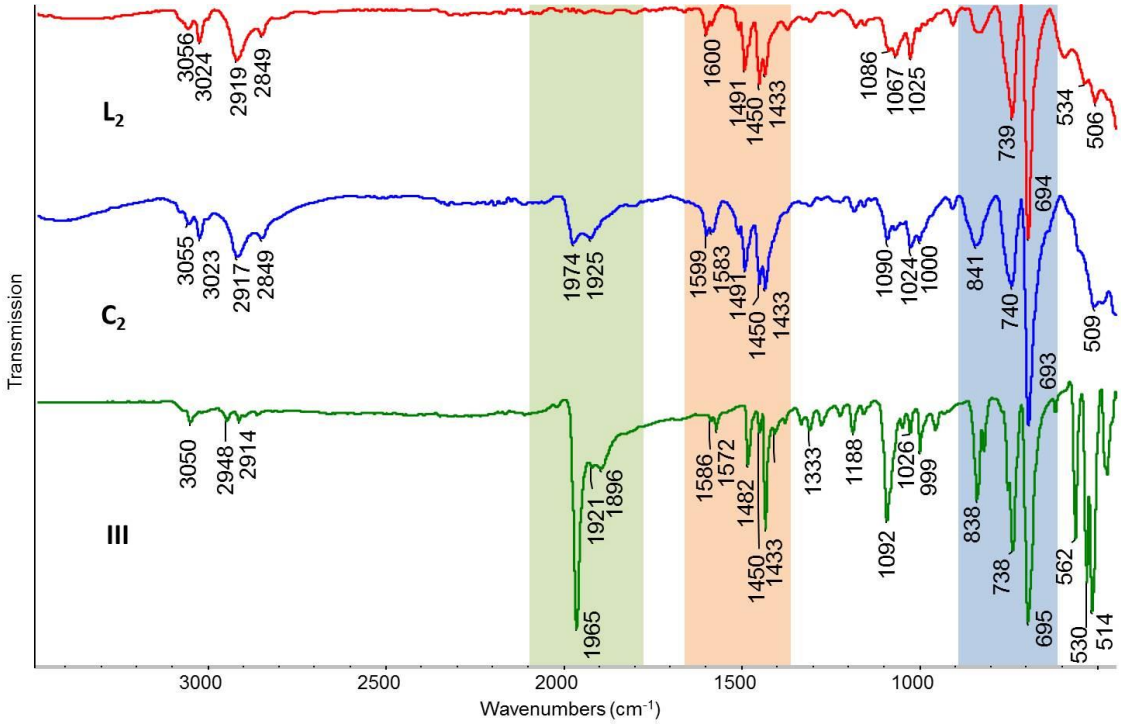

Figure 9 FTIR spectra of resin-bound ligand $\mathbf{L_2}$ (red), the corresponding resin-bound Ru-complex $\mathbf{C_2}$ (blue) and the homogeneous Ru-complex analogue **III** (green).

5.3.4 Raman Spectroscopy

Complementary to FTIR investigations (see chapter 5.3.3), Raman spectroscopic techniques were used to confirm the molecularly defined structure of the supported complex **C_2**. Again, the spectrum of **C_2** (green spectrum) was compared to the free resin-bound ligand **L_2** (blue spectrum) as well as to the non-supported counterpart **III** (red spectrum, Figure 10a). For more detailed illustrations, the wavenumber ranges ν = 2200-1000 cm^{-1} and ν = 1000-100 cm^{-1} are expanded in Figure 10 b and c, respectively. While grey boxes are inserted to highlight bands exclusively observed for the Ru-complexated species **C_2** and **III**, light blue boxes indicate bands solely belonging to the support. The spectra of both resin-bound species show all the distinctive bands associated with the pure non-functionalized polystyrene-based support.[35] Again, the two weak bands at 1976 cm^{-1} and 1921 cm^{-1} for **C_2**, corresponding to CO and the hydride ligand respectively, are in agreement with those obtained for **III** (1968 and 1918 cm^{-1}). The band at 1602 cm^{-1} can be assigned to the deformation vibration of polymeric Ar–H groups, whereas the strong band at 1586 cm^{-1}, which is present in all three compounds, is indicative for vibrations of P–Ar moieties. Furthermore, bands exclusively occurring in the homogeneous and heterogeneous complexes can be found at 1434, 560-524, and 439 cm^{-1}. Finally the bands at 330-336 cm^{-1} and 297-294 cm^{-1} may be assigned to the Ru–Cl stretching vibrations as reported for similar ruthenium complexes.[34]

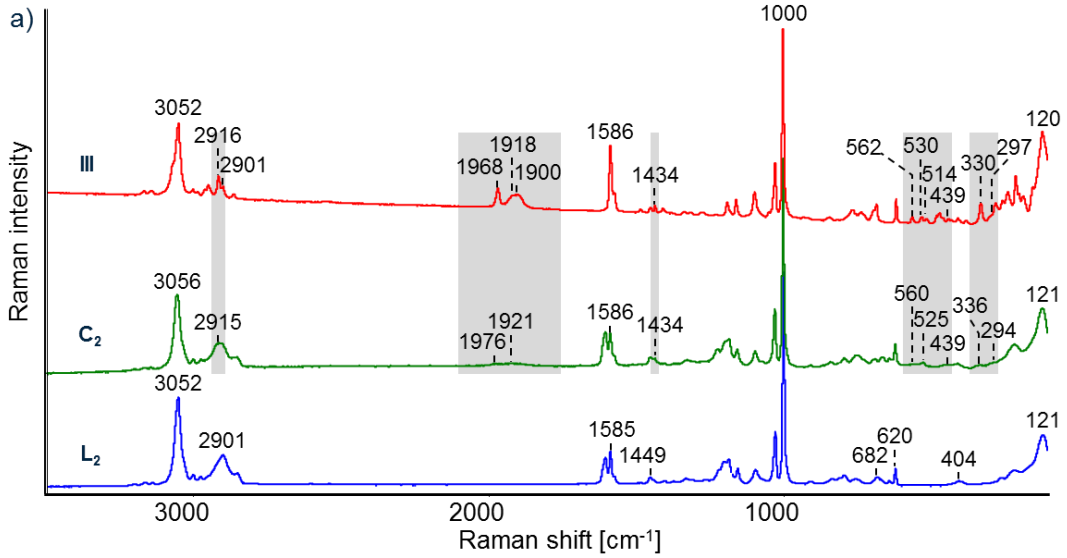

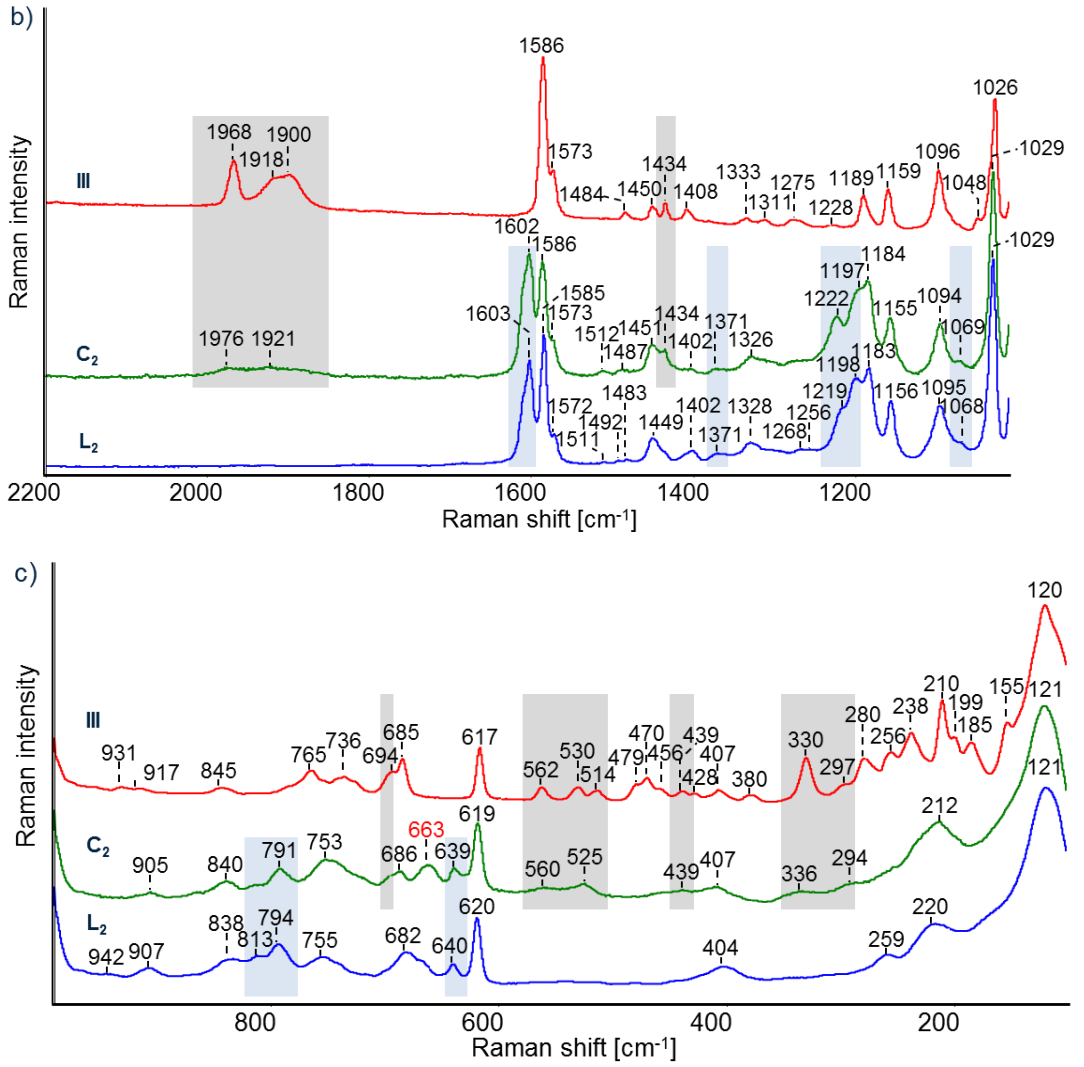

Figure 10 Stacked plot of Raman spectra of supported Triphos ligand **L_2** (blue spectrum), supported Ru-Triphos complex **C_2** (green spectrum) and homogeneous Ru-Triphos complex **III** (red spectrum) in the wavenumber range a) ν = 3500-2400 cm^{-1}, b) ν = 2200-1000 cm^{-1} and c) ν = 1000-100 cm^{-1}. Bands exclusively occurring in the spectra of **C_2** and **III** are highlighted in grey boxes. Bands belonging to the polymeric support are highlighted in blue boxes.

5.4 Application of Supported Ru-Triphos Complexes in Catalysis

5.4.1 Deaminative Hydrogenation of Nitriles to Primary Alcohols

In homogeneous catalysis, systems based on ruthenium-Triphos complexes have been successfully employed in a plethora of transformations (see introduction, chapter 5.1). In particular, hydrogenation reactions of challenging target substrates were studied intensively in recent years.[36] However, reports employing the solution-phase Ru-Triphos complex **III** are limited to alcohol amination reactions[3c-e] and the C–C bond cleavage in lignin model compounds[37].

Recently, Molnár *et al.* reported on the selective hydrogenolysis of *n*-octanenitrile (**4**) to the corresponding primary alcohol using the Ru-Triphos complex **III**.[17] By employing a 1:1 mixture of 1,4-dioxane and water at 140 °C under a H_2 pressure of 10 bar, full conversion of **4** was observed with 73% selectivity towards the desired primary alcohol accompanied by 3% of secondary and 23% of tertiary amine (Table 1, entry 6). Inspired by this result, it was decided to employ the heterogeneous analogue $\mathbf{C_1}$ in the hydrogenolysis of benzonitrile ($\mathbf{S_1}$) and *n*-heptanenitrile ($\mathbf{S_2}$). Mechanistically, the reaction proves to be challenging due to the potential formation of a variety of side products (see Scheme 2, chapter 5.1). In addition to the desired primary alcohol (**G**), the primary amine (**B**), the secondary imine (**C**) and amine (**D**), the tertiary amine (**E**) as well as the primary amide (**H**) could be obtained.

Full conversion of $\mathbf{S_1}$ was observed when using 1.0 mol% of the supported catalyst $\mathbf{C_1}$ under the same conditions as reported for **III** (Table 1, entry 1). Remarkably, 86% selectivity towards the desired benzyl alcohol was reached together with the formation of 10% benzyl amine and minor quantities of **G** and **D**. Moreover, a similar catalyst performance was obtained when lowering the reaction temperature to 120 °C (Table 1, entry 2). A further decrease in temperature to 100 °C had a small detrimental impact on the selectivity towards the alcohol (81%, Table 1, entry 3). A similar result was obtained when reducing the catalyst loading to 0.5 mol% (Table 1, entry 4). The aliphatic substrate $\mathbf{S_2}$ was converted into 1-heptanol with 91% selectivity accompanied by small quantities of amide (2%), primary amine (6%) and secondary amine (2%) using 1.0 mol% of $\mathbf{C_1}$ under the same conditions as reported for *n*-octanenitrile (**3**) (Table 1, entries 5 and 6). Although $\mathbf{S_2}$ and **3** structurally differ in a CH_2 group, the heterogeneous catalyst outperformed its solution-phase analogue **III** with an 18% higher selectivity towards the primary alcohol. Furthermore, no formation of the tertiary amine **E** was observed.

Table 1 Ru-catalyzed hydrogenolysis of nitriles $\mathbf{S_1}$ and $\mathbf{S_2}$ using supported complex $\mathbf{C_1}$.[a]

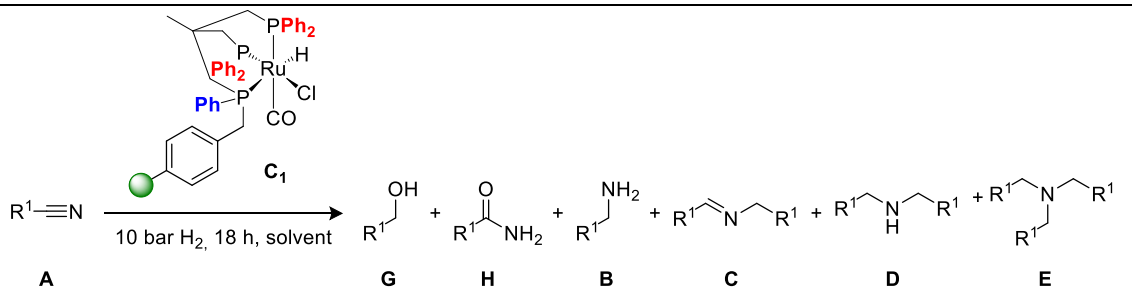

A **G** **H** **B** **C** **D** **E**

4: $R^1 = C_7H_{15}$
$\mathbf{S_1}$: $R^1 = Ph$
$\mathbf{S_2}$: $R^1 = C_6H_{13}$

Entry	Loading [mol%]	Substrate	*T* [°C]	Conv. [%][b]	Selectivity [%][b]					
					G	**H**	**B**	**C**	**D**	**E**
1	1.0	$\mathbf{S_1}$	140	>99	86	2	10	0	2	0
2	1.0	$\mathbf{S_1}$	120	>99	87	2	10	0	2	0
3	1.0	$\mathbf{S_1}$	100	>99	81	2	16	0	2	0
4	0.5	$\mathbf{S_1}$	100	>99	81	1	17	0	1	0
5	1.0	$\mathbf{S_2}$	140	>99	91	2	6	0	2	0
6[c]	**III** (0.5)	**3**	140	>99	73	1	<1	<1	3	23
7[d]	0.5	$\mathbf{S_1}$	100	>99	0	0	99	1	0	0

[a] Conditions: substrate (0.5 mmol), 1,4-dioxane (0.5 mL), water (0.5 mL), H_2 (10 bar), 18 h. [b] Conversion and selectivity determined by GC analysis. [c] Data taken from reference 17. [d] No water was used.

When the hydrogenation of $\mathbf{S_1}$ was performed in the absence of water at 100 °C, full conversion together with 99% selectivity towards benzyl amine was obtained (Table 1, entry 7). This performance is highly impressive for a heterogeneous catalyst, as the use of selectivity enhancing additives was not required and relatively mild reaction conditions were applied. Similar conditions were applied by Beller and co-workers for their solution-phase analogues.[15] Consequently, the application of resin-bound Ru-Triphos catalysts in the selective hydrogenation of nitriles to primary amines was investigated.

5.4.2 Hydrogenation of Nitriles to Primary Amines

Encouraged by the results obtained in the previous catalytic experiments, it was decided to investigate the selective reduction of nitriles to primary amines. Reports on Ru-Triphos systems applied to this transformation remain fairly limited to only a few examples (see chapter 5.1).[14-15,21b] In the case of a solution-phase combination of [Ru(cod)(methallyl)$_2$] with Triphos ligand (**I**), as reported by the group of Beller, 1-haptanenitrile (**S$_2$**) was reduced to 1-heptaneamine in 62% yield under mild conditions (50 °C, 15 bar H_2) in the absence of additives.[15] Changing to the more bulky tripodal phosphorus ligand **II** (see Figure 1, section 5.1) led to a significantly increased catalyst performance achieving quantitative formation of the primary amine under the same conditions. Conversely, the SiO_2 immobilized analogue of Bianchini *et al.* (see Figure 2, **IV**, chapter 5.1) resulted in the selective formation of the secondary imine **C** instead of the primary amine **B**.[21b]

In order to determine the optimized conditions for this reaction, the resin-bound Ru-Triphos complex **C$_1$** was employed in the hydrogenation of **S$_1$** under various conditions and compared to its solution-phase counterpart **III** (Table 2). Using 1.0 mol% of the solid-supported catalyst at 80 °C led to full conversion of **S$_1$** and 98% selectivity towards benzyl amine (Table 2, entry 2). Upon reducing the catalyst loading to 0.5 mol%, the conversion dropped to 48% (Table 2, entry 3). While a comparable selectivity was observed when using THF as a solvent, the activity was lower compared to 1,4-dioxane (37% conversion, Table 2, entry 4). In toluene the catalyst performance further decreased to 24% conversion and only 77% selectivity (Table 2, entry 5). When screening the reaction in more environmentally benign solvents, such as 2-methyltetrahydrofuran (Me-THF), anisole, dimethylcarbonate (DMC) and 1,3-dioxolane, the catalyst performance dropped further (Table 2, entries 6-9). Consequently, 1,4-dioxane was chosen as the most suitable reaction medium providing sufficient polymer swelling properties opposed to ^{i}PrOH, which was found to be the ideal solvent in homogeneously catalyzed nitrile reduction using Ru-Triphos.[15] Interestingly, the homogeneous system proved to be completely inactive when using solvents such as 1,4-dioxane, THF and toluene. Moreover, the same group found that [Ru(cod)(methallyl)$_2$] was the only metal precursor affording any activity in this homogeneous reaction, whereas other Ru sources containing anionic halide or carbonyl ligands remained inactive at reaction temperatures of 50 °C.

Table 2 Optimization of reaction conditions in Ru-catalyzed hydrogenation of $\mathbf{S_1}$ using supported catalyst $\mathbf{C_1}$ und the homogeneous complex **III**.

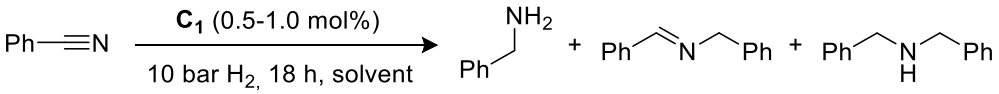

$\mathbf{S_1}$ **B** **C** **D**

Entry	Catalyst [mol%]	Solvent	*T* [°C]	Conversion [%][b]	Selectivity [%][b]		
					B	**C**	**D**
1	0.5	dioxane	100	>99	99	1	0
2	1.0	dioxane	80	>99	98	1	0
3	0.5	dioxane	80	48	97	3	0
4	0.5	THF	80	37	97	3	0
5	0.5	toluene	80	24	73	27	0
6	0.5	Me-THF	80	18	86	6	0
7	0.5	anisole	80	16	44	56	0
8	0.5	DMC	80	2	0	2	0
9	0.5	dioxolane	80	18	39	61	0
10	1.0	dioxane	100	>99	99	1	0
11	**III** (1.0)	dioxane	100	>99	30	68	2
12[c]	Ru/**II** (0.5)	^{i}PrOH	50	>99	>99	<1	<1
13[d]	**IV** (1.0)	*n*-octane	100	95	3	88	5

[a] Conditions: substrate (0.5 mmol), solvent (1.0 mL), H_2 (10 bar), 18 h. [b] Conversion and selectivity determined by GC using dodecane as internal standard. [c] Data taken from ref. 15; reaction conditions: substrate (0.5 mmol), ^{i}PrOH (2 mL), H_2 (15 bar), 17 h. [d] Data taken from ref. 21b; reaction conditions: substrate (2.15 mmol), *n*-octane (30 mL), H_2 (30 bar), 12 h.

Under the slightly elevated conditions used in this screening, the solution-phase catalyst [RuHCl(Triphos)CO] (**III**) achieved full conversion of $\mathbf{S_1}$ but surprisingly led to an unselective mixture of benzylamine (**B**, 30%), *N*-benzylidenebenzylamine (**C**, 68%) and dibenzylamine (**D**, 2%, Table 2, entry 11). In contrast to that, the polymer-bound analogue $\mathbf{C_1}$ selectively yielded 99% of benzyl amine (Table 2, entry 10), which is similar as the *in situ* operated Ru/**II** system of Beller and co-workers (Table 2, entry 12).[15]

In many examples of immobilized homogeneous catalysts, the support often has a detrimental effect on activity and selectivity. However, in this case, the opposite outcome was observed, where the support seems to have a beneficial impact on the

selectivity under the given reaction conditions. One explanation could be a locally high catalyst concentration provided by the specific microenvironment of the swollen polymer structure. A similar effect on linear to branched selectivities of aldehydes was reported by Pittman *et al.* using PS-supported rhodium catalysts in the hydroformylation of 1-pentene.[38] Opposed to the resin-supported Ru-Triphos system, the literature known SiO_2-grafted analogue **IV** gave mainly the secondary imine **C**, instead of the primary amine **B**, as the main product with 95% conversion and 88% selectivity after 12 h (Table 2, entry 13).[21b]

Subsequently, the small resin-bound catalyst library (**C_1-C_5**) was screened in the hydrogenation of **S_1** (Table 3). After 18 hours at 80 °C and at a H_2 pressure of 10 bar , similar catalyst performances were obtained for MF-supported catalyst **C_1**, **C_2** immobilized on JandaJel™ and PS-bound **C_4** (Table 3, entries 1, 2 and 4). This indicates that the type of support has no significant influence on the catalytic outcome. Furthermore, different substituents on the phosphorus atom directly bound to the polymeric support (Ph for **C_1** and **C_2**, ^{t}Bu for **C_4**) did not seem to affect the catalyst activity and selectivity. Supported catalyst **C_3** immobilized on the higher cross-linked MF 4% DVB gave 62% conversion and 97% selectivity (Table 3, entry 3). This can be associated with the lack of solvent dependent gel-like behavior of the higher crosslinked polymer opposed to **C_1**,which consequently reduces the accessibility of the catalytically active site within the support.

Table 3 Screening of supported catalysts **C_1-C_5** in Ru-catalyzed hydrogenation of **S_1**.

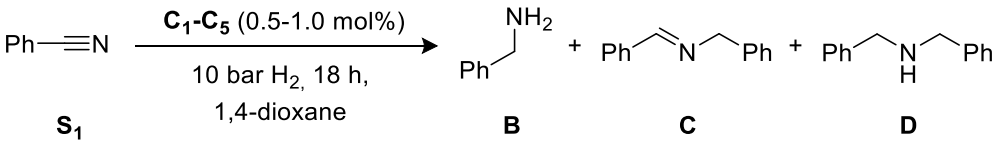

S_1 **B** **C** **D**

Entry	Catalyst [mol%]	*T* [°C]	Conversion [%][b]	Selectivity [%][b]		
				B	**C**	**D**
1	**C_1** (0.5)	80	48	97	3	0
2	**C_2** (0.5)	80	48	96	4	0
3	**C_3** (1.0)	100	62	97	3	0
4	**C_4** (0.5)	80	44	97	3	0
5[c]	**C_5** (0.5)	80	32	0	>99	0

[a] Conditions: substrate (0.5 mmol), 1,4-dioxane (1.0 mL), H_2 (10 bar), 18 h. [b] Conversion and selectivity determined by GC using dodecane as internal standard. [c] After 8 h.

After extending the reaction time to 50 hours, **S_1** was fully converted with 98% selectivity. Unexpectedly, catalyst **C_5** bearing more sterically demanding P(*o*-Tol)$_2$ groups within the Triphos structure resulted in 32% conversion with full selectivity towards the secondary imine **C** after 8 hours (Table 3, entry 5). At a prolonged reaction time of 18 hours, 86% of **S_1** were converted along with a slightly reduced selectivity of 92% towards **C**. However, this nicely showcases that minor alterations in ligand structure can lead to unexpected outcomes and consequently underlines the necessity of catalyst screening. At the same time it demonstrates the power of a modular and hence easily tunable solid-bound Triphos ligand system accessed by using an SPS approach, which makes it highly suitable for automated parallel synthesis.[39]

Next, a range of aromatic and aliphatic mono- and dinitriles were employed to determine the substrate scope using supported catalyst **C_1** under optimized conditions (see Figure 11, **S_1**-**S_{13}**). Among the aromatic nitriles **S_1** and **S_3**-**S_9**, electron-withdrawing *para*-bromo- (**S_3**) and *para*-fluorobenzonitrile (**S_4**) were hydrogenated with relative ease and high selectivity at 80 °C and 100 °C, respectively (Figure 11).

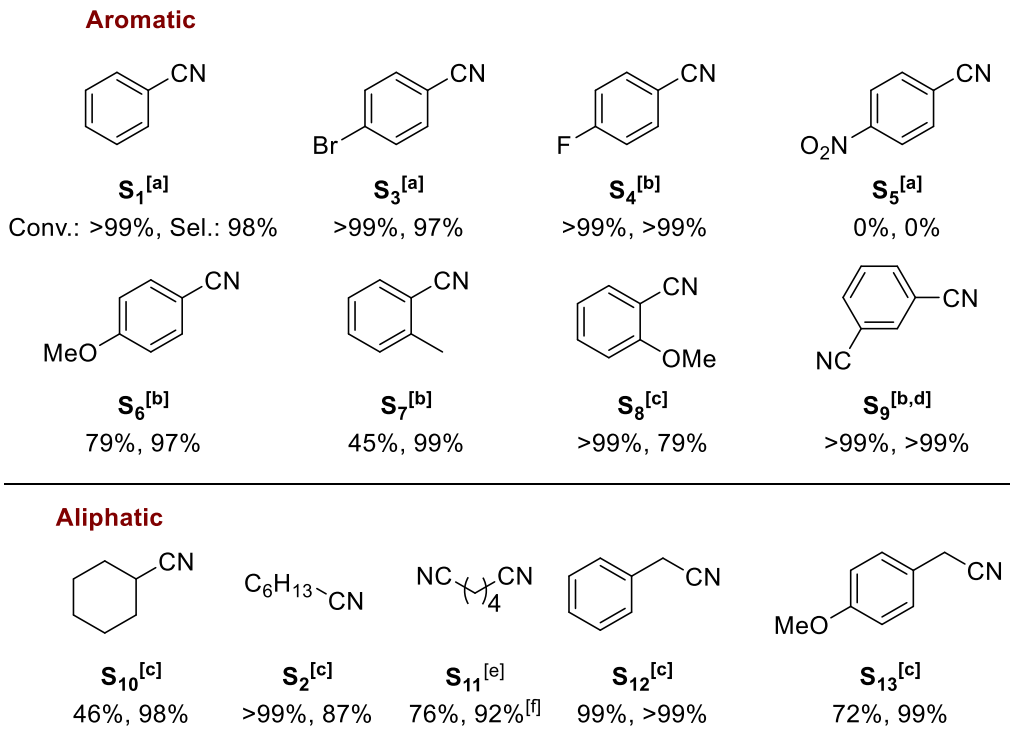

Figure 11 Substrate scope using supported catalyst **C_1** (conversion and selectivity to mono- or diamine indicated below structures). [a] Reaction conditions: substrate (0.5 mmol), [Ru] (1.0 mol%), 1,4-dioxane (1.0 mL), 80 °C, H_2 (10 bar), 18 h. [b] 100 °C. [c] 120 °C. [d] H_2 (30 bar). 24 h, [e] 100 °C, H_2 (30 bar), 24 h. [f] Selectivity towards ω-aminocapronitrile.

When employing **S_3** at 100 °C using only 0.5 mol% of **C_1**, 91% conversion was achieved with 95% selectivity towards the corresponding secondary imine. Nitro-substituted substrate **S_5**, however, led to catalyst decomposition resulting in the formation of black Ru metal as observed in homogeneous deaminative nitrile hydrogenation to primary alcohols. This may be attributed to phosphine oxidation followed by deposition of the metal particles within the porous structure of the polymer. More electron-donating *para*-methoxy groups (**S_6**) gave 79% conversion and 97% selectivity. **S_7**, a substrate featuring a methyl substituent in *ortho*-position proved to be more challenging with only 45% conversion but with excellent selectivity of 99%. **S_8I** bearing an *ortho*-methoxy group was fully converted with 79% selectivity requiring a reaction temperature of 120 °C. The dinitrile 1,3-dicyanobenzene **S_9** was quantitatively converted into the corresponding diamine after 24 h at 100 °C and 30 bar of H_2. Elevated temperatures of 120 °C were also required for the reduction of aliphatic nitriles. While cyclohexanecarbonitrile (**S_{10}**) was selectively hydrogenated to cyclohexylmethanamine with only 46% conversion, heptanenitrile (**S_2**) was predominantly transformed into heptylamine, accompanied by secondary imine and amine. Mainly semihydrogenation of adiponitrile (**S_{11}**) was observed with 92% selectivity towards ω-aminocapronitrile which can serve as a valuable building block for the synthesis of nylon-6.[41] Finally, benzylic nitriles were selectively hydrogenated with excellent to moderate conversions (99% for **S_{12}** and 72% for **S_{13}**).

5.5 Catalytic Recycling

5.5.1 Batch Recycling

Next, the reusability and recyclability of the resin-bound Ru-Triphos catalyst **C_1** were examined in the hydrogenation of **S_1** (Table 4). In order to assess any effect on the catalyst activity, a shorter reaction time of 2 hours per run was chosen. The supernatant solution was filtered off after each cycle followed by addition of fresh substrate stock solution. Within the first four runs, an increase in conversion from 17% (run 1) to 39% (run 4) as well as excellent selectivity towards the desired benzylamine (**B**) was observed (Table 4, entries 1-4).

Table 4 Batch recycling experiments using **C_1** in the hydrogenation of **S_1**.

Run	Conversion [%][b]	Selectivity [%][b]	
		B	**C**
1	17	>99	<1
2	26	>99	<1
3	34	99	1
4	39	99	1
5	36	97	3
6	31	97	3
7[c]	>99	95	5

[a] Conditions: substrate (0.5 mmol), catalyst (1.0 mol%), 1,4-dioxane (1.0 mL), 100 °C, H_2 (10 bar), 2 h. [b] Conversion and selectivity determined by GC using dodecane as internal standard. [c] 18 h.

The gradual raise in catalyst activity could be due to slow formation of the catalytically active species under the given conditions, similar to the induction period reported for the homogeneous [Ru(cod)(methallyl)$_2$]/**II** system by Beller and co-workers.[15] However, in the following two runs, a decrease in catalyst activity was observed (∆3% in run 5, ∆5% in run 6, Table 4, entries 5 and 6), accompanied by a small drop in selectivity to 97%. This could be mainly attributed to mechanical abrasion of the polymeric support and hence the degradation of the specific microenvironment through magnetic stirring, which consequently lead to finely ground particles in the

supernatant solution. When in run 7 the same catalyst was used in the same conditions but with a reaction time of 18 hours, a similar performance compared to the initial screening was observed only differing in the presence of 5% of the secondary imine (Table 4, entry 7 vs Table 2, entry 10). The visual formation of Ru metal deposited within the porous polymer was not observed.

Furthermore, the amount of Ru metal leaching into the product phase was analyzed by ICP-OES after each run. Gratifyingly, no ruthenium in solution was detected above the detection limit (0.07 $mg \cdot l^{-1}$) supporting the assumption of catalyst deactivation being manly caused by deterioration of the polymer rather than by degradation of the molecular structure of the catalyst. These results underline the stability and facile recoverability of the resin-bound Ru-Triphos system retaining a high selectivity throughout the seven recycling experiments. Issues concerning the degradation of the support could be overcome by applying the system in a continuous flow hydrogenation set-up.

5.5.2 Continuous Flow Hydrogenation

Homogeneous catalysts covalently bound to solid polymeric supports represent suitable candidates for application in continuous flow processes. While continuously operated systems facilitate optimization of reaction conditions together with high process reliability, flow conditions could be also beneficial in terms of catalyst long-term stability (see chapter 1.2.4). Both the potential exposure to air and moisture during recycling under batch conditions as well as mechanical degradation of the support can be avoided in a fixed bed reactor.

The hydrogenation of benzonitrile (**S_1**) under flow conditions was investigated by employing the supported catalyst **C_1** in a customized modular microreaction system supplied by Ehrfeld Mikrotechnik BTS (Figure 12). Prior to preparation of the catalyst bed, the resin (200 mg) was swollen in 1,4-dioxane and transferred into the reactor (V = 5 mL). The catalyst bed was layered with glass wool and the remaining volume was filled with glass beads. Via a HPLC pump, the substrate stock solution (0.25 M of **S_1** in 1,4-dioxane) was fed into a micro mixer, where it was combined with H_2 gas. Within the reactor cartridge, the gas-liquid mixture was heated up to reaction temperature before it passed through the catalyst bed. The system pressure was maintained by a back pressure regulator.

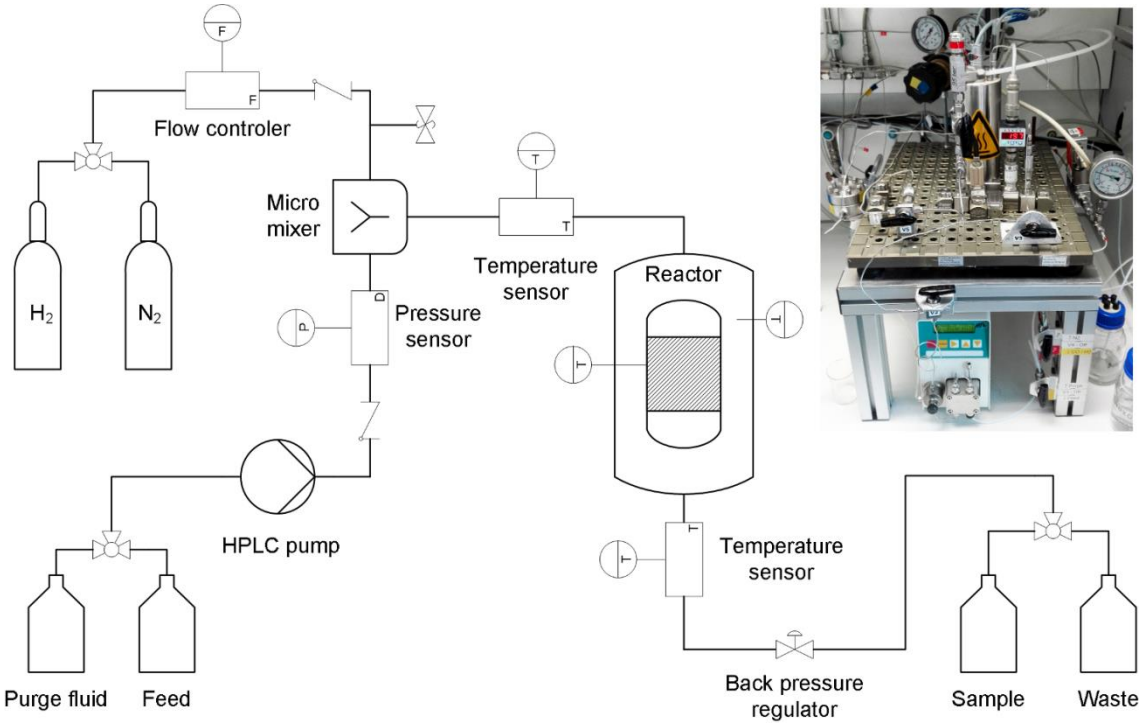

Figure 12 Flow scheme of modular microreactor setup for continuous flow hydrogenation reactions.

In order to investigate the catalyst behavior under various flow conditions, the reaction parameters were gradually altered throughout the initial experiment. The response of the system was studied in eleven different settings of parameters by changing one condition at the time. The flow rate of the feed solution and the H_2 gas as well as reaction temperature and pressure were varied. An overview of all parameter settings and the corresponding final TOS is depicted in Table 5 and Figure 13, respectively. It is important to note that it was aimed for a system pressure of 10 bar in settings 1-3 and 5-11 and 20 bar in setting 4. However, a small blockage within the piping cause elevated pressures of around 17 bar and 29 bar, respectively. Conversion and selectivity towards benzyl amine **B** were monitored by GC analysis and averaged once stable conditions were reached. The results after 97.5 hours on stream are depicted in Figure 13.

Within the first 1.5 hours on stream at a feed flow rate of 0.20 mL·min^{-1}, a H_2 flow of 2.50 mL·min^{-1} and 100 °C fluid temperature, no conversion was observed (Table 5, setting 1). However, after 2.5 hours and a flow rate of 0.10 mL·min^{-1}, 7% of converted starting material was detected (Table 5, setting 2), which is indicative for a lag phase due to slow formation of the catalytically active species as observed in previous batch recycling attempts (see chapter 5.5.1). When changing the flow rate to 0.05 mL·min^{-1}, an average conversion of 83% was reached (Table 5, setting 3). In contrast to high

selectivities obtained in batch catalysis, the product stream was composed of 42% of benzyl amine (**B**) and 58% of secondary imine (**C**). This could be attributed to the length of the catalyst bed. Mechanistically, the primary imine is formed as the intermediate of the first hydrogenation step (see Scheme 1, chapter 5.1). Upon leaving the fixed bed, condensation of the intermediate and benzylamine can occur in the absence of catalyst.

Table 5 Variation of parameters in continuous flow hydrogenation of $\mathbf{S_1}$ using catalyst $\mathbf{C_1}$.

Setting	TOS [h][a]	Flow rate [mL·min^{-1}]	H_2 flow [mL·min^{-1}]	*T* [°C]	*P* [bar]	TOF [h^{-1}][b]	Conv. [%][c,d]	Selectivity [%][d,e]
1	1.5	0.2	2.50	100	15	0.8	0	-
2	2.5	0.10	2.50	100	15	0.8	7	95
3	22.5	0.05	2.50	100	17	4.7	83 (±6.5)	42 (±5.6)
4	26.0	0.10	2.50	100	19	6.4	57 (±1.6)	39 (±1.9)
5	45.5	0.10	2.50	100	29	9.0	80 (±2.5)	42 (±1.8)
6	49.0	0.10	2.50	100	17	5.7	51 (±2.0)	45 (±3.4)
7	51.0	0.10	1.25	100	17	5.5	49 (±0.9)	47 (±2.2)
8	69.0	0.10	1.25	120	17	10.0	89 (±0.5)	67 (±2.4)
9	72.0	0.10	1.25	135	17	11.0	98 (±1.3)	79 (±0.8)
10	75.0	0.10	1.25	150	17	11.2	100 (±0.2)	84 (±0.6)
11	92.5	0.05	1.25	150	17	5.6	100 (±0.0)	85 (±2.1)
12	97.5	0.05	2.50	100	17	4.1	73 (±1.6)	73 (±1.8)

[a] TOS until parameters were altered. [b] TOF (h^{-1}) calculated as flow rate (mL·min^{-1}) x concentration of stock solution (mmol·mL^{-1}) x conversion x 60 / n_{cat} (mmol). [c] Conversion of $\mathbf{S_1}$ determined by GC using dodecane as internal standard. [d] Conversion and selectivity are determined from samples taken every 30 to 60 minutes (values are averaged from at least 3 samples once stable conditions were obtained except for entry 1 and 2). Standard deviation in parenthesis. [e] Selectivity towards benzylamine (**B**).

Increasing the substrate flow rate to 0.10 mL·min^{-1} resulted in 57% conversion and 39% selectivity (Table 5, setting 4). When applying an overall pressure of 29 bar, the selectivity (42%) was not significantly affected, while the activity increased to 80% (Table 5, setting 5). Restoring previous conditions after 49 hours (Table 5, setting 6) led to slightly reduced conversion (51%) and similar selectivity (45%) compared to setting 3. The small differences in activity may be attributed to the system pressure fluctuating between 17 and 19 bar. A marginal decline in conversion (Δ2%) was

observed when reducing the H_2 flow to 1.25 mL·min^{-1} accompanied by a slightly increased selectivity (47%, Table 5, setting 7). Increasing the fluid temperature within the reactor to 120 °C resulted in a significant boost of both conversion (89%) and selectivity (67%, Table 5, setting 8). A further rise to 135 °C after 72 hours achieved nearly full conversion of **S_1** with 79% selectivity towards **B** (Table 5, setting 9). At the final temperature of 150 °C, the catalyst reached a maximum TOF of 11.2 h^{-1} together with 84% selectivity to the desired primary amine (Table 5, setting 10).

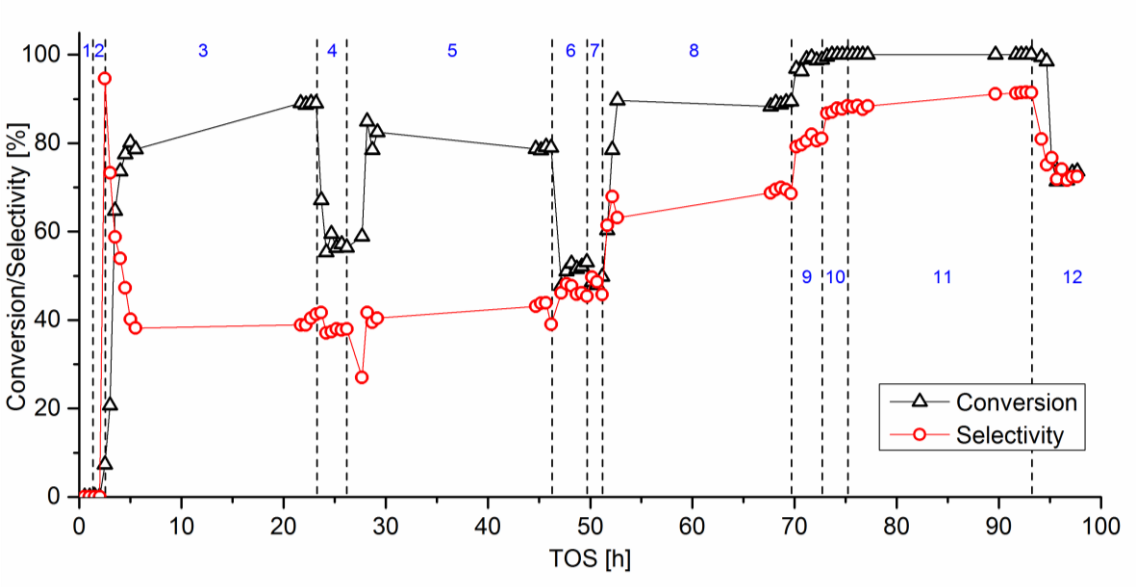

Figure 13 Continuous flow hydrogenation of **S_1** using **C_1**. For conditions in settings 1-12 see Table 5. n_{Cat} = 0.134 mmol, 0,25 M solution of **S_1** in dioxane. Conversion determined by GC using dodecane as internal standard. Selectivity towards benzylamine **B**.

Increasing the residence time by setting the flow rate to 0.05 mL·min^{-1} did not lead to an improved selectivity (85%, Table 5, setting 11). However, significant amounts of secondary amine **D** (up to 8%) were obtained under these conditions. Finally, initial conditions were restored (Table 5, settings 2 vs. 12) resulting in a Δ10% drop in conversion (83% to 73%) after a total 97.5 hours on-stream. Interestingly, a significant rise in selectivity of Δ31% was observed. This may point towards slow catalyst activation in the beginning of the experiment. Upon enhancing the formation of catalytically active species over time, the catalyst to substrate ratio increases within the resin beads. Consequently, more active catalyst is provided to convert the intermediate of the first hydrogenation step to the primary amine prior to the formation of side-products upon leaving the catalyst bed. The amount of Ru metal leached into the product stream was found to be below the detection limit of ICP-OES analysis. The

polymer-supported Ru-Triphos catalyst **C_1** showed a remarkable stability under continuous flow conditions over nearly 98 hours on stream while various reaction conditions during process optimization were applied.

Hence, it was decided to examine the catalyst life-time of **C_1** at constant flow conditions. In this run, a feed flow rate of 0.10 mL·min^{-1}, H_2 flow of 2.50 mL·min^{-1}, 100 °C reaction temperature and a system pressure of 20 bar were chosen to monitor the catalyst performance over nearly 200 h TOS. The substrate conversion, the selectivity towards **B** as well as the cumulative TON are depicted in Figure 14.

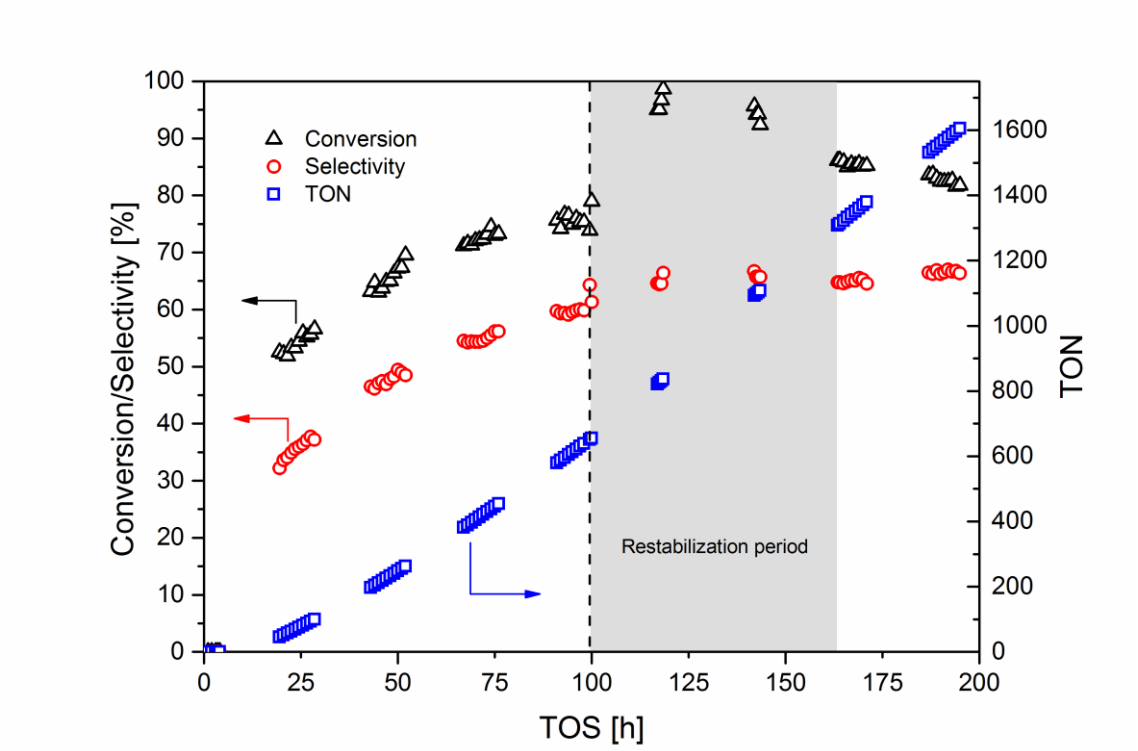

Figure 14 Continuous flow hydrogenation of **S_1** using supported catalyst **C_1**. Conditions: n_{cat} = 0.134 mmol, *T* = 100 °C, 20 bar, 0,25 M **S_1** in dioxane at 0.1 mL·min^{-1}, $\dot{V}(H_2)$ = 2.5 mL·min^{-1}. At 100 h, renewal of feed solution caused malfunctioning of HPLC pump for 1 h (dashed line). Grey area indicates catalyst restabilization period. Conversion determined by GC using dodecane as internal standard. Selectivity towards **B**.

Analogous to the previous flow experiment, an incubation time of at least 4 hours was observed resulting in solely unconverted substrate in the product stream. Again, this could be attributed to the slow formation of the potentially active Ru-hydrido species analogous to the [Ru(cod)(methallyl)$_2$]/**II** system reported by Beller.[15] After 19.5 hours on stream, 53% of the feed was converted with 32% selectivity towards the terminal primary amine **B** demonstrating the acceptable reproducibility compared to the same conditions applied in the previous run (57% conversion, 39% selectivity, see

Table 5, setting 3). Within the following 56 hours, the catalyst activity and selectivity constantly increased to 73% and 56%, respectively. Between 91 and 98 hours on stream, a constant conversion of 76% together with 60% selectivity was reached indicating full activation of the supported catalyst under the given conditions. In order to proceed monitoring the catalyst productivity, the feed stock solution had to be replaced after 98 hours. Unfortunately, this resulted in malfunctioning of the HPLC pump causing a flow outage for 1 hour (dashed line, Figure 14). When reaction conditions were restored, a significant rise in catalyst activity was observed over 35 hours whereas the chemoselectivity was only marginally influenced. Subsequent to this catalyst restabilization period (grey box, Figure 14), constant catalyst performance was recovered after 171 hours on stream resulting in an average conversion and selectivity of 86% and 65%, respectively. Within the remaining 24 hours, a minor drop in activity of about Δ3% was observed. However, lacking a clear indication of catalyst deactivation after 195 hours on stream, the still active supported Ru-Triphos catalyst $\mathbf{C_1}$ achieved a total TON of 1605. Ruthenium metal leached into the product stream could not be detected by ICP-OES analysis. This demonstrates a remarkable long-term stability and hence robustness of the heterogenized complex under continuous flow conditions. Moreover, the flow process emphasizes the advantage over batch recycling methodologies avoiding mechanical deterioration of the polymeric support.

For future investigations, it would be desirable to improve on slow formation of the catalytically active species and hence the incubation time of the catalyst. This could be accomplished by using conditions facilitating catalyst activation in the beginning of a flow run, e.g. higher reactor temperature and system pressure. Both pre-activation with H_2 gas as well as the addition of base have proven to effectively diminish this activation period in homogeneous systems.[15] An increase in catalyst bed length could lead to further improvement regarding the selectivity towards the primary amine as it could provide a sufficient residence time to reduce the concentration of the reactive aldimine intermediate preventing side reactions once the mixture leaves the fully activated catalyst bed.

5.6 Conclusion and Outlook

In this chapter, the solid-phase synthesis of a small library of supported ruthenium complexes **C_1-C_5** based on Triphos-type phosphine ligands **L_1-L_5** was presented. In contrast to previous work within the group, [RuHCl(PPh_3)$_3$CO] was chosen as ruthenium precursor preventing the formation and deposition of Ru metal during the synthesis. Hence, stable Ru-Triphos complexes immobilized on four different polymeric supports were obtained requiring only simple filtration steps during work-up. The successful formation of the desired Ru-complex could be verified by using various analytical techniques such as gel-phase and solid-state NMR, FTIR and Raman spectroscopy. The results obtained are well in line with those obtained for their solution-phase counterpart [RuHCl(Triphos)CO] (**III**).

Subsequently, the supported catalyst **C_1** was employed in the deaminative hydrogenation of nitriles to primary alcohols. While the aromatic substrate benzonitrile (**S_1**) led to a promisingly high selectivity of 87% towards benzyl alcohol, 91% selectivity towards 1-heptanenol were achieved when using *n*-heptanenitrile (**S_2**), which even outperformed the selectivity of homogeneous analogue **III**.

Remarkably, when applying **C_1** in the hydrogenation of **S_1** without the presence of water, very high selectivity of 99% towards benzylamine was obtained. Hence, the small supported catalyst library was screened in the reduction of nitriles to terminal amines. Under mild conditions and without the need of selectivity enhancing additives, the heterogeneous catalysts **C_1-C_4** led to high selectivities for substrate **S_1**. Most aromatic mono- and dinitriles were readily converted with good to excellent selectivities towards the corresponding primary amines, while aliphatic nitriles proved to be more challenging. In contrast to the supported analogues, the homogeneous catalyst **III** gave an unselective mixture of primary amine and secondary imine under the same conditions. The superior selectivity of the heterogeneous catalyst can be attributed to the high catalyst to substrate concentration provided by the local microenvironment of a resin bead suppressing the non-catalytic formation of side-products. Moreover, a marginal change in ligand structure from phenyl groups to *o*-tolyl substituents in **C_5** resulted in nearly selective formation of secondary imine as observed for its SiO_2-grafted analogue **IV**. This tunable selectivity underlines the versatility of the resin-bound Ru-Triphos system and demonstrates the power of the solid-phase synthetic methodology for catalyst discovery.

When tested upon the reusability and recyclability of **C_1** under batch conditions, a constant increase in activity and high selectivity were obtained over four consecutive

cycles indicating slow formation of the active catalyst. In the following two runs, the activity declined due to mechanical degradation of the support.

To overcome this issue, the supported catalyst **C_1** was applied in a fixed bed reactor and used in the reduction of **S_1** under continuous flow conditions. The catalyst performance remained fairly stable over 95 hours when exposed to various reaction conditions. Furthermore, **C_1** demonstrated a remarkable long-term stability indicating no significant loss in activity and selectivity towards benzyl amine after 195 hours on stream. However, the main problem encountered when employing the supported Ru-Triphos system in flow applications was the slow formation of the catalytically active species. Finding an optimized procedure to fully activate the catalyst in order to reduce the incubation time would be highly desirable.

Generally, it would be of great interest to expand the applicability towards the transformation of more challenging substrates, such as esters, keto acids and amides, or employing the system in the reduction of CO_2 to methanol as reported for homogeneous Ru-Triphos systems.[42]

In future, a highly diverse resin-bound Triphos ligand library could be envisioned, where the introduction of up to three different phosphorus moieties into the ligand structure by using SPS in a combinatorial fashion could lead to a higher number of ligand combinations. The proposed modular route depicted in Scheme 5 is based on a neopentyl scaffold modified with three different leaving groups, a strategy reported by Heidel *et al*.[27a] After installing the P(R^2)$_2$ moiety, the backbone can be reacted with a supported lithium phosphide (R^1) followed by introduction of the third P(R^3)$_2$ donor group adapted from the procedure used for the synthesis of supported ligands **L_1-L_5**.

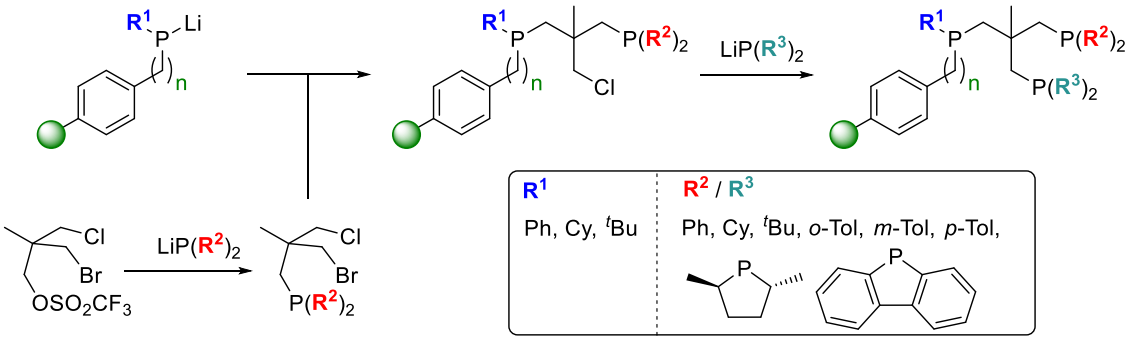

Scheme 5 Proposed modular solid-phase synthetic route towards supported Triphos-type ligands bearing various phosphorus moieties.

5.7 Experimental

General Experimental

All reactions and manipulations were carried out using standard Schlenk techniques under inert atmosphere of purified argon or in an MBraun glovebox unless stated otherwise. All glassware was dried prior to use to remove traces of water. All chemicals were obtained from commercial suppliers and were used as received unless otherwise stated. Diethyl ether and THF were distilled from sodium/benzophenone and toluene was distilled from sodium. Extra dry 1,4-dioxane (99.8%), Me-THF (99+%), anisole (99+%) and DMC were purchased from Acros Organics, degassed and stored over 4 Å molecular sieves. DCM was distilled from calcium hydride. C_6D_6 was thoroughly degassed with Argon and stored over 4 Å molecular sieves. Resin-bound Triphos ligands **L_1-L_5** were prepared by F. J. L. Heutz.[30] Complex **III** was prepared following a literature procedure.[33] NMR spectroscopic analysis was conducted using a Bruker FOURIER 300, an AVANCE II 400 or an AVANCE III 500. ^{1}H-NMR and ^{13}C-NMR experiments were recorded using standard NMR techniques and the chemical shifts (δ) are reported relative to the solvent peak. Gel-phase ^{31}P NMR spectra of all resins were recorded unlocked and without additional shimming in dry THF as a solvent unless mentioned otherwise. Chemical shifts are reported relative to 85% H_3PO_4 in water. Solid-state NMR spectra were acquired using a Bruker Avance III spectrometer equipped with a 9.4 T widebore superconducting magnet. Samples were packed in 4.0 mm ZrO_2 rotors and rotated at MAS rates of 14 kHz (^{1}H, ^{31}P) and 12.5 kHz (^{13}C). Multiplicities are provided using the following abbreviations: s = singlet and br = broad. NMR spectra were processed using TopSpin 3.2 or MestReNova 11.0. IR spectra were recorded on a Shimadzu IRAffinity-1S spectrometer. The Raman spectra were collected on a Renishaw inVia Raman microscope using a 633 nm laser with a laser power of 1.61 mW. The samples were mounted onto object slides and an objective with a magnification of 50x was applied. For the acquisition of each spectrum 10 scans with an irradiation time of at least 20 s per scan were applied. Elemental analyses were measured by Mikroanalytisches Laboratorium Kolbe in Oberhausen, Germany. GC-FID measurements were performed on a HP 6890 using an Agilent HP-5 column. ICP-OES analyses were measured using a Varian 715-ES.

General Procedure for the Synthesis of Resin-Bound Ru-Triphos complexes C_1-C_5

A previously synthesized resin-bound Triphos ligand **L_1** (0.19 mmol, 1.0 equiv), **L_2** (0.10 mmol, 1.0 equiv.), **L_3** (0.13 mmol, 1.0 equiv.), **L_4** (0.20 mmol, 1.0 equiv.) or **L_5** (0.12 mmol, 1.0 equiv.) and [Ru(HCl(PPh_3)$_3$CO] (1.1 equiv.) were weighed into a Schlenk tube. The mixture was suspended in toluene (10 mL) and heated to 80 °C under gentle stirring. The reaction mixture was left at 80 °C with occasional stirring to avoid mechanical abrasion of the resin and the progress of the reaction was monitored by gel-phase ^{31}P NMR. Once full complexation of the resin-bound Triphos ligand was observed, the mixture was cooled to room temperature and the supernatant was removed. The resin-bound complex was washed with three 10 mL portions of THF, three 10 mL portions of DCM followed by three 10 mL portions of Et_2O. After drying *in vacuo* a yellow or orange resin-bound [RuHCl(Triphos)CO] complex (**C_1-C_5**) was obtained. (**C_1-C_5** yields based on ligands **L_1-L_5**).

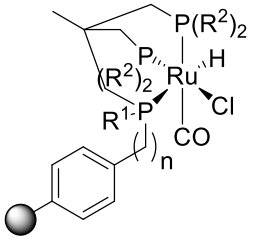

C_1: MF (1% DVB), $R^1 = R^2$ = Ph, n = 1
C_2: JJ, $R^1 = R^2$ = Ph, n = 1
C_3: MF (4% DVB), $R^1 = R^2$ = Ph, n = 1
C_4: PS, R^1 = *t*Bu, R^2 = Ph, n = 0
C_5: MF (1% DVB), R^1 = Ph, R^2 = *o*-Tol, n = 1

C_1: Yellow resin (273.0 mg, 0.18 mmol, 95.0%); ^{31}P NMR (121 MHz, THF:C_6D_6 6:1): δ = 49.8 and 41.8 (1P, br), 15.3 (1P, br), 1.2 (1P, br) ppm; ^{1}H MAS NMR (spinning rate 14 kHz,): δ = -5.80 (br, Ru–H) ppm; IR (solid): $\tilde{\nu}$ = 3055 (m), 3024 (w), 2918 (w), 2850 (w), 1968 (m, CO), 1922 (m, Ru–H), 1600 (w), 1492 (m), 1450 (m), 1433 (m), 1090 (w), 832 (m), 738 (m), 694 (s) cm^{-1}.

C_2: Yellow resin (161 mg, 0,12 mmol, 97.1%): ^{31}P NMR (121 MHz, THF:C_6D_6 6:1): δ = 51.0 and 14.4 (1P, br), 0.8 (1P, br), 1.2 (1P, br) ppm; IR (solid): $\tilde{\nu}$ = 3055 (w), 3023 (w), 2917 (m), 2849 (w), 1975 (m, CO), 1925 (m, Ru–H), 1599 (w), 1580 (w), 1492 (m), 1450 (m), 1433 (m), 1090 (w), 841 (w), 739 (m), 694 (s) cm^{-1}.

C_3: Yellow resin (165 mg, 0,11 mmol, 91.2%): ^{31}P MAS NMR (spinning rate 14 kHz,): δ = 51.8-5.7 (br, 3P) ppm; IR (solid): $\tilde{\nu}$ = 3056 (w), 3023 (w), 2917 (m), 2849 (w), 1970 (m, CO), 1920 (m, Ru–H), 1600 (w), 1582 (w), 1491 (m), 1450 (m), 1433 (m), 1090 (w), 840 (w), 739 (m), 693 (s) cm^{-1}.

C_4: Orange resin (141 mg, 0,13 mmol, 96.3%): ^{31}P MAS NMR (spinning rate 14 kHz,): δ = 51.1-36.9 (m, 1P), 25.8-6.0 (m, 1P), -0.3--13.1 (m, 1P) ppm; ^{13}C MAS NMR (spinning rate 12.5 kHz,): δ = 146.0-128.1 (resin-Ar and P-Ar), 40.5 (resin-CH, P-CH_2, *C*CH_3, C*C*H_3), 32.7 (P-*C*$(CH_3)_3$), 28.4 (P-C$(CH_3)_3$) ppm, CO was not detected; IR (KBr): $\tilde{\nu}$ = 3024 (w), 2918 (m), 2854 (w), 1968 (m, CO), 1922 (m, Ru–H), 1595 (m), 1488 (w), 1432 (s), 1157 (w), 1089 (m), 1046 (w), 1019 (m), 822 (w), 743 (m), 694 (s) cm^{-1}.

C_5: Yellow resin (171 mg, 0,11 mmol, 95.6%): ^{31}P MAS NMR (spinning rate 14 kHz,): δ = 57.3--2.5 (br, 3P) ppm, ^{13}C MAS NMR (spinning rate 12.5 kHz,): δ = 140.6-128.4 (resin-Ar and P-Ar), 40.3 (resin-CH, P-CH_2, *C*CH_3, C*C*H_3), 22.7 (P-*o*-Tol-*C*H_3), ppm, CO was not detected; IR (solid): $\tilde{\nu}$ = 3054 (w), 3024 (w), 2918 (m), 2848 (w), 1968 (m, CO), 1920 (m, Ru–H), 1600 (w), 1492 (w), 1449 (m), 1434 (m), 1095 (w), 826 (w), 742 (m), 695 (s), 532 (m), 471 (m) cm^{-1}.

General Procedure for Deaminative Hydrogenation of Nitriles

The hydrogenation experiments were performed in a stainless steel autoclave charged with an insert suitable for up to 12 reaction vessels (1.5 mL) including Teflon mini stirring bars. Inside a glove box, a reaction vessel was charged with a resin-bound Ru-Triphos complex **C_1** (2.5-5.0 µmol, 0.5-1.0 mol%). Next, to the reaction vessel 0.5 mL of a stock solution of **S_1** or **S_2** (0.5-1.0 M) and the internal standard dodecane (50 mol%) in 1,4-dioxane and 0.5 ml of degassed water were added and the mixture was gently stirred for 5 minutes. Subsequently, the insert loaded with reaction vessels was transferred into the autoclave. The autoclave was purged three times with 10 bar of nitrogen gas followed by three purges with 10 bar of H_2 and then pressurized to 10 bar of H_2 and heated to the desired temperature. The reaction mixtures were gently stirred at 450 rpm for 18 h. The autoclave was cooled to room temperature, depressurized and the conversion was determined by GC-FID measurements using the following column and conditions:

Agilent HP-5 column (30 m, 0.25 mm, 0.1 µm): T_0 = 80 °C, hold for 2 min then ΔT = 10 °C min^{-1} to 160 °C, then ΔT = 15 °C min^{-1} to 240 °C, then ΔT = 15 °C min^{-1} to 300 °C, then hold for 5 min.

Retention times of nitriles and their products:
S$_1$: t_r (nitrile) = 4.53 min, t_r (prim. amine) = 4.88 min, t_r (prim. alcohol) = 5.24 min, t_r (prim. amide) = 9.49 min, t_r (sec. amine) = 13.68 min, t_r (sec. imine) = 13.77 min.
S$_2$: t_r (prim. amine) = 3.96 min, t_r (prim. alcohol) = 4.26 min, t_r (nitrile) = 4.45 min, t_r (prim. amide) = 6.86 min, t_r (sec. amine) = 8.28 min.

General Procedure Nitrile Hydrogenation Experiments
The hydrogenation experiments were performed in a stainless steel autoclave charged with an insert suitable for up to 12 reaction vessels (1.5 mL) including Teflon mini stirring bars. Inside a glove box, a reaction vessel was charged with a resin-bound Ru-Triphos complex **C$_1$-C$_5$** or [RuHCl(triphos)CO] (**III**, 2.5-5.0 µmol, 0.5-1.0 mol%). Next, to the reaction vessel 1.0 mL of a stock solution of **S$_1$-S$_{13}$** (0.25-0.50 M) and the internal standard dodecane (50 mol%) in 1,4-dioxane, toluene, THF, Me-THF, Anisole, DMC or 1,3-dioxolane was added and the mixture was stirred gently for 5 minutes. Subsequently, the insert loaded with reaction vessels was transferred into the autoclave. The autoclave was purged three times with 10 bar of nitrogen gas followed by three purges with 10 bar of H_2 and then pressurized (10-30 bar of H_2) and heated to desired temperature. The reaction mixtures were gently stirred at 450 rpm for 18-50 h. The autoclave was cooled to room temperature, depressurized and the conversion was determined by GC-FID measurements using the following column and conditions:

Agilent HP-5 column (30 m, 0.25 mm, 0.1 µm): T_0 = 80 °C, hold for 2 min then ΔT = 10 °C min^{-1} to 160 °C, then ΔT = 15 °C min^{-1} to 240 °C, then ΔT = 15 °C min^{-1} to 300 °C, then hold for 5 min.

Retention times of nitriles and their products:
S$_1$: t_r (nitrile) = 4.53 min, t_r (prim. amine) = 4.88 min, t_r (sec. amine) = 13.68 min, t_r (sec. imine) = 13.77 min.
S$_2$: t_r (prim. amine) = 3.96 min, t_r (nitrile) = 4.45 min, t_r (sec. imine) = 11.53 min.
S$_3$: t_r (nitrile) = 8.16 min, t_r (prim. amine) = 9.16 min, t_r (sec. imine) = 18.22 min.
S$_4$: t_r (nitrile) = 4.37 min, t_r (prim. amine) = 5.08 min, t_r (sec. imine) = 13.73 min.

S_5: t_r (nitrile) = 9.70 min.

S_6: t_r (prim. amine) = 8.56 min, t_r (nitrile) = 8.65 min, t_r (sec. imine) = 17.63 min.

S_7: t_r (nitrile) = 5.70 min, t_r (prim. amine) = 6.52 min, t_r (sec. imine) = 15.31 min.

S_8: t_r (prim. amine) = 8.17 min, t_r (nitrile) = 8.74 min, t_r (sec. imine) = 16.94 min.

S_9: t_r (dinitrile) = 8.50 min, t_r (monoamine) = 9.82 min, t_r (diamine) = 9.94 min, t_r (sec. imine) = 18.43 min.

S_{10}: t_r (prim. amine) = 4.44 min, t_r (nitrile) = 4.91 min.

S_{11}: t_r (diamine) = 5.93 min, t_r (monoamine) = 6.55 min, t_r (dinitrile) = 7.54 min.

S_{12}: t_r (prim. amine) = 6.08 min, t_r (nitrile) = 6.72 min.

S_{13}: t_r (prim. amine) = 9.71 min, t_r (nitrile) = 10.24 min, t_r (sec. imine) = 11.53 min.

General Procedure for Batch Recycling Experiments

The first nitrile hydrogenation cycle was performed as described above using **C_1** (5 µmol, 1.0 mol%), 1.0 mL of a stock solution of **S_1** in 1,4-dioxane (0.50 M) and the internal standard dodecane (50 mol%) at 100 °C and 10 bar H_2. After 2 hours the autoclave was cooled and depressurized and the reaction vessel was removed. Keeping the catalyst under a H_2 atmosphere using a H_2-filled balloon the supernatant was removed and the resin was washed with three 1 mL portions of THF. Next, new substrate stock solution (0.5 M, 1.0 mL) in 1,4-dioxane was added to the reaction vessel. The autoclave was then charged with the reaction vessel and a new reaction cycle was started. The supernatant was submitted for GC-FID analysis.

Continuous Flow Hydrogenation in Modular Microreaction System

Setup

Continuous flow reactions were performed using a customized Ehrfeld modular cartridge microreactor 240 (www.ehrfeld.com, Figure 12) equipped with a 63 x 10 mm cartridge (5 mL). The stock solution containing substrate **S_1** in 1,4-dioxane (0.25 M) and 25 mol% of *n*-dodecane as internal standard was introduced by a Knauer K-501 HPLC pump (0.001-9.999 mL/min). H_2 was dosed by a Bronkhorst mass flow controller F211CV-050-AAD-33-V (www.bronkhorst.com). The stock solution and the hydrogen gas were mixed in a micromixer before the gas/liquid mixture entered the catalyst bed from the bottom of the reactor. After the micromixer, a pressure sensor was installed to monitor the inlet pressure of the reactor. Two temperature sensors installed before and after the reactor allowed to record the temperature of the reaction mixture. The system pressure was maintained by an Equilibar back pressure valve (www.equilibar.com).

Procedure

200 mg of supported catalyst **C_1** were charged into a Schlenk tube and swollen in 2 mL of dioxane for 10 minutes. Under a flow of Argon, the cartridge layered with glass wool at the bottom was loaded with the suspension. After particle sedimentation and removal of the supernatant solvent the catalyst bed (0.79 mL) was layered with glass wool, the remaining volume of the reactor was filled with glass beads (0.25-0.50 mm) and topped with glass wool again. Next, the cartridge was sealed and inserted into the cartridge reactor under a gentle flow of N_2. At a system pressure of 10-20 bar the setup was flushed with dioxane (0.5 mL·min^{-1}) and H_2 (2.5 mL·min^{-1}) until a constant inlet pressure was reached. After switching to the feed stock solution at a rate of 0.1 mL·min^{-1}, the fluid inside the reactor was heated to the desired temperature. Samples of the product/substrate were collected downstream in vials and analyzed by GC.

5.8 References

[1] a) B. R. Brown, *The organic chemistry of aliphatic nitrogen compounds*, Oxford University, New York, **1994**; b) S. A. Lawrence, *Amines: Synthesis, Properties and Applications*, Cambridge University Press, Cambridge, **2004**; c) P. Roose, K. Eller, E. Henkes, R. Rossbacher, H. Höke,*Amines, Aliphatic*, in *Amines, Aliphatic: Ullmann's Encyclopedia of Industrial Chemistry*, Wiley-VCH, Weinheim, **2015**.

[2] K. S. Hayes, *Appl. Catal. A* **2001**, *221*, 187-195.

[3] a) C. Gunanathan, D. Milstein, *Angew. Chem. Int. Ed.* **2008**, *120*, 8789-8792; b) S. Imm, S. Bähn, M. Zhang, L. Neubert, H. Neumann, F. Klasovsky, J. Pfeffer, T. Haas, M. Beller, *Angew. Chem. Int. Ed.* **2011**, *50*, 7599-7603; c) E. J. Derrah, M. Hanauer, P. N. Plessow, M. Schelwies, M. K. da Silva, T. Schaub, *Organometallics* **2015**, *34*, 1872-1881; d) N. Nakagawa, E. J. Derrah, M. Schelwies, F. Rominger, O. Trapp, T. Schaub, *Dalton Trans.* **2016**, *45*, 6856-6865; e) D. Pingen, J. B. Schwaderer, J. Walter, J. Wen, G. Murray, D. Vogt, S. Mecking, *ChemCatChem* **2018**, *10*, 3027-3033.

[4] a) S. Gomez, J. A. Peters, T. Maschmeyer, *Adv. Synth. Catal.* **2002**, *344*, 1037-1057; b) T. Gross, A. M. Seayad, M. Ahmad, M. Beller, *Org. Lett.* **2002**, *4*, 2055-2058; c) A. F. Abdel-Magid, S. J. Mehrman, *Org. Process Res. Dev.* **2006**, *10*, 971-1031.

[5] a) A. A. N. Magro, G. R. Eastham, D. J. Cole-Hamilton, *Chem. Commun.* **2007**, 3154-3156; b) E. Balaraman, B. Gnanaprakasam, L. J. W. Shimon, D. Milstein, *J. Am. Chem. Soc.* **2010**, *132*, 16756-16758.

[6] a) A. M. Tafesh, J. Weiguny, *Chem. Rev.* **1996**, *96*, 2035-2052; b) M. Orlandi, D. Brenna, R. Harms, S. Jost, M. Benaglia, *Org. Process Res. Dev.* **2018**, *22*, 430-445; c) D. Formenti, F. Ferretti, F. K. Scharnagl, M. Beller, *Chem. Rev.* **2019**, *119*, 2611-2680.

[7] a) C. de Bellefon, P. Fouilloux, *Catal. Rev.* **1994**, *36*, 459-506; b) M. G. Banwell, M. T. Jones, T. A. Reekie, B. D. Schwartz, S. H. Tan, L. V. White, *Org. Biomol. Chem.* **2014**, *12*, 7433-7444.

[8] a) M. Chatterjee, H. Kawanami, M. Sato, T. Ishizaka, T. Yokoyama, T. Suzuki, *Green Chem.* **2010**, *12*, 87-93; b) Y. Li, Y. Gong, X. Xu, P. Zhang, H. Li, Y. Wang, *Catal. Commun.* **2012**, *28*, 9-12; c) H. Yoshida, Y. Wang, S. Narisawa, S. Fujita, R. Liu, M. Arai, *Appl. Catal. A* **2013**, *456*, 215-222.

[9] a) S. Nishimura,*Hydrogenation of Nitriles*, in *Handbook of Heterogeneous Catalytic Hydrogenation for Organic Synthesis*, John Wiley & Sons, New York, **2001**, pp. 254-285; b) B. D. Herzog, R. A. Smiley,*Hexamethylenediamine*, in *Hexamethylenediamine: Ullmann's Encyclopedia of Industrial Chemistry*, Wiley-VCH, Weinheim, Germany, **2012**.

[10] P. Foley, A. Kermanshahi pour, E. S. Beach, J. B. Zimmerman, *Chem. Soc. Rev.* **2012**, *41*, 1499-1518.

[11] a) D. B. Bagal, B. M. Bhanage, *Adv. Synth. Catal.* **2015**, *357*, 883-900; b) S. Werkmeister, K. Junge, M. Beller, *Org. Process Res. Dev.* **2014**, *18*, 289-302.

[12] a) H. Dai, H. Guan, *ACS Catal.* **2018**, *8*, 9125-9130; b) G. A. Filonenko, R. van Putten, E. J. M. Hensen, E. A. Pidko, *Chem. Soc. Rev.* **2018**, *47*, 1459-1483; c) L. Alig, M. Fritz, S. Schneider, *Chem. Rev.* **2019**, *119*, 2681-2751.

[13] J. Coetzee, D. L. Dodds, J. Klankermayer, S. Brosinski, W. Leitner, A. M. Slawin, D. J. Cole-Hamilton, *Chem. Eur. J.* **2013**, *19*, 11039-11050.

[14] T. Suarez, B. Fontal, *J. Mol. Catal.* **1988**, *45*, 335-344.

[15] R. Adam, C. B. Bheeter, R. Jackstell, M. Beller, *ChemCatChem* **2016**, *8*, 1329-1334.

[16] R. Adam, C. B. Bheeter, J. R. Cabrero-Antonino, K. Junge, R. Jackstell, M. Beller, *ChemSusChem* **2017**, *10*, 842-846.
[17] I. G. Molnár, P. Calleja, M. Ernst, A. S. K. Hashmi, T. Schaub, *ChemCatChem* **2017**, *9*, 4175-4178.
[18] a) N. E. Leadbeater, M. Marco, *Chem. Rev.* **2002**, *102*, 3217-3274; b) C. A. McNamara, M. J. Dixon, M. Bradley, *Chem. Rev.* **2002**, *102*, 3275-3300; c) T. J. Dickerson, N. N. Reed, K. D. Janda, *Chem. Rev.* **2002**, *102*, 3325-3344; d) D. E. Bergbreiter, *Chem. Rev.* **2002**, *102*, 3345-3384; e) Q.-H. Fan, Y.-M. Li, A. S. C. Chan, *Chem. Rev.* **2002**, *102*, 3385-3466; f) C. E. Song, S.-g. Lee, *Chem. Rev.* **2002**, *102*, 3495-3524; g) R. van Heerbeek, P. C. J. Kamer, P. W. N. M. van Leeuwen, J. N. H. Reek, *Chem. Rev.* **2002**, *102*, 3717-3756; h) D. J. Cole-Hamilton, *Science* **2003**, *299*, 1702-1706; i) D. J. Cole-Hamilton, R. P. Tooze,*Homogeneous Catalysis — Advantages and Problems*, in *Catalyst Separation, Recovery and Recycling: Chemistry and Process Design* (Eds.: D. J. Cole-Hamilton, R. P. Tooze), Springer Netherlands, Dordrecht, **2006**, pp. 1-8.
[19] a) A. E. C. Collis, I. T. Horváth, *Catalysis Science & Technology* **2011**, *1*, 912-919; b) P. C. J. Kamer, D. Vogt, J. W. Thybaut, *Contemporary Catalysis: Science, Technology, and Applications*, The Royal Society of Chemistry, **2017**.
[20] S. Hübner, J. G. d. Vries, V. Farina, *Adv. Synth. Catal.* **2016**, *358*, 3-25.
[21] a) C. Bianchini, D. G. Burnaby, J. Evans, P. Frediani, A. Meli, W. Oberhauser, R. Psaro, L. Sordelli, F. Vizza, *J. Am. Chem. Soc.* **1999**, *121*, 5961-5971; b) C. Bianchini, V. Dal Santo, A. Meli, W. Oberhauser, R. Psaro, F. Vizza, *Organometallics* **2000**, *19*, 2433-2444; c) P. Barbaro, C. Bianchini, V. Dal Santo, A. Meli, S. Moneti, R. Psaro, A. Scaffidi, L. Sordelli, F. Vizza, *J. Am. Chem. Soc.* **2006**, *128*, 7065-7076.
[22] C. Bianchini, M. Frediani, F. Vizza, *Chem. Commun.* **2001**, 479-480.
[23] R. A. Findeis, L. H. Gade, *Eur. J. Inorg. Chem.* **2003**, *2003*, 99-110.
[24] L. Harmand, S. Samer, J. Andrieu, H. Cattey, M. Picquet, J.-C. Hierso, *Open Org. Chem. J.* **2012**, *6*, 1-11.
[25] a) C. Bianchini, A. Meli, W. Oberhauser, *New J. Chem.* **2001**, *25*, 11-12; b) C. Bianchini, A. Meli, V. Patinec, V. Sernau, F. Vizza, *J. Am. Chem. Soc.* **1997**, *119*, 4945-4954; c) I. Rojas, F. L. Linares, N. Valencia, C. Bianchini, *J. Mol. Catal. A: Chem.* **1999**, *144*, 1-6.
[26] W. Hewertson, H. R. Watson, *J. Chem. Soc.* **1962**, 1490-1494.
[27] a) H. Heidel, G. Huttner, G. Helmchen, *Z. Naturforsch.* **1993**, *48b*, 1681-1692; b) L. Sönchsen, C. Gradert, J. Krahmer, C. Näther, F. Tuczek, *Inorg. Chem.* **2013**, *52*, 6576-6589.
[28] a) D. Obrecht, J. M. Villalgordo,*Introduction, Basic Concepts and Strategies*, in *Solid-Supported Combinatorial and Parallel Synthesis of Small-Molecular-Weight Compound Libraries*, Elsevier Science ltd., Oxford, **1998**, pp. 1-184; b) K. Burgess, *Solid-Phase Organic Synthesis*, John Wiley & Sons, Inc., New York, **2002**; c) M. C. Samuels, B. H. G. Swennenhuis, P. C. J. Kamer,*Solid-phase Synthesis of Ligands*, in *Phosphorus(III) Ligands in Homogeneous Catalysis: Design and Synthesis* (Eds.: P. C. J. Kamer, P. W. N. M. v. Leeuwen), John Wiley & Sons, Ltd, Chichester, **2012**, pp. 463-479.
[29] a) A. Kirschning, W. Solodenko, K. Mennecke, *Chem. Eur. J.* **2006**, *12*, 5972-5990; b) C. Wiles, P. Watts, *Eur. J. Org. Chem.* **2008**, *2008*, 1655-1671; c) C. G. Frost, L. Mutton, *Green Chem.* **2010**, *12*, 1687-1703; d) S. G. Newman, K. F. Jensen, *Green Chem.* **2013**, *15*, 1456-1472; e) F. M. Akwi, P. Watts, *Chem. Commun.* **2018**, *54*, 13894-13928.
[30] F. J. L. Heutz, P. C. J. Kamer, *PhD Thesis* **2016**.
[31] A. Muth, O. Walter, G. Huttner, A. Asam, L. Zsolnai, C. Emmerich, *J. Organomet. Chem.* **1994**, *468*, 149-163.

[32] T. vom Stein, T. Weigand, C. Merkens, J. Klankermayer, W. Leitner, *ChemCatChem* **2013**, *5*, 439-441.
[33] K.-M. Sung, S. Huh, M.-J. Jun, *Polyhedron* **1998**, *18*, 469-479.
[34] H. G. M. Edwards, I. R. Lewis, P. H. Turner, *Inorganica Chim. Acta* **1994**, *216*, 191-199.
[35] B. Altava, M. I. Burguete, E. García-Verdugo, S. V. Luis, M. J. Vicent, *Tetrahedron* **2001**, *57*, 8675-8683.
[36] I. Mellone, F. Bertini, L. Gonsalvi, A. Guerriero, M. Peruzzini, *CHIMIA* **2015**, *69*, 331-338.
[37] T. vom Stein, T. den Hartog, J. Buendia, S. Stoychev, J. Mottweiler, C. Bolm, J. Klankermayer, W. Leitner, *Angew. Chem. Int. Ed.* **2015**, *54*, 5859-5863.
[38] C. U. Pittman, R. M. Hanes, *J. Am. Chem. Soc.* **1976**, *98*, 5402-5405.
[39] M. Renom-Carrasco, L. Lefort, *Chem. Soc. Rev.* **2018**, *47*, 5038-5060.
[40] P. W. N. M. van Leeuwen, J. C. Chadwick, *Homogeneous Catalysts*, Wiley-VCH Verlag GmbH & Co. KGaA, **2011**.
[41] A. J. M. van Dijk, R. Duchateau, E. J. M. Hensen, J. Meuldijk, C. E. Koning, *Chem. Eur. J.* **2007**, *13*, 7673-7681.
[42] S. Wesselbaum, T. Vom Stein, J. Klankermayer, W. Leitner, *Angew. Chem. Int. Ed.* **2012**, *51*, 7499-7502.

List of Publications

Research papers

R. Konrath, F. J. L. Heutz, N. Steinfeldt, N. Rockstroh, P. C. J. Kamer, "Facile Synthesis of Supported Ru-Triphos Catalysts for Continuous Flow Application in Selective Nitrile Reduction", *submitted*.

R. Konrath, F. J. L. Heutz, P. C. J. Kamer, D. Vogt, *Catalyst Separation*, in *Contemporary Catalysis* (Eds.: P. C. J. Kamer, D. Vogt, J. W. Thybaut), The Royal Society of Chemistry, **2017**, pp. 711-747. (**ePub eISBN**: 978-1-78801-233-1)

D. Friedrich, C. Wöckel, S. Küsel, R. Konrath, H. Krautscheid, R. Denecke, B. Abel, "Investigations on the hydrothermal synthesis of pure and Mg-doped nano-$CuCrO_2$", *Am. J. Nano Res. Appl.*, **2014**, *2*, 53-60. (**DOI**: 10.11648/j.nano.s.2014020601.17)

Q. Simpson, R. Konrath, D. W. Lupton, "Enantioselective Pd-Catalysed Deallylative γ-Lactonisation of Propargyl Carbazolone Allyl Carbonates: Mechanistic Insight into their Decarboxylative Allylation", *Austr. J. Chem.*, **2014**, *67*, 1353-1356. (**DOI**: 10.1071/CH14211)

Oral Presentations at Conferences

R. Konrath, F. J. L. Heutz, P. C. J. Kamer, "Solid-Phase Synthesis and Application of Supported Phosphorus Ligand Libraries", *14th European Workshop on Phosphorus Chemistry*, Cluj-Napoca, Romania, **2017**.

R. Konrath, P. C. J. Kamer, "A Supported PNP-Pincer-based Catalyst Library", *XXVIII International Conference on Organometallic Chemistry*, Florence, Italy, **2018**.

R. Konrath, P. C. J. Kamer, "A Supported PNP-Pincer-based Catalyst Library – Applications in Ester and Lactone Hydrogenation", *Annual Meeting of the GDCh-Division Sustainable Chemistry*, Aachen, Germany, **2018**.

R. Konrath, F. J. L. Heutz, N. Steinfeldt, P. C. J. Kamer, “Selective Nitrile Reduction Using Solid-Supported Triphos Ligands: Application in Continuous Flow“, *16th European Workshop on Phosphorus Chemistry*, Bristol, United Kingdom, **2019**.

Poster Presentations at Conferences

R. Konrath, F. J. L. Heutz, N. Steinfeldt, P. C. J. Kamer, “Solid-phase Synthesis of Supported Phosphine-Phosphinite and Phosphine-Phosphite Ligand Libraries“, *13th European Workshop on Phosphorus Chemistry*, Berlin, Germany, **2016**.

R. Konrath, F. J. L. Heutz, S. Wendholt, P. C. J. Kamer, “Solid-Phase Synthesis and Application of Supported Phosphorus Ligand Libraries“, *Universities of Scotland Inorganic Chemistry Conference*, St Andrews, United Kingdom, **2017**.

R. Konrath, P. C. J. Kamer, “A Supported PNP-Pincer-based Catalyst Library – Applications in Ester Hydrogenation“, *51. Jahrestreffen Deutscher Katalytiker*, Weimar, Germany, **2018**.

R. Konrath, P. C. J. Kamer, “Selective Nitrile Reduction Using Solid-Supported Triphos Ligands: Application in Continuous Flow“, *52. Jahrestreffen Deutscher Katalytiker*, Weimar, Germany, **2019**.